PRECLINICAL EVALUATION OF POTENTIAL SYNERGISTIC EFFECT OF NOSCAPINOIDS AND TAXOTERE FOR BREAST CANCER THERAPY

Thesis Submitted to Sambalpur University
for the partial fulfilment of the requirements
of the Degree of

DOCTOR OF PHILOSOPHY
IN
BIOTECHNOLOGY

by

SHRUTI GAMYA DASH

Regd.No.-044/2017/Biotechnology

Under the Joint Supervision of

Supervisor: *Dr. Pradeep K. Naik, Professor, Department of Biotechnology & Bioinformatics, Sambalpur University*

Co-supervisor: *Dr. Manu Lopus, Reader, School of Biological Sciences, UM-DAE Center for Excellence in Basic Sciences, Mumbai*

DEPARTMENT OF BIOTECHNOLOGY AND BIOINFORMATICS
SAMBALPUR UNIVERSITY, JYOTIVIHAR
BURLA- 768 019, ODISHA

DECLARATION

*I hereby declare that, the work reported in the Ph.D. thesis entitled "**Preclinical Evaluation of Potential Synergistic Effect of Noscapinoids and Taxotere for Breast Cancer Therapy**" submitted at **Sambalpur University** is the original report of my research, under the joint guidance of **Dr. Pradeep Kumar Naik**, Dept. of Biotechnology & Bioinformatics and **Dr. Manu Lopus**, Centre of Excellence in Basic Science (UM-DAE-CEBS), Mumbai.*

I have not submitted this work previously to any other organization for any degree or professional qualification. I have confirmed the norms and guidelines given in the ethical code of conduct of the university. Whenever I have used materials (data, theoretical analysis and text) from other sources, I have given due credit to them by citing them in the text of the thesis and given their details in the references.

Date: **(Shruti Gamya Dash)**

COURSE WORK AND COMPREHENSIVE EXAMINATION COMPLETION CERTIFICATE

This is to certify that ***Miss. Shruti Gamya Dash****, bearing Registration No-****044/2017/Biotechnology****, a bonafide Ph.D. scholar of Sambalpur University, Sambalpur, who has successfully completed her course work and comprehensive examination, which is a part of her Ph.D. Programme.*

Date:

(Dr. Pradeep Kumar Naik)
Head of the Department
Dept. of Biotechnology & Bioinformatics
Sambalpur University, Jyoti Vihar, Burla

Dr. Pradeep K. Naik
Professor and Head
Dept. of Biotechnology & Bioinformatics

SAMBALPUR UNIVERSITY
JYOTI VIHAR – 768019
SAMBALPUR, ODISHA
Mob.: +91-9479268802
Fax: (0663) – 2430158
E-mail: *pknaik1973@gmail.com*

CERTIFICATE

*This is to certify that the research work entitled, "**Preclinical Evaluation of Potential Synergistic Effect of Noscapinoids and Taxotere for Breast Cancer Therapy**" submitted by **Shruti Gamya Dash** at **Sambalpur University, Orissa, India** is a bonafied record of her original work carried out under my supervision. This work has not been submitted partially or wholly to any other University or Institute for any degree or diploma. I recommend this thesis in fulfillment for the award of degree of **Doctor of Philosophy** in **Biotechnology.***

Prof. (Dr.) Pradeep Kumar Naik
Dept. of Biotechnology & Bioinformatics,
Sambalpur University, Jyoti Vihar, Burla, Sambalpur, India.
Date:

Dedicated to my parents

ACKNOWLEDGEMENTS

It is my great pleasure to express my deepest gratitude to my Ph.D. supervisor Dr. Pradeep kumar Naik for his enthusiasm, persistent encouragement, constructive criticisms, timely advice and guidance during the course of my entire Ph.D. work. He has been more than a guide to me by being there every single time and leading me through all these years. I could not have imagined having a better advisor and mentor for my Ph.D. study.

I am deeply rejoiced and owe my deep sense of gratitude to my co-supervisor Dr. Manu Lopus, UM-DAE Centre for Excellence in Basic Sciences, Mumbai, for his invaluable advice, moral support and feedback on my research and for always being so supportive of my work during the time I spent at UM-DAE CEBS, Mumbai. I am highly thankful to Dr. Srinivas Kantevari (Organic Chemistry, CSIR-Indian Institute of Chemical Technology, Hyderabad) for helping me out in experimental evaluation.

I have the privilege of extending my sincere thanks to all my reverenced teachers of Department of Biotechnology and Bioinformatics, Sambalpur University who have been kind enough to extend their generosity and help at the sundry phases of my research whenever I approached them during my research tenure.

My appreciativeness is extended to all the staffs of Department of Biotechnology and Bioinformatics who always remain with me and have extended their assistance to me whenever I needed their help that cannot be forgotten.

I extend my thanks to all my lab mates for their inspirational words, co-operation, and encouragement in carrying out my research work. I thank my friends Ms. Sanjukta and Mr. Maruthi Prasad who have helped me in one way or other to achieve the long cherish goal through their support and encouragement.

My special thanks to Mr. Sadananda Naik, Retd. Reader in English cum Principal for the tremendous efforts he has taken to review the language of this thesis. Due to his excellent comments and constructive criticisms, I owe him a debt of gratitude.

Of course, no acknowledgement would be complete without expressing my heartfelt gratitude to my loving parents, Mr. Kanhu Charan Dash and Mrs. Tanuja Dash, for their unwavering love, trust, encouragement, endless patience and for being the pillar of my strength. When I became exhausted, it was their love and support that enabled me to get back on my feet. Both have ingrained me in many admirable qualities and provided me with a solid foundation to endure life. I am also grateful to my sister (Mrs.Shaswati Satapathy) and my Brother-in-Law (Dr. Shasanka mouli Satapathy) for their continuous support, togetherness and love showered on me. Besides, my sweet nephews Swastik & Shashwat who have brought me a new zeal, hope, wonder and a clear conscience to the dreams of possibilities in my life. My family has shown very compassionate, supportive, and silent sacrifices for the sake of my Ph.D. during my tough times, and made me the first graduate from our family. My heartfelt gratitude

goes out to all of my family members, friends, and relatives, whose blessings and prayers made me what I am today.

Above all, I praise the almighty God for blessing me with obligate aptitude and indispensable help of others without which this endeavor would have never been accomplished for granting me the sapience, health and vigor for timely completion of my Ph.D. journey.

This work has been supported by funds from OHEPEE, Govt. of Odisha through World Bank Initiative and Department of Science and Technology, Government of India, in the form of DST-INSPIRE Fellowship to me which is duly acknowledged.

Thank You all!!
Shruti Gamya Dash

(Shruti Gamya Dash)

Table of contents

LIST OF TABLES

LIST OF FIGURES

LIST OF ABBREVIATIONS

1.	Nos	Noscapine
2.	Br-Nos	Bromo noscapine
3.	Br-TMB-Nos	Bromo-trimethoxy benzyl-noscapine
4.	VPN	9-vinyl phenyl-noscapine
5.	Br-Bn-Nos	N-3-Br-Benzyl-noscapine
6.	PYBA-Nos	9-Pyridyl-3-boronic acid noscapine
7.	DOX	Docetaxel
8.	CADD	Computer Aided Drug Design
9.	FDA	Food and Drug Administration
10.	GTP	Guanosine triphosphate
11.	XP	Extra Precision
12.	Gscore	Glide Score
13.	TLC	Thin layer chromatography
14.	NMR	Nuclear Magnetic Resonance
15.	IR	Infrared
16.	MCF-7	Michigan Cancer Foundation-7
17.	ER	Estrogen Receptors
18.	HER2	Human Epidermal Growth Factor Receptor 2
19.	DMEM	Dulbecco's Modified Eagle Medium
20.	RPMI	Roswell Park Memorial Institute Medium
21.	DMSO	Dimethyl sulfoxide
22.	FBS	Fetal bovine serum
23.	MTT	Thiazolyl Blue Tetrazolium Bromide
24.	PBS	Phosphate buffer saline
25.	mg	Milligram
26.	ml	Milliliter
27.	mM	Millimolar
28.	µm	Micromolar
29.	IC_{50}	Inhibitory concentration 50 percent
30.	FIC	Fractional inhibitory concentration
31.	FACS	Fluorescence-activated cell sorting
32.	KDa	Kilo Daltons
33.	PI	Propidium iodide
34.	DAPI	(4′,6-diamidino-2-phenylindole
35.	MgSO4	Magnesium sulfate
36.	EGTA	Ethylene glycol-bis (β-aminoethyl ether) - N,N,N′,N′-tetraacetic acid
37.	SDS PAGE	Sodium dodecyl-sulfate polyacrylamide gel electrophoresis
38.	ANS	8-Anilino-1-naphthalene sulfonic acid
39.	nm	Nanometer

ABSTRACT OF THE DISSERTATION

Docetaxel (DOX) based combination therapy is a novel therapeutic strategy that attracts great interest in breast cancer treatment but its clinical utility got limited due to its side effects. In contrast, noscapine ($C_{22}H_{23}NO_7$), benzylisoquinoline alkaloid was discovered to bind tubulin, arrest dividing cells at mitosis and selectively induced apoptosis to cancer cells without changing the steady state monomer/polymer ratio of tubulin. It was also indicated that, unlike many other microtubule inhibitors, noscapinoids do not significantly promote or hinder microtubule polymerization; rather, they alter the steady-state dynamics of microtubule assembly. This is a unique feature over currently-available antimicrotubule drugs that either overpolymerize microtubules (*taxanes*) or depolymerize them (*vincas*) and hence cause various debilitating toxicities such as leucocytopenias, diarrhea, alopecia and peripheral neuropathies. In addition, noscapine has some other advantage properties as lead molecule: (1) retains activity against paclitaxel-resistant cell lines (1A9/PTX10, 1A9/PTX22) and epothilone-resistant cell line (1A9/A8); (2) a favourable pharmacokinetics (clearance in 6-10 hours); (3) a poor substrate for drug-pumps (polyglycoprotiens and MDR-related proteins) that comprise a major cause of drug resistance; (4) it does not show immunological and neurological toxicities and (5) inhibit tumorigenesis in vivo albeit at high concentrations (~ 300 mg/kg body weight). Although noscapine is cytotoxic in a variety of different cancer cell lines (NCI 60 cell lines panel), the IC_{50} values remain in the high micromolar ranges (~21.1 to 100 μM). To enhance its activity further, efforts have been focused on developing several derivatives of noscapine (we called as noscapinoids) by modification of its scaffold structure at various points.

The combination therapy of anti-microtubule agents is an undiscovered source of chemotherapeutic resources. Presence of multiple drug binding sites on the tubulin,

suggests that a reasonable combination of two or more drugs of this class may increase the efficacy of anticancer drugs and diminish toxic side effects, thereby improving the therapeutic index. In the current dissertation work, we embark upon an approach to rationally designed a novel derivative of noscapine and evaluate its additive effect with the clinically approved anticancer agent, docetaxel (DOX), to enhance the anticancer activity based on the molecular modelling, cellular study and tubulin binding activity.

Molecular docking of 9-vinyl phenyl noscapine (VPN) and DOX onto microtubule revealed a docking score of -4.82 kcal/mol and -6.67 kcal/mol respectively, while the docking score of VPN was changed to -3.23 kcal/mol when it was docked onto the co-complex of tubulin-DOX. Further, the binding free energy ($\Delta G_{bind,PBSA}$) of VPN and DOX with tubulin showed -24.04 and -18.65 kcal/mol respectively, while the binding free energy of DOX was increased further in combination with VPN ($\Delta G_{bind,\ PBSA}$ was reduced to -21.41 kcal/mol), denoting combination effect of both ligands. Similarly, a binding energy of -3.49 and -4.18 kcal/mol respectively was noted by the molecular docking of amino-noscapine and DOX on the microtubule. In contrast, the binding energy was improved significantly (-6.27 kcal/mol) when the DOX was docked to the co-complex of amino-noscapine and tubulin, indicating the combined effect of both the ligands. The individual predicted free energy of binding ($\Delta G_{bind,pred}$) for Br-Bn-Nos and DOX with tubulin was found to be -28.89 kcal/mol and -36.07 kcal/mol based on MM-GBSA as well as -26.21 kcal/mol and -34.65 kcal/mol based on MM-PBSA, respectively. However, the $\Delta G_{bind,pred}$ of Br-Bn-Nos was significantly reduced to -33.02 kcal/mol and -30.24 kcal/mol using MM-GBSA and MM-PBSA in presence of DOX on its binding pocket. Parenthetically, the $\Delta G_{bind,pred}$ of DOX was significantly reduced to -37.17 kcal/mol and -32.80 kcal/mol using MM-GBSA and MM-PBSA in the presence of Br-Bn-Nos on its binding pocket. The reduced $\Delta G_{bind,pred}$ in presence of Br-Bn-Nos and DOX together

indicated a combination effect of both the ligands. The cell killing potential represented in terms of IC_{50} value amounted to 30.17 μM and 19.92 μM for VPN and 0.621 μM and 0.193 μM for DOX, respectively for 48 h and 72 h. The dose dependent cytotoxicity of DOX has been reduced considerably with the combination dose regimen of VPN. The IC_{50} value amounted to 38.07 μM and 28.4 μM for treatment duration of 48 h and 72 h for amino-noscapine. Parenthetically the IC_{50} value was 0.61 μM and 0.08 μM for DOX respectively for the treatment duration of 48 h and 72 h. The cytotoxic effect of DOX was reduced significantly (to 0.05 μM) in combined treatment with amino-noscapine (20 μM). Further, isobologram analysis revealed the synergistic effect of Br-Bn-Nos and DOX in anti-proliferative activity using MCF-7 cell line at 48 h (sum FIC = 0.49) and at 72 h (sum FIC = 0.62). Apropos to the cytotoxic effect, noscapinoids and DOX induced apoptosis to cancer cell by interfering with the cell cycle progression. This study also revealed that the combination dose regimen of noscapinoids and DOX blocks the cell cycle progression at the G2/M transition phase and induced apoptosis to cancer cells more effectively compared to the single regimen. The combined interaction of both agents onto tubulin dimmer was also determined experimentally using purified tubulin, in which a combination regimen of noscapinoids and DOX reduced the fluorescence intensity of tubulin to a higher value (~55% to 68%) compared to the single regimen.

Female athymic nude mice were xenografted with MCF-7 cells and the efficacy of Br-TMB-Nos (150 mg/kg/day) by oral gavage, DOX (1.5 mg/kg/week, i.v.), and in combination (Br-TMB-Nos 300 mg/kg/day+DOX 1.0 mg/kg/week, i.v,) were determined. Tumor volume was reduced to 630 mm^3 with combination treatment, 960 mm^3 with DOX and 1145 mm^3 from the tumor size of 1630 mm^3 from the untreated control group on day 40 post tumour implantation. It is clear from these data that combination treatment of both Br-TMB-Nos and DOX reduces the tumor size quite dramatically compared to single

regimen treatment of Br-TMB-Nos and DOX. Compared to untreated control mice, inhibition of tumor growth by the treatment of Br-TMB-Nos and DOX in single and in combination regimen was statistically significant ($p < 0.001$). Surprisingly, non-significant change in weight loss for Br-TMB-Nos, DOX and in their combination treatment, indicating that Br-TMB-Nos and DOX have a favourable toxicity profile. Our in vivo results demonstrated that a combination has a synergistic effect on a murine breast cancer model induced by the MCF-7.

Taken together, a proof-of-concept has been developed that our study provides compelling evidence that the anticancer potential of noscapine derivatives may be substantially improved when it is used in a combined application with low dose of DOX, could produce synergistic effects on cancer therapies, which is highly promising for enhancing the therapeutic efficacy for preclinical and clinical research.

Keywords: Noscapine; Docetaxel; Apoptosis; Molecular dynamics simulations; Tubulin binding affinity; Tumor

CHAPTER 1

INTRODUCTION

"This chapter describes a general introduction, background of different types of cancers, currently used drugs in cancer therapy and the aims of the thesis."

1.1. Cancer and its statistics

Cancer is generally an abnormal and uncontrolled growth of cells, which at a later stage can invade tissues and metastasize to distant sites within the body. The normal cells convert into cancerous cells due to some mutations and the resultant changes in protein-structure/function or the altered of gene expression patterns that perturb cell proliferation or cell death. Although more prevalent at advanced ages, cancer can affect people of any age including the foetus and is currently one of the leading causes of death. Moreover, the incidence of different types of cancer increases with increasing age worldwide according to the latest GLOBOCAN database. Although substantial advances in the treatment have successfully managed the suffering and the progression of this devastating disease, the complete cure is still largely illusive.

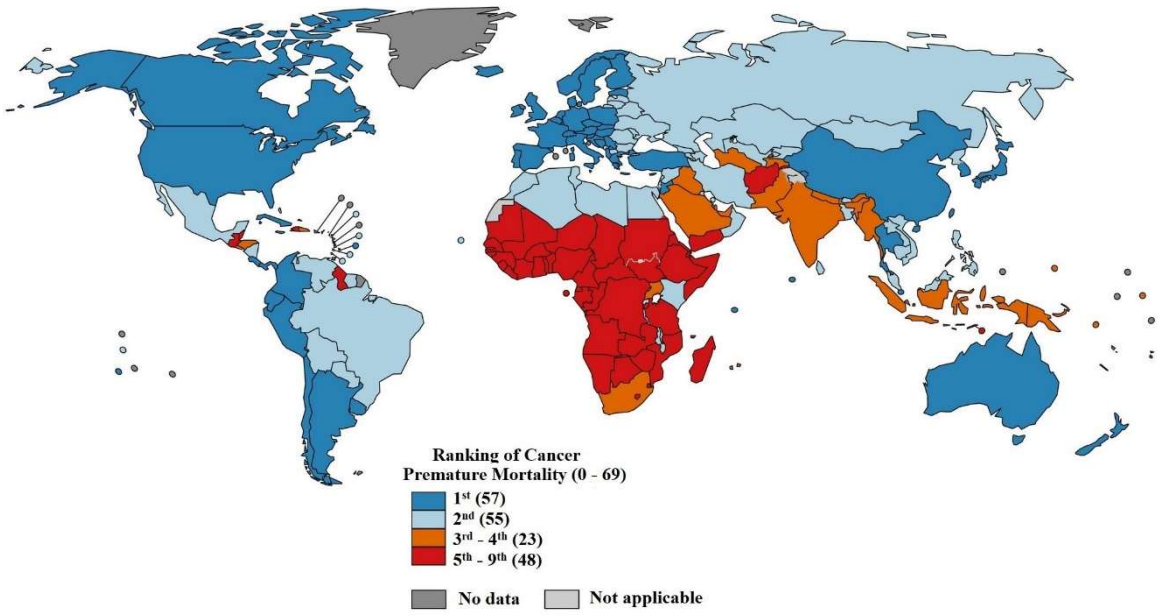

Figure 1.1. Continental distribution of cancer cases. Estimated age-standardized incidence rates (World) in 2019, all cancers, both sexes, all ages. *(Source: Global Cancer Statistics 2020*)

According to the most recent consolidated annual report (National Cancer Institute, National Institutes of Health; the Centres for Disease Control and Prevention; the American Cancer Society and the North American Association of Central Cancer Registries) on the status of cancer (released on February 04, 2021) states that the overall cancer death rates continue to decrease in men, women, and children for all major racial and ethnic groups. Comparatively, women have higher incidence rates of cancer and mortality in the age group of 20 to 49 than the men. According to annual estimates from the American Cancer Society, the death rate from cancer in the US has declined steadily over the last 2 decades. According to the previous report of International Agency for Research on Cancer (IARC) published in December 2013, the global growth rate ascends to 14.1 million new cases and crossed 8.2 million in 2012. Cancer statistics, 2019, published in the journal CA (a Cancer Journal for Clinicians of the American Cancer Society) reported the number of new cancer cases to 1,7,62,450 and deaths to 6,06,880 in the USA. In 2020, it was estimated to be 1,8,06,590 new cancer cases and 6,06,520 cancer deaths in the United States. This report gives data on the incidence rate in 184 nations around the world, comprising 28 kinds of malignancies. The growths analysed worldwide revealed lung (1.8 million, 13.0% of the aggregate), bosom (1.7 million, 11.95% of the aggregate), colorectum (1.4 million, 9.7% of the aggregate), liver (0.8 million, 9.1 percent of the aggregate), and stomach (0.7 million, 8.8 percent of the aggregate); were the most common cancer diagnosed worldwide (Figure 1.2).

Cancer is the world's second most prevalent disease with the highest mortality rate of around 0.3 million deaths per year. According to a 2020 Indian report, tobacco-related cancers are estimated to contribute 3.7 lakhs (27.1%) of the total cancer burden (Mathur et al., 2020). Breast cancers are estimated to contribute 2.0 lakhs (14.8 %) among women, and cervix cancer is reported to contribute 0.75 lakhs (5.4 %), whereas, gastrointestinal

tract cancers are estimated to contribute 2.7 lakhs (19.7 %) of the total cancer incidence both for men and women (The national cancer registry program, India, 2020). Based on the cancer data compiled by ICMR from 2004 to 2010, the number of males, females, and total cancer patients were 3,90,809, 4,28,545, and 8,19,354, respectively. It was depicted that the number of most cases of cancers has gradually improved over time. In Indian communities, all forms of cancers have been identified including pores and skin cancers, lungs, breast, rectum, stomach, dental, pharyngeal, prostate, kidney, cervix, esophagus, blood, etc. Among those lung cancers, the esophagus, belly, and oral cancers are the highest commonplace in men, whereas, in women, cervix and breast cancers are mostly not unusual in India.

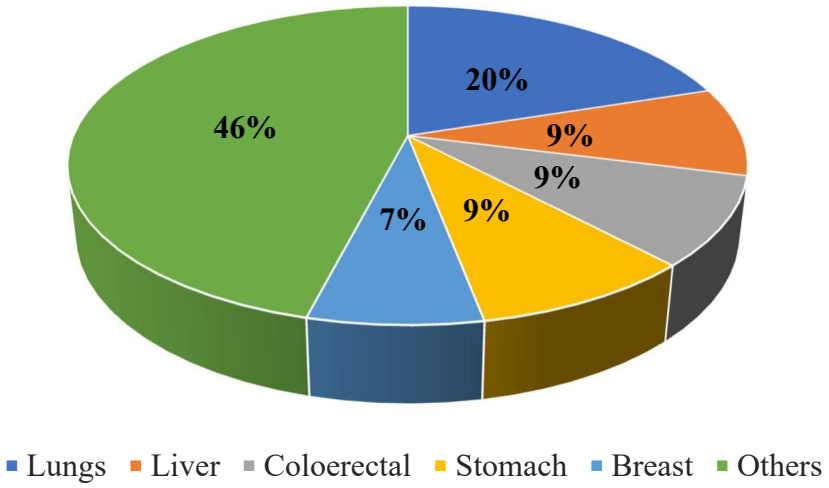

Figure 1.2. The worldwide percentage distribution of cancer types. The incidence of lung cancer was found to be highest in number (20%).

1.2. Modalities of treatment for cancer

The modalities of treatment of cancer depend on their advancement, location and progression stage. Surgery, radiation-based therapy, and chemotherapy are some of the most traditional and widely used therapeutic interventions. The severe side effects associated with the traditional methods of treatment demand a modern and novel approach to cancer treatment. The modern modalities of treatment include hormone-based therapy,

stem cell therapy, immunotherapy, anti-angiogenic modalities, DNA integrity/metabolism, tubulin-binding drugs, and combination therapy (Figure 1.3). The examples of different drugs and their mode of action has been included in Table 1.1 (Zorn et al., 2007; Medeiros et al., 2009; Luh and Liu, 2006; Gerber and Chan, 2008).

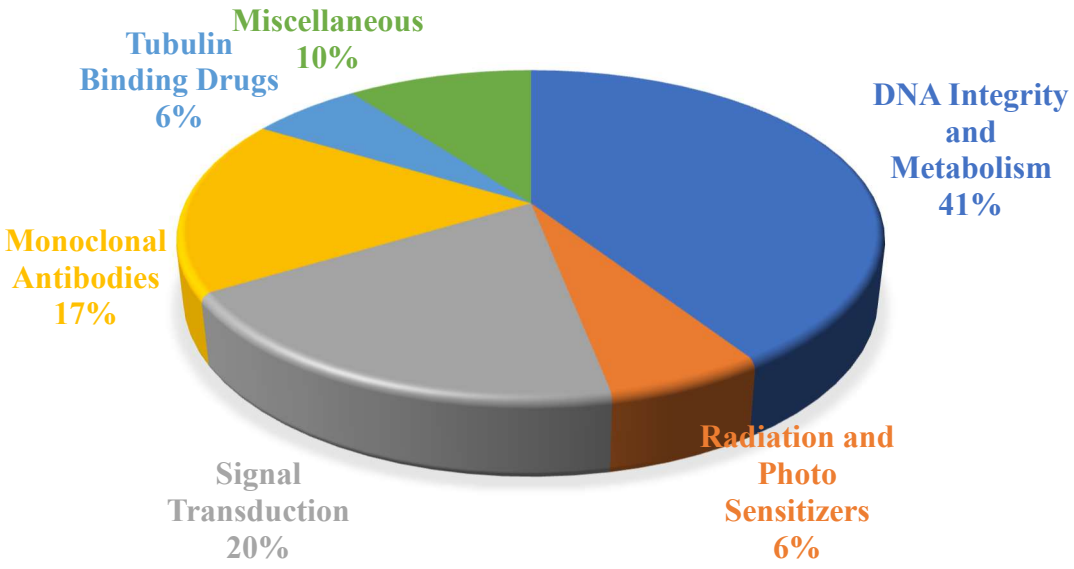

Figure 1.3. Proportions of various mechanisms/drugs currently in use in cancer therapy.

Table 1.1. Drugs currently used for cancer treatment, their mode of action and mechanistic details.

Mode of inhibition	Drugs and their targets
DNA integrity and metabolism	***Folic acid metabolism*:** Dihydrofolate reductase inhibitor (Aminopterin, Methotrexate, Pemetrexed); Thymidylate synthase inhibitor (Raltitrexed, Pemetrexed). ***Purine metabolism*:** Adenosine deaminase inhibitor (Pentostatin); Halogenated/ribonucleotide reductase inhibitors (Cladribine, Clofarabine, Fludarabine); Thiopurine (Thioguanine, Mercaptopurine). ***Pyrimidine metabolism*:** Thymidylate synthase inhibitor (Fluorouracil, Capecitabine, Tegafur, Carmofur, Floxuridine); DNA polymerase inhibitor (Cytarabine); Ribonucleotide reductase inhibitor (Gemcitabine); Hypomethylating agent (Azacitidine, Decitabine). ***Deoxyribonucleotides metabolism*:** Ribonucleotide reductase inhibitor (Hydroxyurea). ***Topoisomerase I inhibitor*:** Camptothecan (Camptothecin, Topotecan, Irinotecan, Rubitecan, Belotecan). ***Topoisomerase II inhibitor***: Podophyllum (Etoposide,

	Teniposide). ***Nitrosoureas****:* Carmustine; Lomustine (Semustine); Fotemustine; Nimustine; Ranimustine; Streptozocin.
	TopoisomeraseII* + *intercalation: Anthracyclines (Aclarubicin, Daunorubicin, Doxorubicin, Epirubicin, Idarubicin, Amrubicin, Pirarubicin, Valrubicin, Zorubicin); Anthracenediones (Mitoxantrone, Pixantrone). ***Crosslinkers*:** *Nitrogen mustards*: Mechlorethamine; Cyclophosphamide (Ifosfamide, Trofosfamide); Chlorambucil (Melphalan, Prednimustine); Bendamustine; Uramustine; Estramustine. ***Alkyl sulfonates****:* Busulfan (Mannosulfan, Treosulfan). ***Aziridines****:* Carboquone; ThioTEPA; Triaziquone; Triethylenemelamine; Platinum (Carboplatin, Cisplatin, Nedaplatin, Oxaliplatin, Triplatin tetranitrate, Satraplatin); Hydrazines (Procarbazine); Triazenes (Dacarbazine, Temozolomide); Altretamine; Mitobronitol; Streptomyces (Actinomycin, Bleomycin, Mitomycin, Plicamycin).
Radiation and photosensitizers	***Radiation therapy***: High-energy radiation from x-rays, gamma rays, neutrons, protons, and other sources. ***Photosensitizers*:** Aminolevulinic acid/Methyl aminolevulinate; Efaproxiral; Porphyrin derivatives (Porfimer sodium, Talaporfin, Temoporfin, Verteporfin).
Signal Transduction	***Receptor tyrosine kinase inhibitors*:** *ErbB*: HER1/EGFR (Erlotinib, Gefitinib, Lapatinib, Vandetanib, Neratinib); HER2/neu (Lapatinib, Neratinib) *RTK class III:* C-kit (Axitinib, Sunitinib, Sorafenib); FLT3 (Lestaurtinib); PDGFR (Axitinib, Sunitinib, Sorafenib); VEGFR (Vandetanib, Semaxanib, Cediranib, Axitinib, Sunitinib, Sorafenib). ***Non recptor tyrosine kinase inhibitors*:** bcr-abl (Imatinib, Nilotinib, Dasatinib), Src (Bosutinib), Janus kinase 2 (Lestaurtinib). ***Enzyme inhibitors***: Farnesyl transferase FI (Tipifarnib); CDK inhibitors (Alvocidib, Seliciclib); proteosome inhibitor PrI (Bortezomib); PDE II inhibitor PhI (Anagrelide); Imp dehydrogenase inhibitor IMPDI (Tiazofurine); Lipoxygenase inhibitor LI (Masoprocol). ***Receptor antagonists/hormones*:** Endothelial receptor antagonist ERA (Atrasentan); retinoid X receptor (Bexarotene); sex steroid (Testolactone).
Tubulin binding drugs	***Inhibit microtubule assembly*:** Vinca alkaloids (Vinblastine, Vincristine, Vinflunine, Vindesine, Vinorelbine) ***Promote microtubule assembly***: Taxanes (Paclitaxel, Docetaxel,

	Larotaxel, Ortataxel, Tesetaxel); Epothilones (Ixabepilone)
Monoclonal antibodies	***Receptor tyrosine kinase*****:** *ErbB*: HER1/EGFR (Cetuximab, Panitumumab); HER2/neu (Trastuzumab). ***Solid tumors***: EpCAM (Catumaxomab, Edrecolomab); VEGF-A (Bevacizumab). ***Leukemia/lymphoma***. *Lymphoid*: CD20 (Rituximab, Tositumomab, Ibritumomab). *Myeloid*: CD52 (Alemtuzumab). *Lymphoid+Myeloid*: CD33 (Gemtuzumab). ***Others*****:** Afutuzumab, Alemtuzumab, Bevacizumab/Ranibizumab, Bivatuzumab mertansine, Cantuzumab mertansine, Citatuzumab bogatox, Dacetuzumab, Etaracizumab, Farletuzumab, Gemtuzumab ozogamicin, Inotuzumab ozogamicin, Labetuzumab, Lintuzumab, Milatuzumab, Nimotuzumab, Oportuzumab monatox, Pertuzumab, Sibrotuzumab, Sontuzumab, Tacatuzumab tetraxetan, Tigatuzumab.
Miscellaneous	Amsacrine; Trabectedin; Retinoids (Alitretinoin, Tretinoin); Arsenic trioxide; Asparagine depleter (Asparaginase/Pegaspargase); Celecoxib; Demecolcine; Elesclomol; Elsamitrucin; Etoglucid; Lonidamine; Lucanthone; Mitoguazone; Mitotane; Oblimersen; Temsirolimus; Vorinostat

Traditionally chemotherapy, the use of chemicals to kill cancer cells, is considered to be the most common in the clinic. The chemical agents execute through different mechanisms such as interference with the metabolism of DNA, the division of the cell, the signal transduction and cytotoxicity (DeVita et al., 2008). However, most of the chemotherapeutics also target normally growing blood-cells in the bone marrow, lining of the gastrointestinal tract, hair-cells within the hair-follicles, thereby causing side effects such as leucocytopoenia, immunocompromise, nausea, vomiting, diarrhoea, hair-loss etc. These immunocompromised patients may thus acquire secondary complications due to sometime lethal infections. A total of 132 cytotoxic chemotherapeutic drugs have been approved by the FDA. These drugs through a variety of their cytotoxic mechanisms often induce cell-death (apoptosis or necrosis) in tumor cells. These drugs are deliberately intended to target and eradicate tumor cells through a genotoxic effect i.e., the release of reactive oxygen species. Normal body cells, however, are also affected to some degree by

these therapeutics (Rodgers et al., 2012). Among the microtubule-targeting chemotherapeutics in clinics, the most common are taxanes and a number of vinca alkaloids for the treatment of a wide variety of human malignancies. Taxanes are the most important class of anti-cancer agents. Paclitaxel (Taxol), derived from bark-extracts of the pacific yew tree, *Taxus brevifolia*, or its derivatives, are administered to patients with breast, ovarian, lung, head and neck, oesophageal, prostate and bladder cancers (Kuruppu et al., 2019). A semisynthetic derivative of taxane is docetaxel, which is used as an effective anticancer agent, derived from extracts of the *Taxus buccata* (Ringel et al., 1991). Similarly, vinca alkaloids, one of the oldest class of therapeutics agents used to treat cancer, are the second most commonly utilized agents in the clinic. These alkaloids have been isolated from *Catharanthus roseus*. Vincristine and Vinblastine are the two main vinca alkaloids and few structural derivatives such as vinorelbine, vindesine and vinflunine are generally used in the clinic for the treatment of different types of cancer (Manfredi & Horwitz 1984). Mechanistically both the groups of drugs targeted to microtubules, interfere with its organization and induce apoptosis to both cancer and normal cells. As a result, both the groups of drugs possess sever toxicity to patients.

1.3. Microtubules: A dynamic target in cancer therapy

1.3.1. Biology of microtubule

Microtubules (MTs) are intracellular tubular structures that, along with actin and intermediate filaments, constitute the dynamic cytoskeleton of nearly all cell types. They continually arrange to form certain specialized super assemblies such as the mitotic apparatus for partitioning duplicated chromosomes during the cell division and then rearrange into normal interphase arrangements (Desai et al., 1997; Howard et al., 2003; Kuruppu et al., 2019). They are not only critical for cell proliferation, but also are required for subcellular-trafficking, signalling, and migration. Microtubules assemble from tubulin,

which itself is a dimer of α-and β-tubulin subunits, each of a molecular weight of ~50,000 Da. Both the tubulin subunits comprise a chain of approximately 450 amino acids compacted into complex structures: a centre of two β-sheets surrounded by α-helices and a bound guanine nucleotide that is non-exchangeable when attached to the α-subunit and is freely exchangeable with the externally added guanine nucleotide when bound to the β-subunit (E-site) (Jordan et al., 2004).

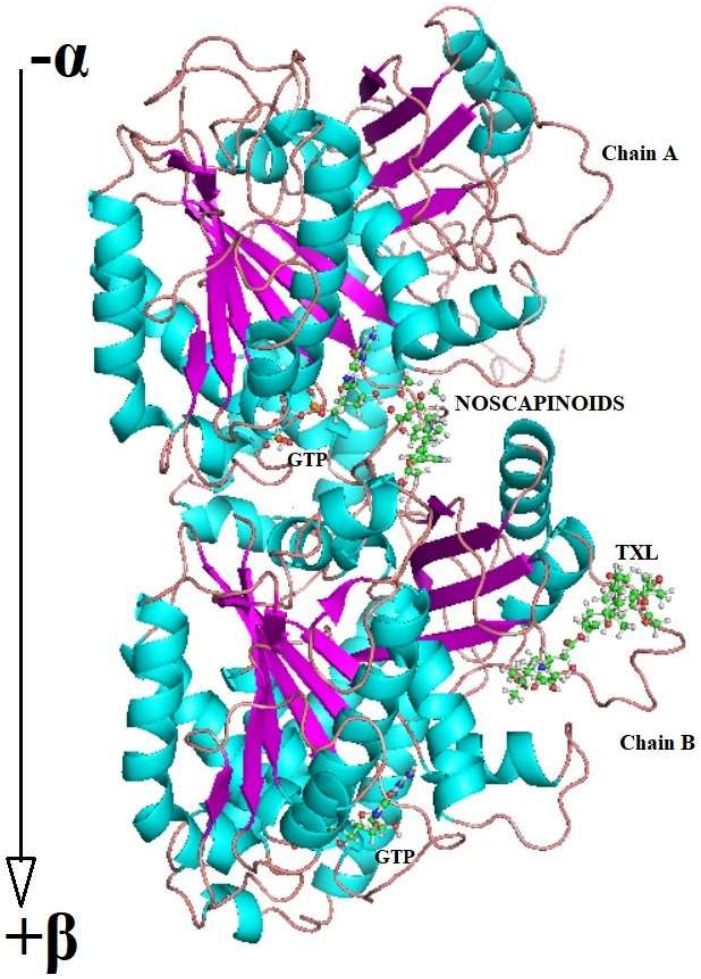

Figure 1.4. Molecular structure of tubulin heterodimer consisting of α- and β-tubulin. Ribbon diagram showing the α- and β-monomers of tubulin from X-ray crystallographic data at a resolution of 2.20 Å viewed from inside of the microtubules. The tubulin consisted of alpha helix, beta strands and loops. The GDP (formed from the hydrolysis of GTP, hydrolyzable site of GTP) and Taxotere are bound to β-monomer and Noscapinoids bound to the interface region. The arrow indicates the growth of the protofilaments during microtubule formation.

The unique functions of microtubules and the primary mechanism of actions of anti-microtubule agents are to relate the dynamic equilibrium between α- and β-tubulin heterodimer subunits and the microtubule polymer. Every monomer is asymmetric with approximate dimensions of 46 × 40 × 65 Å (width, height, and depth, respectively) and consists of a core of two sheets surrounded by helices. Each tubulin subunit is divided dynamically into three domains: the amino-terminal domain containing the nucleotide-binding region, the intermediate domain, and the carboxyl-terminal domain that coordinates drug interactions such as vinblastine and colchicine. This process of microtubule polymerization/depolymerization is referred to as dynamic instability (Figure 1.5). The hydrolysis of GTP at the exchangeable E-site is needed to build up a flux of subunits through the polymer, the addition of tubulin heterodimers to the "plus" end, and dissociating heterodimers from the "minus" end of the microtubules, bringing about in microtubule destabilization (Downing et al., 1998; Rowinsky et al., 2006). Partly also Magnesium ions (Mg2+) are required for assembly because GTP binds as an Mg-GTP complex (Nogales et al., 1999).

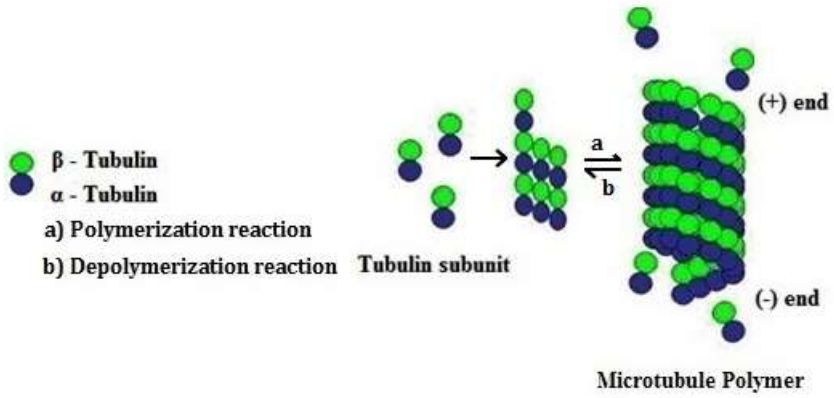

Figure 1.5. Organization of microtubules. The heterodimers of α- and β- tubulin arrange one above the other to form a polymer of protofilament and 13 of these protofilaments arranged side wise to form a microtubule. The heterodimers polymerize at one end called (+) end and at the same time depolymerizes from another end, called as (-) end. The process of polymerization and depolymerization takes place simultaneously that give dynamic structure to microtubule.

The dynamic behaviour of microtubule depends upon the competing role of both stabilizing proteins as well as the microtubule-associated proteins (MAPs: tau, MAP1, MAP2, MAP4, XMAP215), regulatory proteins responsible for microtubule destabilization (stathmin, XKCM1, XKIF2, katanin) and another variable expression of tubulin isotype (Correia et al., 1987). There is another unique dynamic feature of microtubule dynamic: within a population of slowly growing microtubules, certain individual microtubules can transition catastrophically to a rapid depolymerization-phase until they simply disappear. Alternatively, a shortening microtubule can pause randomly at some point in time to grow back again (rescue). This type of dynamic behaviour is termed "dynamic instability".

These include the growth rate, shortening rate, the frequency of transition from the growth to shortening, called a "catastrophe frequency," and the frequency of transition from shortening to growth called a "rescue frequency." (Figure 1.6).

(A)

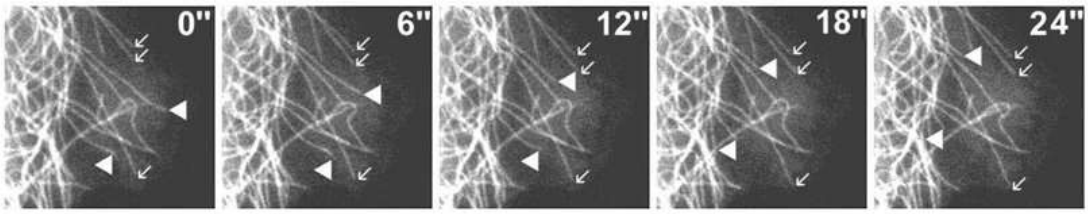

(B)

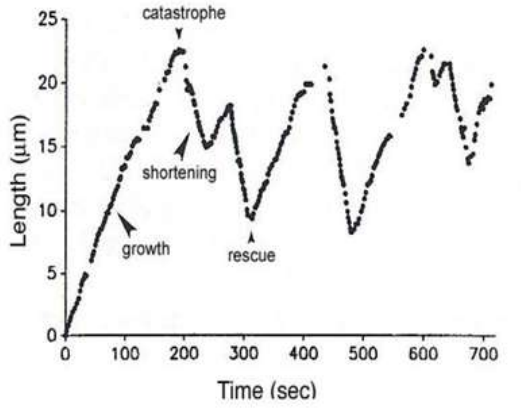

(C)

Dynamic parameters	74 MTs (n=20)
Growth	
Rate (mm/min)	9.15 ± 2.72
Distance (mm)	1.88 ± 0.44
Duration (sec)	14.33 ± 1.22
Shrink	
Rate (mm/min)	12.04 ± 3.63
Distance (mm)	1.99 ± 0.56
Duration (sec)	13.11 ± 1.45
Average pause duration	8.16 ± 2.42
Percentage time per phase	
Growth/ Shrink/ Pause	41.8/36.3/21.8
Rescue frequency (sec-1)	0.077 ± 0.015
Catastrophe frequency (sec-1)	0.086 ± 0.023
Dynamicity (mm/min)	6.61 ± 2.36

Figure 1.6. A gallery of microtubule dynamics and the measured dynamic parameters. (A) A gallery of video frames, 6 seconds apart, showing the plus ends of several microtubules. (B) One representative microtubule plus end behaviour is shown. As time goes in seconds

the microtubule plus end is growing and growing and all of a sudden, the microtubule can revert into a phase of shortening and the shortening can be rescued by another growth phase. So, it is continuously growing and shortening as you can see hardly any pausing between both the phases. (C) The measured dynamic parameters of microtubules (from Ye et al., 1998).

1.3.2. Tubulin-interacting antimitotic agents

The antimitotic agents act by binding specific sites on various structural domains of the tubulin heterodimer either on its unassembled or assembled forms. Three drug-binding domains/sites have been identified, the colchicine binding site, the binding site of vinca alkaloids (α-tubulin) and that of the taxanes (β-tubulin) (Correia et al., 2001). Colchicine binds to the area of the interface and alters the lateral microtubule contact by blocking microtubule polymerization (Jordan et al., 1998). Vinca alkaloids inhibit microtubule assembly by cross-linking the inter-dimer interfaces, thereby sterically deforming the protofilament and inducing formation of alternative polymers of tubulin (Downing et al., 1998; Nogales, 1998). The mechanism of action of taxanes is somewhat different from the other two because it promotes microtubule assembly and bundles them, resulting in significantly stable, non-functional polymers (Wilson et al., 1982; Schiff et al., 1979). Microtubule-interfering agents are graded in two classes. One group of agents such as vinblastine, colchicine, and nocodazole inhibits the polymerization of microtubules (Table 1.2) (Bissery et al., 1991). However, another group induces microtubule polymerization and bundles the microtubules, such as paclitaxel, epothilones, laulimalide, *etc* (Snyder et al., 2001; Schiff and Horwitz, 1980; Bissery et al., 1991) (Table 1.3). While both the groups of microtubule agents behave differently, they all suppress the dynamics of microtubules and interfere with spindle functions and thus arrest cells at mitosis by triggering the control point of the spindle assembly (Jordan and Wilson, 1999; Rudner and Murray 1996).

Table 1.2. Inhibitors of tubulin polymerization and used in clinic as anticancer agents.

Drug	Highest Phase	Indication	Drug type
2-Methoxyestradiol	Phase-I	Cancer	Endogenous metabolite
ABT 751	Phase-II	Breast cancer, Colorectal cancer, Non-small cell lung cancer, Renal cancer	Sulphonamide
ALB 109564(a)	Phase-I	Solid tumors	Semi-synthetic derivative of Madagascar periwinkle flower extract
AVE 8062	Phase-III	Cancer, Sarcoma (Second-line therapy), Solid tumors	Combretastatin A4 analogue
Batabulin	Phase-III	Breast cancer, Colorectal cancer, Glioma, Liver cancer, Non-small cell lung cancer	Synthetic pentafluorophenylsulfonamide
Carbendazim	Phase-I	Cancer, HIV infections	Broad-spectrum benzimidazole fungicide
Cevipabulin	Phase-I	Solid tumors	Tubulin polymerization inhibitors
CYT 997	Phase-II	Glioblastoma, Multiple myeloma, Solid tumors,	Pyridimine amine
Dolastatin analogue	Phase-II	Solid tumors	Synthetic peptide
E 7974	Phase-I	Solid tumors	Synthetic hemiasterlin analogue
EC 0225	Phase-I	Cancer	Folate linked to vinka alkaloid and mitomycin C
EC 145	Phase-II	Cancer	Folate linked to vinka alkaloid
Eribulin	Phase-III	Cancer	Synthetic helichondrin B analogue
Indibulin	Phase-I/II	Cancer	Synthetic small molecule: indolyl-3-glyoxylic acid
LP 261	Phase-I	Solid tumors	Colchicine derivative
MKC 1	Phase-II	Cancer	Small molecule inhibitor
MPC 6827	Phase-I	Cancer	Quinazoline derivative
Noscapine	Phase-I/II	Chronic lymphocytic leukaemia, Multiple myeloma, Non-Hodgkin's	Benzylisoquinoline alkaloid

		lymphoma	
NPI 2358	Phase-II	Lymphoma, Non-small cell lung cancer, Solid tumors	Synthetic analog of NPI-2350 helimide, a natural product isolated from *Aspergillus* sp.
NSC 631570	Phase-II	Cancer, Influenza virus infections	Semi-synthetic compound of thiophosphoric acid and the alkaloid chelidonine
SAR 3419	Phase-II	Non-Hodgkin's lymphoma	Immunoconjugate of anti-CD19 mab conjugated to the cytotoxic agent maytansinoid DM4
SDZ LAV 694	Phase-I	Hodgkin's disease, Non-Hodgkin's lymphoma, Solid tumors	Quinazoline
SGN 35	Phase-II	Cancer	Anti-CD30 antibody attached to a potent, synthetic drug monomethyl auristatin E (MMAE)
Soblidotin	Phase-II	Solid tumors	Dolastatin-10 derivative
Taltobulin	Phase-III	Cancer	Hemiasterlin derivative
Tasidotin	Preclinical	Cancer	Dolastatin-15 analogue
Vincristine liposomal	Phase-III	Cancer	Vinca alkaloid with liposomal delivery system
Vinflunine	Phase-III	Cancer	Vinca alkaloid
Vinorelbine	Phase-II	Cancer	Vinca alkaloid
Vinorelbine emulsion	Phase-I	Cancer	Vinca alkaloid
Vinorelbine liposomal - Hana Biosciences	Phase-I	Cancer	Vinca alkaloid with liposomal delivery system
ZEN 012	Phase-I	Lymphoma, Solid tumors	Small molecule inhibitor (binds to colchicine binding domain)

Table 1.3. Promoters of tubulin polymerization and used in the clinic as anticancer agents.

Drug	Highest Phase	Indication	Drug type
AI 850	Phase-I	Solid tumors	Paclitaxel, in a novel polyoxyethylated castor oil-free hydrophobic microparticle delivery system
ANG 1005	Phase-III	Brain cancer (Metastatic disease), Glioma	Taxane derivative

ARC 100 (TPI-287)	Phase-II	Cancer, Pancreatic cancer, Prostate cancer (Hormone refractory)	3rd generation Taxane to overcome drug resistance
BMS 188797	Phase-II	Cancer	Taxane
BMS 275183	Phase-II	Non-small cell lung cancer, Prostate cancer, Solid tumors	Taxane
BMS 310705	Phase-I	Cancer	Epothilone analog
BMS 753493	Phase-I/II	Solid tumors	Folate receptor targeted epothilone
Cabazitaxel	Phase-III	Breast cancer, Prostate cancer (Hormone refractory)	Taxane
Docetaxel	Phase-II/ Phase-III	Cancer	Taxane
Docetaxel emulsion	Phase-I	Breast cancer	Taxane
DTS 301	Phase-II	Glioblastoma, Oesophageal cancer, Pancreatic cancer	Paclitaxel delivered in copolymer gel ReGel.
EndoTAG 1	Phase-II	Cancer	Positively charged lipid complex to transport paclitaxel
Ixabepilone	Phase-II	Cancer	Epothilone
KOS 1584	Phase-II	Non-small cell lung cancer, Solid tumors	Epothilone
Larotaxel	Phase-III	Cancer	Taxane
Liposome encapsulated docetaxel	Phase-I	Solid tumors	Taxane
Liposome encapsulated paclitaxel	Phase-II	Breast cancer	New formulation of Paclitaxel
Milataxel	Phase-II	Cancer	Taxane analog
NK 105	Phase-III	Solid tumors	Paclitaxel-incorporating polymeric micellar nanoparticle (85 nm in size)
OAS PAC 100	Phase-III	Ovarian cancer (Combination therapy: In combination with carboplatin)	Paclitaxel micellar
Ortataxel	Phase-II	Non-Hodgkin's lymphoma, Renal cancer, Solid tumors	Taxane
Paclitaxel - Bristol-Myers Squibb	Phase-II	Cancer	Paclitaxel
Paclitaxel - Yew Tree Pharmaceuticals	Phase-II	Breast cancer, Ovarian cancer	Taxane

Paclitaxel – Angiotech	Phase-I/II	Inflammation and cancer	Taxane
Paclitaxel-Aphios	Phase-II	Cancer	Taxane
Paclitaxel –Hanmi	Phase-I/II	Cancer	Taxane
Paclitaxel – SuperGen	Phase-I	Solid tumors	Taxane
Paclitaxel liposomal – Aphios	Phase-I	Cancer	Taxane
Paclitaxel nanoparticle - Dabur Pharma	Phase-II	Cancer	Taxane
Paclitaxel nanoparticles - BioAlliance Pharma	Phase-II	Solid tumors	Taxane
Paclitaxel poliglumex	Phase-III	Cancer	Taxane
Paclitaxel polymer implant	Phase-I	Solid tumors	Taxane
Albumin-bound paclitaxel	Phase-III	Cancer	Taxane
Patupilone	Phase-III	Cancer	Epothilone B
Pegylated docetaxel	Phase-I	Solid tumors	Taxane
Sagopilone	Phase-II	Cancer	Epothilone
Simotaxel	Phase-I	Solid tumors	Taxane
Tesetaxel	Phase-II	Cancer	Taxane
TL 310	Phase-I	Cancer	Taxane analog

1.3.3. Challenges associated with the microtubule-targeted drugs

Although the microtubule targeted drugs are used in the treatment of a wide range of different cancers, these are the causative agent of neuropathy, peripheral neuropathy, myeloid toxicity and neutropenia. Such microtubule-binding agents also have some mutagenic properties and therefore secondary tumor risk factor is present. The cells that are exposed to these compounds develop aneuploidy due to lack of aggregation, so the risk of iatrogenic leukemia and/or solid tumors is increased. Moreover, the patients are developing resistance with the treatment of taxotere. Therefore, there is still an emergency for effective drugs with minimal side effects, enhanced solubility, and one that can overcome the mechanism of drug resistance. In a quest of finding such compounds, the naturally available alkaloids have been screened, in particular, the opium alkaloids family.

One of the alkaloids, Noscapine, which is used as safe anti-tussive drug (Karlsson et al., 1990) in the clinic since several decades, has been screened out to have anticancer activity (Ye et al., 1998).

1.3.4. Noscapine a natural opium alkaloid as anticancer agent

Noscapine ($C_{22}H_{23}NO_7$,413.43 Da) a benzylisoquinoline alkaloid was initially described by Professor Pierre-Jean Robiquet in the year 1817 (Wells WAE, 1996) from the opium plant (*Papaver somniferum*) (Figure 1.7). He isolated two natural compounds from opium (*Papaver somniferum*): codeine and noscapine (Yamada et al., 2003). Noscapine is one of the most abundant opium alkaloids (21%), the other prominent alkaloids being morphine (42%), codeine (12%), papaverine (18%), thebaine (6.5%) sanguinarine, berberine, and tubocurarine. Since then, tremendous progress has been made in the development of schemes for total synthesis. Nevertheless, noscapine's availability from natural sources is perhaps more economical than conventional synthetic means. The anticancer effect of noscapine was discovered back in 1998 (Ye et al., 1998). This was achieved through structurally screening a small library of naturally derived compounds that shared structural similarities with toxic MT depolymerizing drugs such as podophyllotoxin, MTC [2-methoxy-5-(2,3,4-trimethoxyphenyl)-2,4,6-cycloheptatrien-1-one] TKB [2,3,4-trimethoxy-4'-acetyl-1,1'-biphenyl], and Colchicine. It was found that noscapine binds stoichiometrically to tubulin (one noscapine molecule for each αβ-tubulin dimer), modify tubulin compliance, and arrest mammalian cells at mitosis phase (Lettre, 1954). Unlike vinca alkaloids and taxanes, however, it does not induce over-polymerization, depolymerization, or any change in the general interphase MT organization. Because of its subtle effect on the kinetic parameters of dynamic instability of MTs, noscapine inhibits mitosis at prometaphase and arrests dividing cancer cells and normal cells in mitosis. Cancer cells, perhaps due to their mutations that compromise cell

cycle checkpoints, often do not sustain arrested mitosis for long time and undergo apoptosis while the arrested normal cells can resume mitosis after drug removal due to metabolic clearance (Warolin and Pierre, 1999). It is reported previously that, different divergent pathways were found to converge in bringing about apoptosis in cancer cells treated with noscapine and its derivatives. These pathways include the induction of stress-activated jun N-terminal kinase, mitochondrial depolarization, downward regulation of cell survival cascades, upward regulation of pro-apoptotic signals, and eventually all converging into caspase 3/7 activation.

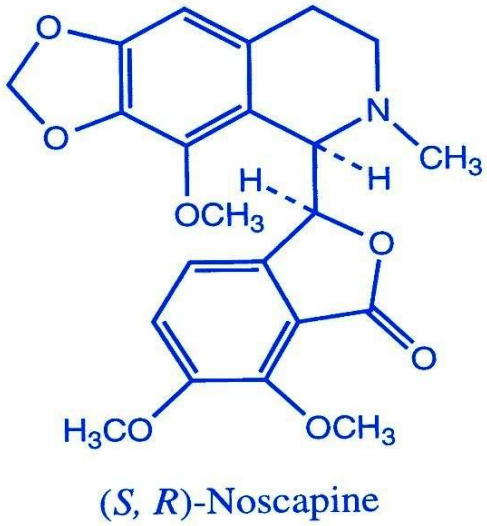

Figure 1.7. The structure of *opium poppy* and the lead molecule, Noscapine.

In comparison to the other MT binding drugs such as taxanes and vinca alkaloids, noscapine offers various advantages in cancer treatment: (a) noscapine arrests a variety of mammalian cancer cells including drug resistant variants in mitosis and targets them for apoptosis (Karlsson et al., 1990; Jordan et al., 1993; Wang et al., 2005) (b) it is a poor substrate for drug pumps (poly glycoproteins and MDR-related proteins) which constitute a major cause of drug resistance (Karlsson et al., 1990) (c) it inhibits progression of murine melanoma, lymphoma, glioblastoma and human breast tumors implanted in nude

mice without detectable toxicity to the rapidly dividing cells and post mitotic cells such as neurons (Karlsson et al., 1990; Jordan et al., 1993; Wang et al., 2005) (d) it does not hinder primary humoral and cellular responses in mice (Drukman and Kavallaris, 2002) (e) it does not cause measurable immunological and neurological toxicity in mice (f) it is orally administered as opposed to other anti-MT drugs that require peritoneal injections or intravenous infusions with a risk of anaphylactic reactions and infection at the injection site causing pain, blood vessel thrombosis or embolism (Karlsson et al., 1990; Jordan et al., 1993; Wang et al., 2005) (g) it has a mean bioavailability of ~30-32 percent over a dose range of 10 mg/kg to 300 mg/kg in mice (Wang et al., 2005). However, noscapine has low cytotoxicity to cancer cells of varying tissue origin. The values of IC_{50} remain within the high micromolar ranges (~21.1 to 100 µM) with the cancer cells of different tissue origin (Table 1.4). To further improve its efficacy, efforts were based on rational drug design and synthesis of new generations of noscapine derivatives for better therapeutic outcomes.

Table 1.4. NCI 60 cell lines screening of Noscapine. From the various cell lines screening, it was found that many cell lines tested were inhibited by the presence of noscapine to various extent (from Ye et al., 1998).

(a) Leukemia cell line	IC_{50} (µM)	(b) CNS cancer	IC_{50} (µM)	(c) Colon cancer	IC_{50} (µM)	(d) Ovarian cancer	IC_{50} (µM)
HL-60(TB)	26.4	SF-268	71.7	COLO205	63.6	IGROV1	62.6
K-562	33	SF-295	30.2	HCC2998	79.5	OVCAR-3	16.5
MOLT-4	23.5	SF-539	30.7	HCT-116	50.5	OVCAR-4	100
RPMI-8226	23.3	SNB-19	80.5	HCT-15	43.3	OVCAR-5	100
SR	38.9	SNB-75	4.87	HT29	40	OVCAR-8	63.5
CCRF-CEM	12.9	U251	41	KM12	45.8	ADR-RES	43.8
				SW-620	27	SK-OV-3	73.1
(e) Melanoma	**IC_{50} (µM)**	**(f) Non-small lung ca**	**IC_{50} (µM)**	**(g) Breast cancer**	**IC_{50} (µM)**	**(h) Renal cancer**	**IC_{50} (µM)**
LOX IMVI	37.2	A549	72.9	MCF7	42.3	786-0	49.9
MALME-3M	33.5	EKVX	100	MDA-MB-231	76.5	A498	100
M14	39.2	HOP-62	71.4	HS 578T	21.1	ACHN	62.6
MDA-MB-435	4.86	HOP-92	100	BT-549	45.7	CAKI-1	63
SK-MEL-2	34.1	H226	100	T-47D	100	RXF 393	100
SK-MEL-28	42.1	H23	79.1	MDA-N	23.1	SN12C	100
SK-MEL-5	48.3	H322M	100	**(i) Prostate cancer**	**IC_{50} (µM)**	TK-10	100
UACC-257	55	H460	39.9	PC-3	50.1	UO-31	69.1
UACC-62	56.9	H522	30.3	DU-145	100		

Nevertheless, noscapine faces some difficulty as its two ring systems *i.e.*, the isoquinoline and the isobenzofuranone are connected by a single rotating -C-C bond

between two chiral centers. Thus, ordinary chemical reactions necessarily lead to a racemic mixture of 4-stereoisomers of noscapine. Out of these, only one stereoisomer, the RS form, is biologically active (Ye et al., 1998; Warolin and Pierre, 1999).

1.3.5. Development of noscapine analogs as potential anticancer agents

To improve noscapine's cytotoxic activity, various analogs have been formulated and chemically synthesized (known as noscapinoids). A series of noscapinoids were formed by functionalizing the natural α-noscapine units of both isoquinoline and isobenzofuranone. Some of these derivatives (Figure 1.8) have far better lists of treatments and better pharmacological profiles. Currently, more than three generations of noscapinoids have been developed, chemically synthesized and their activity have been studied against cancer cell, solubility on water and toxicity to normal cells (Landen et al., 2004; Aneja et al., 2004; Aneja et al., 2006; Santoshi et al., 2011; Naik et al., 2011; Mishra et al., 2011). The first generation of noscapinoids were developed by structural modification of parent noscapine at diversity point ‘A’ and ‘B’ of isoquinoline and diversity point ‘C’ of benzofuranone ring system. Different groups like nitro, azido, an amino and halogenated group like F, Cl, Br, I groups were attached at diversity point ‘A’ and reduced oxygen at diversity point ‘C’ (Figure 1.9) (Aneja et al., 2006).

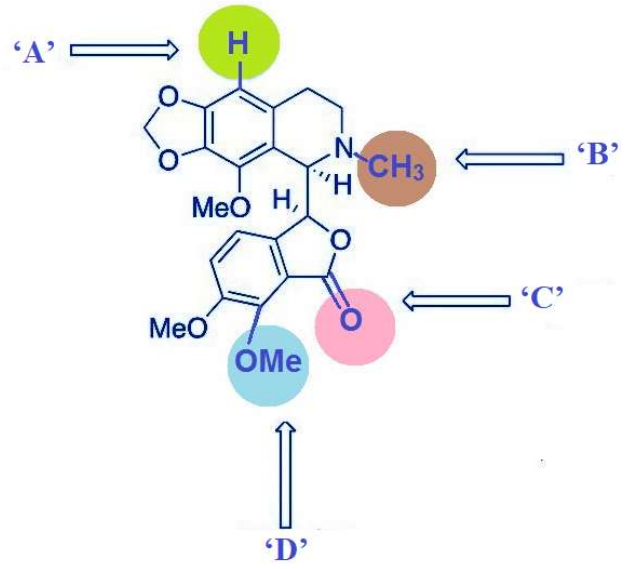

Figure 1.8. Noscapine scaffold and sites of modification.

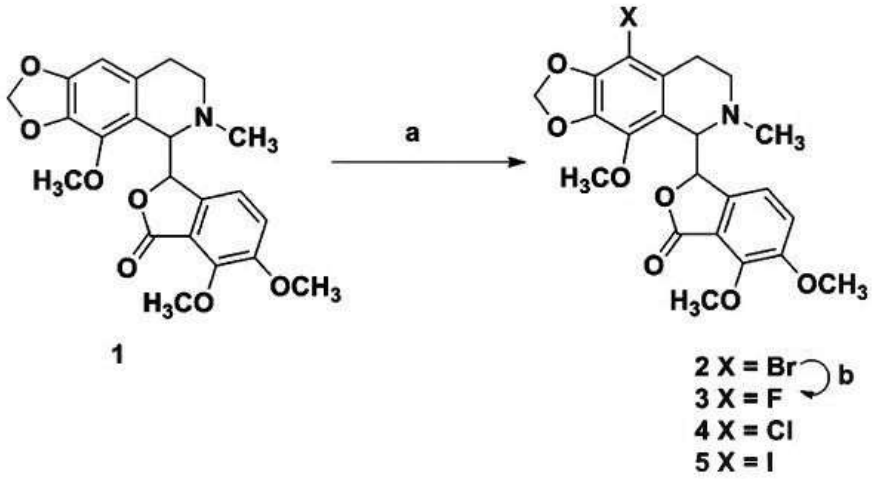

Figure 1.9. Halogenated derivatives of noscapine. All these derivatives showed improved cytotoxic activity compared to lead molecule, noscapine.

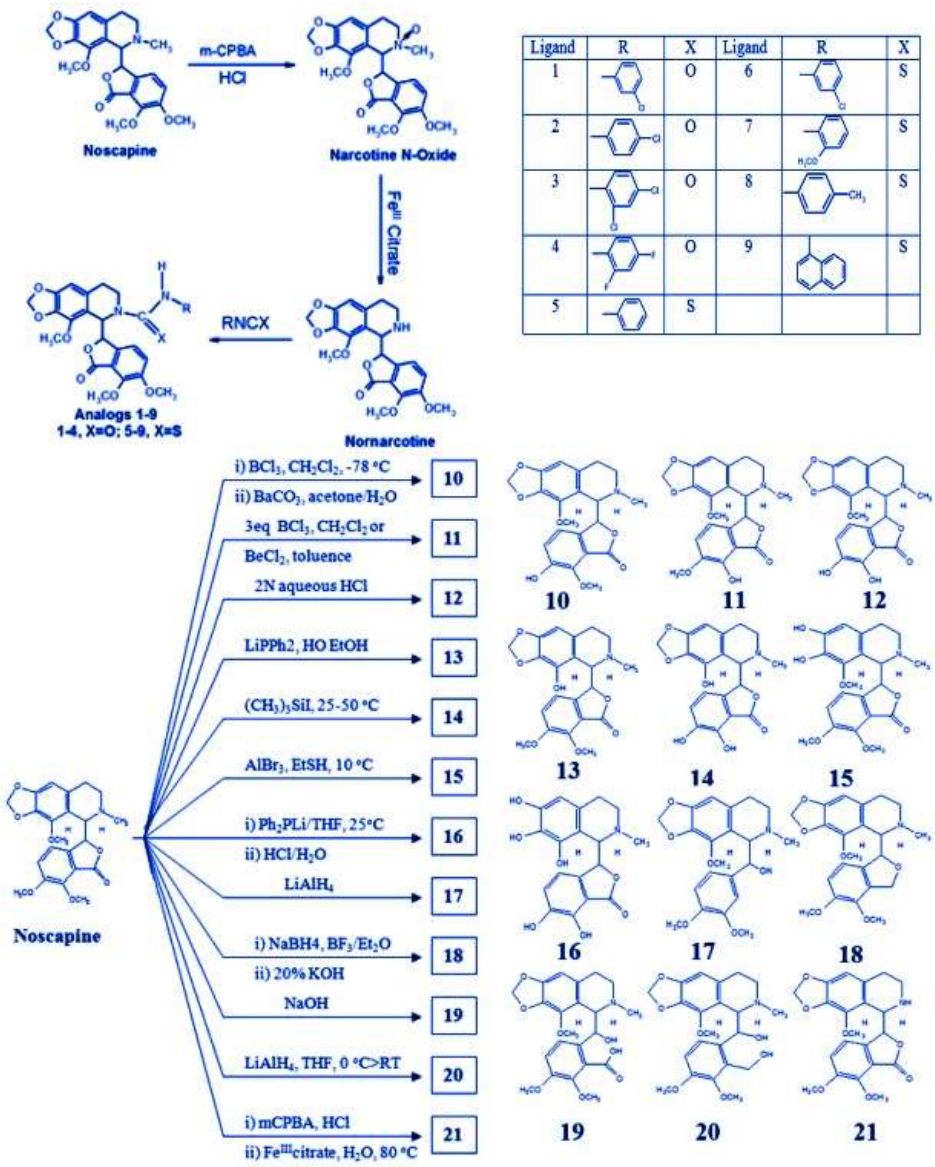

Ligand	R	X	Ligand	R	X
1		O	6		S
2		O	7		S
3		O	8		S
4		O	9		S
5		S			

Figure 1.10. Aryl-derivatives of noscapine. These derivatives were synthesized by functionalization (by deleting or substitution) of various functional groups as mentioned in the noscapine scaffold. All these derivatives showed very little or no improvement in cytotoxicity activity of noscapine.

The first generation noscapinoids were more effective than the parent one (Landen et al., 2004; Aneja et al., 2004; Aneja et al., 2006; Santoshi et al., 2011; Naik et al., 2011; Mishra et al., 2011). The 2nd generation noscapine analogs were synthesized at 7-position benzofuranone noscapine analogs that offered better antiproliferative activity. O-alkylated and asylated which was developed by chemical alteration at diversity point 'D' of parent noscapine (Landen 2004; Aneja et al., 2004; Aneja et al., 2006; Santoshi et al., 2011; Naik

et al., 2011; Manchukonda et al., 2013). Since the first pass *in vitro* experiments remain feasible with several more potent synthetic noscapine analogs, water insolubility has turned into a noteworthy problem for *in vivo* experimentation. Essentially, the presence of substituted isoquinoline and isobenzofuranone ring systems that impart highly hydrophobic structural characteristics can be due to a reduction in aqueous solubility. This lack of adequate solubility would seem to be a challenge for the further development of drugs, while low water solubility would have a direct effect on the absorption and distribution profiles of the test agents, thus compromising bioavailability. Thus, at an early stage of drug development, the solubility characteristics of a drug are immensely important, particularly for animal studies. Provided, the key descriptors of aqueous solubility of a drug are the partition coefficient and TPSA (Topological Polar Surface Area), the integration of information of these parameters is also sought to fine-tune the physicochemical profiles of drugs. To solve all such significant challenges, there is a need for further development of noscapine derivatives. The third generation, noscapinoids manipulated the isoquinoline ring system at diversity point 'B'. All these noscapinoids were superior to parent noscapine based on effectivity. All of these derivatives were normally planned by the functionalization of 'N' in the isoquinoline unit of regular α-noscapine. These subordinates were displayed generous cytotoxicity towards tumor cells of different tissue origins.

Figure 1.11. These derivatives were synthesized by functionalization (by deleting or substitution) of various functional groups as mentioned in the noscapine scaffold. All these derivatives showed very little or no improvement in cytotoxic activity of noscapine.

Enormous numbers of these noscapine derivatives have already been shown to inhibit cell proliferation in a wide variety of tumor cells (NCI 60 disease cell lines). The implanted tumor in xenograft models was successfully regressed (lymphomas, breast, prostate, and melanomas) to a reasonable degree in preclinical mice models by treatment of noscapine and its derivatives. In any case, even with increasing doses as high as 600 mg/kg, the complete remission of the disease was not achieved. Therefore, it is required to generate another generation of noscapine derivatives for better therapeutic outcomes.

Alternatively, the therapeutic efficacy of noscapine could be increased to many folds through combination therapy with the clinically used chemotherapeutics such as docetaxel. The rationality of combination therapy is to use drugs that work through multiple pathways, thereby reducing the risk of developing resistant cancer cells, when drugs of different effects are combined, each drug can be used at its optimal dose without having any side effects. Docetaxel a markedly available, second generation taxane derivative could be a choice for the combination therapy due to its clinical use. The combination of docetaxel with different naturally available anticancer agents has been the subject of numerous studies aimed at reducing the administered dose of docetaxel.

1.4. Clinical trials in cancer

Following the publication of anti-cancer impact of noscapine, many patients with different cancers started using noscapine on their own or by recommendation of their physicians. The Walter Payton Cancer Fund of the Norris Cancer Center, University of Southern California, agreed to sponsor a human trial following numerous anecdotal reports of patients who had failed several traditional chemotherapy agents and

subsequently responded to noscapine. Patients suffering from non-Hodgkin lymphoma /chronic lymphocytic leukaemia are targeted in this Phase I/II trial. It is intended to explain doses of noscapine that are safe and reliable. In trial study, the doses ranged from 1,000 to 3,000 mg per day.

1.5. Computer-aided design of potent and novel noscapine analogs

The discovery and development of drugs is a tedious and expensive process. Computer-aided approaches, such as virtual screening and *de novo* design techniques, play an important role in the drug design ventures. For, placing a drug on the market takes 10–15 years and US$ 500–800 million (Karlsson et al., 1990; Wang et al., 2005). This is why computer-aided drug design (CADD) methods have commonly been used as part of the pharmaceutical industry to increase the product pipeline's efficacy and development (Karlsson et al., 1990; Wu et al., 2006). CADD allows scientists to keep an eye on the most interesting substances so that synthetic and biological research activities can be minimized. In application, the selection of the CADD approaches to be used is sometimes determined by the delivery of target protein 3D structures determined through an experiment. If the target structures are recognized, entirely shape-based approaches that include molecular docking may be used, which employs the goal of 3D systems to design new, lively compounds with advanced potency. The proposed ligands after chemical synthesis and experimental assessment become a hit drug candidate (Figure 1.10). As more structures are becoming available, the structure-based drug designing techniques are the latest equipment to discover amazing and novel molecules.

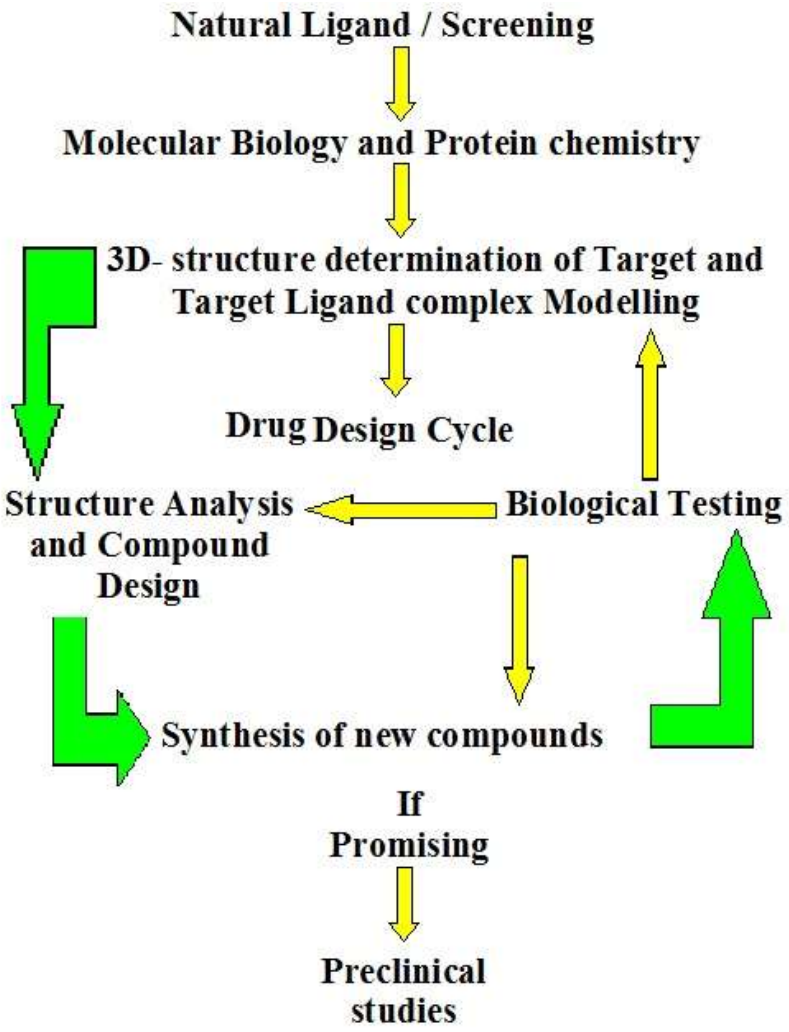

Figure 1.12. The overview of structure-based drug design cycle.

Theoretical calculations, in particular, the approach to molecular docking, appear to be the number one device for gaining such understanding. The docking algorithms provide a desirable binding pose for a compound that fits into the receptor's binding pocket and evaluates its binding affinity by using the scoring function. The scoring capabilities used by docking algorithms, however, are fairly simple. Normally, they do not include complementarity parameters of the shape between binding pocket and ligand as well as the solvation effect in calculating the strength of electrostatic interactions between protein and ligand. Consequently, the use of molecular docking only for the screening of ligands is also problematic and may lead to a reduction in accuracy.

1.6. Organization of the thesis works

In this dissertation work, the more potent derivatives of noscapine were designed through structural modifications on the isoquinoline ring with improved predictive activity, followed by chemical synthesis and experimentally evaluated as anticancer agent. The anticancer activity of these compounds was tested in a single as well as in combination regimen with docetaxel using a human breast cancer cell line, MCF-7. The thesis includes five distinct chapters. Chapter 1, describe a general introduction, background of different types of cancers, currently used drugs in cancer therapy and the aims of the thesis. Chapter 2 include the literature reviews of noscapinoids, applications of Noscapinoids as potential anticancer agent in combination with docetaxel. The details of materials and methods used for the experimentation were included in Chapter 3. The results obtained from various experiments and their significance as anticancer activity were discussed in details in Chapter 4. The overall conclusion and significance of the study was discussed in the conclusion section, Chapter 5.

Objectives of the research work:

1. To develop potent derivatives of Noscapine (called Noscapinoid) with high binding affinity onto α- and β-tubulin heterodimer followed by chemical synthesis and structural characterization.
2. To evaluate the *in vitro* anticancer efficacy of developed noscapinoids using breast cancer cell line (MCF-7). Towards this end we will determine its effect to (i) inhibit cellular proliferation and induce apoptosis to breast cancer cell line, (ii) binding affinity with tubulin, (iii) alteration with cell cycle kinetics, etc.
3. To evaluate the *in vivo* therapeutic efficacy of developed noscapinoids as an inhibitor of localized and metastatic breast cancer using xenograft animal model.

4. To evaluate the toxicity if any of developed noscapinoids based on histopathology and hematology studies using animal model.

5. To determine the combination dose regimen of developed noscapinoids and Docetaxel (a clinically used taxane for metastatic breast cancer therapy) and evaluate its therapeutic outcome using both *in vitro* and *in vivo* models as well as toxicity analysis.

CHAPTER 2

REVIEW OF LITERATURE

"This chapter deals with the literature reviews of noscapinoids, applications of Noscapinoids as potential anticancer agent in combination with docetaxel."

Cancer remains the second deadly disease worldwide after cardiovascular diseases. According to recent estimates from WHO in 2018, cancer accounts for an estimated 10 million deaths globally, particularly in low- and middle-income countries (de Martel et al., 2018; Global Initiative for Cancer Registry Development, 2020). Both external factors such as overuse of tobacco products, alcohol, and unhealthy foods, as well as internal factors, such as genetic mutation and hormonal disorders, are the primary causes for cancer (Zakhari, 1997). Due to uncontrolled cell proliferation and in the absence of cell death, an irregular clump of cells, known as tumors, are developed which expand and metastasize to other parts of the body, leading to complications and at times, mortality.

Chemotherapy, hormone therapy, immunotherapy, cancer vaccine, and biological therapies are the major systemic treatment options widely used for metastatic cancers, while surgery and radiotherapy are the key procedures used for non-metastatic cancers (Wu and Chang, 2010; Arruebo et al., 2011; Schirrmacher, 2019). According to National Cancer Institute (NCI) fact sheet, these frontline therapies rely on the states and localization of cancer. In particular, these treatment modalities are frequently accompanied by severe side effects including genotoxicity, restricted bioavailability, rapid clearance, and limited effect on metastasis. The most commonly used treatment modalities include chemotherapy in which chemical agents have shown promising results either alone or in combination. The chemical agents used in chemotherapeutics include inhibitors of topoisomerase, protein kinases, DNA-binding drugs, and tubulin-binding agents. As an example, doxorubicin, carboplatin, cisplatin, docetaxel, and paclitaxel, etc, are commonly used in clinics, but these agents also have constraints such as cost, side effects, and toxicity to normal healthy cells (Herzog, 2004; Bayat et al., 2017; Liu et al., 2020; Liu et al., 2015).

It is becoming obvious that some chemotherapeutic agents, such as docetaxel (derived from the needles of the European yew tree) have multiple effects and interfere with

some processes involved in the development and metastasis of cancer cells (Beer et al., 2003; Yared and Tkaczuk, 2012). Various tumors have distinct abnormalities in the signalling and growth-stimulation pathways. Understanding the complexities of the mechanism of action of docetaxel in combination with the molecular and genetic changes within a specific tumor may improve therapeutic outcomes in the future.

Docetaxel has been reported to have a wide range of antitumor activity. For example, docetaxel demonstrated 1.3 to 12 fold greater cytotoxicity relative to paclitaxel in several murine and human tumor cell lines. The wide range of activity *in vivo* with murine tumor models and human tumor xenografts produces a similar trend. In addition, docetaxel, unlike paclitaxel, demonstrates linear pharmacokinetics and is stored intracellularly for a longer duration due to variations in drug efflux. Docetaxel is highly effective as monotherapy and combination therapy across a variety of tumor types, including breast, lung, ovarian, head and neck, gastric, and prostate carcinomas (National Centre for Biotechnology Information 2021; Figgitt and Wiseman, 2000). However, primarily because of the poor solubility of these compounds, their clinical use has been somewhat cumbersome and expensive. Also, these drugs are plagued with serious toxicity (particularly, peripheral neuropathies, gastrointestinal toxicity, myelosuppression, and immunosuppression) owing to their non-selective action and extreme over polymerizing or depolymerizing effects on microtubules. Besides, a variety of chemotherapy agents have been successfully developed and tested at the preclinical level (Cortes and Pazdur, 1995; Eisenhauer and Vermorken 1998; Ojima et al., 2016).

2.1. History of noscapine

In 1817, two natural compounds, codeine, and noscapine were extracted from opium poppy by Pierre-Jean Robiquet, a prominent French pharmacist and professor at the Paris Ecole de Pharmacie, a Fellow of the Academie Royale des Sciences (Warolin, 1999).

Noscapine has been identified as a non-narcotic alkaloid and was formerly known as narcotine, anarcotine, or gnoscopine. Earlier pharmacological experiments sought to describe its analgesic (pain-relieving) properties (Rida et al., 2015; National Centre for Biotechnology Information, 2021). It was found to have a very mild analgesic effect (Laties, 2003). However, when taken with morphine, it works synergistically to improve the sedative effects of morphine (Stone et al., 2014) by threefold (Hosseininejad et al., 2017). In addition, noscapine did not induce constipation, unlike other opium alkaloids including morphine, codeine, and papaverine (Malekzadeh et al., 2013). Nevertheless, large clinical applications of noscapine were discovered over the years (Figure 2.1).

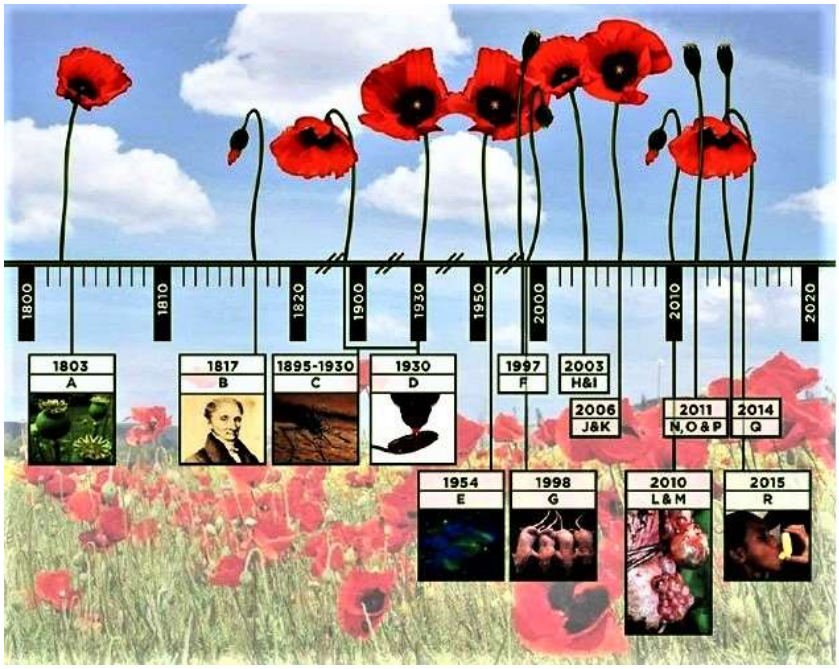

Figure.2.1. Timeline of noscapine-related discoveries. (A) 1803: Jean-François Derosne separates a noscapine-containing salt that he calls "narceine" from poppies. (B) 1817: Pierre-Jean Robiquet purifies noscapine from Derosne's salt. (C) 1895–1930: Noscapine was widely used as an antimalarial (D) 1930: The antitussive action of noscapine was discovered. (E) 1954: Hans Lettr é describes "narcotine" as a weak mitotic poison (F) 1997: Noscapine's ability to antagonize dopamine biosynthesis in PC12 cells was discovered. (G) 1998: Mouse models reveal the *in vivo* anticancer activity of noscapine against various malignancies. (H) 2003: Noscapine's antistroke activity was discovered. (I) 2003: Brominated noscapine analogue was synthesized. (J) 2006: A variety of noscapine halo derivatives were synthesized and characterized. (K) 2006: A nitro-derivative of noscapine was synthesized. (L) 2010: Brominated noscapine analogs were found to induce autophagy in macrophages and prostate cancer cells. (M) 2010: Experiments reveal that noscapine may have therapeutic value in polycystic ovarian syndrome. (N) 2011: Amino-noscapine

was synthesized and characterized. (O) 2011: Poly (ethylene glycol)-grafted gelatin nanoparticles customized to deliver noscapine intracellularly with long-circulating half-lives were synthesized and characterized. (P) 2011: Second-generation benzofuranone ring-substituted derivatives of noscapine analogs were synthesized and characterized. (Q) 2014: Third-generation water-soluble derivatives of noscapine were synthesized and characterized. (R) 2015: Inhalable nanostructured lipid particle containing a brominated noscapine derivative was synthesized and characterize (Source: *from Rida et.al, 2015*).

In 1930, the antitussive effect of noscapine was discovered. Since then, it has been used as an antitussive drug in the clinic and for the treatment of bronchial asthma (Bolser 2006; Ukena et al., 2008; Bateman et al., 2008; Mahmoudabad, & Rahimi-Moghaddam, 2009). It is administered orally in the form of tablets, lozenges, or syrup, or in a rectal suppository form.

2.2. Noscapine as an anti-cancer agent

The cytotoxic effect of noscapine was first discovered in 1954 (Lettre, 1954). Similar studies were also reported by National Cancer Institute, the United States in 1958. However, further findings failed to demonstrate substantial *in vivo* antitumor activity until a group led by Prof. Harish Joshi, at Emory University School of Medicine, Atlanta, Georgia has identified its anticancer activity in 1998 (Ye et al., 1998). It was also demonstrated that noscapine interferes with microtubules and induces apoptosis in cancer cells (Ye et al., 1998). The research work done by the scientists at Emory University on noscapine has very significant consequences. They were able to reduce the size of breast cancer tumors implanted in mice by 80 % within three weeks by treating animals with noscapine. Similar studies were also carried out with mice implanted with a tumor of human bladder cancer and against the murine lymphoid tumor. The authors concluded that noscapine decreases tumor size quite significantly, with no apparent weight loss or any tissue toxicity observed after treatment with noscapine (Ye et al., 1998). In addition, an oral dosage of noscapine did not hinder primary immune response, which is critically dependent on lymphoid cell

proliferation. It was revealed that noscapine has the potential to be an important chemotherapeutic agent for human cancer treatment (Ke et al., 2000).

Consequently, experiments were conducted to assess the efficacy of noscapine against other cancer types. It includes ovarian cancer (Zhou et al., 2002), malignant melanoma (Landen et al., 2002), bladder cancer (Ye et al., 1998), and glioblastoma (Landen et al., 2004). To determine the exact mechanism by which noscapine prevents the division of cancer cells, comprehensive experiments were performed by Dr. Joshi and his team and published in numerous medical journals (Zhou et al., 2002; Zhou et al., 2002; Ye et al., 2001).

2.3. Development of noscapine analogs as potential anticancer agents

To improve the anticancer activity of noscapine various analogs have been designed and chemically synthesized (known as noscapinoids). Some of these derivatives have far better lists of treatments and better pharmacological profiles than the parent compound. Currently, more than three generations of noscapinoids have been developed, chemically synthesized and their anticancer activities have been experimentally studied against cancer cells of different tissue origin (Aneja et al., 2006; Santoshi et al., 2011; Naik et al., 2011; Mishra et al., 2011). These generations of noscapinoids represent chemical modifications of the functional groups of noscapine that have been demonstrated to significantly attenuate its biological activity.

2.3.1. Halogen and Cyclic ether derivatives of noscapine

These derivatives of noscapine were developed by substitution of halogen groups at the 9th position of noscapine (Figure 2.2). These derivatives were demonstrated to have a

better therapeutic effect compared to noscapine. For example, 9'-bromonoscapine (9'-Br-Nosc) and reduced 9'-bromonoscapine (Rd 9'-Br-Nosc) were able to bind more effectively to tubulin and were able to prevent mitosis at a much lower effective dose (ED50) than the parent compound noscapine. In certain cell lines, they showed as high as 20 to 40 times more potency than noscapine (Aneja et al., 2006; Naik et al., 2011).

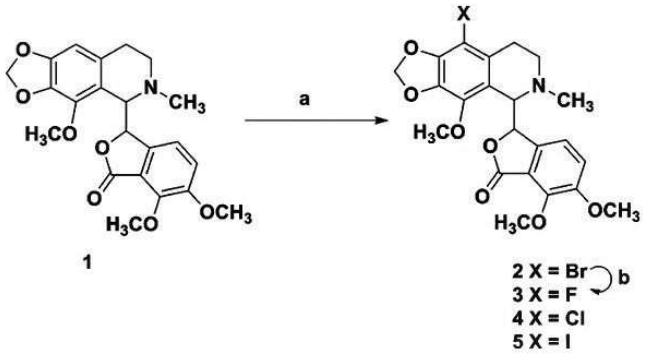

Figure 2.2. Halogenated noscapinoids: '*a*' represents bromine water and hydrogen bromide for bromo noscapine; sulfuryl chloride and chloroform for chloro noscapine; fluorine, Amberlyst-A (a slightly basic resin with alkyl amine functionality), and tetrahydrofuran for fluoro noscapine; and pyridine–iodine chloride and acetonitrile for iodo noscapine.

A large spectrum of biological activity was also demonstrated by these compounds. Among, the groups of noscapinoids, halogenated noscapinoids are implemented for their impact on the proliferation of cancer cells, antitumor potency, and associated risks (Aneja et al., 2006). These compounds were formulated by halogenating noscapine through chemical challenges as outlined in Figure 2.2. These compounds were demonstrated to arrest cell mitosis at the G2/M phase with more efficacy than noscapine, leading to selective cancer cell apoptosis (Mukhtar et al., 2014; Manchado et al., 2012). The computational blind docking approach revealed a binding site at the interface of α- and β- tubulin, overlapping with colchicine binding site for the noscapine and its derivatives with tubulin (Naik et al., 2011). A cyclic ether derivative of 9'-fluoronoscapine (Figure 2.3) was synthesized by Aneja et al., in the year 2007. It was found to be a promising anti breast cancer agent (Aneja et al., 2007). It arrested the cell cycle at the G2/M phase and induced apoptosis. The cyclic

ether derivatives of noscapine were chemically synthesized by reduction of noscapine in presence of boron trifluoride dietherate, and adding to it dropwise a solution of sodium borohydride in dry THF at 0 ˚C.

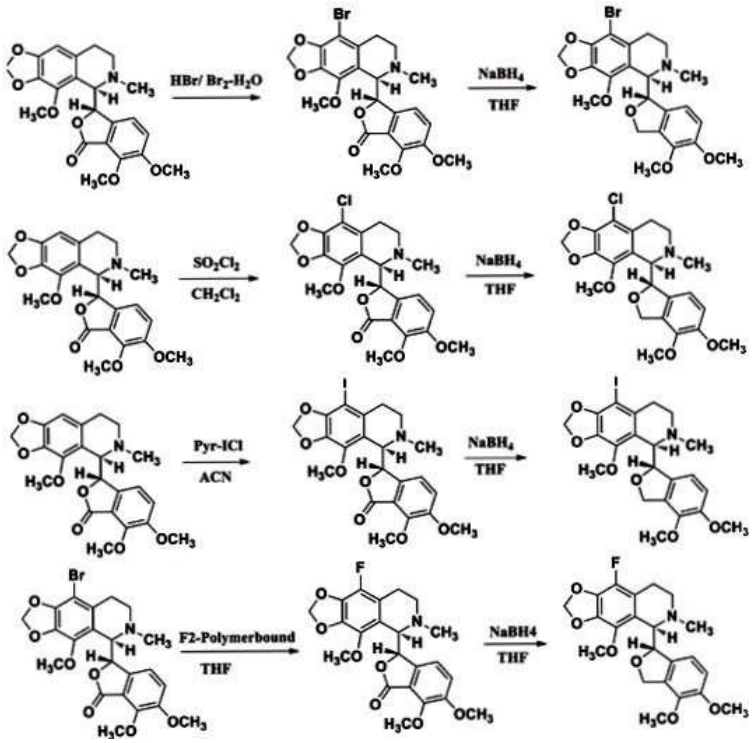

Figure 2.3. Cyclic ether halogenated derivatives (*viz.* reduced 9-fluoronoscapine (Rd-9-F-nos); reduced 9-chloronoscapine (Rd-9-Cl-nos); reduced 9-bromonoscapine (Rd-9-Br- nos) and reduced 9-iodonoscapine (Rd-9-I-nos)) of noscapine. These derivatives were synthesized from the halogenated derivatives.

2.3.2. Nitro-derivative of noscapine

The nitro-derivative of noscapine (Figure 2.4) was developed by adding a nitro group at the C-9' position of the isoquinoline ring of noscapine (Aneja et al., 2006). It inhibits the proliferation of ovarian cancer cells of paclitaxel-resistant mutant cells, human lymphoblastoid cells, and their vinblastine- and teniposide-resistant variants (Aneja et al., 2006). Further, it blocks the cell cycle progression at the G2/M phase and induced apoptosis in cancer cells. Surprisingly, there was no substantial inhibition of the proliferation of normal human fibroblast cells (Aneja et al., 2006; Otto & Sicinski 2017).

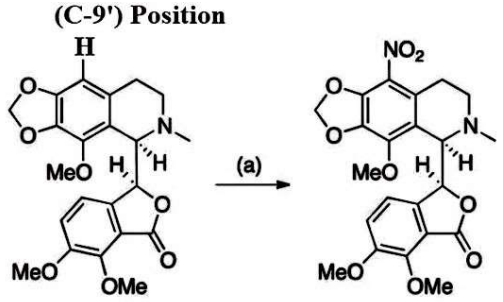

Figure 2.4. Nitro noscapine (9-Nitro-noscapine) is a product of aromatic nitration of noscapine in the presence of silver nitrate in trifluoracetic anhydride and acetonitrile (Aneja et al., 2006). (Synthetic scheme of nitro-noscapine)

2.3.3. Azido-derivative of noscapine

The azido-derivative of noscapine (Figure 2.5) was developed by adding an azido group at the C-9' position of the isoquinoline ring of noscapine. It has been illustrated as superior efficacy in killing human acute lymphoblastic leukemia cells (Santoshi et al., 2011).

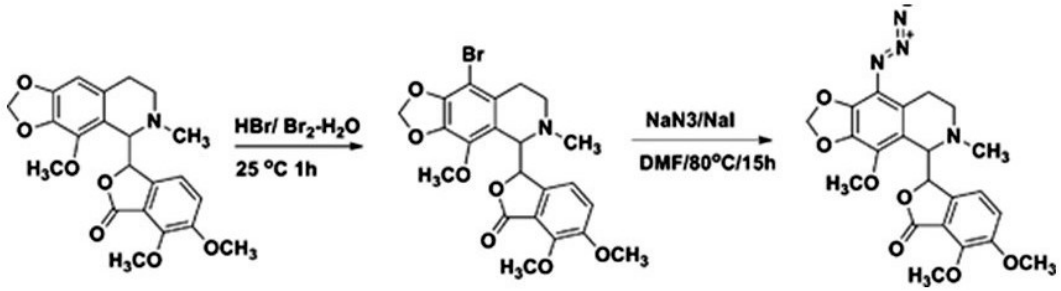

Figure 2.5. Azido noscapine: Azido noscapine (9-azido noscapine) was synthesized by first converting noscapine to bromo noscapine followed by treatment with sodium azide and sodium iodide.

2.3.4. Amino derivative of noscapine

The amino-derivative of noscapine (Figure 2.6) was developed based on the binding free energies of various noscapinoids, estimated in combination with a surface generalized Born (SGB) continuum solvation model using the linear interaction energy (LIE) method (Naik et al., 2011). The assessment of the binding free energy revealed that amino noscapine binds tubulin more strongly than the parent compound. It inhibits the proliferation of cancer

cells of different types more effectively compared to noscapine (Naik et al., 2011). However, it did not directly influence the extent of polymerization/depolymerization of tubulin subunits.

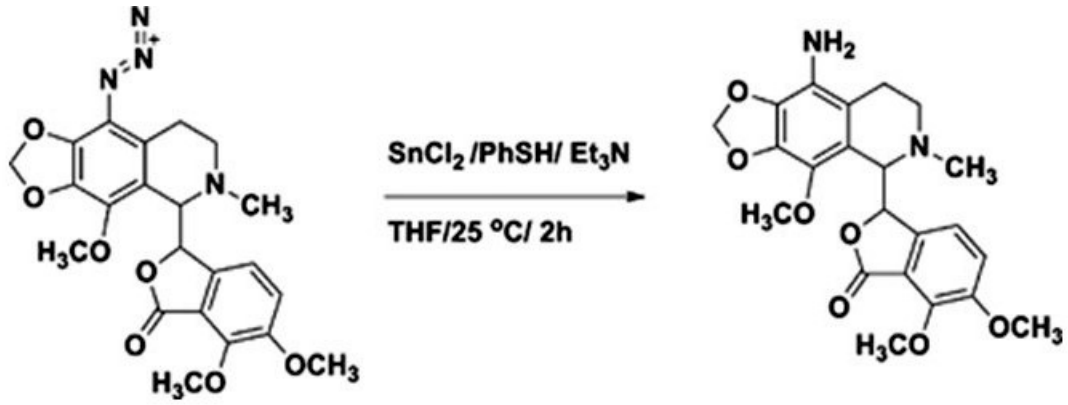

Figure 2.6. Amino noscapine: Amino noscapine (9-amino noscapine) possesses an amine group at the 9-position of the quinoline ring and is synthesized from azido noscapine (Aneja et al., 2006).

2.3.5. Biaryl type derivatives of noscapine

As per the earlier literature, natural α-noscapine has biaryl binding sites, which shows close similarity to colchicine. Colchicine's use as an anticancer agent is strictly limited because of its toxic side effects. Only a few natural products with biaryl architectural design are potent antimitotic agents that affect the tubulin-microtubule steady state (Figure 2.7).

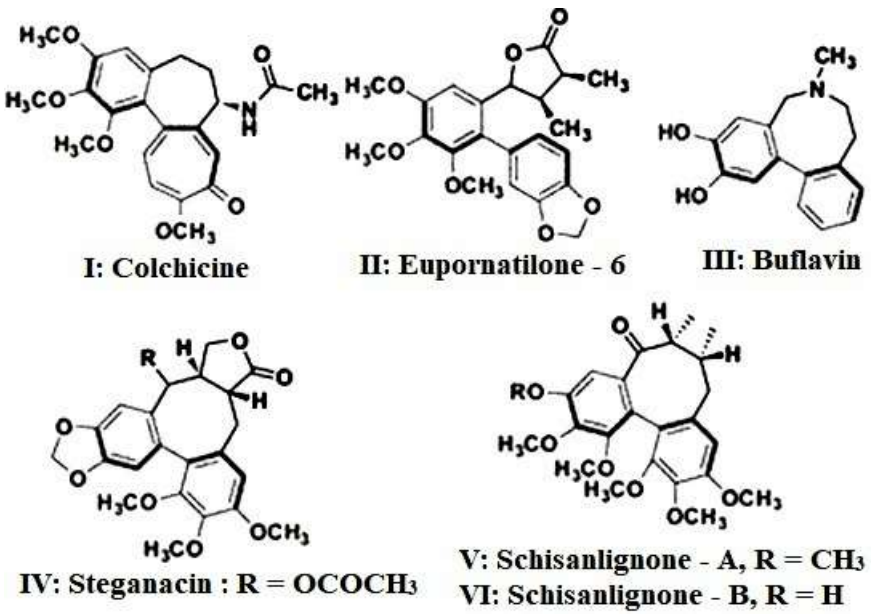

Figure 2.7. Biaryl pharmacophore is a major structural component of natural and synthetic derivatives that act as microtubule targeting agents.

Inspired by this, many novel biaryl type α -noscapine congeners were developed by implementing biaryl ring architecture into the natural α -noscapine skeleton and testing them as anticancer agents (Manchukonda et al., 2014). It was revealed that all of the newly designed biaryl noscapine analogs (figure 2.8) bind to tubulin with a higher affinity than that of the parent molecule and were found very promising for a variety of cancer types (Manchukonda et al., 2014).

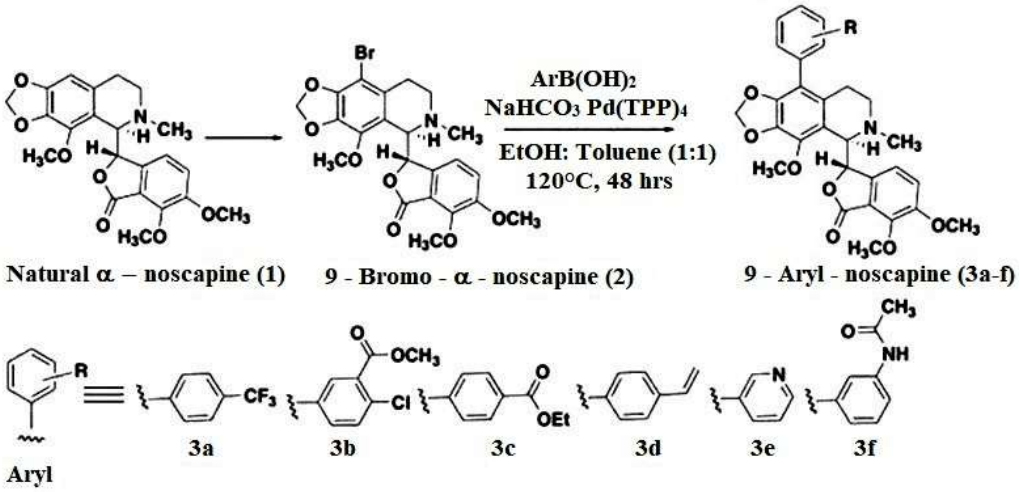

Figure 2.8. Biaryl derivatives of noscapine.

2.3.6. Benzofuranone ring substituted noscapinoids

The 2nd generation noscapine analogs (Figure 2.9) were developed by chemical alteration at diversity point 'C' of parent noscapine (Aneja et al., 2006; Mishra et al., 2011; Naik et al., 2012; Anderson et al., 2005). These analogs were also revealed better activity compared to noscapine. These derivatives inhibit the assembly of microtubules in a concentration-dependent manner and have shown effective in inhibiting the proliferation of lymphoma and cell lines of lung, breast, prostate, and pancreatic cancer.

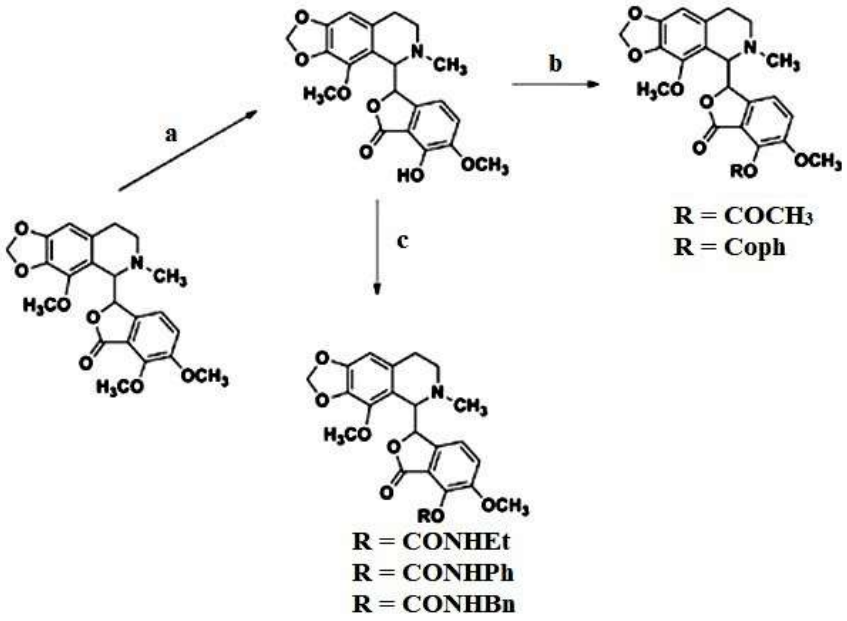

Figure 2.9. Benzofuranone derivatives of noscapine, the second generation of noscapinoids *a* depicts sodium azide/sodium iodide, dimethylformamide (DMF) at 140° C, 4h *b*, represents dimethylamino pyridine, acetic anhydride, acetonitrile at 50° C, 6h for compound 3 potassium carbonate, dimethylformamide and benzyl chloride at 80°C, for 8 h for compound 4. *c*, represents Dimethylamino pyridine, dichloromethane and isocyanate at room temperature for 6-8 h.

2.3.7. Targetin–folate conjugated noscapine

For the targeted delivery of noscapine specifically to aggressive tumor cells, noscapine was conjugated with a folate group at the C-9 position (Figure 2.10) (Naik et al.,

2012). The folate group is a natural ligand for cellular folate receptor alpha (FRα), which is over-expressed on some solid tumors such as ovarian epithelial cancers (Ross et al., 1994; Parker et al., 2005). Conjugation of noscapine with the folate group significantly improved the uptake of noscapine to cancer cells (Naik et al., 2012).

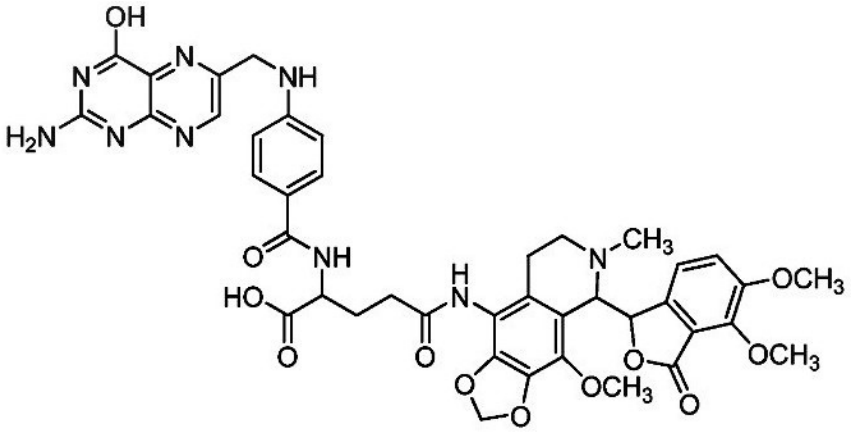

Figure 2.10. Molecular structure of Folate-noscapine (Targetin).

2.3.8. Third-generation noscapinoids

The third generation of noscapinoids were obtained by inducing structural modification at diversity point D of noscapine (Figure 2.11) based on the insights obtained from the previous generations of noscapinoids (Manchukonda et al., 2013). Similar to previously reported derivatives, third-generation noscapinoids have comparable or enhanced binding affinities. In addition, these congeners of noscapine were demonstrated strong cytotoxicity to a number of cancer cells of different tissue origins (Manchukonda et al., 2013). These compounds have delayed the progression of the cell cycle at the G2/M stage and induced apoptotic cell death in cancer cells. For this sequence of compounds, the apoptotic indices were substantially greater compared to noscapine.

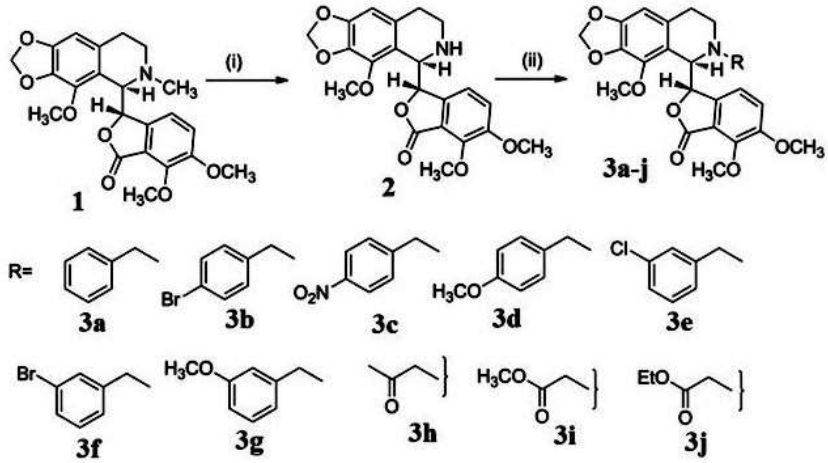

Figure 2.11. Chemical synthesis of third generation noscapinoids from noscapine as starting material. (i) *a*, meta-chloroperoxybenzoic acid and dichloromethane; *b*, 2N hydrochloric acid; *c*, Iron (II) Sulfate Heptahydrate; (ii) Bromo methane, potassium iodide, K_2Cr_3, and Acetone.

2.4. Molecular mechanism of action of noscapine

Noscapine binds to tubulin and alters tubulin conformation, suppresses the dynamics of microtubule assembly, blocks cell cycle progression at mitosis, and then cause apoptotic cell death in many cancer cells types (Ye et al., 1998; Landen et al., 2002; Zhou et al., 2002a; Zhou et al., 2002b; Zhou et al., 2003). From a pharmacological perspective, noscapinoids are arguably the most eminent microtubule drugs, effective against multidrug-resistant cancer cell lines (Zhou et al., 2003), affect cancer cells differently than the normal diving cells (Landen et al., 2002), have a better pharmacokinetic profile (Aneja et al., 2007) with no significant side effects (Aneja et al., 2007; Sharma et al., 2010). Since the discovery of the therapeutic properties of noscapine, new findings related to its activities and its mechanisms of action have been unveiled. Previously it was shown that noscapinoids binds to tubulin and alters microtubule dynamics *in vitro* and *in vivo* (Ye et al., 1998; Zhou et al., 2003). However, where noscapinoids bind specifically to tubulin is still not known. The best way to understand the site of interaction of ligand-receptor is to obtain the crystal structure and

this has not been successful so far. This is so far only possible for drugs that stabilize microtubules (Nogales 1998; Ravelli et al., 2004; Nettles, 2004).

Noscapine has a different mode of action for activation of apoptosis during cell cycle progression, one of them is the activation of cyclin-dependent kinase pcdc2. Noscapine induced apoptosis in murine cell carcinoma by activating p34cdc2. The role of p34cdc2 in the cell cycle has been studied by Ye et al., (1998) and found that prolonged activation of the kinase induces the cell to be mitotically arrested and it was also reported that the kinase has a major role in apoptosis induced by noscapine (Pucci et al., 2000). The JNK pathway also called the c-Jun-N-terminal kinase pathway, is a cassette of the MAPK signaling pathway (Yan et al., 2016). The pathway activates during the number of cellular responses one of them is stress-induced apoptosis. Activation of JNK during apoptosis by microtubule targeted drug has been reported in paclitaxel resistance cancer cell line.

Tumor cells are hypoxic in nature which expresses HIF-1α, a transcription factor activated by hypoxia. Studies reported that dimer of HIF-1α and HIF-β induces angiogenesis (Ziello et al., 2007). HIF-1α induces the expression of an angiogenetic promoter like vascular endothelial growth factor (VEGF). Suppression of HIF-1α and subsequent inactivation of VEGF by noscapine have also been reported (Zhang & Luo, 2018; Rida et al., 2015; Newcomb et al., 2006). Another angiogenetic promoter is NF-κB, further, it has been reported that the pathway involves chemoresistance to certain cancer cells and finds the noscapine induced inactivation of NF-κB signaling along with TNF, IKK, VEGF as well as MMP-9 (Pucci et al., 2000). The antagonistic effect of noscapine in fibrosis of human lungs fibroblast culture cells has been reported by (Kach et al., 2014). It has also been reported that treatment with noscapine increases in caspase level that leads to DNA fragmentation and apoptosis in various types of cancer cells

(Abotaleb et al., 2018; Liu et al., 2019) by altering the ratio of pre apoptotic (BAX) and apoptotic protein (BCL2).

2.5. Combination therapy of noscapine with currently use tubulin binding drugs

Combination therapy using microtubule-targeted drugs is an exciting source of chemotherapeutic wealth due to the presence of diverse drug binding sites on tubulin. It suggests that a rational combination of two or more drugs of this class might be able to enhance the anti-cancer efficacy and reduce toxic side effects, thereby improving the therapeutic index. The general rationale for employing combination therapy is twofold. Firstly, when multiple drugs with different molecular targets are applied, the cancer adaptation process such as cancer cell mutations can be delayed. Secondly, when multiple drugs target the same cellular pathway, they could function synergistically for higher therapeutic efficacy and higher target selectivity. The combination regimes used clinically are categorized based on their mechanisms of action that include: (1) the combination of non-specific small molecular chemotherapeutic agents and (2) the combination of target-specific biological and small molecular chemotherapeutic agents (Masui et al., 2013). Taxanes are another class of chemotherapeutic agents, extracted initially from natural sources and then synthetically derivatized, like paclitaxel (Taxol), Docetaxel, and Taxotere (Nabholtz et al., 2000; Ojima, et al., 2016).

Taxanes have a mechanism of action to interrupt the role of microtubules. For cell division, microtubules are necessary and taxanes stabilize the microtubule, thus inhibiting the process of division of cells (Stanton et al., 2011). Taxanes experience difficulty in pharmaceutical formulation due to their low water solubility and this also results in reduced bioavailability. In addition, their clinical utility is limited due to the development of

associated severe side effects. In contrast, noscapine is a safer orally active antimicrotubule agent that showed *in vitro* and *in vivo* antitumor activity against a variety of cancers including tumors resistant to conventional antimicrotubular agents without any significant side effects (Ye et al., 1998; Laden et al., 2002; Zhou et al., 2003).

Previously, noscapine has been used in combination with platinum analogs for the evaluation of anticancer activity (Chougule et al., 2011). Also, it was demonstrated, the use of noscapine in augmenting cisplatin's antitumor activity *in vitro* and *in vivo*, against lung cancer (Chougule et al., 2011). Similarly, noscapine was used in combination with doxorubicin for the management of triple-negative breast cancer and with fewer adverse side effects as compared to the conventional chemotherapeutics regimens based on *in vitro* and *in vivo* study (Chougule et al., 2011).

Drugs that target microtubules, such as taxols, are important chemotherapeutic drugs in the clinical management of breast cancer. However, these drugs are plagued with serious toxicity. Besides, patients have developed resistance against taxols, suggesting a need for anti-microtubule agents that have no severe side effects. It is becoming well-appreciated that a toxic drug at its maximum tolerated dose given intermittently is not necessarily better and there exists an opportunity to reduce its dose levels by using combinatorial regimens of drugs that have either different targets or different binding sites onto the same target. Thus, in this study, we are approaching breast cancer therapy by developing a promising analog of noscapine that is non-toxic to normal tissues and by optimizing its synergistic combination with docetaxel for better therapeutic outcomes.

CHAPTER 3

MATERIALS AND METHODS

"This chapter deliberates the synthesis of the promising derivatives of noscapine, their characterization, and optimizing its synergistic combination with docetaxel. The experimental techniques used in the study involved in silico approach, in vitro biochemical and cellular analysis as well as in vivo animal models for the analysis of the anticancer activity of noscapinoids alone and in combination regimen with docetaxel"

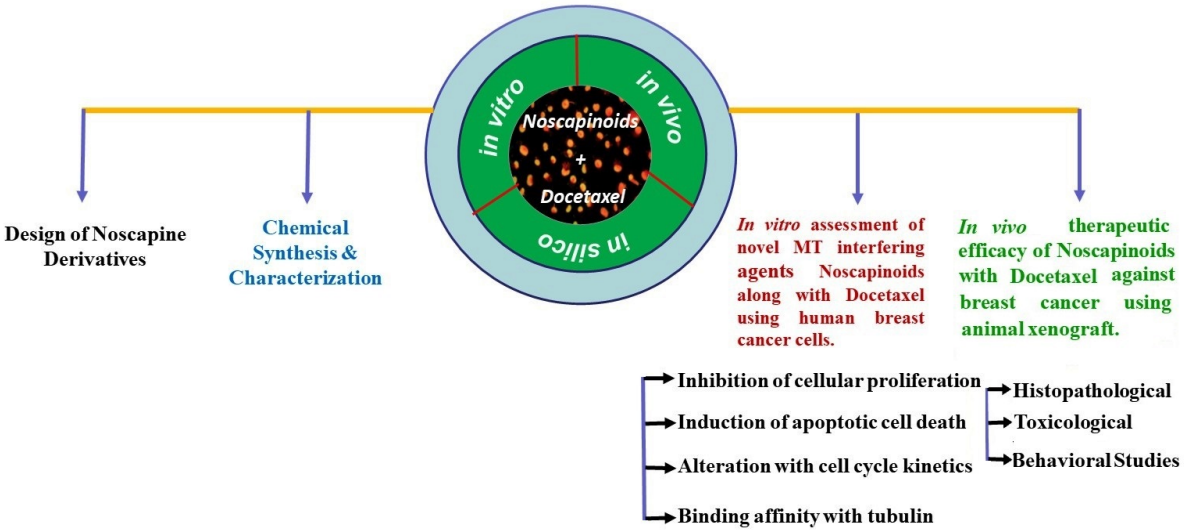

3.1. Design of noscapine derivatives

Several derivatives of noscapine have been developed previously, which are at a different level of preclinical and clinical trials. The availability of several derivatives along with their experimental activity can be utilized to develop several new derivatives through structure-activity relationship study. We approach to chemically synthesized a panel of novel derivatives of noscapine by derivatization at different site points of the noscapine followed by experimental evaluation in single as well as in combination regimen with docetaxel.

3.2. Protein preparation

The co-crystal structure of the tubulin with derivative of noscapine (amino-noscapine), PDB ID: 6Y6D (resolution 2.20 Å) (Oliva et al., 2020) was used for molecular docking and rescoring. A complex consisting of both 'α' and 'β' chains of the protein was acquired after a manual inspection and cleaning of the structure. The errors in the PDB files were removed as per the procedure reported earlier (Santoshi and Naik, 2014). The hydrogen atoms were added and the protein structure was prepared using protein preparation wizard (Schrodinger software package). All water molecules have been removed from the complex. The multi-step Schrödinger Protein Preparation tool (PPrep) was used for final protein preparation. PPrep neutralizes side chains that are not close to the binding cavity and do not participate in salt bridges. This step is then followed by constrained minimization of co-crystallized complex, which redirects side chain hydroxyl groups and mitigates potential steric clashes. Exponentially weaker restraints (tethering force constants 3, 1, 0.3, 0.1) were applied to non-hydrogen atoms only. The complex obtained was energy minimized using OPLS 2005 force field with Polack-Ribiere Conjugate Gradient (PRCG) algorithm (Polak and Ribiere, 1969). The minimization was

stopped either after 5,000 steps of minimizations or after the energy gradient converged below 0.001 kcal/mol.

3.2.1. Ligand preparation

The molecular structures of noscapine derivatives such as Br-noscapine (Br-Nos), Amino-noscapine (Amino-Nos), Br-trimethoxy benzyl-noscapine (Br-TMB-Nos), N-3-Br-Benzyl-noscapine (Br-Bn-Nos), 9-vinyl phenyl-Noscapine (VPN-Nos) and 9-Pyridyl-3-boronic acid noscapine (PYBA-Nos) were built using the builder feature in Maestro (Schrodinger software package). All these structures were energy minimized using macromodel (Schrodinger software package) with OPLS 2005 force field. Polak-Ribiere Conjugate Gradient (PRCG) algorithm. Complete geometric optimization of these structures was performed using Jaguar (Schrodinger software package). Hybrid density functional theory with Becke's three-parameter exchange potential and the Lee-Yang-Parr correlation functional (B3LYP) (Lee et al., 1988; Becke, 1993) and 3-21G* basis set (Binkley et al., 1980; Gordon et al., 1982; Pietro et al., 1982) were used for geometric optimization. Using ligprep (Schrodinger software package), each structure was assigned an appropriate bond order. A number of structures with different ionization states, tatomers, stereochemistry and ring conformations were generated by ligprep utility from each input structure. This program automatically generated all possible stereoisomers (default value of 32 was used) for each ligand. In addition, with the support of ligprep, a unique low-energy ring conformation for each stereoisomer with correct chirality was generated. These geometrically optimized structures of noscapine derivatives were used for Glide (grid-based ligand docking with energetics) docking.

3.2.2. Molecular docking

Molecular docking of noscapine derivatives and docetaxel with their respective binding sites was performed using the ‘‘Extra Precision’’ (XP) mode of Glide docking (Friesner et al., 2004; Halgren et al., 2004) (version 4.5, Schrodinger Inc.). The detailed algorithm of Glide docking has been reported earlier (Friesner et al., 2004; Halgren et al., 2004). Briefly, Glide approximates a systematic search of positions, orientations, and conformations of the ligand in the receptor binding site using a series of hierarchical filters. The shape and properties of the receptor are represented on a grid by several different sets of fields that provide progressively more accurate scoring of the ligand pose. Two concentric cubes were specified at the binding site: the bounding box, which must include the center of mass of any appropriate ligand pose, and the enclosing box, which must encompass all the atoms of the ligand pose in order to effectively dock into the binding site. During the docking process, Glide also conducted conformational searches for each input structure. A set of initial ligand conformations were generated through an exhaustive search of the torsional minima and the conformers are clustered in a combinatorial fashion. Each cluster characterized by a common conformation of the core and an exhaustive set of side chain conformations is docked as a single object in the first stage. The search begins with a rough positioning and scoring phase that significantly narrows the search space and reduces the number of poses to be further considered to a few hundred. These selected poses are energy minimized on precomputed OPLS-2005 van der Waals and electrostatic grids for the receptor. In the final stage, the 5–10 lowest-energy poses obtained in this fashion are subjected to a Monte Carlo sampling in which nearby torsional minima are examined and the orientation of peripheral groups of the ligand is refined. The minimized poses are then rescored using the GlideScore. In this work, an inner grid box of 12Å x 12Å x 12Å was defined to confine the mass center of the

docked ligand. Besides, an enclosing grid box of size ≤ 24Å in comparison to the co-complex ligand, amino noscapine in the crystal structure was defined which occupied all the atoms of the docked poses. The scale factor of 0.4 for van der Waals radii was applied to atoms of protein with absolute partial charges less than or equal to 0.25. The algorithm generated 10000 poses, out of which only 1000 poses were used for the minimization (conjugate gradients), and the final refined structures having the lowest energy conformations were evaluated for the favourable Glide docking score. Energy minimization protocol included a dielectric constant of 4.0 and 1000 steps of conjugate gradient minimizations. Upon completion of each docking calculation, 100 poses per ligand were generated and the best docked structure was chosen using a Glide Score (Gscore) function. Glide Score is a more advanced variant of ChemScore (Eldridge et al., 1997) with components focused on force fields and additional terminology that account for solvation and repulsive interactions. Using a model energy score (Emodel), which combines the energy grid score, Gscore and the ligand's internal strain, the selection of the best pose is made. Owing to its high accuracy, Glide docking is extensively used by pharmaceutical industries and research institutions to analyze drug-target interactions and to design potential drug candidates with enhanced activities (Perola et al., 2004; Zhou et al., 2007; Cross et al., 2009; Li et al., 2010). A single best conformation for noscapinoids and docetaxel was considered based on minimum docking score for MD simulation (Snyder et al., 2001).

3.2.3. Molecular dynamic simulations

Co-complex of tubulin with both noscapinoids and docetaxel (Tubulin+Noscapinoids+Docetaxel) were obtained from co-docking of docetaxel (DOX) and noscapinoids onto tubulin heterodimer (complex_1). GTP, GDP and magnesium ions

were retained in the complex. Similarly, co-complex of tubulin-noscapinoids (complex_2) and tubulin_DOX (Complex_3) were obtained by removing atoms of DOX and noscapinoids from complex_1, respectively. Complex 4 with tubulin only, without DOX and noscapinoids, was also obtained. All simulations were performed using Amber 16 simulation suite (Case et al., 2016; Wang et al., 2006). The parameters for all ligands such as DOX, Br-Bn-Nos, VPN-Nos, PYBA-Nos, Br-Nos, Amino-Nos, Br-TMB-Nos, GTP and GDP were estimated using Antechamber program of Amber 16 suite (Wang et al., 2006). All atomic point charges were calculated using AM1-BCC charge model (Jakalian et al., 2002). Topologies and internal coordinates for all the complexes were generated using tleap program in Amber16. Missing Hydrogens were added and parameters were assigned to Protein and ligands using FF14SB and GAFF force-fields, respectively (Maier et al., 2015). Each molecular system was neutralized by adding counterions and was subsequently solvated using TIP3P water model in a truncated octahedron with the distance of 12 Å between the atoms of protein and wall of the box (Jorgensen et al., 1983). Once the topologies and internal co-ordinates for all complexes were obtained, three rounds of minimization were performed on each complex to relax the system and amend the bad contacts. Position restraints of 10 kcal/Å^2 and 2 kcal/Å^2 were imposed on the protein system for the first and the second rounds respectively, to relax the water molecules around protein. No restraints were imposed in the third round. After removal of bad contacts through minimization, all four molecular systems were equilibrated at 300 K and 1 atm for 500 ps. The equilibrated systems were then run for 100 ns each with time step of 2 fm. The cut-off for non-bonded interaction was 10 Å, electrostatics was calculated using Particle Mesh Ewald (PME) and bonds were constrained using shake algorithm (Ryckaert et al., 1977; Darden et al., 1993; Essmann et al., 1995). Langevin thermostat was used to regulate the temperature of simulations. Co-ordinates were written

every 20 ps to write 5000 frames for each molecular system. CPPTAJ implemented in Ambertools was used to analyze trajectories for Root Mean square deviation analyses (PTRAJ and CPPTRAJ, 2013).

3.3. Chemical synthesis of noscapine derivatives

All the derivatives of noscapine were chemically synthesized from the parent molecule, noscapine as the starting material. It is a very challenging, tedious and time-consuming task to synthesize the derivatives of noscapine, due to its highly responsive C-C bond between isoquinoline and isobenzofuranone ring components which is labile to strong acids and base. However, with the amalgamation of proper solvents and taking parent noscapine as a starting material we have optimized the reaction conditions without affecting the sensitive C-C bond. All the reactions were regulated by thin-layer chromatography (precoated silica plates and visualization under UV light). All the intermediates and final products were structurally characterized by ^{1}H and ^{13}C NMR spectra in $CDCl_3$ on AVANCE-300MHz, 400 MHz, and 500 MHz spectrometer. The high-resolution spectra were recorded with an ESI source (IICT, Hyderabad) on QSTAR XL hybrid MS/MS system (Applied Bio systems/MDS sciex, foster City, USA). The final products are mentioned in the respective schemes.

All reactions were executed with magnetic stirring in oven-dried flasks. Analytical thin layer chromatography (TLC) conducted on silica gel GF254 pre-coated plates tracked all the experiments. The plates were visualized under UV illumination at 254 nm for UV active materials after elution. Further visualization was accomplished with staining with PMA and charring on a hot plate. Solvents were extracted in a vacuum and heated at 35 °C in a water bath. For column chromatography, silica gel thinner than 200 mesh was used. Columns were prepared in hexane as a silica gel slurry and prior to calibrated with the

suitable solvent/solvent mixture. Using the suitable solvent method, the compounds were loaded conveniently or as a concentrated solution. The elution was supported by applying pressure with an air pump. Unless stated otherwise, yields apply to chromatographically and spectroscopically homogeneous materials. With the aid of ChemBioOffice 2017, appropriate names for all the new compounds were given. Samples were determined with a melting point apparatus from Fischer-Johns and are uncorrected. Analytical HPLC (SPD-M20A, make: Shimadzu) was used to assess the purity of all compounds (>96%) used for biological screening using an eluted ODS column with a gradient acetonitrile-water mixture. As neat liquids or KBr pellets, IR spectra have been documented and absorption in cm^{-1} is confirmed. NMR spectra were measured in suitable solvents on 300 (Bruker) and 500 MHz (Varian) spectrometers using TMS as an internal standard or solvent signals as secondary standards and chemical shifts on δ scales have been seen. Multiplicities of NMR signals are designated as s (singlet), d (doublet), t (triplet), q (quartet), br (broad), m (multiplet, for unresolved lines), etc. On a 75 MHz spectrometer, ^{13}C NMR spectra were obtained. Using ESI-QTOF mass spectrometry, high-resolution mass spectrums have been obtained. With a Roudolph Digipol 781 polarimeter at 25 ^{o}C, optical rotations were analysed. Without further purification, the commercially available solvents hexane, CH_2Cl_2, and EtOAc were used as such. Natural α-noscapine and Docetaxel used in this study have been purchased and are used as such from Sigma-Aldrich. The reaction schemes for the synthesis of noscapine derivatives are mentioned below.

Chemical synthesis of 9-Bromo-Noscapine:

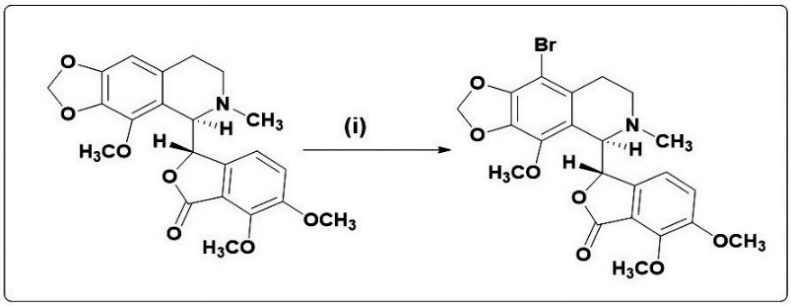

Reaction Scheme 1. Synthesis of 9-Bromo-Noscapine: Reaction Conditions. (i) 48% HBr, bromine water, room temperature, 2h, 90% yield.

(S)-3-((R)-9-bromo-4-methoxy-6-methyl-5,6,7,8-tetrahydro-[1,3]dioxolo[4,5-g]isoquinolin-5-yl) -6,7-dimethoxyisobenzofuran-1(3H)-one: To a suspension of natural α- noscapine (4.0 g, 9.7 mmol) in 48% aqueous HBr solution (15 mL) was added with continuous stirring freshly prepared saturated bromine water (~50 mL) drop wise at room temperature until the orange precipitate appeared (~1.0 h). The reaction mixture was stirred further at RT for 30 min to attain completion, the reaction mixture was adjusted to pH 10 by the addition of 25% aqueous ammonia solution, extracted with chloroform (3 x 25 mL), dried with anhydrous Na_2SO_4, evaporated under reduced pressure. The crude residue was subjected to silica gel column chromatography eluted with 3:7 Ethyl acetate: Hexane (3:7) gave pure 9-bromo-noscapine (4.3g, 90%) as white solid. mp 170ºC; $[\alpha]_D^{25}$= -106.8 (c=1, Dichloromethane); ^{1}H NMR (300 MHz, $CDCl_3$): δ 6.96 (d, J= 8.30 Hz, 1H), 6.26 (d, J= 8.30 Hz, 1H), 6.02 (s, 2H), 5.39 (d, J= 4.72 Hz, 1H), 4.27 (d, J= 4.72 Hz, 1H), 4.07 (s, 3H), 3.99 (s, 3H), 3.87 (s, 3H), 2.83-2.74 (m, 1H), 2.67-2.57 (m, 1H), 2.51 (s, 3H), 2.49-2.42 (m, 1H), 2.02-1.91 (m, 1H). ^{13}C NMR (75 MHz, $CDCl_3$): δ 167.9, 152.2, 147.6, 146.4, 141.1, 139.9, 134.1, 130.2, 119.5, 118.9, 118.2, 117.4, 101.0, 95.5, 81.2, 62.2, 60.8, 59.3, 56.7, 48.3, 45.1, 25.8. MS (ESI) m/z 492 $[M+H]^+$; HR-MS (ESI) Calcd for $C_{22}H_{22}NO_7Br$ $[M+H]^+$:492.0657, found: 492.0636. The ^{1}H-NMR, ^{13}C-NMR and mass

spectra (ESI and HR-MS) of the final product, Br-Nos are included as supporting material in the appendix.

Chemical synthesis of 9-Vinyl Phenyl-Noscapine:

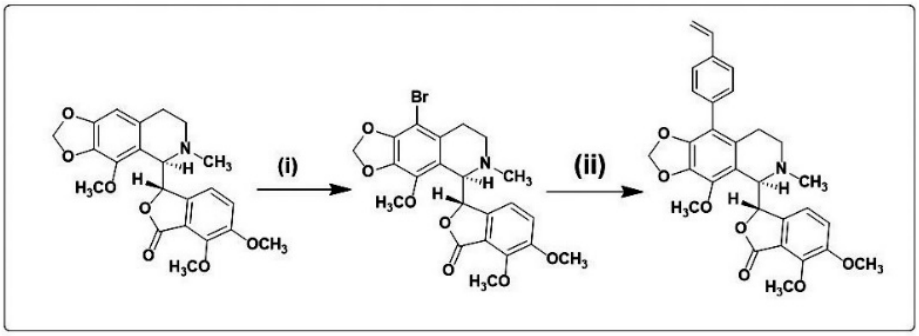

Reaction Scheme 2. Reaction Conditions. (i) 48% HBr, Bromine-water, room temperature, 2h, (ii) 4-Vinyl boronic acid, Pd (TPP)$_4$, $NaHCO_3$, EtOH/Toluene, 120^{o}C, 48 h, 62% yield

(S) - 6,7-Dimethoxy-3- (R) - 4 - methoxy-6-methyl – 9 - (4-vinylphenyl) - 5,6,7,8 - tetrahydro-[1,3] dioxolo [4,5-g] isoquinolin-5-yl) isobenzofuran-1(3H) - zone (9-VP-Nos): To a solution of 9-bromonoscapine (2.0 g, 4.1 mmol) in ethanol/toluene (1:1, v/v, 100 mL), $Pd(PPh_3)_4$ (0.59g, 0.49 mmol), $NaHCO_3$ (8.2 mmol) and 4-vinylphenyl boronic acid (1.25 g, 8.2 mmol) were added sequentially, and the contents were stirred for 48 h at 120 ^{o} C. After the starting material was completely consumed in the reaction (judged by TLC), reaction mixture was cooled to room temperature, the solvents were evaporated under vacuum. The crude residue was extracted into dichloromethane (3 x 25 mL) and washed with brine solution. The organic layer was collected and passed through a Na_2SO_4 bed and later removed under reduced pressure. The crude residue was chromatographed over a triethylamine silica gel bed, using pet. ether/ethyl acetate (7:3) as eluents, to give pure compound as colourless solid. (1.32g) Yield: 62%; m.p: 120-122 ^{o}C; $[\alpha]_D^{25}$ 120.22 (c = 1, dichloromethane); ^{1}H NMR (300 MHz, $CDCl_3$): δ 7.40 (d, J = 8.24 Hz, 2H), 7.17 (d, J = 8.24 Hz, 2H), 6.97 (d, J = 8.16 Hz, 1H), 6.74-6.66 (dd, J = 10.81 Hz,

17.51 Hz, 1H) 6.10 (s, 1H), 5.98 (s, 1H), 5.91 (s, 1H), 5.74 (d, J = 17.51 Hz, 1H), 5.48 (s, 1H), 5.25 (d, J = 10.81 Hz, 1H), 4.47 (s, 1H), 4.10 (s, 6H), 3.90 (s, 3H), 2.66-2.54 (m, 4H), 2.27-2.13 (m, 2H), 1.77-1.64 (m, 1H). ^{13}C NMR (75 MHz, $CDCl_3$): δ 157.9, 152.2, 147.7, 146.0, 143.6, 140.9, 139.6, 136.7, 133.7, 133.5, 130.7, 130.1, 126.0, 120.4, 117.8, 116.1, 114.2, 100.8, 81.9, 62.3, 61.1, 59.5, 56.9, 50.8, 46.6, 27.0, 23.2, 29.6. MS (ESI): m/z 538 $[M+Na]^+$; HRMS (ESI): Calcd for $C_{30}H_{29}NO_7$ $[M+Na]^+$; 538.1841; found: 538.1848. The ^{1}H-NMR, ^{13}C-NMR and mass spectra (ESI and HR-MS) of the final product, VPN-Nos are included as supporting material in the appendix.

Chemical synthesis of 9-Amino-Noscapine:

The amino-noscapine was synthesized from the lead molecule, noscapine as per the method described earlier (Naik et al., 2011; Joshi et al., 2014). First of all, bromo-noscapine was synthesized from the noscapine by adding hydrobromic acid (~40 mL) and bromine water (~250 mL). The bromo-noscapine was converted to azido-noscapine in presence of sodium azide (40.63 mmol) and sodium iodide (4.063 mmol). Finally, amino-noscapine was synthesized from azido-noscapine by adding a solution of $SnCl_2$ in THF (10 mL), thiophenol and triphenylamine. The detailed of the synthetic scheme was mentioned below. The amino-noscapine was structurally elucidated based on ^{1}H NMR (300 MHz), ^{13}C NMR (75 MHz), HRMS, etc. and are included as supporting information in the appendix.

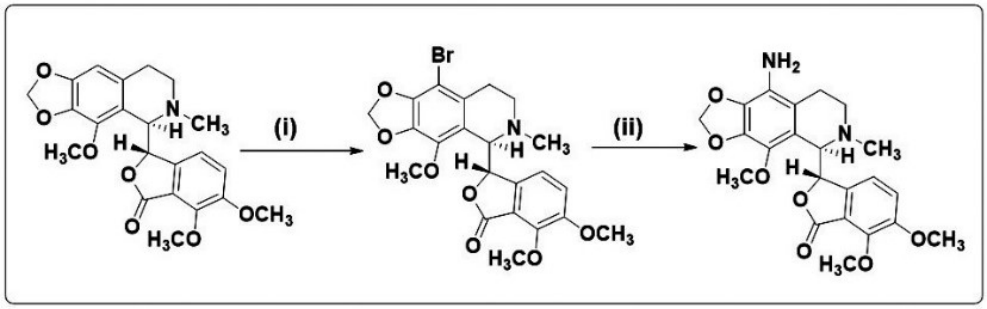

Reaction Scheme 3. Synthesis of 9-amino-noscapine. (i) HBr/Bromine water at 25 °C/1h, (ii) NaN_3/NaI in DMF at 80 °C/15h, (iii) $SnCl_2$/PhSH/Et_3N in THF at 25 °C/2h.

^{1}H NMR (300 MHz, $CDCl_3$) δ 6.93 (d, J= 8.3 Hz, 1H), 6.10 (d, J=8.3 Hz, 1H), 5.93 (s, 2H), 5.53 (d, J=3.77Hz, 1H), 4.34 (d, J=3.77, 1H), 4.07 (s, 3H), 3.90 (s, 3H), 3.85 (s, 3H), 3.25 (s, 2H), 2.70-2.59 (m, 1H), 2.53 (s, 3H), 2.47-2.20(m, 2H), 1.80-1.59 (m, 1H). ^{13}C NMR (75 MHz, $CDCl_3$) δ 168.07, 152.10, 147.69, 141.29, 135.34, 134.86, 133.80, 121.88, 119.88, 118.26, 117.94, 117.69, 117.19, 100.89, 81.70, 62.23, 60.79, 59.62, 56.77, 48.36, 45.53, 21.00. IR (KBr) 3437, 3362, 2924, 2853, 1750, 1652, 1615, 1494, 1459, 1388, 1265, 1159, 1115, 1036, 801, 711, 656, 514, 405. MS (ESI) m/z 429 $[M+H]^+$; HR-MS (ESI) Calcd for $C_{22}H_{24}N_2O_7$ $[M+H]^+$:429.1661, found:429.1673.

Chemical synthesis of N-3-Br- Benzyl Noscapine:

The starting solution of (S)-6,7-dimethoxy-3-((R)-4-methoxy-5,6,7,8 tetrahydro [1,3] dioxolo [4,5-g] isoquinolin-5yl) isobenzofuran-1(3H)-one (200 mg, 0.50 mmol) in acetone (5 mL), was added to potassium carbonate (1.10 mmol), potassium iodide (0.5 mmol) and 3-Bromo benzyl bromide (0.55 mmol) and stirred at room temperature (RT) for 1 h. The crude reaction mixture was filtered and evaporated under vacuum, water (5 mL) and dichloromethane (2 X 10 mL) was added, organic layer was dried over Na_2SO_4 and concentrated under reduced pressure. The crude residue was purified by the silica gel column chromatography with hexane/ethyl acetate (70:30) to yield as solid product. The detailed synthetic scheme is mentioned below. The ^{1}H NMR spectra, ^{13}C NMR spectra and the ESI mass spectral data of the final product Br-Bn-Nos are included as the supporting material in the appendix.

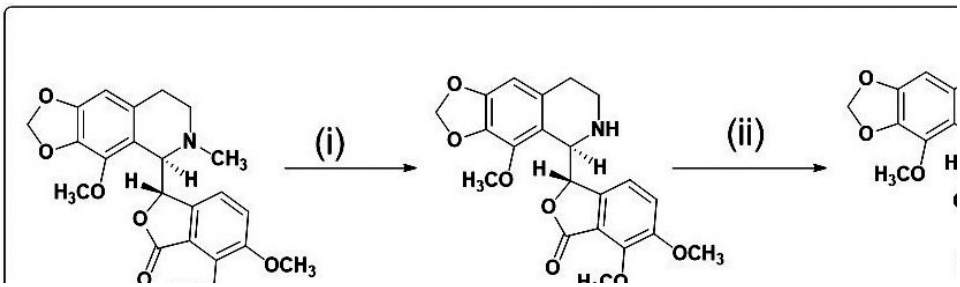

Reaction Scheme 4. Reaction Conditions.: (i) a: m-CPBA, DCM; b: 2N HCl; C: $FeSO_4.7H_2O$; (ii) 3-Bromo benzyl bromide, KI, K_2CO_3, Acetone, RT, 97% yield.

(S)-3-((R)-6-(3-bromobenzyl)-4-methoxy-5,6,7,8tetrahydro-[1,3]dioxolo[4,5-g]isoquino lin-5-yl)-6,7dimethoxyisobenzofuran-1(3H)-one : Yield: 97%; mp 65 °C; [α]D25 = 52.0 (c = 1, Dichloromethane); IR νmax (cm^{-1}): 3503, 2940, 2837, 1759, 1621, 1498, 1387, 1271, 1212, 1039, 891, 785, 695. ^{1}HNMR: (300 MHz, $CDCl_3$): δ 7.40-7.30 (m, 2H), 7.24-7.09 (m, 2H), 6.99 (d, J= 8.30 Hz, 1H), 6.34 (s, 1H), 6.15 (d, J= 8.30 Hz, 1H), 5.95 (s, 2H), 5.66 (d, J= 3.96 Hz, 1H), 4.60 (d, J= 3.96 Hz, 1H), 4.17-4.06 (m, 4H), 4.04 (s, 3H) 3.87, (s, 3H), 3.63 (d, J= 13.78 Hz, 1H), 2.50-2.37 (m, 2H), 2.32-2.19 (m, 1H), 2.07-1.92 (m, 1H). ^{13}CNMR (75 MHz, $CDCl_3$): δ 168.1, 152.2, 148.5, 147.9, 141.5, 140.4, 134.0, 131.8, 131.4, 130.0, 129.7, 127.3, 122.2, 118.1, 117.7, 116.6, 102.4, 100.7, 81.6, 81.1, 62.5, 61.1, 59.5, 59.3, 56.7, 45.4, 26.8. MS (ESI) m/z 568 $[M+H]^+$. HRMS (ESI) Calcd for $C_{28}H_{26}BrNO_7$ $[M+H]^+$: 568.41, found: 568.41.

Chemical synthesis of Bromo-Trimethoxy Benzyl-Noscapine:

To a solution of Br-OH-Nos (2.4 g, 5 mM) in toluene (10 mL) and N-methyl pyrrolidone (NMP, 10 mL), was sequentially added sodium hydride 60% in mineral oil (0.24 g, 6.0 mM), 3,4,5-trimethoxybenzyl bromide (2.60 g, 10 mM) and a catalytic amount of tetrabutylammonium iodide (100 mg) at room temperature. The reaction mixture was heated at 70 ˚C for 2 h, cooled to room temperature, and concentrated under vacuum. The crude residue was treated with water (20 mL), extracted with diethyl ether (3 x 20 mL),

the organic solvent was washed with brine, dried over anhydrous sodium sulfate, filtered and rotary evaporated under vacuum. The residue thus obtained was purified over silica gel column chromatography eluted with hexane: ethyl acetate (1:5) to give pure Br-TMB-Nos (2.7 g, 82%) as pale-yellow solid. The structural characterization of Br-TMB-Nos was carried out based on Infrared spectroscopy (IR), Nuclear magnetic resonance (NMR) spectra (1H-NMR at 300 and 500 MHz, 14C-NMR at 75 MHz), high-resolution mass spectra (HRMS) by using ESI-QTOF mass spectrometry. The melting point of the compound was measured with a Fischer-Johns melting point apparatus and was uncorrected. The compound was HPLC purified to 96% (SPD-M20A, make: Shimadzu) using the ODS column eluted with a gradient mixture of acetonitrile-water.

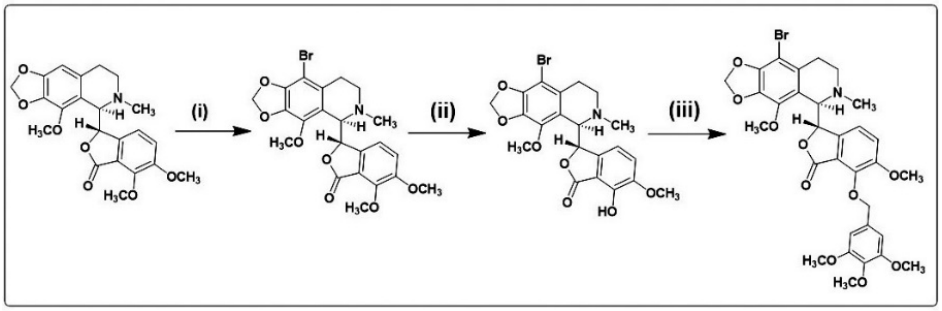

Reaction Scheme 5. Reaction Conditions: (i) Br_2-H_2O in 48% Aqueous HBr, 2 h, RT, 90% (ii) NaN_3/NaI, DMF, 4 h, 135–140 ºC, 75% (iii) 3,4,5 Trimethoxybenzyl bromide/NaH/ TBAI, Toluene: NMP (1:1), 70 ºC, 2 h, 82% yield.

(S)-3-((R)-9-bromo-4-methoxy-6-methyl-5,6,7,8tetrahydro-[1,3]dioxolo[4,5-g] isoquinolin-5-yl)-6-methoxy-7((3,4,5-trimethoxybenzyl)oxy)isobenzofuran-1(3H)-one: Mp 76 °C; [α] D25 = -63.7 (c=1, $CHCl_3$). IR, (KBr): 2941, 2839, 1760, 1593, 1499, 1445, 1373, 1124, 1035, 1008, 936, 820, 727, 633, 580, 525, cm 1. ^{1}H NMR (500MHz, $CDCl_3$): δ 7.01 (d, J=8.24 Hz, 1H), 6.89 (d, J= 6.86 Hz, 1H), 6.87 (s, 2H), 6.24 (d, J= 8.08 Hz, 1H), 6.03 (d, J= 1.3 Hz, 1H), 6.01 (d, J= 1.3 Hz, 1H), 5.52 (d, J= 4.27 Hz, 1H), 5.32 (q, J= 11.29 Hz, 2H), 4.34 (d, J= 4.27 Hz, 1H), 3.90 (s, 3H), 3.89 (s, 3H), 3.87 (s, 6H), 3.82 (s,

3H), 2.61-2.51 (m, 2H), 2.49 (s 3H), 2.42-2.34 (m, 1H), 1.90-1.81 (m, 1H). ^{13}C NMR (125MHz, $CDCl_3$): δ 168.1, 152.9, 152.5, 146.4, 145.8, 141.0, 139.7, 137.4, 134.0, 132.6, 130.2, 120.1, 118.6, 118.2, 117.6, 105.2, 101.0, 95.5, 81.0, 75.6, 60.7, 60.6, 59.2, 56.7, 56.0, 48.0, 44.9, 25.6. MS (ESI) m/z: 659 $[M+H]^+$. HRMS (ESI) Calcd for $C_{31}H_{33}BrNO_{10}$ $[M+H]^+$: 659.21364, found: 659.21084. The ^{1}H-NMR, ^{13}C-NMR and mass spectra (ESI and HR-MS) of the final product, Br-TMB-Nos are included as supporting material in the appendix.

Chemical synthesis of 9-3-Pyridyl-Noscapine:

We have chemically synthesized the PYBA-Nos, by coupling of 3-Pyridyl boronic acid functionality at the C-9 position of noscapine scaffold. At the starting point of our synthetic strategy, 9-bromonoscapine (200 mg, 0.41 μmol) (1) was developed from the natural α-noscapine, using bromine water (48% aq. HBr) by modifying the reaction conditions. To a solution of 9-bromo noscapine **(2)** was added ethyl acrylate, Pd(PPh3)4 (0.049 μmol), sodium bicarbonate (0.82 μmol) and 3-pyridyl boronic acid (0.82 μmol), under nitrogen. The reaction mixture was heated at 120 ^{0}C for 48 h; post completion, the reaction was brought to room temperature under reduced pressure, water (10 mL) was added, extracted with dichloromethane (3X25 mL), and combined organic portions were washed with water, dried over anhydrous sodium sulphate and concentrated. The crude residue was column chromatographed over silica gel, using 25% ethyl acetate in hexanes to give pure colourless solid compounds.

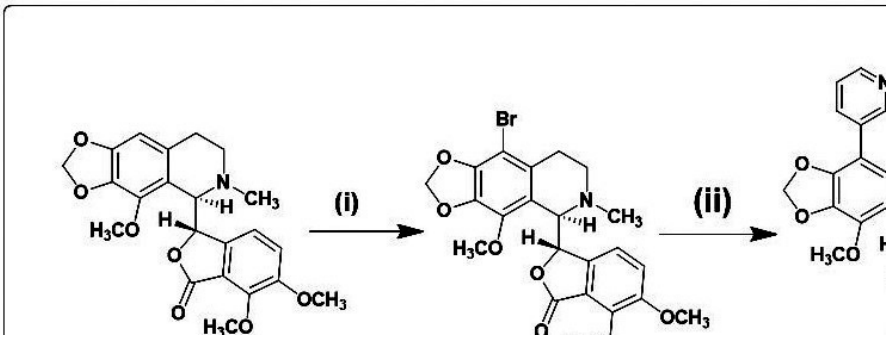

Reaction Scheme 6: Synthesis of 9-3-Pyridyl noscapine: Reaction Conditions. (i) 48% HBr, Bromine water, room temperature, 2h, 90% (ii) 3-Pyridyl boronic acid, $Pd(TPP)_4$, $NaHCO_3$, EtOH/Toluene,120^oC, 48 h, 62%.

(S)-6,7-Dimethoxy-3-((R)-4-methoxy-6-methyl-9-(pyridin-3-yl)-5,6,7,8-tetrahydro[1,3]dioxolo[4,5-g]isoquinolin-5-yl)isobenzofuran-1(3H)-one: Yield: 62%; mp: 193 ^0C; [α]D 25 124.25 (c = 1, dichloro methane); ^1H NMR (500 MHz, $CDCl_3$): δ 8.52 (s, 1H), 8.43 (s, 1H) 7.56 (d, J= 7.64 Hz, 1H), 7.30 (t, J= 6.65 Hz, 1H), 6.98 (d, J= 8.54 Hz, 1H), 6.12 (d, J= 7.61 Hz, 1H), 5.99 (s, 1H), 5.92 (s, 1H), 5.43 (d, J= 4.74 Hz, 1H), 4.43 (d, J= 4.74 Hz, 1H), 4.11 (s, 3H), 4.08 (s, 3H), 3.88 (s, 3H), 2.67–2.60 (m, 1H), 2.55 (s, 3H), 2.22–2.14 (m, 2H), 1.79–1.69 (m, 1H). ^{13}C NMR (75 MHz, $CDCl_3$): δ 167.9, 152.3, 150.7, 148.36, 147.6, 146.4, 140.7, 140.2, 137.3, 133.7, 130.7, 130.3, 130.2, 123.1, 120.4, 118.2, 117.5, 100.9, 81.8, 62.2, 61.0, 59.4, 56.8, 50.6, 46.6, 26.8; IR (KBr): 3412, 2938, 1756, 1637, 1497, 1445, 1273, 1082, 1032, 943, 815, 714 cm^{-1} ; MS (ESI): m/z 513 $[M+Na]^+$; HRMS (ESI): Calcd for $C_{27}H_{26}N_2O_7$ $[M+Na]^+$; 513.1637; found: 513.1615. The ^1H-NMR, ^{13}C-NMR and mass spectra (ESI and HR-MS) of the final product, PYBA-Nos are included as supporting material in the appendix.

3.4. Cell culture and reagents

The natural lead compounds, noscapine and docetaxel, were obtained from Sigma. All the chemical reagents and media used for cell culture were obtained from Sigma. In

this study, a human breast cancer cell line, MCF-7 was used, which was obtained from the cell repository of the National Centre for Cell Science Pune, Maharashtra, India. MCF-7 is a human breast cancer cell line with estrogen, progesterone and glucocorticoid receptors (Horwitz et al., 1975). MCF-7 cells are ideal for *in vitro* breast cancer studies because they preserve some ideal features of mammary epithelial cells, such as estrogen processing in the form of estradiol via estrogen receptors (ER) in the cell cytoplasm. In addition to retaining estrogen sensitivity, MCF-7 cells are also sensitive to cytokeratin. It is the first hormone receptor breast cancer cell line. When grown *in vitro*, the cell line is capable of forming domes and processing estradiol via cytoplasmic estrogen receptors. Growth can be inhibited by using tumor necrosis factor alpha (TNF alpha) and treatment of MCF-7 cancer cells with anti-estrogens can modulate insulin-like growth factor proteins, which ultimately have the effect of a reduction in cell growth. Scientists have found that although MCF-7 cells are easy to propagate, they are generally a slow-growing population. MCF-7 doubling time is typically 30-40 hours. MCF-7 cells are fairly large adherent cells, with a typical cell size measuring 20-25 microns (Camarillo et al., 2014).

MCF-7 cells were cultured using DMEM/RPMI medium supplemented with 10 % fetal bovine serum (FBS) and growth factors such as EGF (100 mg/ml), Insulin (10 mg/ml), Hydrocortisone (1 mg/ml) and 1% antibiotic. All cells were maintained in 5 % CO_2 humidified chamber.

3.4.1. *In vitro* assessments of cytotoxicity of designed compounds

Inhibition of cellular proliferation of MCF-7 was assessed by 3-(4, 5-dimethylthiazol-2-yl)-2,5, ditetrazolium bromide (MTT). Briefly, MCF-7 cells (3×10^3) were seeded into 96 well plates. After post-attachment, the cells were treated with different concentrations of noscapine derivatives (VPN-Nos, Br-Bn-Nos, PYBA-Nos, Br-

Nos, Amino-Nos, Br-TMB-Nos) and docetaxel in single as well as in combination regimen and were maintained in complete medium for 48 hr and 72 hr. To estimate the viability of cells, we have treated them with 10 µl of MTT (5 mg/ml) for 4 h at 37 ˚C and formazan crystals were dissolved in DMSO. Optical density was obtained at 570 nm using in a multimode flash reader (Varioskan, Thermo Scientific). The IC_{50} values for the concentration of drugs needed to destroy a 50 % cell have been calculated using the online tool Quest GraphTM IC_{50} Calculator (AAT Bioquest, Inc., Sunnyvale, CA, USA, https://www.aatbio.com/tools/ic50-calculator).

3.4.2. Drug combination effect study using isobologram analysis

The cumulative effect of drugs in terms of additive, synergistic, or antagonistic effect is studied by the most classical approach called Isobologram analysis. This method has been proven and mathematically demonstrated. As the combinations of noscapinoids and docetaxel have been used in a non-constant dose ratio, a normalized isobologram for the designed drugs at their ED_{50} was constructed.

The fractional inhibitory concentration (FIC) was interpreted by the following formula:

$$FIC = \frac{Conc.of\ drug\ in\ combination\ to\ produce\ IC_{50}}{Conc.\ of\ drug\ alone\ require\ to\ produce\ IC_{50}}$$

The sum FIC value for each of the preparations determined by the following formula was used to classify the drug–drug interaction.

$$Sum\ FIC = \frac{IC_{50}\ of\ drug\ A\ in\ combination}{IC_{50}\ of\ drug\ A\ alone} + \frac{IC_{50}\ drug\ B\ in\ combination}{IC_{50}\ of\ drug\ B\ alone}$$

Sum FIC < 0.5 represents substantial synergism, sum FIC < 1 represents synergism, sum FIC = 1 represents additive interaction, sum FIC ≥ 1 represents antagonism. An

Isobologram was plotted to show the drug interaction as per the method proposed earlier (Pandey et al., 2016).

3.4.3. Cell cycle analysis using flow cytometer

In Dulbecco's Modification of Eagle's Medium (DMEM), MCF-7 cells were cultivated with 4.5 g/l glucose and L-glutamine, supplemented by 10% bovine fetal serum and 1% penicillin/streptomycin. For cell cycle analysis, MCF-7 ($1X10^5$) cells were seeded in a 6-well culture plate overnight and then the cells were treated with IC_{50} concentrations of noscapinoids (Br-Bn-Nos, VPN-Nos, PYBA-Nos, Br-Nos, Amino-Nos, Br-TMB-Nos) and DOX in single as well as in combination regimen. Cells were incubated for 48 hours. After specified treatment time, the cells were harvested using trypsin-EDTA, washed with phosphate buffered saline (PBS) and fixed in 70% ethanol for 30 minutes. After fixation, the cells were washed and stained with staining solution that included RNase (5µg/ml), propidium iodide (5µg/ml) and Triton X (0.1%). The cells were analyzed in a flow cytometer (FACS Calibur) for the effect of drug treatment on different phases of cell cycle.

3.4.4. Apoptosis analysis using flow cytometer

Choline phospholipids such as phosphatidylcholine and sphingomyelin (PS) are exposed to the external leaflet during apoptosis, whereas aminophospholipids (phosphatidylserine, phosphatidylethanolamine) are positioned exclusively on the lipid bilayer's cytoplasmic surface (Ji et al., 2017). The identification of PS by the fluorochrome-tagged 36 KDa anticoagulant protein Annexin V permits apoptotic incidence to be reliably calculated. Only in the presence of mM concentrations of divalent calcium ions, this probe reversibly binds to phosphatidylserine residues. Apoptosis in

cancer cells has been identified by Annexin-V-FITC detection kit (Sigma –Aldrich,USA) based on instruction provided by manufacture.

MCF-7 cells (5 X 10^4) were seeded in 35 mm plates. After 24 hours of attachment, cells were treated with IC_{50} concentrations of noscapinoids (Br-Bn-Nos, VPN-Nos, PYBA-Nos, Br-Nos, Amino-Nos, Br-TMB-Nos) and docetaxel in single as well as in combination regimen and incubated for indicated time intervals at 37 °C in 5% CO_2. The cells were then stained with propidium iodide (PI) and Annexin-V-Alexa Fluor 488 (BD Pharmingen, San Diego, CA, USA) according to the manufacturer's protocol. Percentage of apoptotic cells was assessed using BD FACS Calibur (San Jose, CA, USA).

3.4.5. Morphological examination using DAPI staining

The nuclear morphology of cells treated with the noscapinoids was evaluated by staining the cells with DAPI and imaging with fluorescence microscopy. In brief, MCF-7 cells (3 x 10^3 cells) were grown on poly-l-lysine coated coverslips in 6-well plates and treated with noscapinoids (Br-Bn-Nos, VPN-Nos, PYBA-Nos, Br-Nos, Amino-Nos, Br-TMB-Nos) and docetaxel in single as well as in combination regimen for 48 hours. The cells were then washed twice with ice-cold PBS. The coverslips were fixed with 70% ethanol and stained using DAPI, followed by imaging using an inverted fluorescent microscope (Nikon Eclipse Ts2R-FL). Apoptotic cells were identified as changes in cellular morphology (e.g., nuclear condensation, membrane blebs formation, and apoptotic bodies).

3.4.6. Foci formation assay

MCF-7 cells (2 x 10^3 cells) were plated in six-well culture dishes in the presence of reduced serum (2%) medium. DMSO was added as a control to the culture medium.

Every second day, drugs were replenished, and the assay was carried out for 15 days, as previously mentioned (Tiwari et al., 2015; Palanisamy et al., 2010). After staining with crystal violet, foci (>5 μm) were counted under phase contrast Olympus microscope (Tokyo, Japan).

Tubulin binding assay to determine the binding affinity of noscapinoid and docetaxel in single and in combination doses

3.4.7. Tubulin purification

Microtubules were isolated and purified from the goat brain through alternative cycles of GTP-dependent polymerization and depolymerisation in PEM buffer (50 mM pipes, 3 mM MgSO4, 1 mM EGTA, pH 6.8) (Mahaddalkar et al., 2015). The purified microtubules were preserved at -80 °C. The purified tubulin was estimated using the Bradford method as well as by SDS PAGE (Bradford, 1976).

3.4.8. Tryptophan Quenching Assay

Tubulin (2 μM) was incubated in a water bath with our test compounds (PYBA-Nos, Br-TMB-Nos) and docetaxel at a required concentration alone as well as in combination with DOX at indicated concentration in PEM buffer (50 mM pipes, 3 mM $MgSO_4$, 1 mM EGTA, pH 6.8) for 45 min at 35˚C. The samples were excited at 295 nm and emission was measured at 310-400 nm. For the spectrofluorometric titrations a FlouroMax ® 4 spectrofluorometer (Horiba Scientific, Edison, NJ) assisted by Fluor Essence 3.5 software was used.

3.4.9. ANS (8-Anilino-1-naphthalene sulfonic acid)-binding assay

ANS binding assay was performed to verify the structural integrity of the tubulin in presence of the noscapinoids and DOX in single as well as in combination regimen. Tubulin (2 μM) was incubated with the desired concentration of noscapinoids and DOX alone and in combination regimens at 35 ºC for 30 min in PEM buffer. ANS (50 μM) was added and the samples were incubated in dark at 25 ºC for 15 min. The samples were excited at 370 nm and the emission was measured at 400–540 nm using a Flourolog 3 spectrofluorometer (Horiba Scientific, Edition, NJ) assisted by Fluor Essence 3.5 software. The assays were repeated two times.

3.4.9.1. *In vivo* therapeutic efficacy of noscapinoid and docetaxel as single agents and in drug combination in inhibiting breast carcinomas in a xenograft model.

All experimental protocols involved in this study were approved by Institutional Animal Ethics Committee of NIPER, Hyderabad (1548/PO/Re/2011/CPCSEA) and followed by the guidelines of "Committee for the Purpose of Control and Supervision of Experiments on Animals" of Govt. of India. About 8 to 10 weeks old female BALB/c athymic nude mice were housed in the Animal Care Facility. Suspensions of $1x10^6$ human breast adenocarcinoma estrogen receptor positive cell line MCF-7 cells in 0.2 ml of PBS were inoculated subcutaneously into the anterior flank. After 7-10 days when the tumors were palpable, treatment of the test compound, PYBA-Nos and Br-TMB-Nos in single as well as in combination with docetaxel were administrated by oral gavage. The mice were randomly divided into 2 groups. Group-1 (control) consisting of 5 animals received daily gavage of vehicle solution (acidified water, pH 4.0) only, whereas group-2 consisting of 10 animals were treated with 100 mg/kg body weight of our test drugs in the same vehicle solution by daily gavage. Tumor volumes were determined on alternative days by

measuring tumors in three perpendicular diameters using vernier calipers and their volume was determined as Π/6 (length x width x height) (Tomayko and Reynolds, 1989). The control group of mice was euthanized at day 30 owing to their large tumor volumes—this served as the end-point for control animals. Accordingly, this endpoint was used to compare tumor size in untreated mice with those administered with our targeted compounds.

3.4.9.2. Histopathological and hematological analyses

On day 30, tumor-bearing mice treated with 100 mg/kg body weight of PYBA-Nos and Br-TMB-Nos in single as well as in combination with docetaxel by oral gavage daily and untreated tumor bearing mice were given an overdose (0.2 ml) of 3.5% chloral hydrate, blood was taken from the heart, and CBC analysis was performed using a CBC instrument (CDC Technologies, Oxford, CT). Next, animals were perfused with a 3% paraformaldehyde and 2% glutaraldehyde mixture in PBS (pH 7.4) and liver, kidney, spleen, lung, heart, brain, intestines and tumor were removed and processed for histopathological analysis. Tissues were embedded in paraffin, sectioned and stained with hematoxylin and eosin. The tissues were observed under the microscope for toxicity evaluation.

Chapter 4

RESULT and DISCUSSION

"This chapter provides information of the synthesized noscapinoids and its combined effect with docetaxel based on their molecular modelling and cellular study. Poor clinical prospects of the current chemotherapy have triggered the development of new treatment modalities such as combination therapy for breast cancer. The results obtained from theoretical prediction were validated through experiments by tubulin-binding assay in different conditions."

4.1. Molecular modelling

According to the earlier reports, it was revealed that noscapine and its derivatives bind to tubulin and alters microtubule dynamics both *in vitro* and *in vivo* (Ye et al., 1998; Zhou et al., 2002a; Zhou et al., 2002b; Landen et al., 2002; Zhou et al., 2003; Checchi et al., 2003; Aneja et al., 2006; Joshi et al., 2010). Besides, the clinically use chemotherapeutics, docetaxel is also reported to bind to tubulin at a different binding site. Noscapinoids bind at the interface of α- and β-tubulin (Naik et al., 2011; Oliva et al., 2020), whereas the binding of docetaxel was biased to β-tubulin (Snyder et al., 2001). Since both noscapinoids and docetaxel bind to tubulin at different sites, we are interested to determine their binding affinity when both of them docked at their respective binding site onto tubulin. We have performed two cycles of molecule docking with tubulin. In the first cycle, docetaxel was docked onto its binding site and similarly the noscapinoids were docked onto noscapine binding site using Glide XP docking (Dash et al., 2020). All the noscapinoids docked well into their binding site with docking score ranged from -4.41 to -8.99 kcal/mol (Table 4.1). Similarly, docetaxel docked well with a docking score of -6.67 kcal/mol. Further, the docking energy for all the noscapinoids vary in between -37.13 to -57.61 kcal/mol. Their binding with tubulin was much more favourable with van der Waal interaction with the energy score ranged from -28.76 to -45.90 kcal/mol (Table 4.1).

Table 4.1. Molecular docking results (Glide XP_{score}) and the relevant energy parameters of designed derivatives of noscapine and docetaxel in single as well as in combination with tubulin.

Ligands	Glide XP_{score} (kcal/mol)	Glide E_{vdw} (kcal/mol)	Glide E_{coul} (kcal/mol)	Glide Energy (kcal/mol)
Docetaxel	-6.67	-41.63	-8.46	-50.09
9-vinyl phenyl-Noscapine	-4.82	-39.86	-8.16	-48.02
9-vinyl phenyl-Noscapine + Docetaxel	-3.23	-32.83	-9.27	-42.10
Amino-Noscapine	-6.27	-31.16	-5.97	-37.13

Amino-noscapine + Docetaxel	-3.49	-43.27	-6.46	-49.97
Br Bn-Noscapine	-6.03	-39.07	-5.46	-52.53
Br Bn-Noscapine + Docetaxel	-4.99	-31.67	-8.29	-35.97
Br TMB-Noscapine	-7.24	-42.758	-6.445	-49.202
Br TMB-Noscapine+ Docetaxel	-4.37	-45.902	-11.713	-57.615
PYBA-Noscapine	-8.99	-28.76	-10.19	-51.19
PYBA-Noscapine + Docetaxel	-5.67	-40.99	-9.01	-37.78
Bromo-Noscapine	-4.41	-31.37	-9.65	-41.02
Bromo-Noscapine + Docetaxel	-3.81	-39.44	-16.16	-52.95

The DOX-tubulin complex was taken in the second cycle and all the noscapinoids were docked onto the noscapine binding site. Presence of DOX on its binding site interfered with the binding of noscapinoids and altered the docking score to -3.23 to -6.03 kcal/mol (Table 4.1). The binding of docetaxel induced the conformational changes to tubulin and thus influenced the binding of noscapinoids onto their binding site, indicating a combination effect of both the ligands.

4.2. MD simulation of the complex

The binding of both noscapinoids and DOX with tubulin were evaluated independently (Tub-Noscapinoids and Tub-DOX complexes) as well as in combination with tubulin (Tub-DOX+Noscapinoids) by a molecular dynamic simulation of 100 ns. To analyse the system's stability, the root means square deviations (RMSD) of Cα-atoms were computed for all frames over the entire duration of simulation. The fluctuation in the RMSD of Cα carbon atoms were very small after equilibration and all of the systems were found to be stable after 20 ns of simulation (Figure 4.1a & b). The root mean square fluctuations (RMSF) of Cα-atoms were also measured to see if there were any changes in residue flexibilities during the entire duration of MD simulation. The residues with higher RMSF tend to show more flexibility (Figure 4.2a & b). Both noscapinoids and DOX were found to bind with tubulin during the entire duration of the simulation. However, the top most five ligand-tubulin complexes based on the lowest total energy from the MD simulation

trajectory were obtained to generate the average structure in order to analyse the binding mode of ligands.

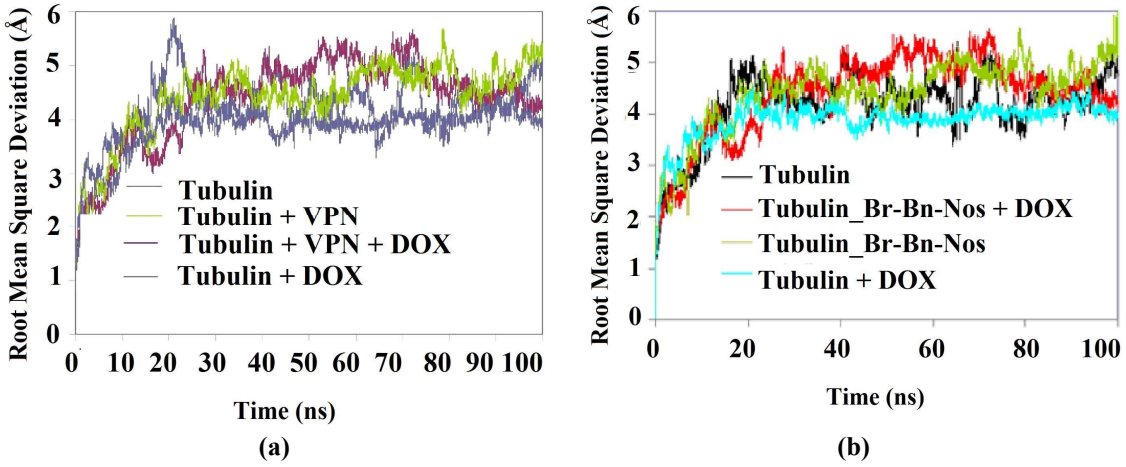

Figure 4.1. (a) Representative figures of root mean square deviations (RMSD) of Cα carbon atoms of tubulin only and in complex with (a) 9-Vinyl-phynyl-Noscapine (VPN) (Tubulin + VPN) and (b) N-3-Br-Benzyl-Noscapine (Tubulin+Br Bn-Nos) in single regimen as well as in combination with docetaxel (Tubulin + DOX + VPN, Tubulin + Br Bn-Nos + DOX) during 100 ns of MD simulation. The relative fluctuation in the RMSD of the Cα atoms is very small after ~ 20 ns of the simulation. The time step of 20fs was used during the simulation that generated 5,000 frames which were used to generate the average structure.

Both noscapinoids and DOX were found to accommodate well inside the binding cavity. The noscapinoids docked well at the interface of α- and β- tubulin, whereas the binding of DOX is biased more towards β-tubulin (Synder et al., 2000; Canales et al., 2011; Winefield et al., 2008). Their binding mode with the tubulin was represented in two steps: (a) receptor residues that have strong interactions with the ligand, such as a favourable hydrogen-bonding interaction, and (b) receptor residues that are close to the ligand, but whose interactions with the ligand are weak or diffuse, such as hydrophobic interaction.

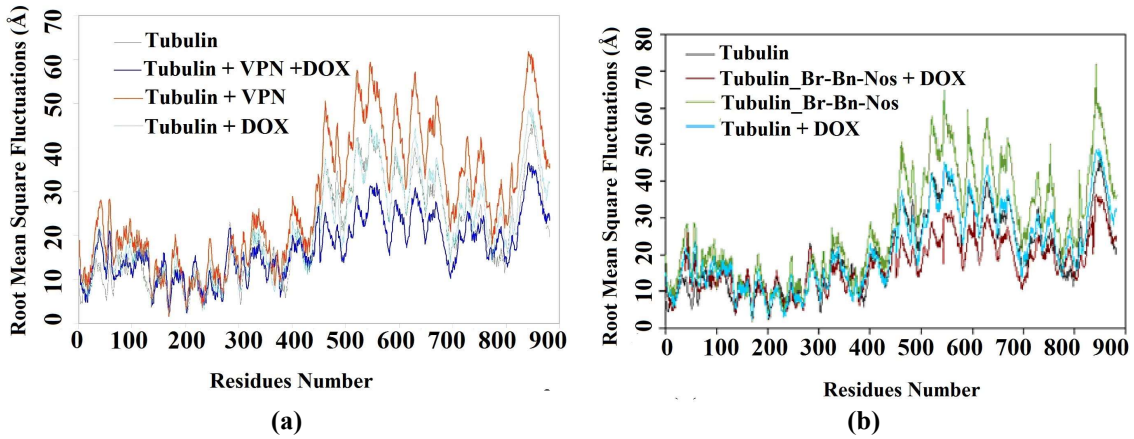

Figure 4.2. Representative figures of root mean square fluctuation (RMSF) of the residues of tubulin in the bound form of the ligands (a) 9-Vinyl-phynyl-noscapine (VPN) and (b) N-3-Br-Benzyl-noscapine (Br-Bn-Nos) in single as well as in combination with docetaxel (DOX) with the tubulin heterodimer. Different levels of flexibility of these residues were noticed in the bound form of tubulin with VPN, Br-Bn-Nos and DOX in single as well as in combination. Most of the residues showed flexibilities > 5 Å in case of tubulin bound with VPN, Br-Bn-Nos and DOX compared to the free tubulin heterodimer, indicating that these residues seem to be more flexible as a result of binding.

The differential mode of interactions of noscapinoids and DOX with the residues of tubulin is represented in the ligplot. The binding site amino acids involved in the binding of noscapinoids independently and in the presence of DOX were found albite different, which may be due to the change in conformation of tubulin in presence of DOX (Figure 4.3a-f). As seen in the figure several hydrogen bonds and hydrophobic interactions are involved in their binding sites.

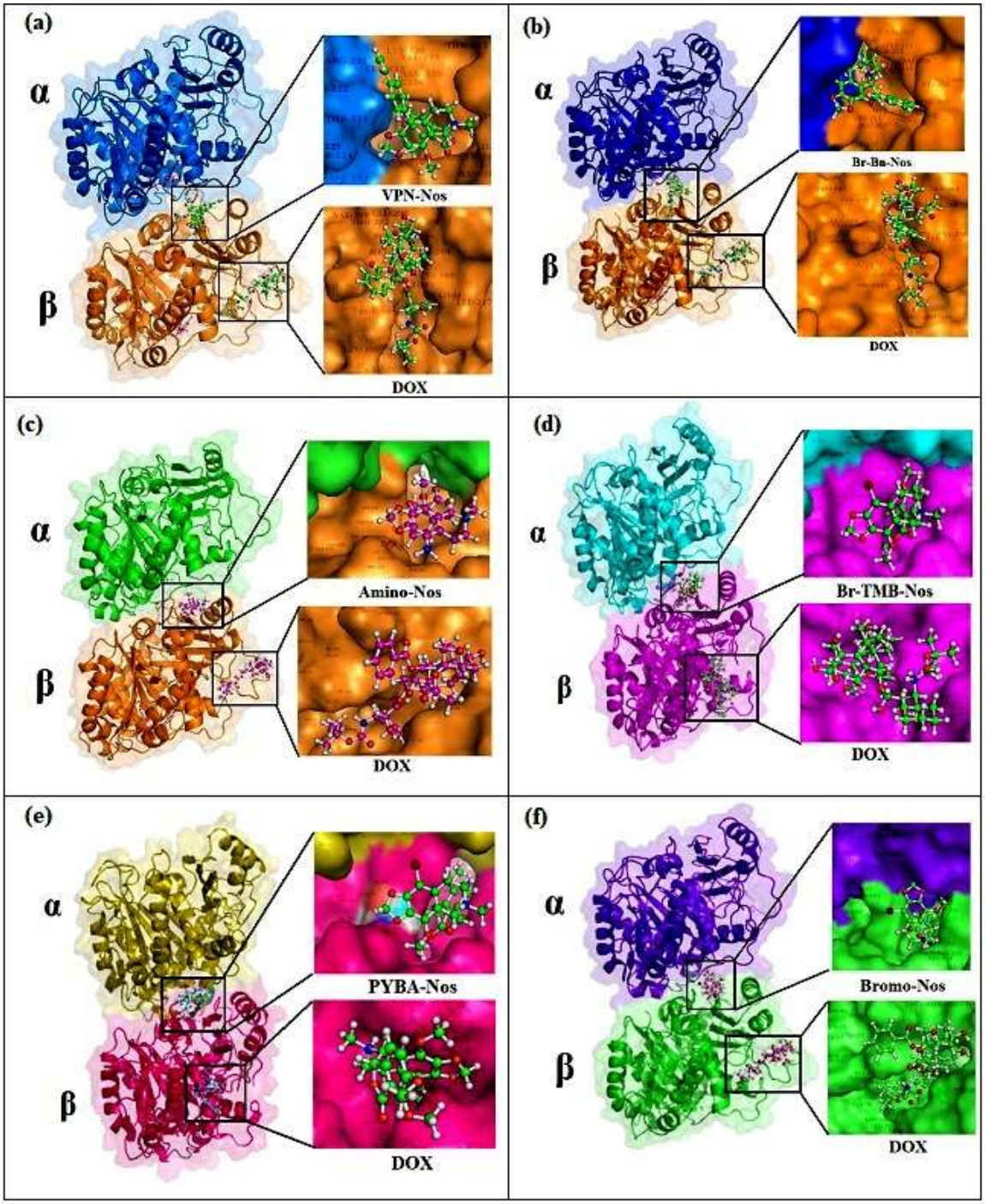

Figure 4.3. (a)VPN (b)Br-Bn-Nos (c)Amino-Nos (d) Br-TMB-Nos (e) PYBA-Nos (f) Brmo-Nos and DOX are well accomodated inside their respective binding site of tubulin. Snapshot of the ligands are obtained from the MD simulation. The binding site is represented as macromodel surface according to α- and β- tubulin.

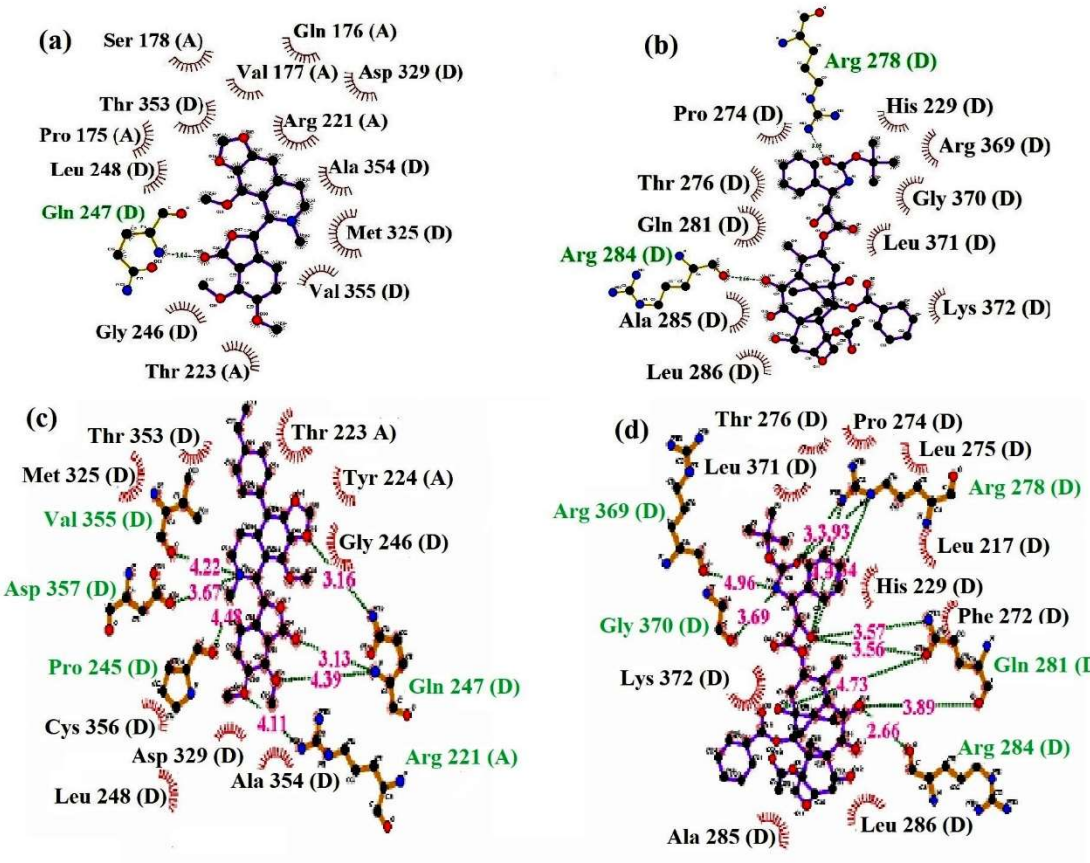

Figure 4.4. The ligplot analysis showing the interaction of binding site amino acids with (a) Tubulin_VPN and (b) Tubulin_Docetaxel when both the molecules docked independently into their respective binding sites. Further, the change in binding site amino acids when both the molecules docked together into their binding sites is shown in (c) Tubulin-VPN and Tubulin-DOX. The binding site amino acids were found to be albite different when both VPN and DOX were docked independently or in together.

The differential mode of interactions of compounds VPN and DOX with the residues of tubulin are represented in the ligplot. The differences in amino acids for binding of VPN with tubulin independently and in combination with DOX were mainly because of the change in conformation of tubulin due to binding of DOX (Figure 4.4) (Dash et al., 2020). As seen in the figure several hydrogen bonds and hydrophobic interactions are involved in their binding. The amino acids of the binding site involved in the binding of VPN are Gln 247 (D),Val 355(D), Leu 248(D), Glu 207(A), Asn 357(D), Lys 394(A), Thr 353 (D),Thr 223 (A), Ala 354 (D), Arg 221 (A),Gly 246 (D) and the DOX are Thr 276 (D), Leu 275 (D), Arg 278 (D), Leu 275 (D), Leu 217 (D), Pro 247 (D), Leu 217 (D), His 229 (D), Phe 272

(D), Gln 281(D), Arg 284 (D), Leu 286 (D), Ala 285 (D), Lys 372 (D), Gly 370 (D), Arg 369 (D), Leu 371 (D). A total of seven hydrogen bonds contributed to the interactions of VPN with the binding pocket of tubulin. Similarly binding of DOX involves eleven hydrogen bonds. In contrast there is a significant difference in the amino acids involved in the interaction of VPN as well as DOX in the co-complex of tubulin with both the ligands together (Appendix Table 4.2). This clearly explains the changes in the binding mode of VPN and DOX when both the ligands were docked together with the tubulin, indicating a chance of combination effect.

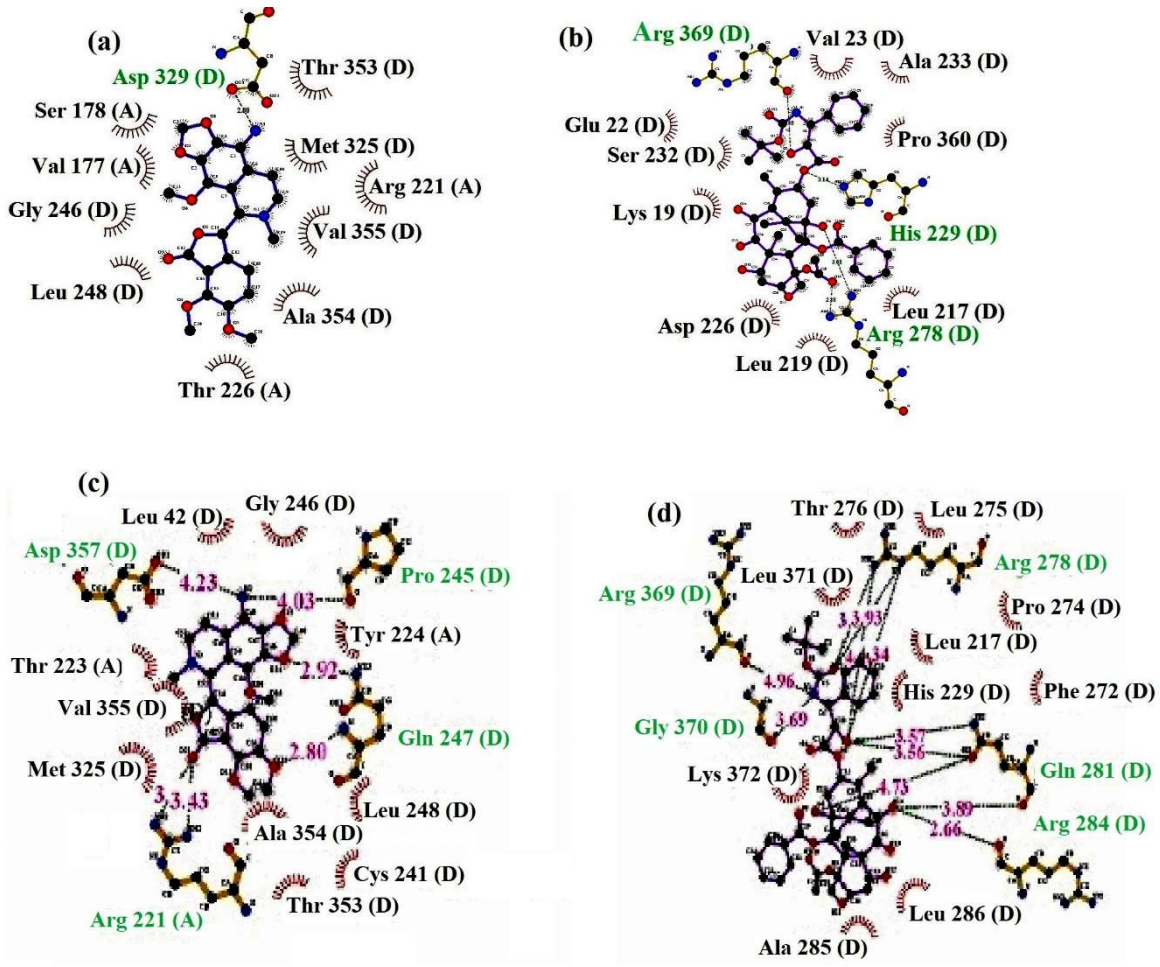

Figure 4.5. The ligplot analysis showing the interaction of binding site amino acids with (a) Tubulin_Amino and (b) Tubulin_Docetaxel when both the molecules docked independently into their respective binding sites. Further, the change in binding site amino acids when both the molecules docked together into their binding sites is shown in (c) Tubulin-Amino and Tubulin-DOX. The binding site amino acids were found to be albite different when both amino and DOX were docked independently or in together.

The amino acids of the binding site involved in the binding of Amino-Nos are Glu 247(D), Val 355(D), Leu 245(D), Leu 42 (D), Pro 245(A), Arg 221(A), Asn 357 (D), Thr 223 (A), Met 325 (D),Cys 241 (D),Ala 354 (D) (Figure 4.5 (a)), and the DOX are Thr 276 (D), Leu 275 (D), Arg 278 (D),Pro 247 (D), Leu 217 (D),His 229 (D), Phe 272 (D), Gln 281(D), Arg 284 (D), Leu 286 (D),Ala 285 (D), Lys 372 (D), Gly 370 (D), Arg 369 (D), Leu 371 (D). (Figure 4.5 b). The binding of Amino-Nos involved 6 hydrogen bonds (dashed lines) with different bond lengths. Similarly binding of DOX involved 13 hydrogen bonds with the binding site residues. Besides, hydrogen bonding, good number of hydrophobic interactions were involved in the binding of amino nos and DOX with binding site residues (Appendix Table 4.3).

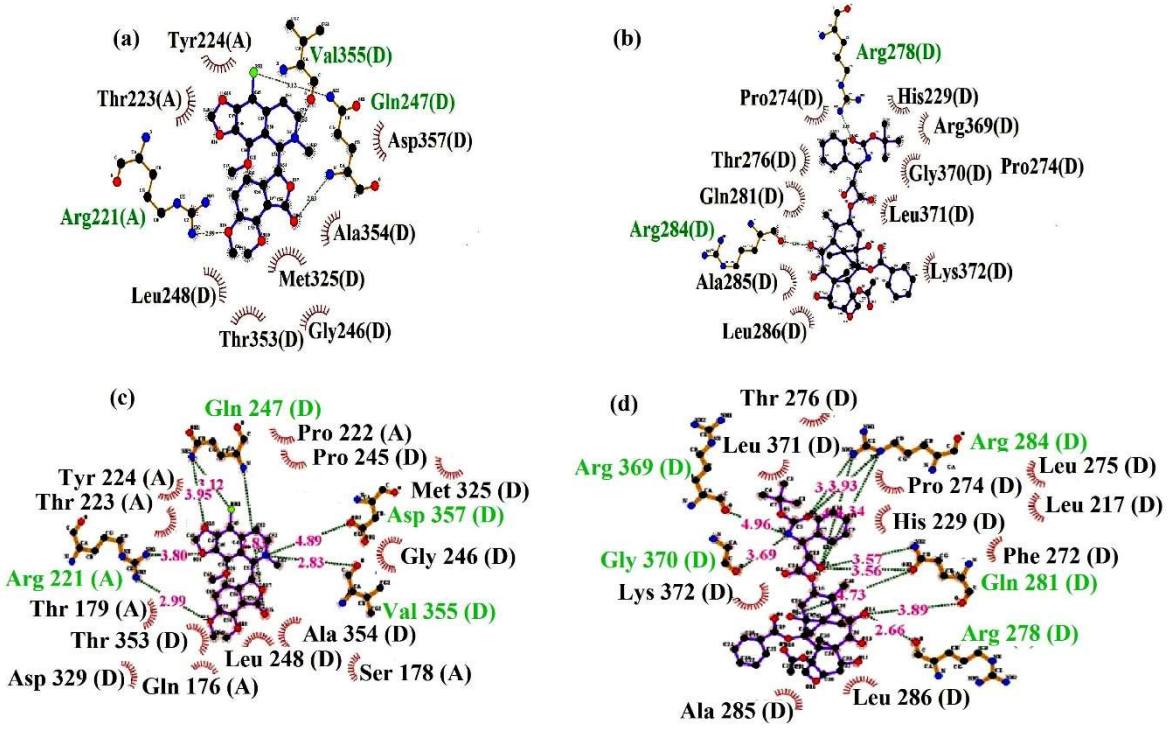

Figure 4.6. The ligplot analysis showing the interaction of binding site amino acids with (a) Tubulin_Bromo and (b) Tubulin_Docetaxel when both the molecules docked independently into their respective binding sites. Further, the change in binding site amino acids when both the molecules docked together into their binding sites is shown in (c) Tubulin-Bromo and Tubulin-DOX. The binding site amino acids were found to be albite different when both bromo and DOX were docked independently or in together.

Binding of Bromo-Nos involved 7 hydrogen bonds (dashed lines), each with a distinct bond length, while docetaxel binding involved 13 hydrogen bonds with the binding site residues. The different amino acids involved in the interaction of Bromo-Nos are Glu 247 (D), Pro 222 (A),Pro 245 (D), Met 325 (D),Asp 357 (D), GLy 246 (D),Ala 354 (D), Leu 248 (D),Thr 353 (D), Thr 179 (A and Arg 221 (A) (Figure 4.6 a) and in DOX are Thr 276 (D), Leu 275 (D), Arg 278 (D),Pro 247 (D), Leu 217 (D),His 229 (D), Phe 272 (D), Gln 281(D), Arg 284 (D), Leu 286 (D),Ala 285 (D), Lys 372 (D), Gly 370 (D), Arg 369 (D), Leu 371 (D) (Figure 4.6b). Moreover, good numbers of hydrophobic interactions were involved in the binding of Bromo-Nos and DOX with the respective binding site residues (Appendix Table 4.4). The significant difference in amino acids, clearly explains the changes in the binding mode of Bromo-Nos and DOX when both the ligands were docked together with the tubulin.

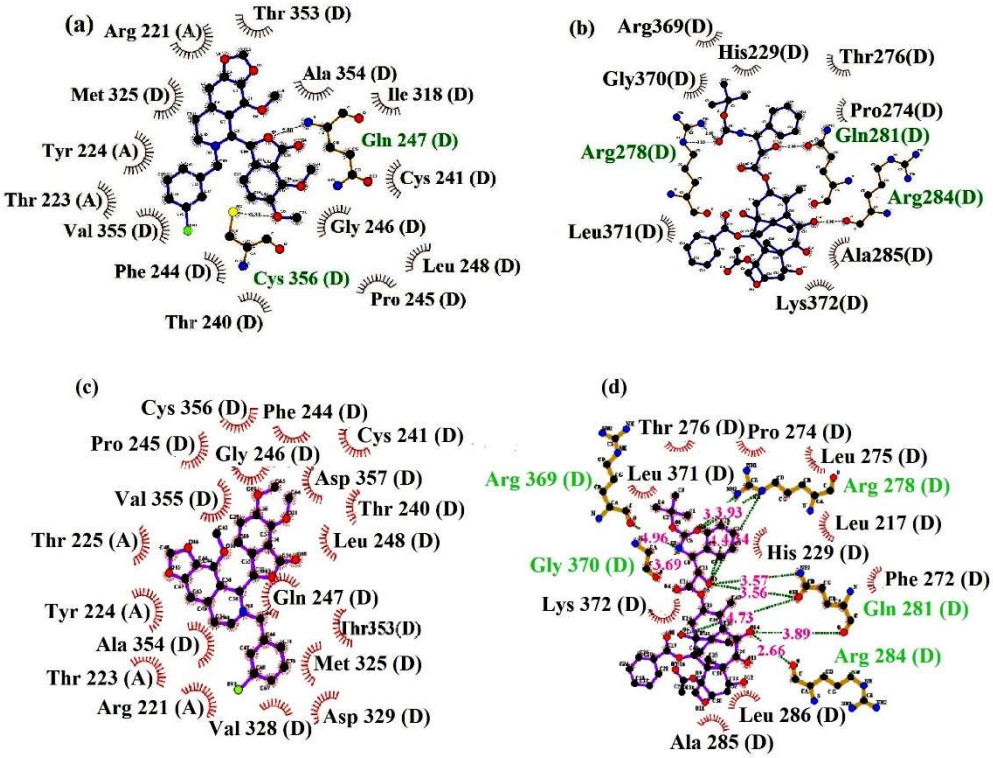

Figure 4.7. The ligplot analysis showing the interaction of binding site amino acids with (a) Tubulin_Br-Bn-Nos and (b) Tubulin_Docetaxel when both the molecules docked independently into their respective binding sites. Further, the change in binding site amino acids when both the molecules docked together into their binding sites is shown in (c)

Tubulin-Br-Bn-Nos and Tubulin-DOX. The binding site amino acids were found to be albite different when both Br-Bn-Nos and DOX were docked independently or in together.

The amino acids of the binding site involved in the binding of Br-Bn-Nos are Cys 356(D), Phe 244 (D), Cys 241 (D), Asp (D), Leu 248 (D), Gln 247 (D), Thr 353 (D), Met 325 (D), Val 328 (D), Arg 221 (A), Thr 223 (A), Ala 354 (D), Tyr 224 (A), Thr 225 (A), Val 355 (D), Pro 245 (D), Cys 356 (D) (Figure 4.7a). It was seen that no hydrogen bonds were involved in the interactions of Br-Bn-Nos with the tubulin binding pocket. Whereas, binding of DOX involved 12 hydrogen bonds. The amino acids Thr 276 (D), Leu 275 (D), Arg 278 (D), Leu 275 (D), Leu 217 (D), Pro 247 (D), Leu 217 (D), His 229 (D), Phe 272 (D), Gln 281(D), Arg 284 (D), Leu 286 (D), Ala 285 (D), Lys 372 (D), Gly 370 (D), Arg 369 (D), Leu 371 (D) (Figure 4.7b) contributed hydrophobic interactions with DOX (Appendix Table 4.5).

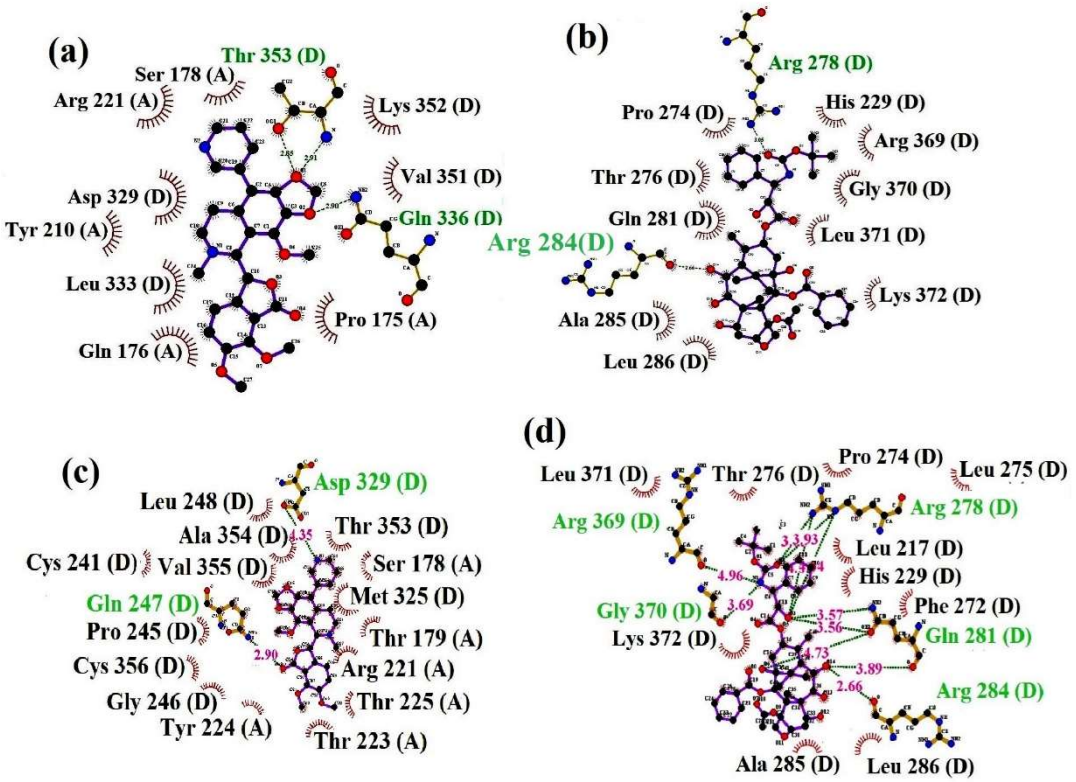

Figure 4.8. The ligplot analysis showing the interaction of binding site amino acids with (a) Tubulin_PYBA-Nos and (b) Tubulin_Docetaxel when both the molecules docked

independently into their respective binding sites. Further, the change in binding site amino acids when both the molecules docked together into their binding sites is shown in (c) Tubulin-PYBA-Nos and Tubulin-DOX. The binding site amino acids were found to be albite different when both PYBA-Nos and DOX were docked independently or in together.

The amino acids involved in PYBA-Nos binding include Arg 221 (A), Ser 178 (A), Thr 353 (D), Lys 352 (D), Val 351(D), Gln 336(D), Pro 175(A), Gln 176 (A), Leu 333 (D), Tyr 210 (A), Asp 329 (D), Arg 221 (A) (Figure 4.8 a). Binding mode of PYBA-Nos with the binding pocket is accompanied by two hydrogen bonds. In addition to hydrogen bonding, a large number of hydrophobic interactions were involved in the binding of PYBA-Nos to binding site residues (Appendix Table 4.5). The amino acids that contributed to the binding of DOX include, Thr 276 (D), Leu 275 (D), Arg 278 (D), Leu 275 (D), Leu 217 (D), Pro 247 (D), Leu 217 (D), His 229 (D), Phe 272 (D), Gln 281(D), Arg 284 (D), Leu 286 (D), Ala 285 (D), Lys 372 (D), Gly 370 (D), Arg 369 (D), Leu 371 (D). A total of 13 hydrogen bonds were involved in the biding of DOX with the binding site residues (Figure 4.8 b).

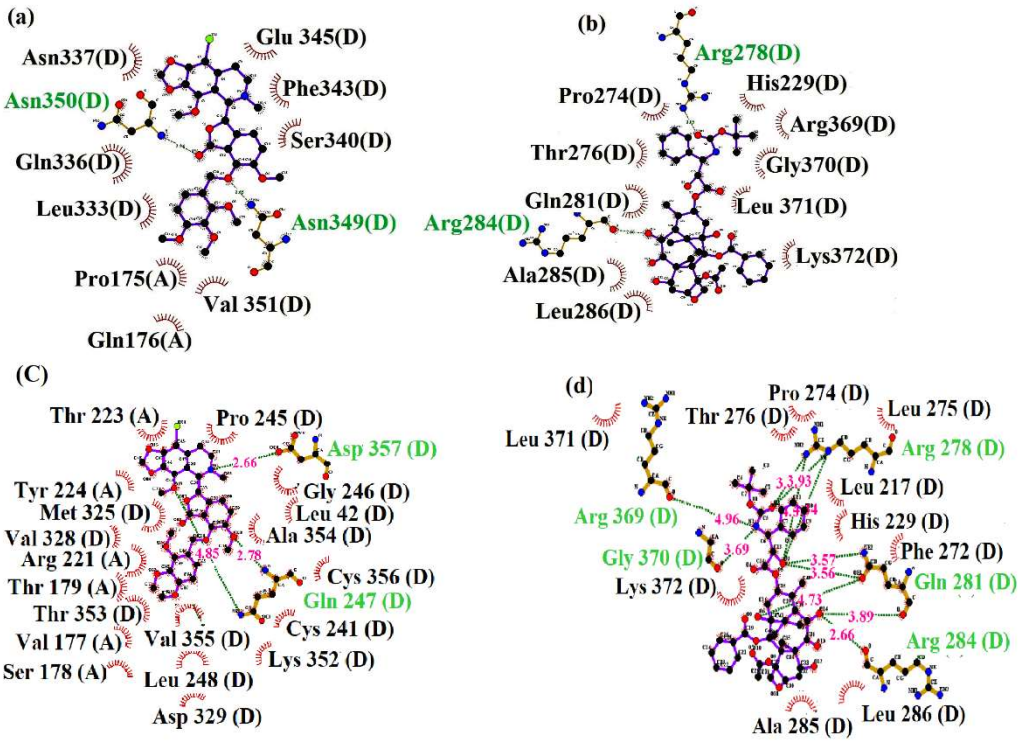

Figure 4.9. The ligplot analysis showing the interaction of binding site amino acids with (a) Tubulin_Br-TMB-Nos and (b) Tubulin_Docetaxel when both the molecules docked independently into their respective binding sites. Further, the change in binding site amino acids when both the molecules docked together into their binding sites is shown in (c) Tubulin- Br-TMB-Nos and Tubulin-DOX. The binding site amino acids were found to be albite different when both Br-TMB-Nos-Nos and DOX were docked independently or in together.

The interactions of Br-TMB-Nos with the binding pocket of tubulin include three hydrogen bonds with distances of 2.66 Å, 4.85 Å, and 2.78 Å. Besides, hydrogen bonding, good number of hydrophobic interactions were involved in the binding of Br-TMB-Nos with binding site residues (Appendix Table 4.7). The amino acids involved in the binding of Br-TMB-Nos are: Pro 245 (D), Asp 357 (D), Gly 246 (D), Leu 42(D), Ala 354 (D), Cys 356 (D), Gln 247 (D), Cys 241(D), Lys 352 (D), Asp 329(D), Ser 178 (A), Leu 248 (D), Thr 353 (D), Thr 179 (A), Arg 221 (A), Val 328 (D), Met 325 (D), Tyr 224 (A), Thr 223 (A) and the amino acids involved in the binding of DOX are Thr 276 (D), Leu 275 (D), Arg 278 (D), Leu 275 (D), Leu 217 (D), Pro 247 (D), Leu 217 (D), His 229 (D), Phe 272 (D), Gln 281(D), Arg 284 (D), Leu 286 (D), Ala 285 (D), Lys 372 (D), Gly 370 (D), Arg 369 (D), Leu 371 (D).

4.3. Proliferation of cancer cells is inhibited by noscapinoids and DOX in single as well as in combination regimen

Inspired by the *in-silico* prediction of binding affinity of the six potent derivatives of noscapine with tubulin dimer, we evaluated its efficacy in inhibiting proliferation of MCF-7 cells in single as well as in combination regimen with DOX. Understanding the pharmacological and biological properties of a chemotherapeutic agent requires determining the half-maximal (50%) inhibitory concentration (IC_{50}). The method for determining IC_{50} has become simpler and can be conducted after the invention of a colorimetric technique the 3-(4,5-dimethylthiazol-2-yl)-2,5-diphenyltetrazolium bromide (MTT) assay. The MTT

assay evaluates a compound's cytotoxicity by evaluating changes in intracellular NAD(P)H-dependent oxidoreductase activity (Tolosa et al., 2015; Aleshin et al., 2015). The initial status of living cells is defined by the optical densities (ODs) of the control wells, the mean of which is set to a survival rate of 100% (*i.e.*, inhibitory rate of 0%). The concentration corresponding to a survival rate of 50% is defined as the IC_{50} value.

The anti-proliferative activity for both VPN and DOX increases with the increasing concentration in single as well as in combination regimen (Figure 4.10a). The IC_{50} value amounted to 30.17 μM and 19.92 μM, respectively for 48 h and 72 h with VPN. Similarly, the IC_{50} value amounted to 0.621 μM and 0.193 μM, respectively for 48 h and 72 h with DOX. Surprisingly, the inhibition of cellular proliferation was significantly achieved with the combination dose regimens of both VPN and DOX. The approximately 50% inhibition of cellular proliferation was found to be at VPN (50μM) and DOX (0.01μM). The dose dependent cytotoxicity of DOX has been enhanced considerably with the combination dose regimen of VPN (Dash et al., 2020).

Parenthetically, the derivative of noscapine, Br-Bn-Nos inhibited proliferation of MCF-7 cells in a dose dependant manner with IC_{50} values of 11.5 μM and 7.71μM respectively at 48 h and 72 h. Similarly, the DOX showed IC_{50} values of 0.39 μM and 0.016 μM against MCF-7 cells. The combination effect of both Br-Bn-Nos and DOX on proliferation of MCF-7 has also determined and included in Figure 4.10b.

Further, the interaction between both the agents has also been investigated using their sum FICs and isobologram plots (Figure 4.11a). At 48 h and 72 h, the cumulative FICs value was 0.8 and 0.76 respectively. The isobolographic plot of VPN and docetaxel revealed that the two drugs have synergistic antiproliferative efficacy after 48 h and 72 h of administration. The sum FICs value was found to be 0.49 and 0.62 respectively at 48 h and 72 h. The isobologram of Br-Bn-Nos (Figure 4.11b) with DOX suggested that the

combination regimen has synergistic antiproliferative activity at 48 h and 72 h exposure (sum FIC <1).

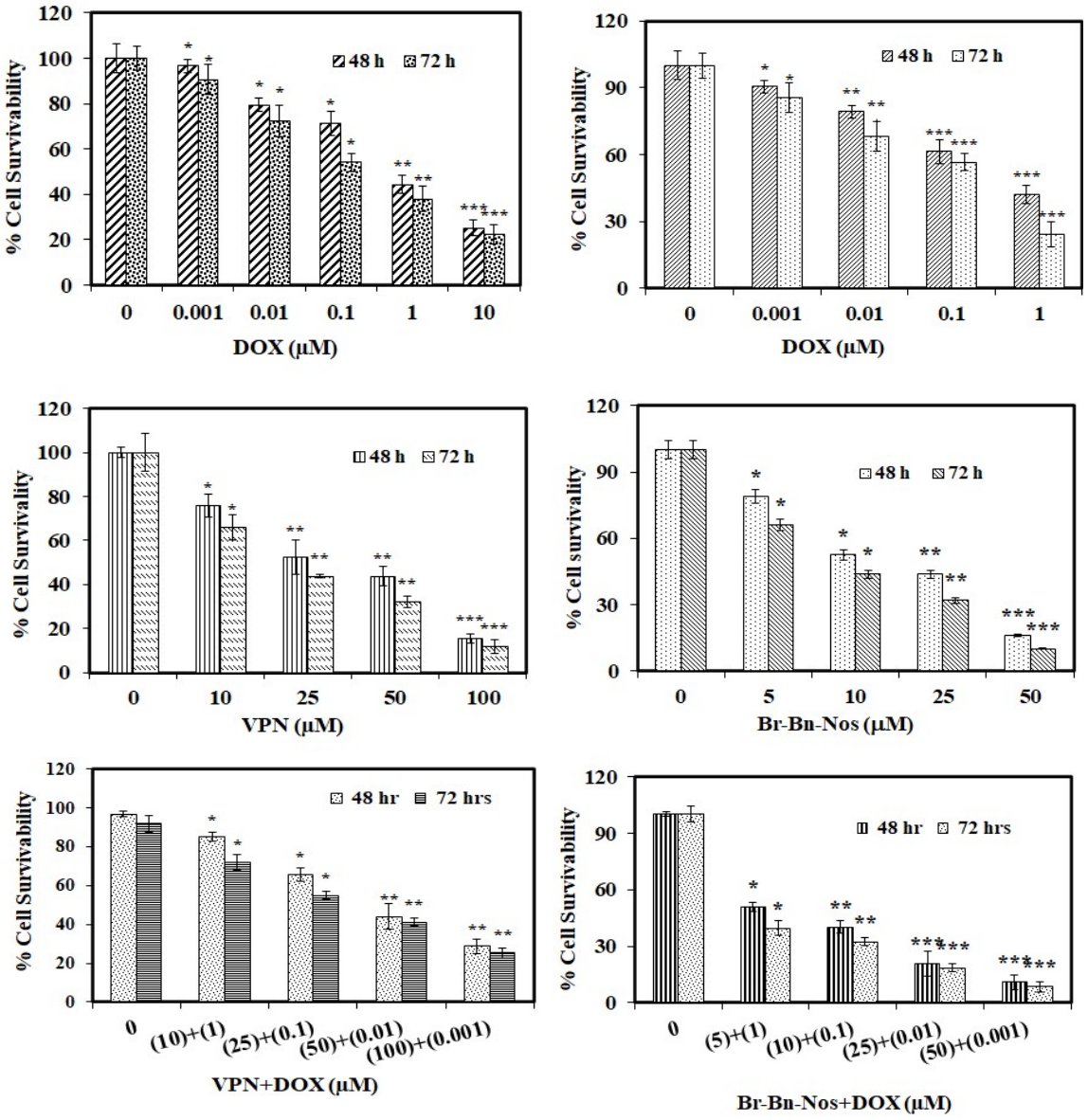

Figure 4.10. The inhibition of cellular proliferation of human breast cancer cell, MCF-7 with the treatment of (a) VPN and DOX in single as well as in combination regimen at different concentration after 48 h and 72 h post-treatment. In contrast, the approximately 50% inhibition of cellular inhibition was achieved in a combination regimen of VPN (50µM) and DOX (0.01µM) after 48h and 72h post-treatment. (b) Br Bn-Nos and DOX in single as well as in combination regimen at different concentrations inhibit cellular proliferation of human breast cancer cell, MCF-7 after 48 h and 72 h treatment. In contrast, approximately 50% inhibition of cellular inhibition was achieved in a combination regimen of Br Bn-Nos (5µM) and DOX (0.001µM) after 48 h and 72 h post-treatment. The graph is presented as mean ± SD, (n = 3), and considered significant if *p < 0.05, **p < 0.01, ***p < 0.001 compared to the control.

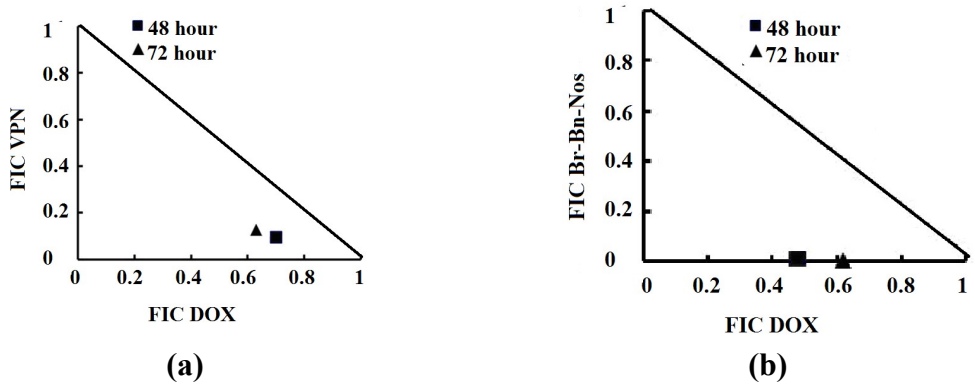

Figure 4.11. Representative figures of Isobolograms analysis showing *in vitro* interactions between (a) VPN and DOX (b) Br-Bn-Nos and DOX. Sum FIC < 0.5 represents substantial synergism, sum FIC< 1 represents synergism, sum FIC 1 represents additive interaction, sum FIC >1 represents antagonism.

Similarly, the Amino-Nos has a dose-dependent cytotoxicity effects in the MCF-7 cell line. The antiproliferative activity increases with the increasing concentration of Amino-Nos and DOX in single as well as in combination. The percentage of cell survivability was reduced to ~50% at 38.7 µM and 28.4 µM respectively at 48 h and 72 h of treatment with Amino-Nos (Figure 4.12 a). In contrast, the DOX revealed the dose dependent cytotoxicity of 0.61 µM and 0.08 µM respectively at 48 h and 72 h (Figure 4.12 a). Further, the combination dose of Amino-Nos (20 µM) and DOX (0.05 µM) revealed reduction in ~50% cell survival at 48 h and 72 h of treatment. The decrease in the concentration of DOX in combination with Amino-Nos in comparison to single regimen treatment revealed a chance of combination effect of both the drugs (Dash et al., 2020).

The anti-proliferative activity for both Bromo-Nos and DOX increases with the increasing concentration in single as well as in combination regimen. The IC_{50} value amounted to 35.17 µM and 20.92 µM, respectively for 48 h and 72 h with Bromo-Nos. In contrast, the IC_{50} value amounted to 0.521 µM and 0.093 µM, respectively for 48 h and 72 h with DOX. Approximately 50% inhibition of cellular proliferation was found with the combination treatment of Bromo-Nos (20µM) and DOX (0.05µM). The dose dependent

cytotoxicity of DOX has been reduced considerably with the combination dose regimen of Bromo-Nos (Figure 4.12 b).

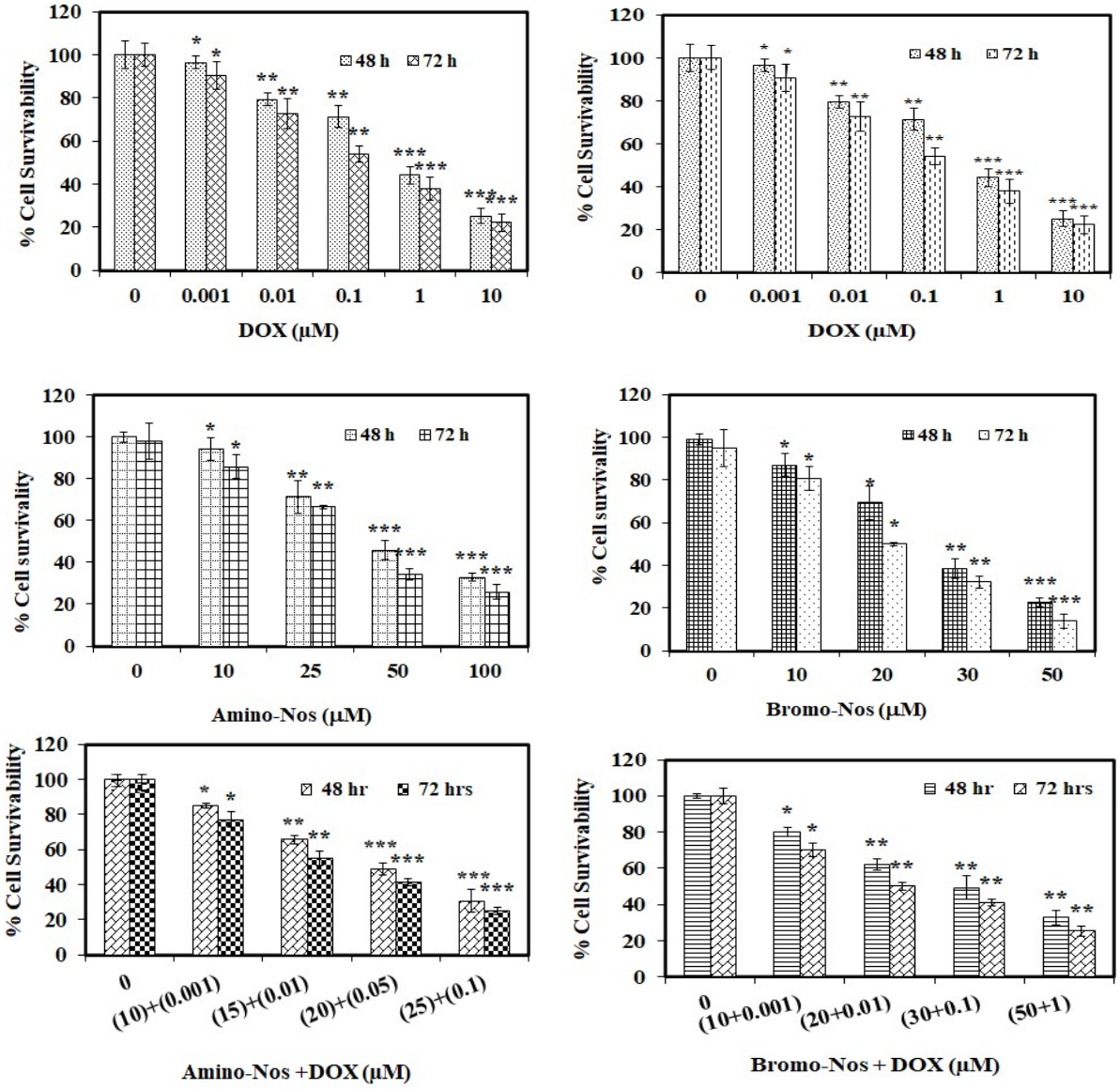

Figure 4.12. Reduction in percentage of cell survivability with the treatment of (a) Amino-nos and DOX (b) Bromo-nos and DOX in single as well as in combination regimen for MCF-7 cancer cell. The graph is presented as mean ± SD, (n = 3), and considered significant if *p < 0.05, **p < 0.01, ***p < 0.001 compared to the control.

Moreover, we determined the efficacy of Br-TMB-Nos and DOX in inhibiting the proliferation of human breast cancer cells (MCF-7) in both single and combination regimens. With the increasing concentration of Br-TMB-Nos and DOX both in single and in combination, the antiproliferative activity was found to be increased significantly (Figure

4.13 a). The IC_{50} value for Br-TMB-Nos was found to be 10.461 µM and 8.266 µM for 48 h and 72 h of treatments. In contrast, the IC_{50} value for DOX was found to be 0.033 µM and 0.014 µM for 48 h and 72 h of treatments. Our results showed that the combination dose of Br-TMB-Nos (25 µM) and DOX (0.01µM) revealed a reduction in cell survival to ~50% at 48 h and 72 h of treatment. Therefore, the dose-dependent cytotoxicity of DOX may be reduced considerably with the combination dose regimen of Br-TMB-Nos.

Anti-proliferative potential for both PYBA-Nos and DOX found to increase with increasing concentration including both single and in combination regimens (Figure 4.13 b). The IC_{50} values were 11.0 µM and 8.4 µM, respectively, for the PYBA-Nos after 48 h and 72 h of treatment. Likewise, the IC_{50} value amounted to 0.028 µM and 0.015 µM with DOX for 48 h and 72 h, respectively. Approximately 50% inhibition of cellular proliferation was achieved in the combination regimen of PYBA (10 µM) and DOX (0.1 µM) after 48 h and 72 h post-treatment. The findings showed that PYBA and DOX significantly decreased the dosage and time dependent viability of MCF-7 cells compared to control, both in the single and in the combination regimen.

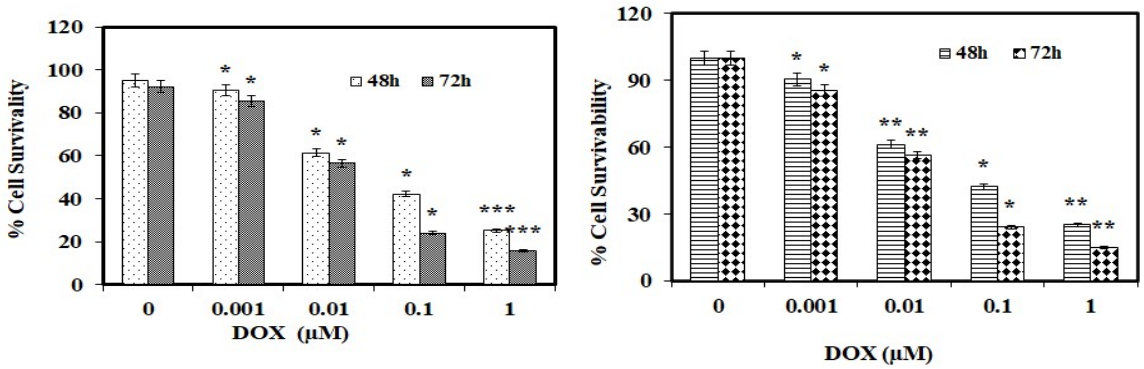

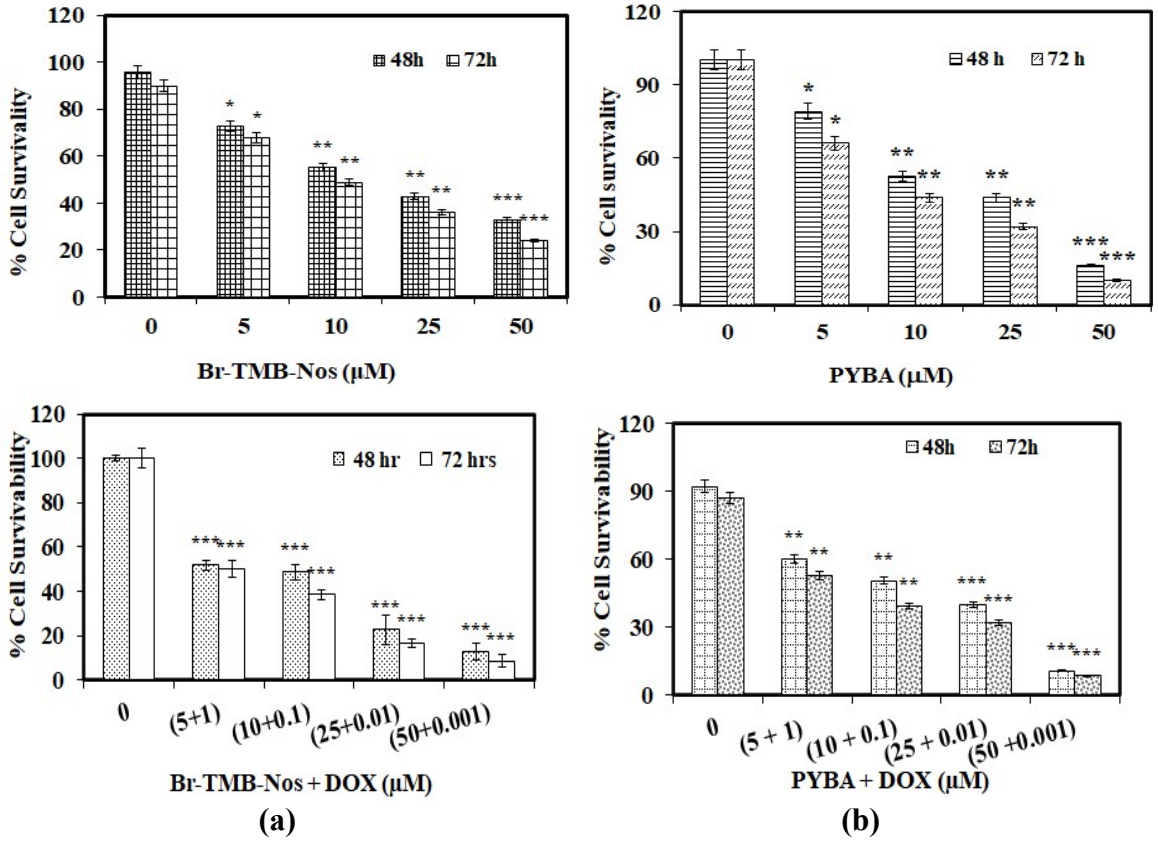

Figure 4.13. Reduction in percentage of cell survival in MCF-7 human breast cancer cell with the treatment of (a) Br-TMB-Nos and DOX (b) PYBA-Nos and DOX in single as well as in combination regimen at different concentration after 48 h and 72 h post-treatment for MCF7 cancer cell. Cell viability was detected by MTT assay. The graph is presented as mean ± SD, (n = 3), and considered significant if *p < 0.05, **p < 0.01, ***p < 0.001 compared to the control.

4.4. Effects of noscapinoids and dox using single and in combination regimen on cell cycle progression analysis

The effectivity of six derivatives of noscapine and docetaxel on the cell at the required concentration on the cell cycle profile of MCF-7 was evaluated by the induction of cell death using fluorescently labeled DNA deposition as a promising predictor of cell cycle progression and cell death. The unreplicated pattern of 2N DNA represent the G1 phase, while the cells with duplicated 4N DNA describe the G2/M phases. Cells with less than 2N DNA represent the dying cells in which the DNA degrades to varying degrees. We want to examine the effect of both Docetaxel and noscapinoids on cell cycle progression of MCF-7 cells with single and in their combination treatment. The cells were treated with varying

concentration of the noscapinoids in single and in combination regimen with docetaxel and the cell cycle distribution was evaluated. High cell aggregation during the G2/M transition phase compared to untreated cells was observed in the FACS analysis.

Inhibition in the progression of cell cycle of MCF-7 with treatment of VPN (20 µM) and DOX (0.5 µM) in single regimen as well as in combination regimen (25 µM VPN+0.05 µM DOX) was evaluated using flow cytometer. Both the compounds showed an increase in the sub-G1 cell populations compared to the control after 24 h of treatment in single and in combination regimen. The representative two-dimensional disposition of cell cycle profile is included in Figure 4.14 The sub-G1 population with treatment of VPN was increased to 8.12%, whereas with DOX it was increased to 16.1% and in combination it was further increased to 19.4 % in comparison to control. A cell must lose enough DNA to appear in the sub-G1 area, indicating both the compounds, VPN and DOX in single as well as in combination induce apoptosis to cancer cell. Maximum cells were arrested at the G2/M transition phase (Dash et al., 2020).

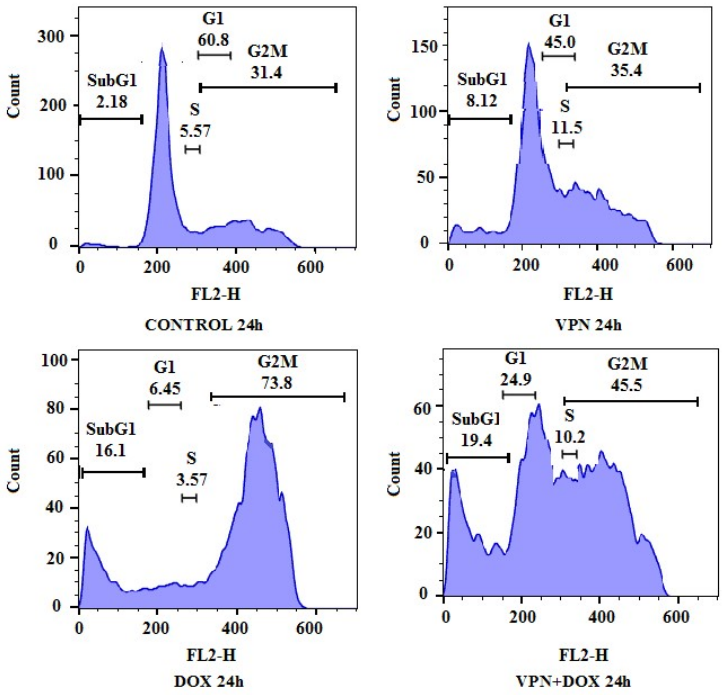

Figure 4.14. Panels (A) to (D) depicts the cell cycle distribution of MCF-7 cells in a two-dimensional disposition as determined by flow cytometry at 24 h of treatment with 20 µM

of VPN, 0.5 µM of DOX as single regimen and 25 µM of VPN + 0.05 µM of DOX in combination regimen. Results represent cell cycle progression at mitosis followed by the appearance of a characteristic hypodiploid (sub-G1) DNA peak is indicative of apoptosis.

Similarly, 25 µM of Amino-Nos and 0.5 µM of DOX in single regimen and 25 µm Amino-Nos+0.05 µm DOX in combination treatment effectively arrest cell cycle progression and induced cell death. The sub-G1 population with the treatment of amino-noscapine was increased to 9.62%, whereas with DOX it was increased to 15.4% and in combination it further increased to 32.6 % in comparison to control (Dash et al.,2020).

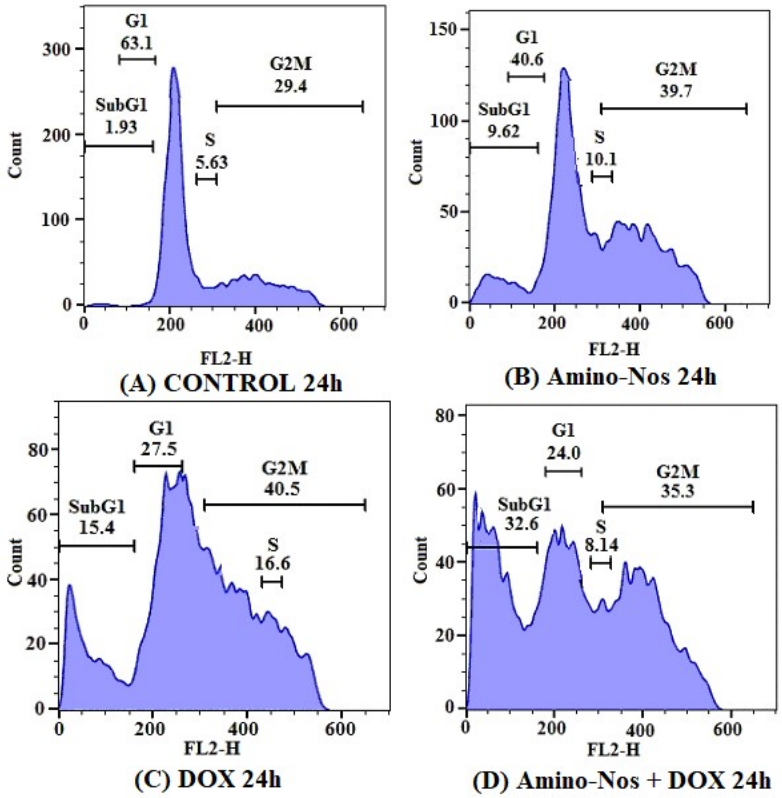

Figure 4.15. Panels (A) to (D) depicts the cell cycle distribution of MCF-7 cells treated with 25 µM of Amino-Nos, 0.5 µM of DOX in single regimen, and 25 µM of Amino-Nos + 0.05 µM of DOX in combination regimen as determined by flow cytometry at 24 h. Results represent cell cycle progression at mitosis followed by the appearance of a characteristic hypodiploid (sub-G1) DNA peak is indicative of apoptosis.

Further, the MCF-7 cancer cells were treated with Br-Bn-Nos (20 µM) and DOX (0.1 µM) in the single regimen as well as in the combination regimen (25 µM Br-Bn-Nos+0.01 µM DOX) and the cell cycle progression was evaluated via flow cytometric analysis. As shown in figure 4.16, cells were shown an increment in the sub-G1 phase

compared to the control after 48 h of treatment in single and in combination regimen. The sub-G1 population with treatment of Br-Bn-Nos was increased to 15.4%, whereas with DOX it was increased to 16.1% and in combination it further increased to 23.2% compared to control. The combination effect of both Br-Bn-Nos and DOX on cell cycle progression could be useful for induction of apoptosis.

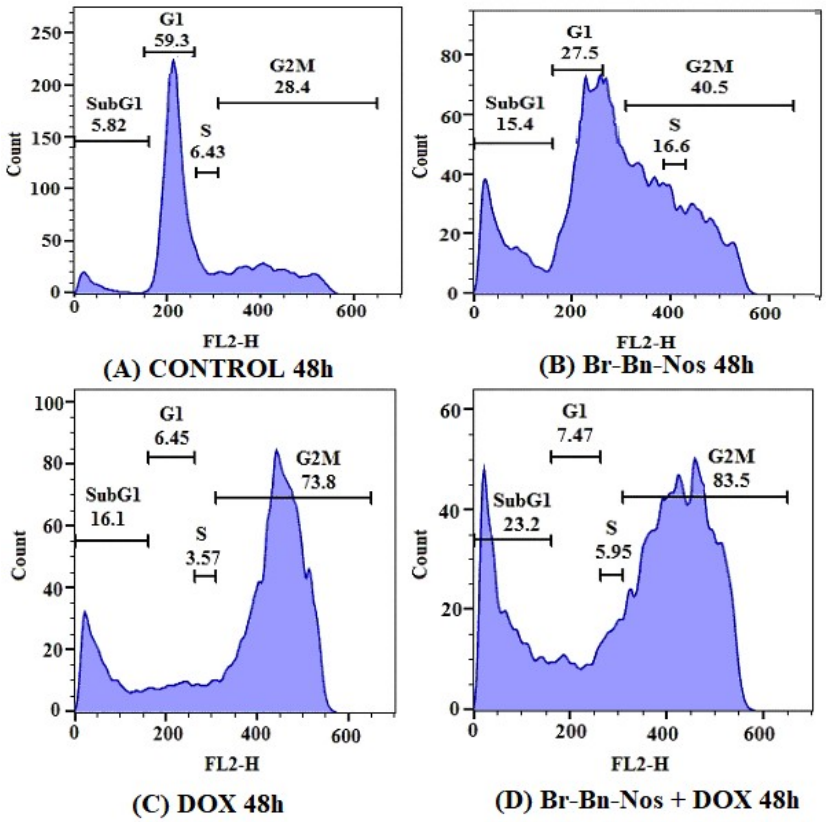

Figure 4.16. Figure A-D depict represented figures of analysis of cell cycle distribution in a two-dimensional disposition as determined by flow cytometry in MCF-7 cells treated with 20 µM of Br- Bn-Nos, 0.1µM of DOX as single regimen and 25 µM of Br-Bn-Nos + 0.01µM of DOX in combination regimen. Both Br Bn-Nos and DOX inhibit cell cycle progression at mitosis followed by the appearance of a characteristic hypodiploid (sub-G1) DNA peak, indicative of apoptosis.

The effect of Br-TMB-Nos (10 µM) and DOX (0.1 µM) in single as well as in their combination regimen (25 µM Br-TMB-Nos+0.01 µM DOX) on the cell cycle progression of MCF-7 cells was investigated by FACS. The untreated cells exposed to vehicle solvent (DMSO) showed a typical cell cycle profile with 63.1% in G1 phase, 5.63% in S phase, and 29.4% in G2/M phase (Figure 4.17). However, after 24 h treatment with Br-TMB-Nos and

DOX in single and in combination regimen showed an increase in the sub-G1 cell populations compared to the control. After 24 h treatment the Br-TMB-Nos showed only 34.4% in G1 phase, 14.2% in S phase, and 38.7% in G_2/M phase. Parenthetically, treatment with DOX after 24h revealed 6.86% in G1 phase, 3.33% in S phase and 73.5% in G2/M phase. In contrast, the combination effect of both Br-TMB-Nos and DOX after 24 h revealed 23% in G1 phase, 8.23% in S phase and 39.2% in G2/M phase. The sub-G1 population was increased to 12.6% with treatment of Br-TMB-Nos, whereas with DOX it was increased to 16.4% and in combination, it further increased to 29.6 % compared to control. Therefore, both the compounds, Br-TMB-Nos and DOX alone as well as in combination showed promising activity in MCF-7 cells which is an event reminiscent of apoptosis to the cancer cell. Maximum percentages of cells were arrested at the G_2/M transition phase.

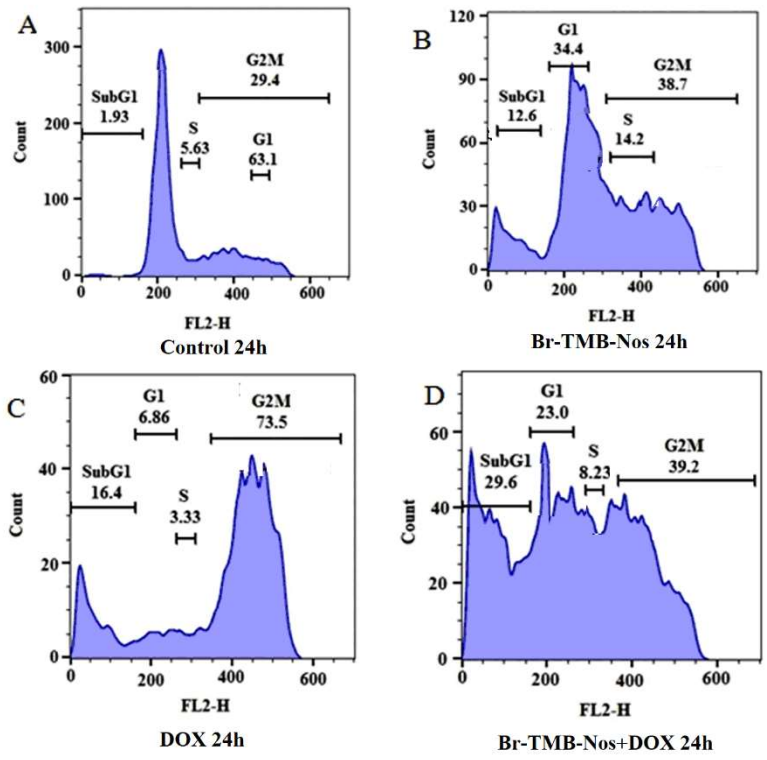

Figure 4.17. Figure A-D depict represented figures of analysis of cell cycle distribution in a two-dimensional disposition as determined by flow cytometry in MCF-7 cells with the treatment of Br-TMB-Nos (10 µM) and DOX (0.1 µM) in single as well as combination (25 µM of Br-TMB-Nos + 0.01 µM of DOX) for 24 hrs. The cells were arrested in the G_2/M

phase of cell cycle followed by the appearance of hypodiploid DNA peak (sub-G1) which indicates the apoptosis.

The effect of PYBA-Nos and DOX on the cell cycle profile of MCF-7 using FACS confirmed the induction of cell death (Figure 4.18). Fluorescently labelled DNA deposition is a reliable indication of cell cycle profile and cell death. The G1 process is represented by cells with 2N DNA, while cells with duplicated 4N DNA represents G2 and M phases. Cells in the DNA replication process with peaks of 2N and 4N reflect the S phase in which DNA is being synthesised, whereas cells with less than 2N DNA indicated that the cells are in dying stages. The treatment of MCF-7 cells with test compound PYBA-Nos for 24 h resulted in massive perturbations of the cell cycle profile. The FACS data suggests high deposition of cells in the G2/M phase at 24 hours of treatment with PYBA-Nos (25 μm) and DOX (0.01 μm) in single and in combination regimens (25 μm PYBA-Nos+0.01 μm DOX), relative to untreated cells. A characteristic hypodiploid DNA content peak (sub-G1) was shown to increase at 24 h of treatment relative to the G2/M block. Fragmented DNA is demonstrated by the progressive generation of cells with hypodiploid DNA content, suggesting dying of cells.

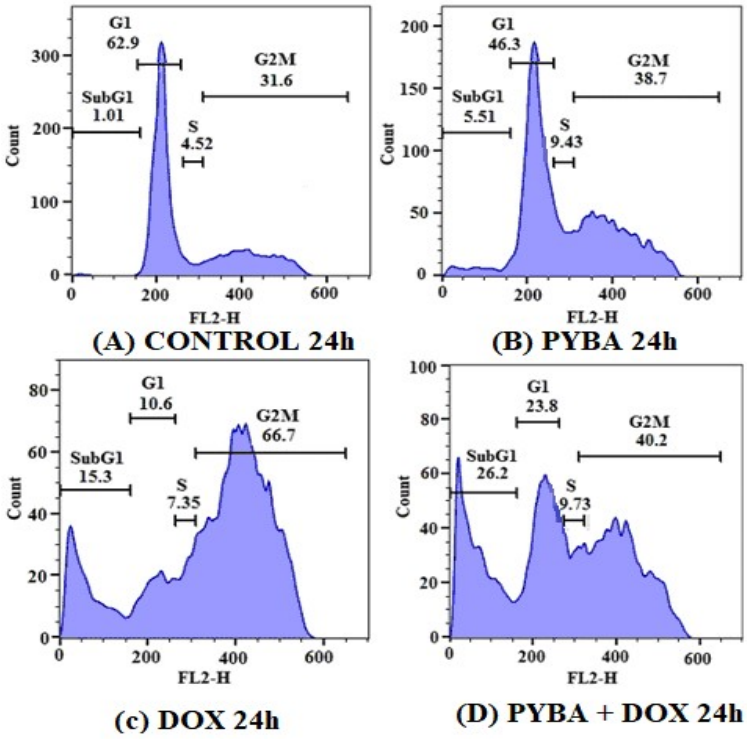

Figure 4.18. Panels (A) to (D) depicts cell cycle distribution of MCF-7 cells in a two-dimensional disposition as determined by flow cytometry at 24h of treatment with 25 µM of PYBA-Nos, 0.01 µM of DOX as single regimen and 25 µM of PYBA-Nos+0.01 µM of DOX in combination regimen. Results represent cell cycle progression at mitosis followed by the appearance of a characteristic hypodiploid (sub-G1) DNA peak is indicative of apoptosis.

Inhibition in the progression of cell cycle of MCF-7 with treatment of Br-Nos (25 µM) and DOX (0.01 µM) in single regimen as well as in combination regimen (25 µM Br-Nos+0.01 µM DOX) was also evaluated using flow cytometer. Both the compounds showed an increase in the sub-G1 cell populations compared to the control after 24 h of treatment in single and in combination regimen. The representative two-dimensional disposition of cell cycle profile is included in Figure 4.19. The sub-G1 population with treatment of Br-Nos was increased to 7.57%, whereas with DOX, it was increased to 16.4% and in combination it further increased to 23.2 % in comparison to control. High cell aggregation during the G2/M transition phase at 24 h of treatment compared to untreated cells was observed in the FACS analysis.

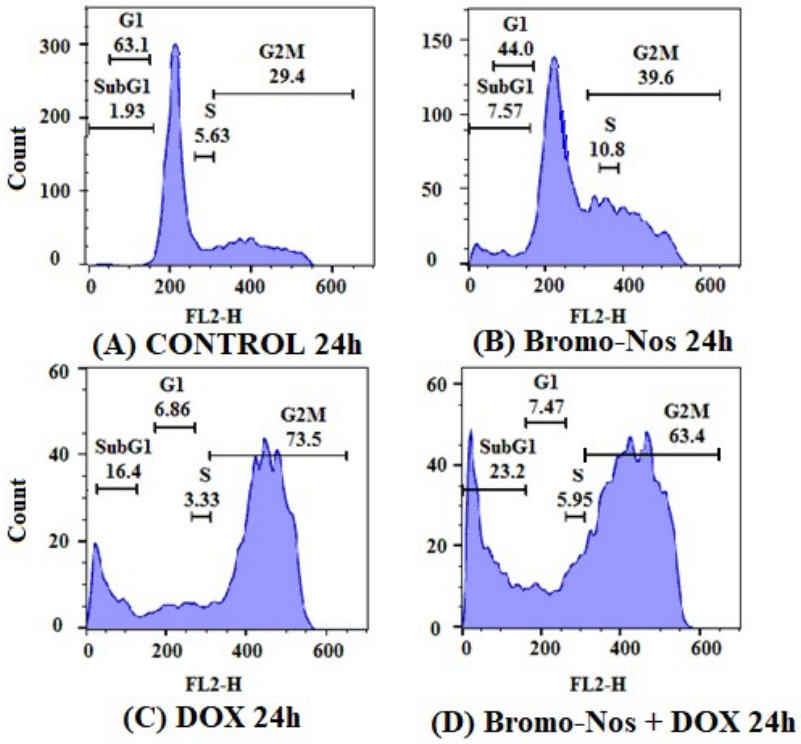

Figure 4.19. Bromo-Nos and DOX suppress the progression of the cell cycle at mitosis, indicated by characteristic hypodiploid (sub-G1) DNA peak, indicative of apoptosis. Figure A-D demonstrates the two-dimensional cell cycle distribution analysis as assessed by flow cytometry in MCF-7 cells treated with 25 μM of Bromo-Nos, 0.01 μM of DOX in single regimen, and 25 μM of Bromo-Nos + 0.01 μM of DOX in combination regimen.

4.5. Induction of apoptosis to MCF-7 cancer cells with the treatment of noscapinoids and DOX in single and in combination regimen

Biochemically, the apoptotic phase is characterized by alterations in the lipid composition between the two plasma membrane leaflets, *i.e*., phosphatidylserine, usually translocated to the outer leaflet, which can be determined by using a fluorescent dye, Annexin V. In contrast, the cell impairment DNA-binding fluorescent dye *i.e.,* propidium iodide can only enter the cells at the stage of late apoptosis when membrane permeability is compromised. Apoptotic cells can be quantified by FACS analysis. There were very few apoptotic cells (~2%) in the untreated cell cultures, which were assigned as the background cell death.

We approached to determine the induction of apoptotic cell death to breast cancer cell, MCF-7 by treatment of VPN and DOX in single as well as in combination regimen. In

FACS, green Annexin V staining was used together with an impermeant red DNA binding dye, 7-Amino-Actinomycin (7-AAD), to quantitate the population of apoptotic, necroptotic and necrotic cells. The results depict the density plots of 7-Amino-Actinomycin (7-AAD) versus PE conjugated Annexin V fluorescence obtained from untreated control and treated MCF-7 cells. Cells negative for both 7-AAD and Annexin V staining were viable cells (in the lower left quadrant: Q3); 7-AAD-negative, Annexin V-positive cells were early apoptotic cells (in the lower right quadrant: Q4); 7-AAD-positive, Annexin V-positive cells were primarily late apoptotic/necrotic cells (in the upper right quadrant: Q2); and the 7-AAD-positive but annexin V-negative cells were necrotic cells (in the upper left quadrant: Q1). As anticipated, MCF-7 cells treated with both VPN (20 μM) and DOX (0.5 μM) in single as well as in combination regimen (VPN 25 μM +DOX 0.05 μM) for a duration of 24 h resulted in significant increase of apoptotic cells compared to control untreated cells (Figure 4.20). The percentage of early apoptotic cells were measured to be 4.79%, 10.9%, 20.4% and late apoptotic cells were estimated to 5.97%, 3.8%,16.9%, respectively with treatment of VPN and DOX in single as well as in combination regimen after 24 h of post-treatment. The control untreated cell culture contained only very few early apoptotic (0.83% after 24 h post-treatment) and late apoptotic cells (2.17% after 24 h post-treatment), which were considered as the background cell death due to regular trauma during cell culture (Figure 4.20) (Dash et al., 2020). This is mainly because we have taken unstained cell for gating and put the stained control cells in the FACS analysis as per the standard protocol (Ji et al., 2017; Sivakumaran et al., 2018; Fan et al., 2018).

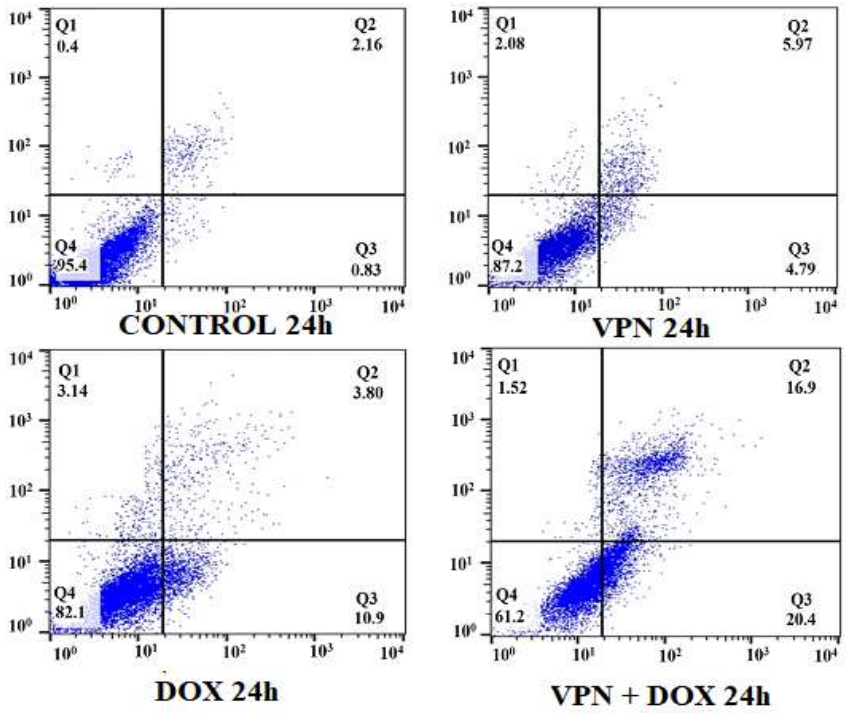

Figure 4.20. Induction of apoptosis caused by VPN (20 µM) and DOX (0.5 µM) alone and in their combination regimen (VPN, 25 µM+DOX, 0.05 µM) based on flow cytometric analysis. PE/Annexin V staining was used in combination with 7-Amino-Actinomycin (7-AAD) to distinguish among 4 subpopulations: cells negative for both 7-AAD and Annexin V staining were viable cells (in the lower left quadrant: Q3); 7-AAD-negative, Annexin V-positive cells were early apoptotic cells (in the lower right quadrant: Q4); 7-AAD-positive, Annexin V-positive cells were primarily late apoptotic/necrotic cells (in the upper right quadrant: Q2); and the 7-AAD-positive but annexin V-negative cells were necrotic cells (in the upper left quadrant: Q1).

Similarly, MCF-7 cells treated with Amino-Nos (25 µm) for 24 h showed both early and late apoptosis (4.12% and 2.42%) respectively. In contrast DOX (0.5 µm) demonstrates early and late apoptosis, 10.9% and 3.80% after 24 h. The combination treatment of DOX (0.05 µm) and amino-noscapine (25 µm) showed increased rate of early and late apoptosis (15.1% and 11.9%) 24 h post treatment (Figure 4.21).

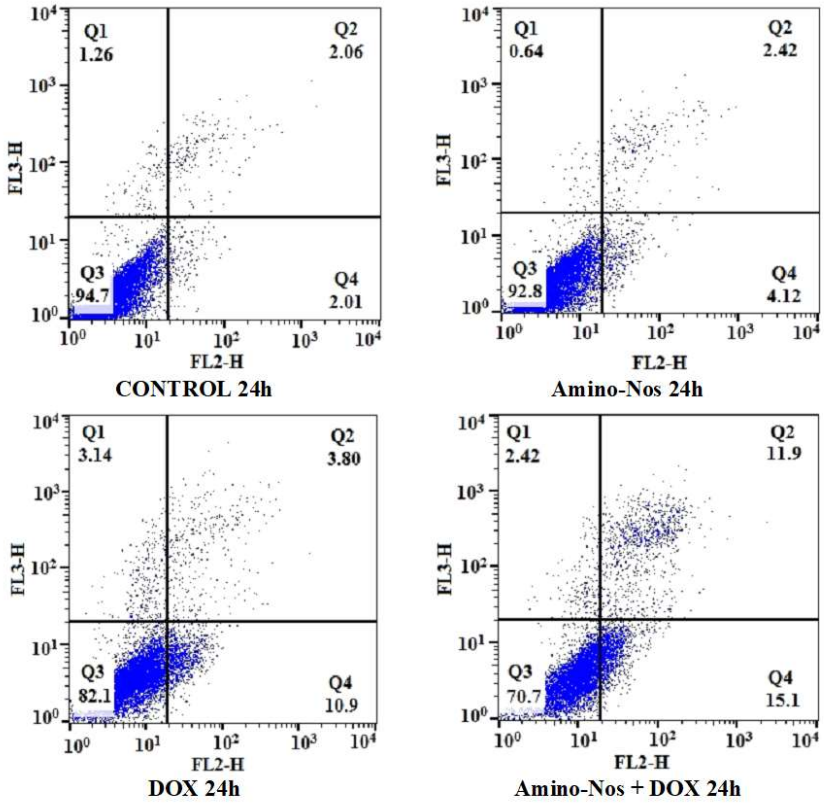

Figure 4.21. Induction of apoptosis caused by Amino-Nos (25 µM) and DOX (0.5 µM) alone and in their combination regimen (Amino-Nos, 25 µM+DOX, 0.05 µM) based on flow cytometric analysis.

The percentage of early and late apoptotic cells treated with combination of Br-Bn-Nos (25 µm) + DOX (0.01 µm) was 24.1% and 20.3%, which was significantly high compared to single regimen treatment with 25 µm Br-Bn-Nos (11.0 % and 3.73 %) or 0.1 µm DOX (10.9 % and 3.80 %) respectively after 48 h in comparison to control untreated cells. This study demonstrated that the proposed combination effect of Br-Bn-Nos and DOX not only induced apoptosis to cancer cell, but also provided a promising prospect to reduce the toxicity of DOX.

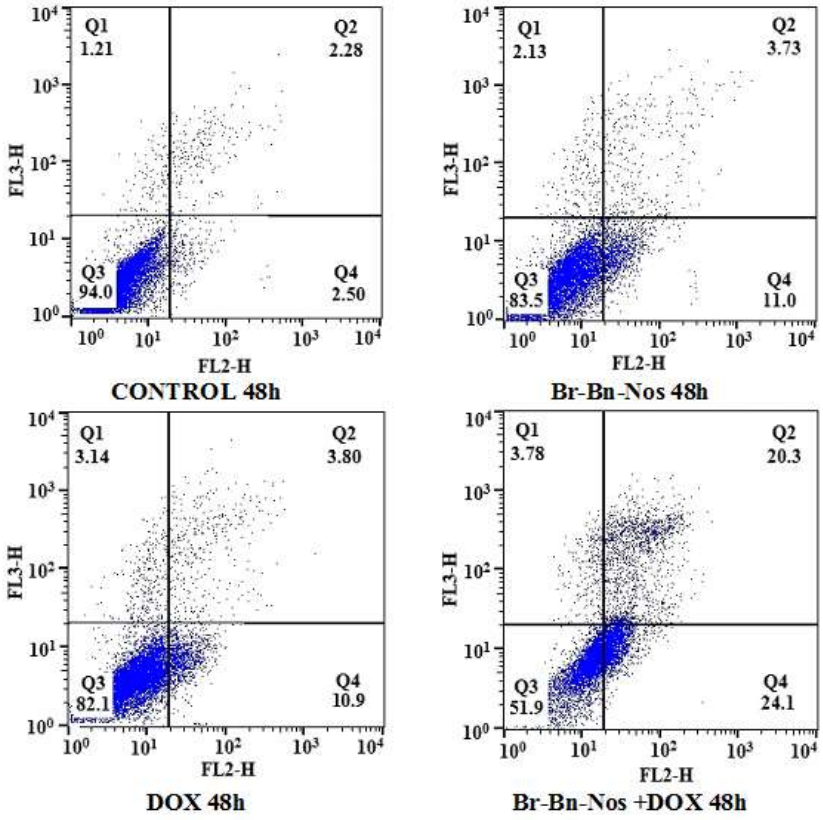

Figure 4.22. Flow cytometric observation of apoptosis cell death induced by Br-Bn-Nos alone and in combination with DOX. PE conjugate of Annexin V was used in combination with 7-Amino-Actinomycin (7-AAD) to distinguish among 3 subpopulations: PE^{--} and 7-AAD^{--} population indicates viable cells (bottom left quadrant); PE^{--} and 7-AAD^{+} population indicates early apoptotic cells (lower right quadrant); PE^{+} and 7-AAD^{+} population indicate late apoptotic cells (top right quadrant).

We next evaluated the induction of apoptosis by Br-TMB-Nos and DOX in single as well as in combination regimen; using 7-Amino-Actinomycin (7-AAD) versus PE-conjugated Annexin V fluorescence staining kit via flow cytometer. It was revealed that the number of apoptotic MCF-7 cells increased significantly after treatment of Br-TMB-Nos (10 μM) and DOX (0.1 μM) individually and in combination regimen (Br-TMB-Nos 25 μM+DOX 0.01 μM) for a duration of 24 h compared to the control group.

Cells in the first quadrant were necrotic cells, which were Annexin V negative cells. The second quadrant represented the late apoptotic cells that were both Annexin V and 7-AAD-positive cells, due to a loss of plasma membrane integrity. The third quadrant included normal viable cells and were not stained with either Annexin V or 7-AAD. The fourth

quadrant included the early apoptotic cells which were Annexin V positive cells. A significant increase in early and late apoptotic cells were identified with the treatment of Br-TMB-Nos and DOX in single as well as in combination regimen in comparison to the control group. The percentage of early apoptotic cells measured were 5.33%, 13.5%, 27.8%, and estimated late apoptotic cells were 6.37%, 4.77%, 13.7%, respectively with the treatment of Br-TMB-Nos and DOX in single as well as in combination regimen. The control untreated cells contain only very few early and late apoptotic cells (1.16 % and 2.17%), which were considered as the background cell death due to regular trauma during cell culture (Figure 4.23). This is mainly because we have taken unstained cells for gating and put the stained control cells in the FACS analysis as per the standard protocol (Sivakumaran et al., 2018; Fan et al., 2019; Ji et al., 2017).

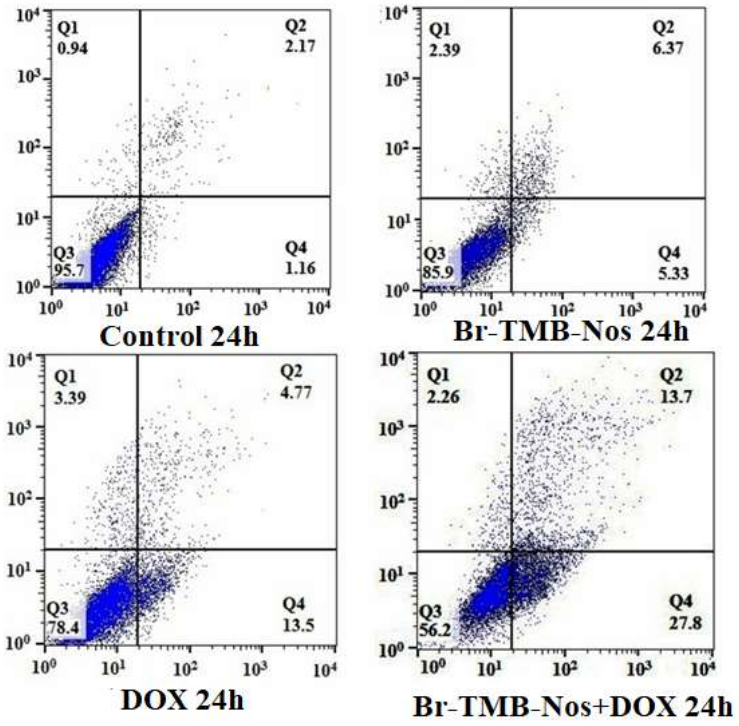

Figure 4.23. Flow cytometry analysis of phosphatidylserine (PS) exposure in MCF-7 cells treated with Br-TMB-Nos alone and in combination with DOX based on flow cytometric analysis for 24 h and compared with non-treated control cells. Representative results of three independent experiments.

Further, the noscapine derivative PYBA-Nos individually and in combination with DOX was evaluated in the induction of apoptotic cell death in breast cancer cells.

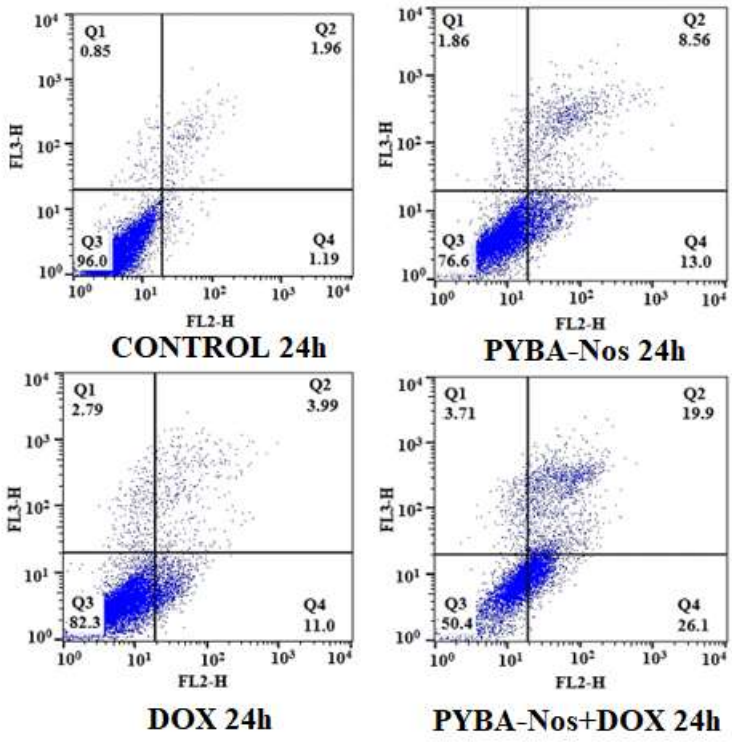

Figure 4.24. Flow cytometry analysis of phosphatidylserine (PS) exposure in MCF-7 cells treated with PYBA-Nos alone and in combination with DOX based on flow cytometric analysis for 24 hours and compared with non-treated control cells. Representative results of three independent experiments.

Figure 4.24 demonstrated the density plots obtained from untreated control and treated MCF-7 cells using 7-Amino-Actinomycin (7-AAD) against PE conjugated Annexin V fluorescence. As expected, the amount of early and late apoptotic cells was 26.1 % and 19.9 % with the combination treatment of PYBA-Nos (25 μm) + DOX (0.01 μm) which were remarkably high compared to single regimen treatment with 25 μm of PYBA-Nos (13.0 % and 8.56 %) or 0.01 μm of DOX (11.0 % and 3.99 %). This finding revealed that the combined effect of PYBA-Nos and DOX would not only efficiently induce apoptosis in cancer cells, but also represent a promising potential of reducing toxicity of DOX.

Parenthetically, significantly high percentage of early apoptotic cells of 12,5%, 14.1% and 21.3% as well as late apoptotic cells of 7.90%, 10.5% and 32.1%, respectively were found with the treatment of Br-Nos and DOX in single as well as in combination regimen after 24 hours (Figure 4.25). The control untreated cell contained only very few early apoptotic (2.01% after 24 h post-treatment) and late apoptotic cells (2.14% after 24 h post-treatment), which were considered as the background cell death.

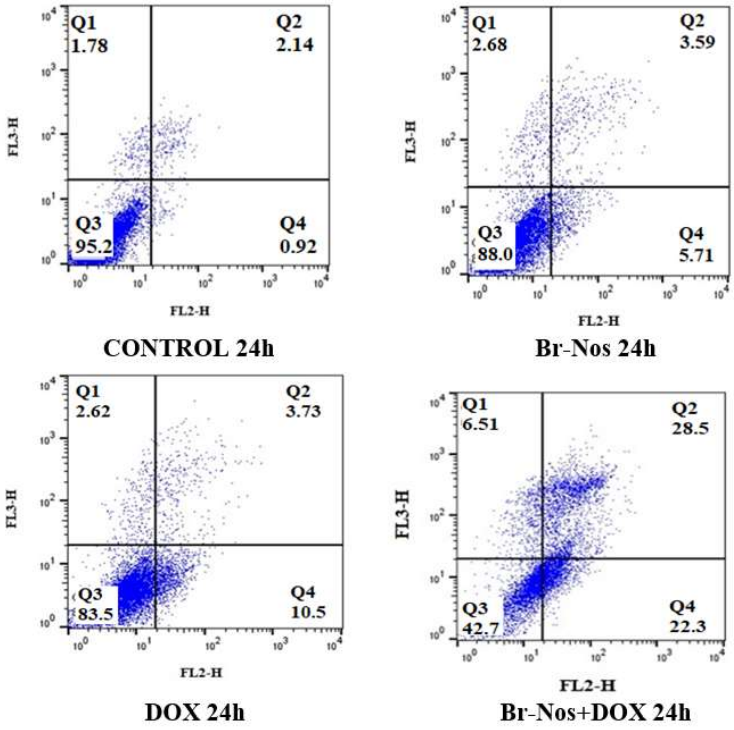

Figure 4.25. Flow cytometry analysis of phosphatidylserine (PS) exposure in MCF-7 cells treated with Br-Nos alone and in combination with DOX based on flow cytometric analysis for 24 hours and compared with non-treated control cells. Representative results of three independent experiments.

4.6. DAPI staining

The induction of apoptosis to cancer cells were observed under the inverted fluorescence microscope after treatment of noscapinoids and DOX in single as well as in combination. The apoptotic cells have significant alteration in the membrane architecture, blebbing of plasma membrane, chromatin condensation and chromosomal breakdown (apoptotic bodies) which could be visualized using the 4′, 6-diamidino-2-phenylindole

(DAPI) fluorescent dye. The compounds in both single and in combination, efficiently induced apoptosis to cancer cell as revealed in the (Figure 4.26).

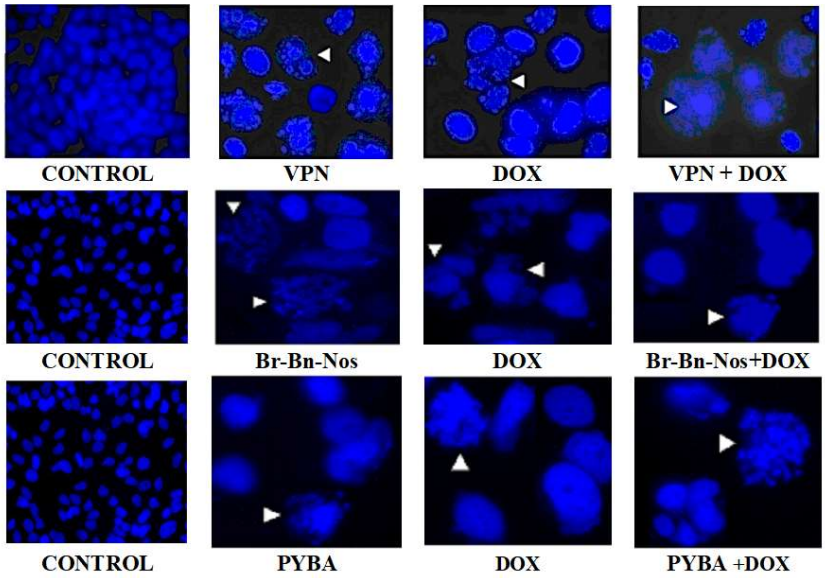

Figure 4.26. Morphologic indicators of apoptotic cell death include chromatin condensation along with nuclear envelope and plasma membrane blebbing followed by formation of small apoptotic bodies. Representative panels show morphological evaluation of nuclei stained with DAPI in the absence and presence of the Noscapinoids (10 µM) and DOX (0.01 µM) in single as well as in combination regimen with docetaxel. Several typical features of apoptotic cells such as condensed chromosomes, numerous fragmented micronuclei, and apoptotic bodies are evident (indicated by white head arrows) upon 48 hours of drug treatment. (Scale bar = 15 µm).

We also validated the results by an immunofluorescence-based focus-forming assay using noscapinoids and DOX in single as well as in combination and we got the similar results represented in figure 4.27.

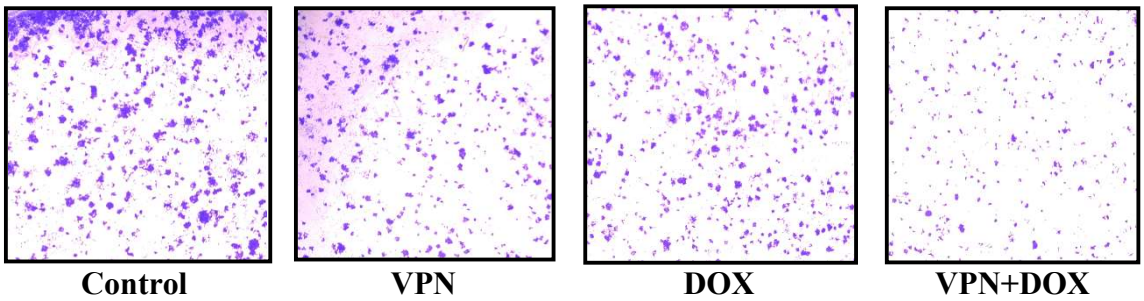

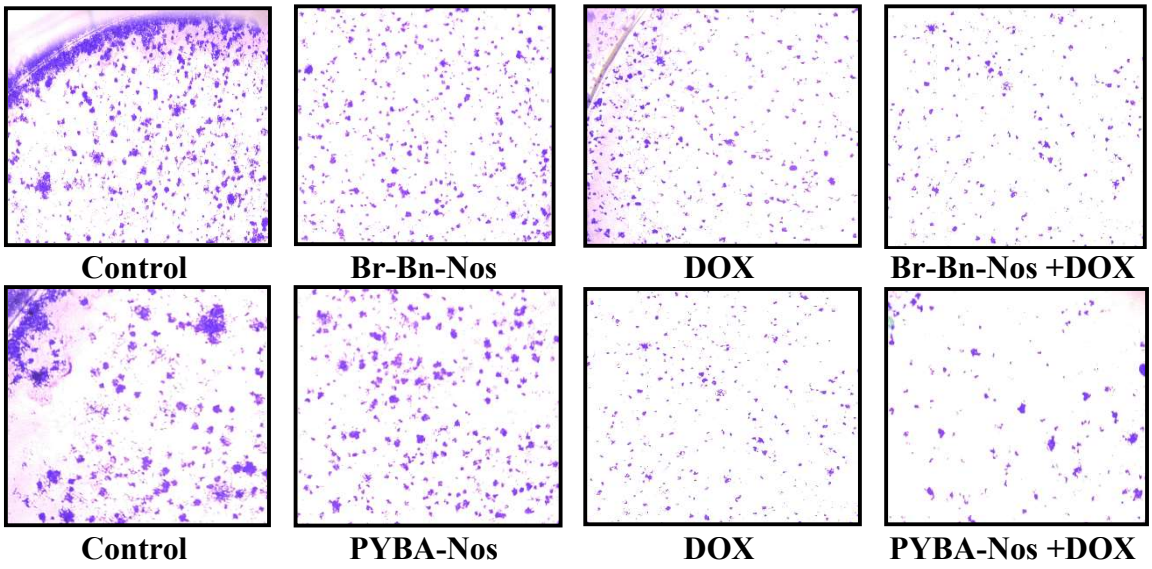

Figure 4.27. Foci formation assay using MCF-7 cells (treated with selected derivatives of noscapinoids (10 μM) and DOX (0.01 μM) in single as well as in combination regimen with docetaxel.

4.7. Tubulin binding activity of noscapinoids and DOX in single as well as in combination treatment (Tryptophan Quenching Assay)

The innate ability of proteins to display the intrinsic fluorescence provided a way to understand the environmental changes after interaction with the quencher. Tubulin is autofluorescence due to presence of tryptophan amino acid. Tryptophan (Trp), tyrosine (Tyr) and phenylalanine (Phe) are the three natural aromatic amino acids that are fluorescent in nature, but Trp does have highest fluorescence quantum yield (Sood et al., 2018). Any alteration in the conformation of protein due to ligand binding decreases the emission fluorescence - a standard tool used to recognize a ligand binding with protein. In order to experimentally validate our findings based on molecular modelling study with respect to the tubulin-binding affinity of noscapinoids and DOX in single as well as in their combination; we determined the quenching of fluorescence intensity of tubulin with the treatment of both the agents in single as well as in combination regimen. The decrease in fluorescence intensity with the treatment of Br-TMB-Nos (25 μm) and DOX (0.1 μm) suggested the binding of both the compounds to tubulin. The percentage reduction in fluorescence

intensity was 30.03 % and 52 %, respectively in the presence of 25 μm Br-TMB-Nos and 0.1 μm DOX. Further reduction in fluorescence intensity of 62.7% respectively (Figure 4.28a) were observed in the combination treatment (DOX 0.01 μm + Br-TMB-Nos 25 μm). The proportional percentage of reduction in fluorescence intensity was 32.39 % and 50.03 % respectively in the presence of 25 μm PYBA-Nos and 0.1 μm DOX and 61 % in the combination of DOX (0.01 μm) and PYBA (25 μm) (Figure 4.28b). The dynamic reduction in fluorescence intensity of tubulin in presence of noscapinoids and docetaxel in single as well as in combination regimen indicated the binding of both the compounds with tubulin.

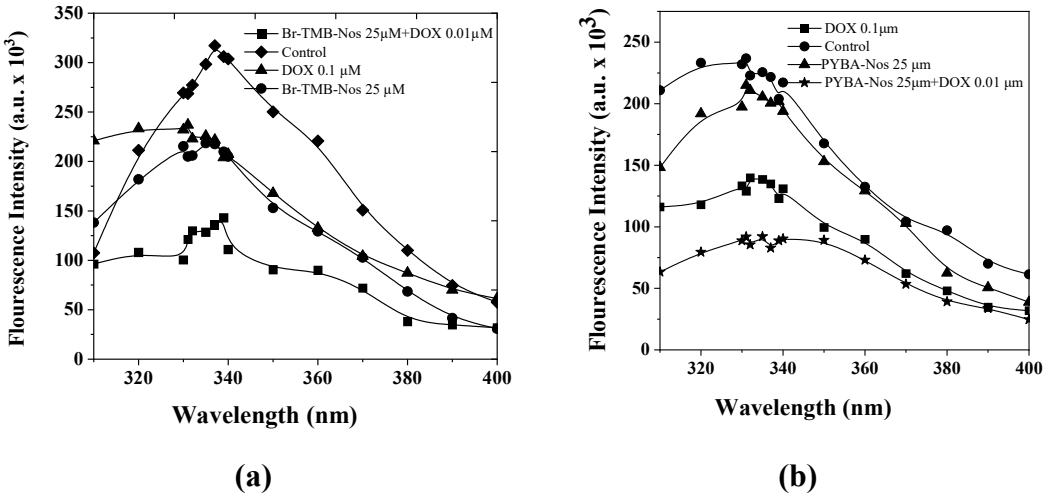

Figure 4.28. Representative figures of decrease of fluorescence intensity of tubulin by (a) PYBA-Noscapine and (b) Br-TMB-Noscapine in single as well as in combination regimen with docetaxel (DOX). Tubulin (2 μM) was incubated with indicated concentration of noscapinoids and DOX alone as well as in combination and the emission spectra were collected (310 nm – 400 nm). The graph is a representative of three independent experiments.

4.8. Effects of noscapinoids and DOX on ANS-tubulin fluorescence in single and combination treatment

In order to further investigate the conformational changes in tubulin due to binding of noscapinoids and DOX in single as well as in combination regimen, we probed the purified tubulin with ANS (8-anillino-1-naphthalenesulfonic acid). ANS is a fluorescent probe that bound to hydrophobic patches on proteins and improves the fluorescence when

attached to protein. An increase in ANS fluorescence of tubulin suggests a loss of protein structural integrity. Purified tubulin with the treatment of PYBA-Nos and DOX showed an increase in tubulin-ANS fluorescence intensity (Figure 4.29). It displayed a 25.07% increase in fluorescence intensity at 25 µM PYBA-Nos, and 42.39% in presence of 0.1 µM of DOX compared to unbound tubulin. Similarly, in combination treatment with PYBA-Nos (25 µM) and DOX (0.01 µM) the tubulin-ANS fluorescence intensity was further increased to 52.25%. We also analysed the effect of Br-TMB-Nos (25 µm) and DOX (0.1 µm) on transitions of tubulin conformation. Treatment of tubulin with Br-TMB-Nos and DOX in single and in combination demonstrated a significant improvement in tubulin-ANS fluorescence intensity (Figure 4.29a).

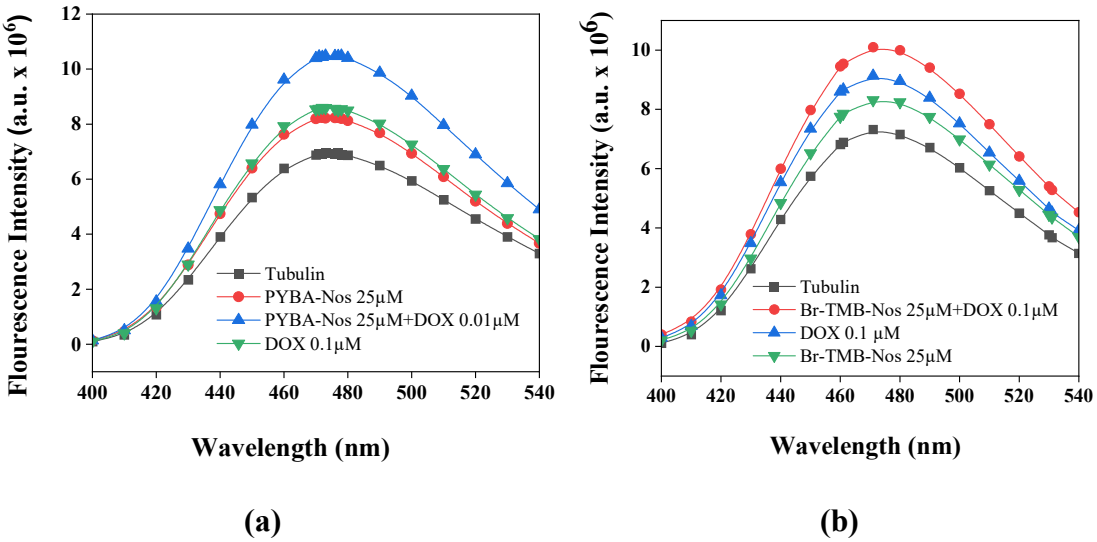

Figure 4.29. Representative figures of enhancement of tubulin-ANS fluorescence by (a) PYBA-Noscapine and (b) Br-TMB-Noscapine in single as well as in combination regimen with docetaxel (DOX). Tubulin (2 µM) was incubated with Noscapinoids at desired concentration with DOX and in their combination, regimen followed by incubation with ANS (50 µM). The samples were excited at 380 nm and the emission spectra were collected (400 nm – 500 nm).

The fluorescence intensity was increased to 34.28 % with the treatment of 25 µM of Br-TMB-Nos, 42.29 % with 0.1 µM of DOX compared to unbound tubulin. In contrast, combination effect of both the compounds, DOX 0.01 µM + Br-TMB-Nos 25 µM, increased the fluorescence intensity of the tubulin-ANS to 52 % respectively (Figure 4.29b).

4.9. Reduction in tumor volume with treatment of Br-TMB-Nos and DOX in single and in combination regimen against MCF-7 xenograft animal model

Treatment with Br-TMB-Nos (150 mg/kg/day), DOX (1.5 mg/kg/week, i.v), or in combination (Br-TMB-Nos 300 mg/kg/day+DOX 1.0 mg/kg/week, i.v,) considerably decreased tumour volume in comparison to control ($P < 0.001$) (Figure. 4.30A). Tumor volume was reduced to 630 mm^3 with combination treatment, 960 mm^3 with DOX and 1145 mm^3 from the tumor size of 1630 mm^3 from the untreated control group on day 40 post tumour implantation. On 40^{th} day tumor cell inoculation, mice were sacrified and tumors were removed and weighted. All untreated mice developed solid tumors in sizes ranging from 4.5g to 10.5 g (mean 7.8 ± 2.0 g). Whereas, among the treated groups the tumor size was significantly regressed and showed only small palpable tumors. Figure 4.30B shows the mean tumor weight±standard error of control and experimental mice. Compared to untreated control mice, inhibition of tumor growth by the treatment of Br- TMB-Nos and DOX in single and in combination regimen was statistically significant ($p < 0.001$). It is clear from these data that combination treatment of both Br-TMB-Nos and DOX reduces the tumor size quite dramatically compared to single regimen treatment of Br-TMB-Nos and DOX. In addition, we did not observe any apparent weight loss after drug treatment compared to control group of mice (Figure 4.30C).

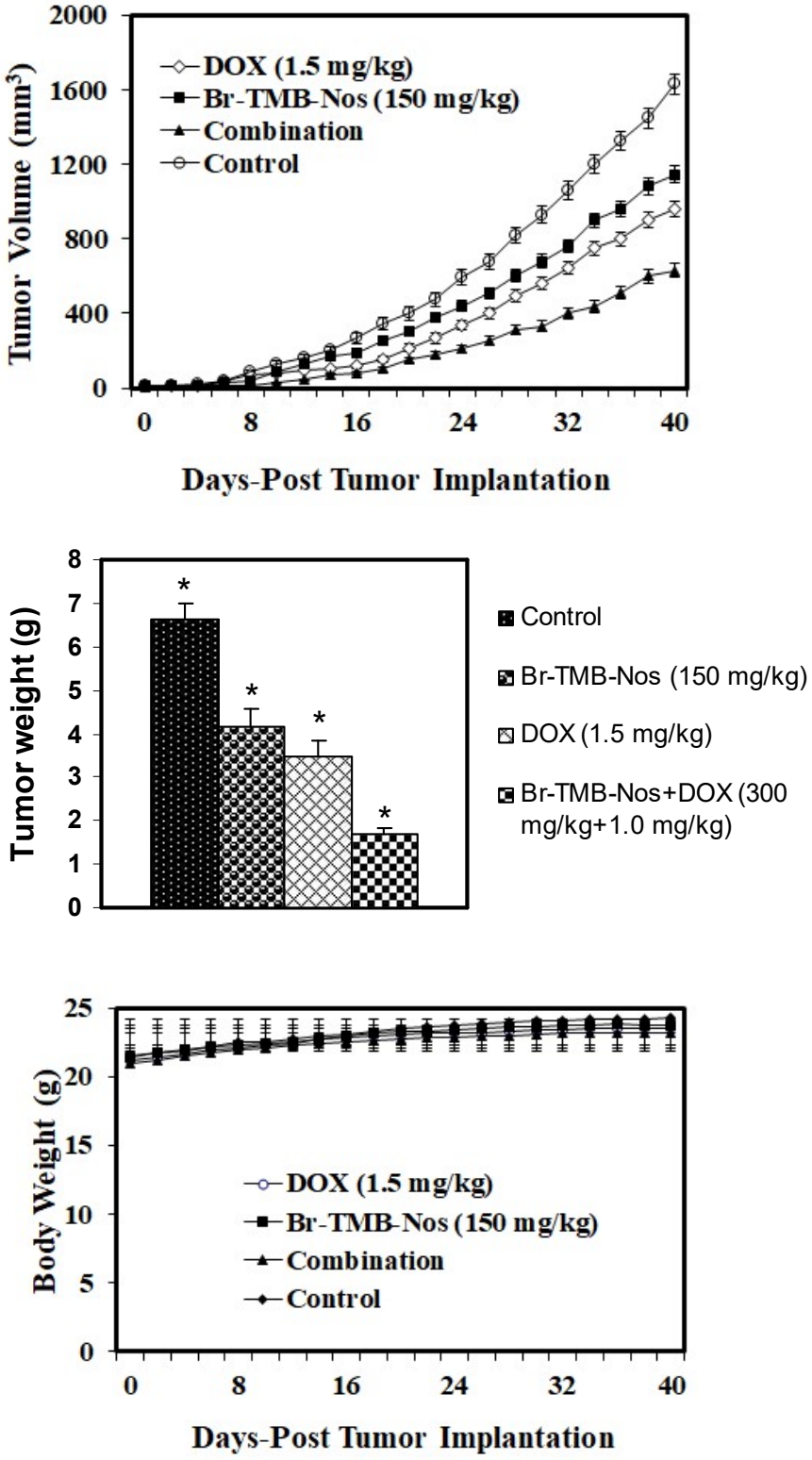

Figure 4.30. (A) Progression profile of tumor growth kinetics of in-vivo antitumor effect of therapeutics doses of Br-TMB-Nos and DOX alone and in combination regimen on human MCF-7 tumor xenograft model (tumor volumes, $mm^3 \pm$ SEM), (B) and measurement of body weight following Br TMB-Nos alone, DOX alone and in combination regimen. Female nude mice with xenograft MCF-7 tumors received various treatments for 30 days starting

on day 7 post tumor implantation. The mice were treated with Br-TMB-Nos (150mg/kg/day), DOX (1.5 mg/kg i.v.) and Br-TMB-Nos 300 mg/kg/day+DOX 1.0 mg/kg/week. Control group received vehicle only. Statistical significance of the difference in tumor volume of treatment groups compared with control. $P<0.01$ (*, significantly different from untreated controls; **, significantly different from Br-TMB-Nos and DOX single treatments). This experiment was repeated twice.

4.9.1. Treatment of Br-TMB-Nos and DOX in single and in combination does not cause any detectable toxicity

The severe side effects during chemotherapeutics are a major concern in the treatment of cancer patients. Tubulin binding agents for example, vinca alkaloids and taxanes, while clinically approved, are known to cause adverse side effects (Rowinsky et al., 1997). As a result, there is a need to identify a drug regimen that is both safe and well-tolerated. We examined the liver, kidney, spleen, lung, heart, brain, and colon of tumor-bearing mice to see if Br-TMB-Nos and DOX in single as well as in combination treatment causes toxicity to normal tissues. Treatment with the compound Br-TMB-Nos at daily doses of 150 mg/kg, DOX at a tolerated dose of 1.5 mg/kg body weight once in a week and in their combination treatment (Br-TMB-Nos 300 mg/kg/day+DOX 1.0 mg/kg/week, iv) failed to reveal any detectable pathological abnormalities in normal tissues involved in normal cell proliferation. Figure 4.31 collated at 200x magnification of H&E staining of paraffin-embedded 5.0 micron-thick sections of the liver, kidney, spleen, lung, heart, colon, and brain. Microsections of brain did not reveal any infracted areas. The liver showed normal hepatic lobular architecture. The kidneys revealed normal glomeruli, proximal and distal tubules, interstitium and blood vessels. The heart muscle showed normal morphology among the groups. The lung tissue showed normal alveoli and bronchial airways. Furthermore, we observed differences in hematological parameters between treated and control animals.

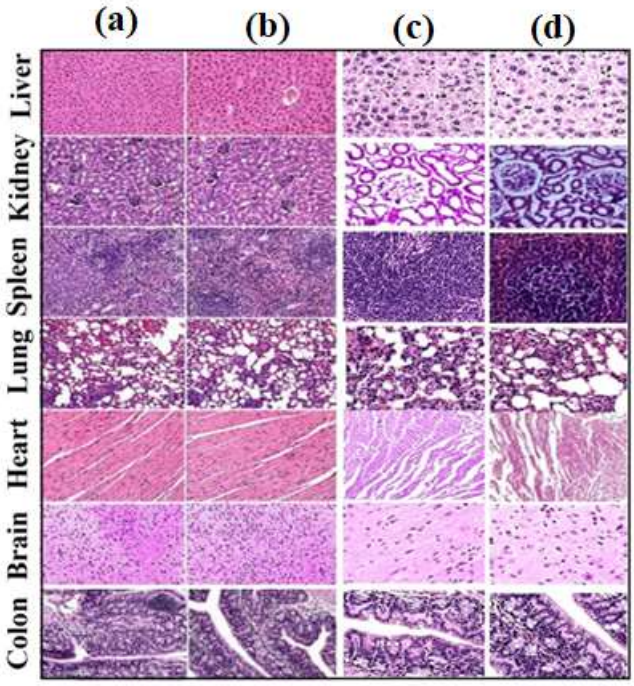

Figure 4.31. Represent H&E staining of paraffin-embedded 5.0 micron-thick sections of (a)Vehicle, (b) Br-TMB-Nos (150 mg/kg/day), (c) DOX (1.5 mg/kg/week), (d) (Br-TMB-Nos 300 mg/kg/day + DOX 1.0 mg/kg/week, the colon, brain, heart, lung, spleen, kidney and liver at a magnification of 200x.

Conclusion

Tubulin remains a persistent and promising target for anti-cancer therapy. This is well validated by the already approved clinically used drug classes such as toxoids and vincas. Tubulin binding drugs such as taxanes and vinca alkaloids are the most efficient anticancer agents for breast cancer treatment (Chougule et al., 2011). Docetaxel is widely used as a chemotherapy agent for patients with advanced breast cancer who have failed to respond to other treatments (Kleeberg et al., 2003). However, docetaxel-related serious side effects such as neutropenia, fluid retention, hair loss, nail changes and hypersensitivity reactions can compromise its clinical efficacy (Baker et al., 2009). Controlling side effects associated with docetaxel therapy may improve the quality of life and treatment outcomes in cancer patients. Chemotherapeutics side effects are also associated with increased in free radicals and related oxidative damage in normal human cells (Weijl et al., 1997). It is becoming well-appreciated that a toxic drug at its maximum tolerated dose given intermittently is not necessarily better and there exists an opportunity to reduce its dose levels by using combination regimens of drugs that display synergistic interactions (Jordan and Wilson, 2004). Poor clinical prospects of the current chemotherapeutic agents have triggered the development of new treatment modalities such as combination therapy for breast cancer. However, due to the emergence of drug resistance and the subsequent serious side effects, their therapeutic utility is limited (Doddapaneni et al., 2016). In contrast, noscapine, a less toxic orally administered anti-microtubule agent, clearly indicates antitumor activity *in vitro* and *in vivo* against a number of cancers (Laden et al., 2002; Zohu et al., 2002; Zhou et al., 2006). Noscapinoids as anticancer agents influence subtly modulate microtubule dynamicity, making them gentler than other microtubule-targeting drugs currently on the market (Stanton et al., 2011; Zhang & Kanakkanthara, 2020; De Bono et al., 2015; Seetharaman and Rajan,

1995). The ability to modify and synthesize noscapine with new derivatives, as well as the drug's efficacy against multiple cancer cell lines, demonstrates the drug's potency and signifies the future encampment of noscapinoids for cancer treatment. This distinguishing feature of noscapinoids is driving it to the forefront of research into cellular activities that rely on microtubule dynamics. Superior microtubule-interfering agents with increased antiproliferative activity were found to be water-soluble analogues, inhibiting cancer cell proliferation effectively in comparison to the lead molecule. The determination of the optimum mass ratio is another important factor for each component within a combination drug delivery system. Therefore, to decrease the severe side effects of docetaxel and increase its anti-cancer effectiveness we adopted a combination treatment with the derivatives of noscapine. Our present *in vitro* study showed that a combination of noscapinoids and docetaxel is effective against MCF-7 cells by inhibiting cell proliferating assay, inducing apoptosis and cell cycle kinetics suggesting a novel therapeutic strategy to improve the treatment efficiency of breast cancer therapy.

The extensive molecular modelling study involving molecular docking, molecular dynamic simulation and MM-GBSA/MM-PBSA calculation revealed strong binding of both noscapinoids and docetaxel with tubulin. Further, both the drug molecules were found to bound with tubulin during the entire period of simulation and were well accommodated within the binding cavity. The calculated binding energy of noscapinoids and docetaxel in terms of molecular docking and MM-GBSA/MM-PBSA was found to be significantly reduced when both the molecules were co-docked together onto tubulin compared to their single interaction, indicating combination effect of both the molecules. In a quest of experimentally validate the chances of combination effects of noscapionoids, (Br-Bn-Nos, VPN-Nos, PYBA-Nos, Br-Nos, Amino-Nos, Br-TMB-Nos) with docetaxel (DOX), these noscapinoids were chemically synthesised as per the synthetic scheme

published earlier. We have performed extensive cellular and biochemical assays to validate the improvement in anticancer activity when both the class of molecules were applied in combination compared to their single regimen treatment. Antiproliferative activity of noscapinoids and docetaxel in single as well as in combination regimen using MCF-7 breast cancer cells revealed significant improvement in their activity when applied in combination compared to single regimen treatment. Further, isobolographic method of evaluation between both the class of molecules revealed a synergistic antiproliferative activity. Similarly, the combination regimen of noscapinoids and docetaxel effectively interfered with the cell cycle progression of cancer cells compared to their single regimen treatment. It was also observed that cytotoxicity of noscapinoids is mediated by perturbed DNA synthesis, delayed cell cycle progression at S phase, enhanced fragmentation of DNA in the sub G1 population, arrest of cell cycle at G2/M phase and subsequently induced apoptosis. The induction of apoptosis to cancer cell is clearly evidenced by altered plasma membrane asymmetry and fragmentation of nuclear DNA. Further, the theoretical prediction of co-binding of both the molecules with microtubule was experimentally validated based on tubulin binding assay with purified tubulin. We found significantly high binding affinity between both the molecules when applied in combination compared to single regimen treatment. The antitumor activity of noscapinoids and docetaxel in their single regiment treatment and in their combination, effect was evaluated by taking a xenograft nude mice model and administrating both the molecules in single as well as in combination regimen. We administered a normal therapeutic dose of one noscapinoid derivative, Br-TMB-Nos 300 mg/kg/day by oral gavage and docetaxel 1.0 mg/kg/week by i.v. injection to assess the combination potential of the two drugs. Our *in vivo* results demonstrated that a combination treatment of both the molecules exhibited a synergistic effect. The tumor volume was found to be significantly regressed in combination treatment

compared to single regimen treatment. Surprisingly, no toxicity has been noticed with the vital organs or in blood biochemistry in either single or in combination treatment, indicating that high doses of noscapinoids and low doses of docetaxel have a favourable toxicity profile.

In conclusion all these results taken together based on molecular modelling, cellular, biochemical studies and *in vivo* animal experiments revealed the combination effect of noscapinoids and docetaxel, compensating for the lack of previous docetaxel-based combination therapy studies. Finally, we established a proof-of-concept that a rational combination of noscapinoids and docetaxel could generate synergistic effects on cancer treatment, which is a highly promising and novel approach for the treatment of breast cancer.

REFERENCES

- Abotaleb, M., Samuel, S. M., Varghese, E., Varghese, S., Kubatka, P., Liskova, A., & Büsselberg, D. (2018). Flavonoids in Cancer and Apoptosis. *Cancers*, *11*(1), 28. https://doi.org/10.3390/cancers11010028.
- Aleshin, V. A., Artiukhov, A. V., Oppermann, H., Kazantsev, A. V., Lukashev, N. V., & Bunik, V. I. (2015). Mitochondrial Impairment May Increase Cellular NAD(P)H: Resazurin Oxidoreductase Activity, Perturbing the NAD(P)H-Based Viability Assays. *Cells*, *4*(3), 427–451. https://doi.org/10.3390/cells4030427.
- Anderson, J.T., Ting, A.E., Boozer, S., Brunden, K.R., Danzig, J., Dent, T., Harrington, J.J., Murphy, S.M., Perry, R., Raber, A., Rundlett, S.E., Wang, J., Wang, N., and Bennani, Y.L. (2005). Discovery of S-phase arresting agents derived from noscapine. *Journal of medicinal chemistry*, *48*(8), 2756-2758. https://doi.org/10.1021/jm0494220.
- Aneja, R., Kalia, V., Ahmed, R., and Joshi, H.C. (2007). Nonimmunosuppressive chemotherapy: EM011-treated mice mount normal T-cell responses to an acute lymphocytic choriomeningitis virus infection. *Molecular Cancer Therapy*, 6, 2891-2899.
- Aneja, R., Vangapandu, S. N., Lopus, M., Viswesarappa, V. G., Dhiman, N., Verma, A., Chandra, R., Panda, D., & Joshi, H. C. (2006). Synthesis of microtubule-interfering halogenated noscapine analogs that perturb mitosis in cancer cells followed by cell death. *Biochemical pharmacology*, *72*(4), 415–426. https://doi.org/10.1016/j.bcp.2006.05.004
- Aneja, R., Vangapandu, S.N., & Joshi, H.C. (2006). Synthesis and biological evaluation of a cyclic ether fluorinated noscapine analog. *Bioorganic & medicinal chemistry*, *14*(24), 8352-8358. https://doi.org/10.1016/j.bmc.2006.09.012.
- Aneja, R., Vangapandu, S.N., Lopus, M., Chandra, R., Panda, D., and Joshi, H.C. (2006). Development of a novel nitro-derivative of noscapine for the potential treatment of drug-resistant ovarian cancer and T-cell lymphoma. *Molecular pharmacology*, *69*(6), 1801-1809. https://doi.org/10.1124/mol.105.021899.

- Arruebo, M., Vilaboa, N., Sáez-Gutierrez, B., Lambea, J., Tres, A., Valladares, M., and González-Fernández, A. (2011). Assessment of the evolution of cancer treatment therapies. *Cancers*, *3*(3), 3279-3330. https://doi.org/10.3390/cancers3033279.
- Baker, J., Ajani, J., Scotté, F., Winther, D., Martin, M., Aapro, M. S., & von Minckwitz, G. (2009). Docetaxel-related side effects and their management. European journal of oncology nursing : the official journal of European Oncology Nursing Society, 13(1), 49–59. https://doi.org/10.1016/j.ejon.2008.10.003.
- Bateman, E.D., Hurd, S.S., Barnes, P.J., Bousquet, J., Drazen, J.M., FitzGerald, M., Gibson, P., Ohta, K., Byrne, P.O., Pedersen, S.E., Pizzichini, E., Sullivan, S.D., Wenzel, S.E., Zar, H.J. (2008). *European Respiratory Journal* 31: 143-178; https://doi.org/ 10.1183/09031936.00138707.
- Bayat Mokhtari, R., Homayouni, T.S., Baluch, N., Morgatskaya, E., Kumar, S., Das, B., and Yeger, H. (2017). Combination therapy in combating cancer. *Oncotarget*, *8*(23), 38022-38043. https://doi.org/10.18632/oncotarget.16723.
- Becke, A.D. (1993). A new mixing of Hartree-Fock and local density-functional theories. The Journal of Chemical Physics, 98, 1372-1377. https://doi.org/10.1063/1.464304.
- Beer, T.M., El-Geneidi, M., and Eilers, K.M. (2003). Docetaxel (taxotere) in the treatment of prostate cancer. *Expert review of anticancer therapy*, *3*(3), 261-268. https://doi.org/10.1586/14737140.3.3.261.
- Binkley, J.S., Pople, J.A., & Hehre, W.J. (1980). Self-consistent molecular orbital methods. 21. Small split-valence basis sets for first-row elements. Journal of the American Chemical Society, 102, 939-947. https://doi.org/10.1021/ja00374a017.
- Bissery, M.C., Guenard, D., Gueritte-Voegelein, F., & Lavelle, F. (1991). Experimental antitumor activity of taxotere (RP 56976, NSC 628503), a taxol analogue. *Cancer research*, *51*(18), 4845-4852.
- Bolser D.C. (2006). Cough suppressant and pharmacologic protussive therapy: ACCP evidence-based clinical practice guidelines. *Chest*, *129* (1 Suppl), 238S-249S. https://doi.org/10.1378/chest.129.1_suppl.238S.

- Bradford, M.M., (1976). A rapid and sensitive method for the quantitation of microgram quantities of protein utilizing the principle of protein-dye binding. Analytical Biochemistry, 72, 248-254. doi: 10.1006/abio.1976.9999.
- Canales, A., Rodríguez-Salarichs, J., Trigili, C., Nieto, L., Coderch, C., Andreu, J. M., Paterson, I., Jiménez-Barbero, J., & Díaz, J. F. (2011). Insights into the interaction of discodermolide and docetaxel with tubulin. Mapping the binding sites of microtubule-stabilizing agents by using an integrated NMR and computational approach. *ACS chemical biology*, *6*(8), 789–799. https://doi.org/10.1021/cb200099u.
- Case, D.A., Betz, R.M., Cerutti, D.S., Cheatham, T.E. III, Darden, T.A., Duke, R.E., Giese, T.J., Gohlke, H., Goetz, A.W., Homeyer, N., Izadi, S., Janowski, P., Kaus, J., Kovalenko, A., Lee, T.S., LeGrand, S., Li, P., Lin, C., Luchko, T., Luo, R., Madej, B., Mermelstein, D., Merz, K.M., Monard, G., Nguyen, H., Nguyen, H.T., Omelyan, I., Onufriev, A., Roe, D.R., Roitberg, A., Sagui, C., Simmerling, C.L., Botello-Smith, W.M., Swails, J., Walker, R.C., Wang, J., Wolf, R.M., Wu, X., Xiao, L., & Kollman, P.A. (2016). AMBER 2016, University of California, San Francisco.
- Checchi, P. M., Nettles, J. H., Zhou, J., Snyder, J. P., & Joshi, H. C. (2003). Microtubule-interacting drugs for cancer treatment. *Trends in pharmacological sciences*, *24*(7), 361–365. https://doi.org/10.1016/S0165-6147(03)00161-5
- Chougule, M. B., Patel, A. R., Jackson, T., & Singh, M. (2011). Antitumor activity of Noscapine in combination with Doxorubicin in triple negative breast cancer. *PloS one*, *6*(3), e17733. https://doi.org/10.1371/journal.pone.0017733.
- Chougule, M., Patel, A.R., Sachdeva, P., Jackson, T., and Singh, M. (2011). Anticancer activity of Noscapine, an opioid alkaloid in combination with Cisplatin in human non-small cell lung cancer. *Lung cancer (Amsterdam, Netherlands)*, *71*(3), 271-282. https://doi.org/10.1016/j.lungcan.2010.06.002.
- Correia, J. J., & Lobert, S. (2001). Physiochemical aspects of tubulin-interacting antimitotic drugs. *Current pharmaceutical design*, *7*(13), 1213–1228. https://doi.org/10.2174/1381612013397438.

- Correia, J.J., Beth, A.H., & Williams, R.C., Jr (1988). Tubulin exchanges divalent cations at both guanine nucleotide-binding sites. *The Journal of biological chemistry*, *263*(22), 10681-10686.
- Cortes, J. E., and Pazdur, R. (1995). Docetaxel. *Journal of clinical oncology: official journal of the American Society of Clinical Oncology*, *13*(10), 2643-2655. https://doi.org/10.1200/JCO.1995.13.10.2643.
- Cross JB, Thompson DC, Rai BK, Baber JC, Fan KY, Hu Y and Humblet C (2009). Comparison of several molecular docking programs: pose prediction and virtual screening accuracy. Journal of Chemical Information and Modeling 49: 1455-1474.
- Darden, T., York, D., & Pedersen, L. (1993). Particle mesh Ewald: An N. log (N) method for Ewald sums in large systems. The Journal of Chemical Physics, 98(12), 10089-10092. https://doi.org/10.1063/1.464397.
- Dash, S. G., Kantevari, S., Pandey, S. K., & Naik, P. K. (2021). Synergistic interaction of N-3-Br-benzyl-noscapine and docetaxel abrogates oncogenic potential of breast cancer cells. *Chemical biology & drug design*, *98*(3), 466–479. https://doi.org/10.1111/cbdd.13902
- Dash, S. G., Suri, C., Nagireddy, P., Kantevari, S., & Naik, P. K. (2020). Rational design of 9-vinyl-phenyl noscapine as potent tubulin binding anticancer agent and evaluation of the effects of its combination on Docetaxel. *Journal of biomolecular structure & dynamics*, 1–14. Advance online publication. https://doi.org/10.1080/07391102.2020.1785945.
- De Martel, C., Georges, D., Bray, F., Ferlay, J., and Clifford, G.M. (2020). Global burden of cancer attributable to infections in 2018: a worldwide incidence analysis. *The Lancet. Global health*, *8*(2), e180-e190. https://doi.org/10.1016/S2214-109X(19)30488-7.
- DeBono, A., Capuano, B., & Scammells, P. J. (2015). Progress Toward the Development of Noscapine and Derivatives as Anticancer Agents. *Journal of medicinal chemistry*, *58*(15), 5699–5727. https://doi.org/10.1021/jm501180v.
- Desai, A., & Mitchison, T.J. (1997). Microtubule polymerization dynamics. *Annual review of cell and developmental biology*, *13*, 83-117. https://doi.org/10.1146/annurev.cellbio.13.1.83.

- DeVita, V.T., Jr, & Chu, E. (2008). A history of cancer chemotherapy. *Cancer research*, *68*(21), 8643-8653. https://doi.org/10.1158/0008-5472.CAN-07-6611.
- Diaz, J.F., & Andreu, J.M. (1993). Assembly of purified GDP-tubulin into microtubules induced by taxol and taxotere: reversibility, ligand stoichiometry, and competition. *Biochemistry*, *32*(11), 2747-2755. https://doi.org/10.1021/bi00062a003.
- Doddapaneni, R., Patel, K., Chowdhury, N., & Singh, M. (2016). Noscapine chemosensitization enhances docetaxel anticancer activity and nanocarrier uptake in triple negative breast cancer. *Experimental cell research*, *346*(1), 65–73. https://doi.org/10.1016/j.yexcr.2016.05.006.
- Downing, K. H., & Nogales, E. (1998). Tubulin structure: insights into microtubule properties and functions. *Current opinion in structural biology*, *8*(6), 785-791. https://doi.org/10.1016/s0959-440x(98)80099-7.
- Downing, K., & Nogales, E. (1998). New insights into microtubule structure and function from the atomic model of tubulin. *Eur Biophys J* **27,** 431-436. https://doi.org/10.1007/s002490050153
- Drukman, S., & Kavallaris, M. (2002). Microtubule alterations and resistance to tubulin-binding agents (review). *International journal of oncology*, *21*(3), 621-628.
- Eisenhauer, E.A., and Vermorken, J.B. (1998). The taxoids. Comparative clinical pharmacology and therapeutic potential. *Drugs*, *55*(1), 5-30. https://doi.org/10.2165/00003495-199855010-00002.
- Eldridge, M. D., Murray, C. W., Auton, T. R., Paolini, G. V., & Mee, R. P. (1997). Empirical scoring functions: I. The development of a fast empirical scoring function to estimate the binding affinity of ligands in receptor complexes. Journal of computer-aided molecular design, 11(5), 425–445. https://doi.org/10.1023/a:1007996124545.
- Essmann, U., Perera, L., Berkowitz, M.L., Darden, T., Lee, H., & Pedersen, L.G. (1995). A smooth particle mesh Ewald method. The Journal of Chemical Physics, 103(19), 8577-8593. https://doi.org/10.1063/1.470117.

- Fan, B., Shi, S., Shen, X., Yang, X., Liu, N., Wu, G., Guo, X., & Huang, N. (2019). Effect of HMGN2 on proliferation and apoptosis of MCF-7 breast cancer cells. Oncology letters, 17(1), 1160-1166. https://doi.org/10.3892/ol.2018.9668.
- Figgitt, D.P., and Wiseman, L.R. (2000). Docetaxel: an update of its use in advanced breast cancer. *Drugs*, *59*(3), 621-651. https://doi.org/10.2165/00003495-200059030-00015.
- Friesner, R.A., Banks, J.L., Murphy, R.B., Halgren, T.A., Klicic, J.J., Mainz, D.T., Repasky, M.P., Knoll, E.H., Shelley, M., Perry, J.K., Shaw, D.E., Francis, P., & Shenkin, P.S. (2004). Glide: a new approach for rapid, accurate docking and scoring. 1. Method and assessment of docking accuracy. Journal of Medicinal Chemistry, 47, 1739-1749.
- Gerber, D.E. & Chan, T.A. (2008). Recent advances in radiation therapy. Am Fam Physician, 78 pp 1254-62.
- Global Initiative for Cancer Registry Development. Lyon: International Agency for Research on Cancer; 2020 (https://gicr.iarc.fr/about-the-gicr/the-value-of-cancer-data/, accessed February 2021).
- Gordon, M.S., Binkley, J.S., Pople, J.A., Pietro, W.J., & Hehre, W.J. (1982). Self-consistent molecular-orbital methods. 22. Small split valence basis sets for second-row elements. Journal of the American Chemical Society, 104, 2797-2803. https://doi.org/10.1021/ja00374a017.
- Gueritte-Voegelein, F., Guenard, D., Lavelle, F., Le Goff, M. T., Mangatal, L., & Potier, P. (1991). Relationships between the structure of taxol analogues and their antimitotic activity. *Journal of medicinal chemistry*, *34*(3), 992-998. https://doi.org/10.1021/jm00107a017.
- Halgren, T.A., Murphy, R.B., Friesner, R.A., Beard, H.S., Frye, L.L., Pollard, W.T., & Banks, J.L., (2004). Glide: a new approach for rapid, accurate docking and scoring. 2. Enrichment factors in database screening. Journal of Medicinal Chemistry 47, 1750-1759. https://doi.org/10.1021/jm0306430.
- Hamel, E., & Lin, C.M. (1981). Glutamate-induced polymerization of tubulin: characteristics of the reaction and application to the large-scale purification of tubulin. Archives of Biochemistry and Biophysics, 209, 29-40. doi: 10.1016/0003-9861(81)90253-8.

- Herzog T.J. (2004). Recurrent ovarian cancer: how important is it to treat to disease progression. *Clinical cancer research: an official journal of the American Association for Cancer Research*, *10*(22), 7439-7449. https://doi.org/10.1158/1078-0432.CCR-04-0683
- Horwitz, K. B., Costlow, M. E., & McGuire, W. L. (1975). MCF-7; a human breast cancer cell line with estrogen, androgen, progesterone, and glucocorticoid receptors. *Steroids*, *26*(6), 785–795. https://doi.org/10.1016/0039-128x(75)90110-5
- Hosseininejad, S.M., Amini Ahidashti, H., Bozorgi, F., Goli Khatir, I., Montazar, S.H., Jahanian, F., and Amooei Khanabbasi, M. (2017). Efficacy and Safety of Combination Therapy with Ketorolac and Morphine in Patient with Acute Renal Colic; A Triple-Blind Randomized Controlled Clinical Trial. *Bulletin of emergency and trauma*, *5*(3), 165-170.
- Howard, J., & Hyman, A.A. (2003). Dynamics and mechanics of the microtubule plus end. *Nature*, *422*(6933), 753-758. https://doi.org/10.1038/nature01600.
- Jakalian, A. Jack, D.B., & Bayly, C.I. (2002). Fast, efficient generation of high quality atomic charges. AM1-BCC model: II. Parameterization and validation, The Journal of Computational Chemistry, 23, 1623-1641. doi: 10.1002/jcc.10128.
- Ji, Y., Yu, M., Qi, Z., Cui, D., Xin, G., Wang, B., Jia, W., & Chang, L. (2017). Study on apoptosis effect of human breast cancer cell MCF-7 induced by lycorine hydrochloride via death receptor pathway. *Saudi pharmaceutical journal : SPJ : the official publication of the Saudi Pharmaceutical Society*, *25*(4), 633–637. https://doi.org/10.1016/j.jsps.2017.04.036
- Jordan, A., Hadfield, J. A., Lawrence, N. J., & McGown, A. T. (1998). Tubulin as a target for anticancer drugs: agents which interact with the mitotic spindle. *Medicinal research reviews*, *18*(4), 259–296. https://doi.org/10.1002/(sici)1098-1128(199807)18:4<259::aid-med3>3.0.co;2-u .
- Jordan, M. A., & Wilson, L. (2004). Microtubules as a target for anticancer drugs. *Nature reviews. Cancer*, *4*(4), 253–265. https://doi.org/10.1038/nrc1317.
- Jordan, M.A., & Wilson, L. (1999). The use and action of drugs in analyzing mitosis. *Methods in cell biology*, *61*, 267-295. https://doi.org/10.1016/s0091-679x(08)61986-x.

- Jordan, M.A., Toso, R.J., Thrower, D., & Wilson, L. (1993). Mechanism of mitotic block and inhibition of cell proliferation by taxol at low concentrations. *Proceedings of the National Academy of Sciences of the United States of America*, *90*(20), 9552-9556. https://doi.org/10.1073/pnas.90.20.9552.

- Jorgensen, W.L., Chandrasekhar, J., Madura, J.D., Impey, R.W., & Klein, M.L. (1983). Comparison of simple potential functions for simulating liquid water. The Journal of chemical physics, 79(2), 926-935. https://doi.org/10.1063/1.445869.
- Joshi, H.C Aneja, R. and Vangapandu, S.N. (2014). Noscapine analogs and their use in treating cancers (Patent No. 8889705). Emory University Link: https://www.freepatentsonline.com/8889705.html.
- Joshi, H.C., Salil A, Bughani, U & Naik PK (2010). Noscapinoids: a new class of anticancer drugs demand biotechnological intervention. In Medicinal Plant Biotechnology, CABI South Asia Edition, UK, 2010, pp. 303-320.
- Kach, J., Sandbo, N., La, J., Denner, D., Reed, E.B., Akimova, O., Koltsova, S., Orlov, S.N., and Dulin, N.O. (2014). Antifibrotic effects of noscapine through activation of prostaglandin E2 receptors and protein kinase A. *The Journal of biological chemistry*, *289*(11), 7505-7513. https://doi.org/10.1074/jbc.M113.546812.

- Karlsson, M.O., Dahlstrom, B., Eckernas, S.A., Johansson, M., & Alm, A.T. (1990). Pharmacokinetics of oral noscapine. *European journal of clinical pharmacology*, *39*(3), 275-279. https://doi.org/10.1007/BF00315110.

- Ke, Y., Ye, K., Grossniklaus, H. E., Archer, D. R., Joshi, H. C., & Kapp, J. A. (2000). Noscapine inhibits tumor growth with little toxicity to normal tissues or inhibition of immune responses. *Cancer immunology, immunotherapy: CII*, *49*(4-5), 217–225. https://doi.org/10.1007/s002620000109.
- Kleeberg, U. R., Fink, M., Tessen, H. W., Nennecke, A., Hentschel, S., & Bartels, S. (2013). Adjuvant therapy reduces the benefit of palliative treatment in disseminated breast cancer - own findings and review of the literature. Onkologie, 36(6), 348–356. https://doi.org/10.1159/000351253.
- Konzett, H., and Rothlin, E. (1954). Zur Wirkung von Narkotin auf den Hustenreflex und auf die Bronchialmuskulatur [The effect of narcotine on cough

reflex and on bronchial musculature]. *Experientia*, *10*(11), 472-473. https://doi.org/10.1007/BF02170409.

- Kuruppu, A.I., Paranagama, P., & Goonasekara, C.L. (2019). Medicinal plants commonly used against cancer in traditional medicine formulae in Sri Lanka. *Saudi pharmaceutical journal: SPJ : the official publication of the Saudi Pharmaceutical Society*, *27*(4), 565-573. https://doi.org/10.1016/j.jsps.2019.02.004.

- Landen, J. W., Lang, R., McMahon, S. J., Rusan, N. M., Yvon, A. M., Adams, A. W., Sorcinelli, M. D., Campbell, R., Bonaccorsi, P., Ansel, J. C., Archer, D. R., Wadsworth, P., Armstrong, C. A., & Joshi, H. C. (2002). Noscapine alters microtubule dynamics in living cells and inhibits the progression of melanoma. *Cancer research*, *62*(14), 4109–4114.

- Landen, J.W., Hau, V., Wang, M., Davis, T., Ciliax, B., Wainer, B.H., Van Meir, E. G., Glass, J.D., Joshi, H.C., & Archer, D.R. (2004). Noscapine crosses the blood-brain barrier and inhibits glioblastoma growth. *Clinical cancer researc-: an official journal of the American Association for Cancer Research*, *10*(15), 5187-5201. https://doi.org/10.1158/1078-0432.CCR-04-0360

- Landen, J.W., Lang, R., McMahon, S.J., Rusan, N.M., Yvon, A.M., Adams, A.W., Sorcinelli, M.D., Campbell, R., Bonaccorsi, P., Ansel, J.C., Archer, D.R., Wadsworth, P., Armstrong, C. A., and Joshi, H.C. (2002). Noscapine alters microtubule dynamics in living cells and inhibits the progression of melanoma. *Cancer research*, *62*(14), 4109-4114.
- Laties, V.G. Behavior (2003). Analysis and the growth of behavioral pharmacology. *BEHAV ANALYST* 26, 235-252. https://doi.org/10.1007/BF03392079.
- Lee, C., Yang, W., & Parr, R. G. (1988). Development of the Colle-Salvetti correlation-energy formula into a functional of the electron density. *Physical review. B, Condensed matter*, *37*(2), 785–789. https://doi.org/10.1103/physrevb.37.785.

- Lettre, H. (1954). Synergists and antagonists of mitotic poisons. *Annals of the New York Academy of Sciences*, *58*(7), 1264–1275. https://doi.org/10.1111/j.1749-6632.1954.tb45907.x.
- Li X, Li Y, Cheng T, Liu Z and Wang R (2010). Evaluation of the performance of four molecular docking programs on a diverse set of protein-ligand complexes. Journal of Computational Chemistry 31: 2109-2125.
- Liu, B., Ezeogu, L., Zellmer, L., Yu, B., Xu, N., and Joshua Liao, D. (2015). Protecting the normal in order to better kill the cancer. *Cancer medicine*, *4*(9), 1394-1403. https://doi.org/10.1002/cam4.488.
- Liu, C., Yang, S., Wang, K., Bao, X., Liu, Y., Zhou, S., Liu, H., Qiu, Y., Wang, T., & Yu, H. (2019). Alkaloids from Traditional Chinese Medicine against hepatocellular carcinoma. *Biomedicine & pharmacotherapy = Biomedecine & pharmacotherapie*, *120*, 109543. https://doi.org/10.1016/j.biopha.2019.109543.
- Liu, T., Wan, Y., Xiao, Y., Xia, C., and Duan, G. (2020). Dual-Target Inhibitors Based on HDACs: Novel Antitumor Agents for Cancer Therapy. *Journal of medicinal chemistry*, *63*(17), 8977-9002. https://doi.org/10.1021/acs.jmedchem.0c00491.
- Luh, S.P., & Liu, H.P. (2006). Video-assisted thoracic surgery--the past, present status and the future. *Journal of Zhejiang University. Science. B*, *7*(2), 118–128. https://doi.org/10.1631/jzus.2006.B0118.
- Macht, Di. (1916). A pharmacologic and clinical study of papaverin. *Arch Intern Med (Chic)*; XVII (61): 786-805. https://doi.org/10.1001/archinte.1916.00080120077003.
- Mahaddalkar, T., Suri, C., Naik, P. K., & Lopus, M. (2015). Biochemical characterization and molecular dynamic simulation of β-sitosterol as a tubulin-binding anticancer agent. *European journal of pharmacology*, *760*, 154–162. https://doi.org/10.1016/j.ejphar.2015.04.014
- Mahmoudian, M., & Rahimi-Moghaddam, P. (2009). The anti-cancer activity of noscapine: a review. *Recent patents on anti-cancer drug discovery*, *4*(1), 92–97. https://doi.org/10.2174/157489209787002524.
- Maier, J.A., Martinez, C., Kasavajhala, K., Wickstrom, L., Hauser, K.E., & Simmerling, C. (2015). ff14SB: Improving the accuracy of protein side chain and

backbone parameters from ff99SB. Journal of Chemical Theory and Computation, 11, 3696-3713. https://doi.org/10.1021/acs.jctc.5b00255.

- Malekzadeh, M.M., Khademi, H., Pourshams, A., Etemadi, A., Poustchi, H., Bagheri, M., Khoshnia, M., Sohrabpour, A.A., Aliasgari, A., Jafari, E., Islami, F., Semnani, S., Abnet, C. C., Pharoah, P.D., Brennan, P., Boffetta, P., Dawsey, S.M., Malekzadeh, R., and Kamangar, F. (2013). Opium use and risk of mortality from digestive diseases: a prospective cohort study. *The American journal of gastroenterology*, *108*(11), 1757-1765. https://doi.org/10.1038/ajg.2013.336.
- Manchado, E., Guillamot, M., & Malumbres, M. (2012). Killing cells by targeting mitosis. *Cell death and differentiation*, *19*(3), 369–377. https://doi.org/10.1038/cdd.2011.197.
- Manchukonda, N. K., Naik, P. K., Sridhar, B., & Kantevari, S. (2014). Synthesis and biological evaluation of novel biaryl type α-noscapine congeners. *Bioorganic and Medicinal Chemistry Letters,* 24(24), 5752-575.
- Manchukonda, N.K., Naik, P.K., Santoshi, S., Lopus, M., Joseph, S., Sridhar, B., & Kantevari, S. (2013). Rational design, synthesis, and biological evaluation of third generation α-noscapine analogues as potent tubulin binding anti-cancer agents. *PloS one*, *8*(10), e77970. https://doi.org/10.1371/journal.pone.0077970.
- Manchukonda, N.K., Naik, P.K., Santoshi, S., Lopus, M., Joseph, S., Sridhar, B., and Kantevari, S. (2013). Rational design, synthesis, and biological evaluation of third generation α-noscapine analogues as potent tubulin binding anti-cancer agents. *PloS one*, *8*(10), e77970. https://doi.org/10.1371/journal.pone.0077970.
- Manfredi, J.J., & Horwitz, S.B. (1984). Taxol: an antimitotic agent with a new mechanism of action. *Pharmacology & therapeutics*, *25*(1), 83-125. https://doi.org/10.1016/0163-7258(84)90025-1.
- Masui, K., Gini, B., Wykosky, J., Zanca, C., Mischel, P.S., Furnari, F.B., and Cavenee, W.K. (2013). A tale of two approaches: complementary mechanisms of cytotoxic and targeted therapy resistance may inform next-generation cancer treatments. *Carcinogenesis*, *34*(4), 725-738. https://doi.org/10.1093/carcin/bgt086.

- Mathur, P., Sathishkumar, K., Chaturvedi, M., Das, P., Sudarshan, K.L., Santhappan, S., Nallasamy, V., John, A., Narasimhan, S., Roselind, F. S., & ICMR-NCDIR-NCRP Investigator Group (2020). Cancer Statistics, 2020: Report from National Cancer Registry Programme, India. *JCO global oncology*, *6*, 1063-1075. https://doi.org/10.1200/GO.20.00122.

- Medeiros, L. R., Rosa, D. D., Bozzetti, M. C., Fachel, J. M., Furness, S., Garry, R., Rosa, M. I., & Stein, A. T. (2009). Laparoscopy versus laparotomy for benign ovarian tumour. *The Cochrane database of systematic reviews*, (2), CD004751. https://doi.org/10.1002/14651858.CD004751.pub3

- Mishra, R.C., Karna, P., Gundala, S.R., Pannu, V., Stanton, R.A., Gupta, K.K., Robinson, M.H., Lopus, M., Wilson, L., Henary, M., & Aneja, R. (2011). Second generation benzofuranone ring substituted noscapine analogs: synthesis and biological evaluation. *Biochemical pharmacology*, *82*(2), 110-121. https://doi.org/10.1016/j.bcp.2011.03.029.

- Mukhtar, E., Adhami, V. M., & Mukhtar, H. (2014). Targeting microtubules by natural agents for cancer therapy. *Molecular cancer therapeutics*, *13*(2), 275–284. https://doi.org/10.1158/1535-7163.MCT-13-0791.
- Nabholtz, J.M., Tonkin, K., Smylie, M., Au, H.J., Lindsay, M.A., and Mackey, J. (2000). Chemotherapy of breast cancer: are the taxanes going to change the natural history of breast cancer?. *Expert opinion on pharmacotherapy*, *1*(2), 187-206. https://doi.org/10.1517/14656566.1.2.187.
- Naik, P.K., Chatterji, B.P., Vangapandu, S.N., Aneja, R., Chandra, R., Kanteveri, S., and Joshi, H.C. (2011). Rational design, synthesis and biological evaluations of amino-noscapine: a high affinity tubulin-binding noscapinoid. *Journal of computer-aided molecular design*, *25*(5), 443-454. https://doi.org/10.1007/s10822-011-9430-4.
- Naik, P.K., Chatterji, B.P., Vangapandu, S.N., Aneja, R., Chandra, R., Kanteveri, S. and Joshi, H.C. (2011). Rational design, synthesis and biological evaluations of amino-noscapine: a high affinity tubulin-binding noscapinoid. Journal of Computer Aided Molecular Design, 25(5): 443-54. doi: 10.1007/s10822-011-9430-4.

- Naik, P.K., Lopus, M., Aneja, R., Vangapandu, S.N., and Joshi, H.C. (2012). *In silico* inspired design and synthesis of a novel tubulin-binding anti-cancer drug: folate conjugated noscapine (Targetin). *Journal of computer-aided molecular design*, *26*(2), 233-247. https://doi.org/10.1007/s10822-011-9508-z.
- National Center for Biotechnology Information (2021). PubChem Compound Summary for CID 148124, Docetaxel. Retrieved March 29, 2021 from https://pubchem.ncbi.nlm.nih.gov/compound/Docetaxel.
- National Center for Biotechnology Information (2021). PubChem Compound Summary for CID 275196, Noscapine. Retrieved March 29, 2021 from https://pubchem.ncbi.nlm.nih.gov/compound/Noscapine.
- Nettles, J.H., Li, H., Cornett, B., Krahn, J.M., Snyder, J.P., and Downing, K.H. (2004). The binding mode of epothilone A on alpha, beta-tubulin by electron crystallography. *Science (New York, N.Y.)*, *305*(5685), 866-869. https://doi.org/10.1126/science.1099190.
- Newcomb, E. W., Lukyanov, Y., Schnee, T., Ali, M. A., Lan, L., & Zagzag, D. (2006). Noscapine inhibits hypoxia-mediated HIF-1alpha expression andangiogenesis in vitro: a novel function for an old drug. *International journal of oncology*, *28*(5), 1121–1130.
- Nogales, E. A (1999). Structural view of microtubule dynamics. *CMLS, Cell. Mol. Life Sci.* **56,** 133-142 (1999). https://doi.org/10.1007/s000180050012.
- Nogales, E., Whittaker, M., Milligan, R.A., & Downing, K.H. (1999). High-resolution model of the microtubule. *Cell*, *96*(1), 79-88. https://doi.org/10.1016/s0092-8674(00)80961-7.
- Nogales, E., Wolf, S.G., and Downing, K.H. (1998). Structure of the alpha beta tubulin dimer by electron crystallography. *Nature*, *391*(6663), 199-203. https://doi.org/10.1038/34465.
- Ojima, I., Lichtenthal, B., Lee, S., Wang, C., and Wang, X. (2016). Taxane anticancer agents: a patent perspective. *Expert opinion on therapeutic patents*, *26*(1), 1-20. https://doi.org/10.1517/13543776.2016.1111872.
- Oliva, M.A., Prota, A.E., Rodriguez Salarichs, J., Bennani, Y.L., Jimenez barbero, J., Bargsten, K., Canales, A., Steinmetz, M.O., and Diaz, J.F. (2020). Structural basis of noscapine activation for tubulin binding. J Med Chem (63):8495-8501.

- Otto, T., & Sicinski, P. (2017). Cell cycle proteins as promising targets in cancer therapy. *Nature reviews. Cancer*, *17*(2), 93–115. https://doi.org/10.1038/nrc.2016.138.
- Palanisamy, N., Ateeq, B., Kalyana-Sundaram, S., Pflueger, D., Ramnarayanan, K., Shankar, S., Han, B., Cao, Q., Cao, X., Suleman, K., Kumar-Sinha, C., Dhanasekaran, S. M., Chen, Y. B., Esgueva, R., Banerjee, S., LaFargue, C. J., Siddiqui, J., Demichelis, F., Moeller, P., Bismar, T. A., … Chinnaiyan, A. M. (2010). Rearrangements of the RAF kinase pathway in prostate cancer, gastric cancer and melanoma. *Nature medicine*, *16*(7), 793–798. https://doi.org/10.1038/nm.2166.
- Panda, D., Chakrabarti, G., Hudson, J., Pigg, K., Miller, H.P., Wilson, L., & Himes, R.H. (2000). Suppression of microtubule dynamic instability and treadmilling by deuterium oxide. Journal of Biochemistry, 39, 5075-5081. doi: 10.1021/bi992217f.
- Pandey, S. K., Biswas, S., Gunjan, S., Chauhan, B. S., Singh, S. K., Srivastava, K., Singh, S., Batra, S., & Tripathi, R. (2016). Pyrrolidine-Acridine hybrid in Artemisinin-based combination: a pharmacodynamic study. *Parasitology*, *143*(11), 1421–1432. https://doi.org/10.1017/S0031182016000937
- Parker, N., Turk, M.J., Westrick, E., Lewis, J.D., Low, P.S., and Leamon, C.P. (2005). Folate receptor expression in carcinomas and normal tissues determined by a quantitative radioligand binding assay. *Analytical biochemistry*, *338*(2), 284-293. https://doi.org/10.1016/j.ab.2004.12.026.
- Perola E, Walters WP and Charifson PS (2004). A detailed comparison of current docking and scoring methods on systems of pharmaceutical relevance. Proteins 56: 235-249.
- Pietro, W.J., Francl, M.M., Hehre, W.J., Defrees, D.J., Pople, J.A., & Binkley, J.S. (1982). Self-consistent molecular orbital methods. 24. Supplemented small split-valence basis sets for second-row elements. Journal of the American Chemical Society, 104, 5039-5048. https://doi.org/10.1021/ja00383a007.
- Polak E, Ribiere G (1969) Revue Francaise Inf Rech Oper, Serie Rouge 16:35-43.
- PTRAJ and CPPTRAJ (2013). Software for Processing and Analysis of Molecular Dynamics Trajectory Data. Journal of Chemical Theory and Computation, 9(7), 3084-3095. https:// doi.org/10.1021/ct400341p.

- Pucci, B., Kasten, M., and Giordano, A. (2000). Cell cycle and apoptosis. *Neoplasia (New York, N.Y.)*, *2*(4), 291-299. https://doi.org/10.1038/sj.neo.7900101.
- Ravelli, R.B., Gigant, B., Curmi, P.A., Jourdain, I., Lachkar, S., Sobel, A., and Knossow, M. (2004). Insight into tubulin regulation from a complex with colchicine and a stathmin-like domain. *Nature*, *428*(6979), 198-202. https://doi.org/10.1038/nature02393.

- Rida, P. C., LiVecche, D., Ogden, A., Zhou, J., & Aneja, R. (2015). The Noscapine Chronicle: A Pharmaco-Historic Biography of the Opiate Alkaloid Family and its Clinical Applications. *Medicinal research reviews*, *35*(5), 1072–1096. https://doi.org/10.1002/med.21357.

- Rida, P.C., LiVecche, D., Ogden, A., Zhou, J., & Aneja, R. (2015). The Noscapine Chronicle: A Pharmaco-Historic Biography of the Opiate Alkaloid Family and its Clinical Applications. *Medicinal research reviews*, *35*(5), 1072-1096. https://doi.org/10.1002/med.21357.

- Ringel, I., & Horwitz, S.B. (1991). Studies with RP 56976 (taxotere): a semisynthetic analogue of taxol. *Journal of the National Cancer Institute*, *83*(4), 288-291. https://doi.org/10.1093/jnci/83.4.288.

- Rodgers, G.M., 3rd, Becker, P.S., Blinder, M., Cella, D., Chanan-Khan, A., Cleeland, C., Coccia, P. F., Djulbegovic, B., Gilreath, J. A., Kraut, E. H., Matulonis, U.A., Millenson, M.M., Reinke, D., Rosenthal, J., Schwartz, R.N., Soff, G., Stein, R.S., Vlahovic, G., & Weir, A.B., 3rd (2012). Cancer- and chemotherapy-induced anemia. *Journal of the National Comprehensive Cancer Network: JNCCN*, *10*(5), 628-653. https://doi.org/10.6004/jnccn.2012.0064.

- Ross, J.F., Chaudhuri, P.K., and Ratnam, M. (1994). Differential regulation of folate receptor isoforms in normal and malignant tissues in vivo and in established cell lines. Physiologic and clinical implications. *Cancer*, *73*(9), 2432-2443. https://doi.org/10.1002/1097-0142(19940501)73:9<2432::aid cncr2820730929>3.0.co;2-s.

- Rowinsky, E.K., & Calvo, E. (2006). Novel agents that target tublin and related elements. *Seminars in oncology*, *33*(4), 421–435. https://doi.org/10.1053/j.seminoncol.2006.04.006.

- Rowinsky, E.K., & Donehower, R.C. (1991). The clinical pharmacology and use of antimicrotubule agents in cancer chemotherapeutics. *Pharmacology & therapeutics*, *52*(1), 35-84. https://doi.org/10.1016/0163-7258(91)90086-2.

- Rudner, A.D., & Murray, A.W. (1996). The spindle assembly checkpoint. *Current opinion in cell biology*, *8*(6), 773-780. https://doi.org/10.1016/s0955-0674(96)80077-9.

- Ryckaert, J.P., Ciccotti, G., & Berendsen, H.J. (1977). Numerical integration of the cartesian equations of motion of a system with constraints: molecular dynamics of< i> n</i>-alkanes. Journal of Computational Physics, 23(3), 327-341.
- Santoshi, S., & Naik, P. K. (2014). Molecular insight of isotypes specific β-tubulin interaction of tubulin heterodimer with noscapinoids. *Journal of computer-aided molecular design*, *28*(7), 751–763. https://doi.org/10.1007/s10822-014-9756-9.

- Santoshi, S., Naik, P.K., & Joshi, H.C. (2011). Rational design of novel anti-microtubule agent (9-azido-noscapine) from quantitative structure activity relationship (QSAR) evaluation of noscapinoids. *Journal of biomolecular screening*, *16*(9), 1047-1058. https://doi.org/10.1177/1087057111418654.

- Schiff, P.B., & Horwitz, S.B. (1980). Taxol stabilizes microtubules in mouse fibroblast cells. *Proceedings of the National Academy of Sciences of the United States of America*, *77*(3), 1561-1565. https://doi.org/10.1073/pnas.77.3.1561.

- Schiff, P.B., Fant, J., & Horwitz, S.B. (1979). Promotion of microtubule assembly in vitro by taxol. *Nature*, *277*(5698), 665-667. https://doi.org/10.1038/277665a0.
- Schirrmacher, V. (2019). From chemotherapy to biological therapy: A review of novel concepts to reduce the side effects of systemic cancer treatment (Review). *International journal of oncology*, *54*(2), 407-419. https://doi.org/10.3892/ijo.2018.4661.
- Seetharaman, J. and Rajan, S.S. (1995). Crystal and molecular structure of noscapine. *Zeftschrm furKristamographic* 210, 111-113.

- Sharma, P.K., Kumar, S., Kumar, P., Kaushik, P., Kaushik, D., Dhingra, Y., and Aneja, K.R. (2010). Synthesis and biological evaluation of some pyrazolylpyrazolines as anti-inflammatory-antimicrobial agents. *European journal of medicinal chemistry*, *45*(6), 2650-2655. https://doi.org/10.1016/j.ejmech.2010.01.059.
- Sivakumaran, N., Samarakoon, S.R., Adhikari, A., Ediriweera, M.K., Tennekoon, K.H., Malavige, N., Thabrew, I. & Shrestha, R.L.S. (2018). Cytotoxic and Apoptotic effects of Govaniadine isolated from Corydalis govaniana Wall. Roots on Human Breast Cancer (MCF-7) Cells. BioMed Research International, 3171348. doi: 10.1155/2018/3171348.
- Snyder, J. P., Nettles, J. H., Cornett, B., Downing, K. H., & Nogales, E. (2001). The binding conformation of Taxol in beta-tubulin: a model based on electron crystallographic density. *Proceedings of the National Academy of Sciences of the United States of America*, *98*(9), 5312–5316. https://doi.org/10.1073/pnas.051309398.
- Snyder, J.P., Nettles, J.H., Cornett, B., Downing, K.H., & Nogales, E. (2001). The binding conformation of Taxol in tubulin: A model based on electron crystallographic density. *Proceedings of the National Academy of Sciences of the United States of America,* 98(9), 5312-5316. doi: 10.1073/pnas.051309398.
- Sood, D., Kumar, N., Rathee, G., Singh, A., Tomar, V, and Chandra,R. (2018).Mechanistic Interaction Study of Bromo-Noscapine with Bovine Serum Albumin employing Spectroscopic and Chemoinformatics Approaches. Scientific Reports, 8(16964).
- Stanton, R. A., Gernert, K. M., Nettles, J. H., & Aneja, R. (2011). Drugs that target dynamic microtubules: a new molecular perspective. *Medicinal research reviews*, *31*(3), 443–481. https://doi.org/10.1002/med.20242.
- Stone, L.S., German, J.P., Kitto, K.F., Fairbanks, C.A., and Wilcox, G.L. (2014). Morphine and clonidine combination therapy improves therapeutic window in mice: synergy in antinociceptive but not in sedative or cardiovascular effects. *PloS one*, *9*(10), e109903. https://doi.org/10.1371/journal.pone.0109903.
- Tiwari, R., Pandey, S. K., Goel, S., Bhatia, V., Shukla, S., Jing, X., Dhanasekaran, S. M., & Ateeq, B. (2015). SPINK1 promotes colorectal cancer progression by

downregulating Metallothioneins expression. *Oncogenesis*, *4*(8), e162. https://doi.org/10.1038/oncsis.2015.23.

- Tolosa, L., Donato, M. T., & Gómez-Lechón, M. J. (2015). General Cytotoxicity Assessment by Means of the MTT Assay. *Methods in molecular biology (Clifton, N.J.)*, *1250*, 333–348. https://doi.org/10.1007/978-1-4939-2074-7_26.
- Ukena, D., Fishman, L., and Niebling, W.B. (2008). Bronchial asthma: diagnosis and long-term treatment in adults. *Deutsches Arzteblatt international*, *105*(21), 385-394. https://doi.org/10.3238/arztebl.2008.0385.
- Wang, J., Wang, W., Kollman, P.A., & Case, D.A. (2006). Automatic atom type and bond type perception in molecular mechanical calculations. The Journal of Molecular Graphics and Modelling, 25, 247-260. doi: 10.1016/j.jmgm.2005.12.005.
- Wang, Y., O'Brate, A., Zhou, W., & Giannakakou, P. (2005). Resistance to microtubule-stabilizing drugs involves two events: beta-tubulin mutation in one allele followed by loss of the second allele. *Cell cycle (Georgetown, Tex.)*, *4*(12), 1847-1853. https://doi.org/10.4161/cc.4.12.2264.
- Warolin C. (1999). Pierre-Jean Robiquet: (Rennes, 14 janvier 1780 - Paris, 29 avril 1840) [Pierre-Jean Robiquet]. *Revue d'histoire de la pharmacie*, *47*(321), 97-110.
- Warolin C. (1999). Pierre-Jean Robiquet: (Rennes, 14 janvier 1780 - Paris, 29 avril 1840) [Pierre-Jean Robiquet]. *Revue d'histoire de la pharmacie*, *47*(321), 97-110.
- Weijl, N. I., Cleton, F. J., & Osanto, S. (1997). Free radicals and antioxidants in chemotherapy-induced toxicity. Cancer treatment reviews, 23(4), 209–240. https://doi.org/10.1016/s0305-7372(97)90012-8.
- Wells WA. (1996). The spindle-assembly checkpoint: aiming for a perfect mitosis, every time. Trends in Cell Biology. 6(6), 228-234. https://doi.org/10.1016/0962-8924(96)10018-0.
- Wilson, L., Jordan, M.A., Morse, A., & Margolis, R.L. (1982). Interaction of vinblastine with steady-state microtubules in vitro. *Journal of molecular biology*, *159*(1), 125-149. https://doi.org/10.1016/0022-2836(82)90035-3.

- Winefield, R. D., Entwistle, R. A., Foland, T. B., Lushington, G. H., & Himes, R. H. (2008). Differences in paclitaxel and docetaxel interactions with tubulin detected by mutagenesis of yeast tubulin. *ChemMedChem*, *3*(12), 1844–1847. https://doi.org/10.1002/cmdc.200800288.

- Wu, H., Chang, D., & Huang, C. (2006). Targeted Therapy for Cancer, 2(2), 57-66.

- Wu, H.C., and Chang, D.K. (2010). Peptide-mediated liposomal drug delivery system targeting tumor blood vessels in anticancer therapy. *Journal of oncology*, *2010*, 723798. https://doi.org/10.1155/2010/723798.

- Yamada, T., Mori, Y., Hayashi, R., Takada, M., Ino, Y., Naishiro, Y., Kondo, T., & Hirohashi, S. (2003). Suppression of intestinal polyposis in Mdr1-deficient ApcMin/+ mice. *Cancer research*, *63*(5), 895-901.

- Yan, D., An, G., & Kuo, M. T. (2016). C-Jun N-terminal kinase signalling pathway in response to cisplatin. *Journal of cellular and molecular medicine*, *20*(11), 2013–2019. https://doi.org/10.1111/jcmm.12908.

- Yared, J.A., and Tkaczuk, K.H. (2012). Update on taxane development: new analogs and new formulations. *Drug design, development and therapy*, *6*, 371-384. https://doi.org/10.2147/DDDT.S28997.

- Ye, K., Ke, Y., Keshava, N., Shanks, J., Kapp, J.A., Tekmal, R R., Petros, J., & Joshi, H.C. (1998). Opium alkaloid noscapine is an antitumor agent that arrests metaphase and induces apoptosis in dividing cells. *Proceedings of the National Academy of Sciences of the United States of America*, *95*(4), 1601-1606. https://doi.org/10.1073/pnas.95.4.1601.

- Ye, K., Zhou, J., Landen, J. W., Bradbury, E. M., and Joshi, H. C. (2001). Sustained activation of p34 (cdc2) is required for noscapine-induced apoptosis. *The Journal of biological chemistry*, *276*(50), 46697-46700. https://doi.org/10.1074/jbc.C100550200.

- Zakhari, S. (1997). Alcohol and the cardiovascular system: molecular mechanisms for beneficial and harmful action. *Alcohol health and research world*, *21*(1), 21-29.

- Zhang, D., & Kanakkanthara, A. (2020). Beyond the Paclitaxel and Vinca Alkaloids: Next Generation of Plant-Derived Microtubule-Targeting Agents with

Potential Anticancer Activity. *Cancers*, *12*(7), 1721. https://doi.org/10.3390/cancers12071721.

- Zhang, X., & Luo, H. (2018). Effects of thalidomide on growth and VEGF-A expression in SW480 colon cancer cells. *Oncology letters*, *15*(3), 3313–3320. https://doi.org/10.3892/ol.2017.7645.
- Zhou Z, Felts AK, Friesner RA and Levy RM (2007). Comparative performance of several flexible docking programs and scoring functions: enrichment studies for a diverse set of pharmaceutically relevant tergets. Journal of Chemical Information and Modeling 47: 1599-1608.
- Zhou, J., Gupta, K., Aggarwal, S., Aneja, R., Chandra, R., Panda, D., & Joshi, H. C. (2003). Brominated derivatives of noscapine are potent microtubule-interfering agents that perturb mitosis and inhibit cell proliferation. *Molecular pharmacology*, *63*(4), 799–807. https://doi.org/10.1124/mol.63.4.799.
- Zhou, J., Gupta, K., Yao, J., Ye, K., Panda, D., Giannakakou, P., & Joshi, H. C. (2002). Paclitaxel-resistant human ovarian cancer cells undergo c-Jun NH2-terminal kinase-mediated apoptosis in response to noscapine. *The Journal of biological chemistry*, *277*(42), 39777–39785. https://doi.org/10.1074/jbc.M203927200.
- Zhou, J., Gupta, K., Yao, J., Ye, K., Panda, D., Giannakakou, P., & Joshi, H. C. (2002). Paclitaxel-resistant human ovarian cancer cells undergo c-Jun NH2-terminal kinase-mediated apoptosis in response to noscapine. *The Journal of biological chemistry*, *277*(42), 39777–39785. https://doi.org/10.1074/jbc.M203927200.

- Zhou, J., Liu, M., Aneja, R., Chandra, R., Lage, H., & Joshi, H.C. (2006). Reversal of P glycoprotein mediated multidrug resistance in cancer cells by the c-jun NH2-terrminal kinase. *Cancer Research,* 66, 445-452. https://doi: 10.1158/0008-5472.CAN-05-1779.

- Zhou, J., Panda, D., Landen, J. W., Wilson, L., & Joshi, H. C. (2002). Minor alteration of microtubule dynamics causes loss of tension across kinetochore pairs and activates the spindle checkpoint. *The Journal of biological chemistry*, *277*(19), 17200–17208. https://doi.org/10.1074/jbc.M110369200.

- Ziello, J. E., Jovin, I. S., & Huang, Y. (2007). Hypoxia-Inducible Factor (HIF)-1 regulatory pathway and its potential for therapeutic intervention in malignancy and ischemia. *The Yale journal of biology and medicine*, *80*(2), 51–60.
- Zorn, K.C., Gofrit, O.N., Steinberg, G.D., Arieh, L., & Shalhav, M.D. (2007). Evolution of Robotic Surgery in the Treatment of Localized Prostate Cancer. *Curr. Treat. Options in Oncol.* **8,** 197–210 https://doi.org/10.1007/s11864-007-0028-y.

APPENDICES

Supporting Information of 9-Vinyl phenyl noscapine (VPN)

Copies of ^{1}H, ^{13}C NMR and mass spectra (ESI and HR-MS) of

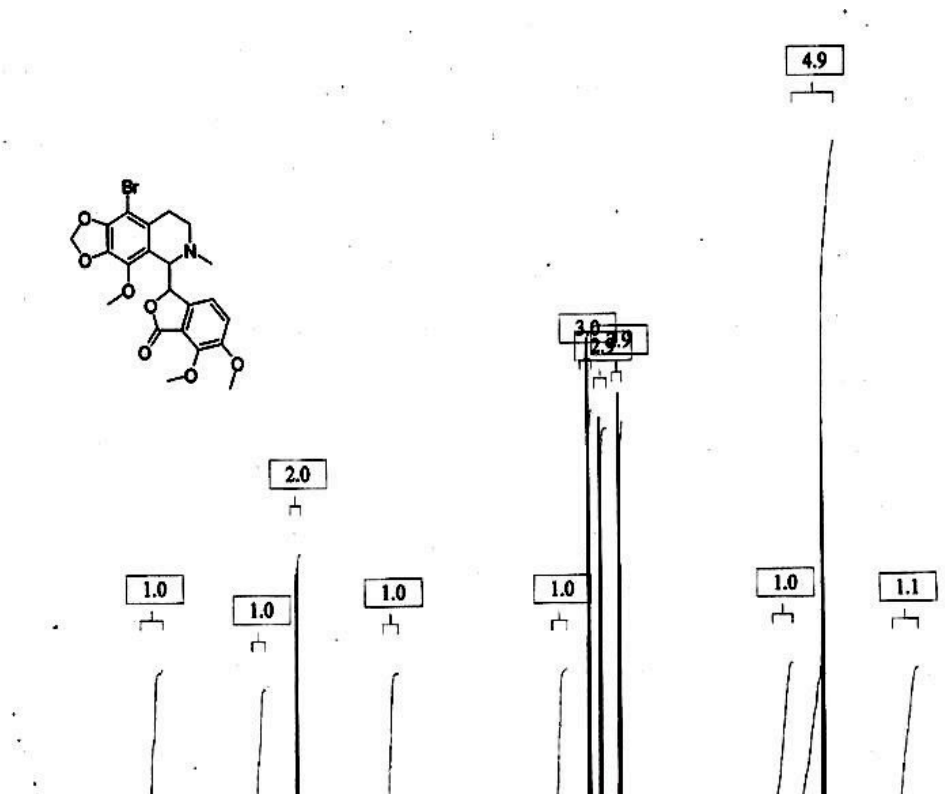

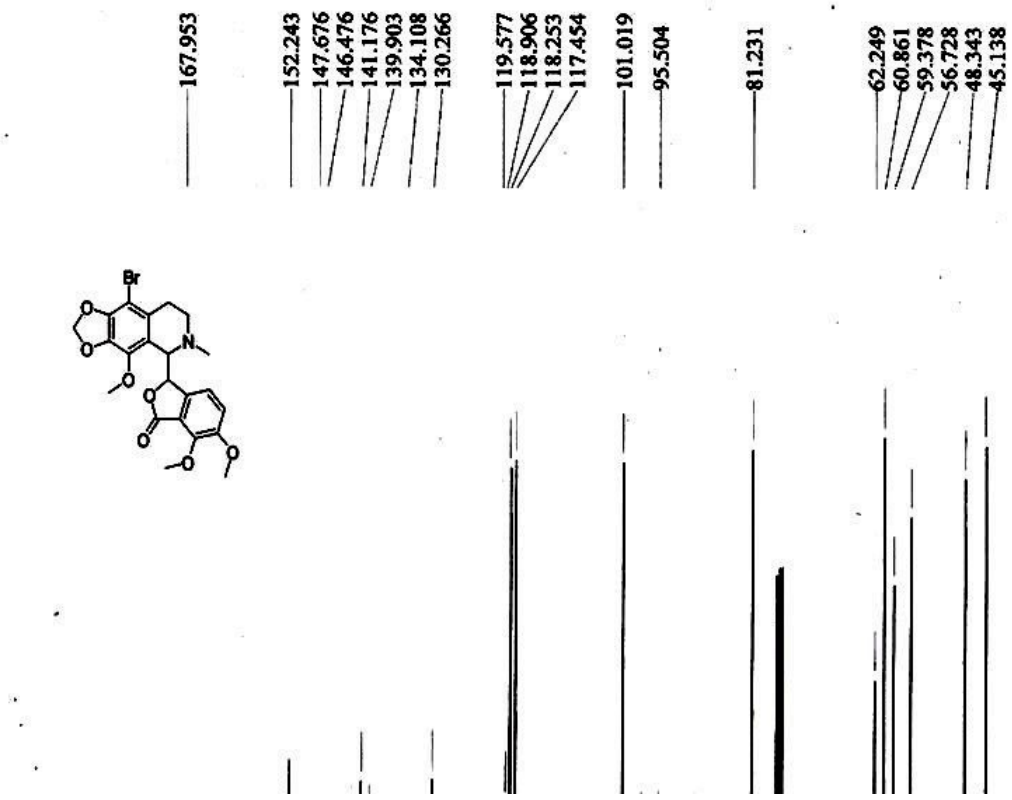
167.953
152.243
147.676
146.476
141.176
139.903
134.108
130.266
119.577
118.906
118.253
117.454
101.019
95.504
81.231
62.249
60.861
59.378
56.728
48.343
45.138
Br

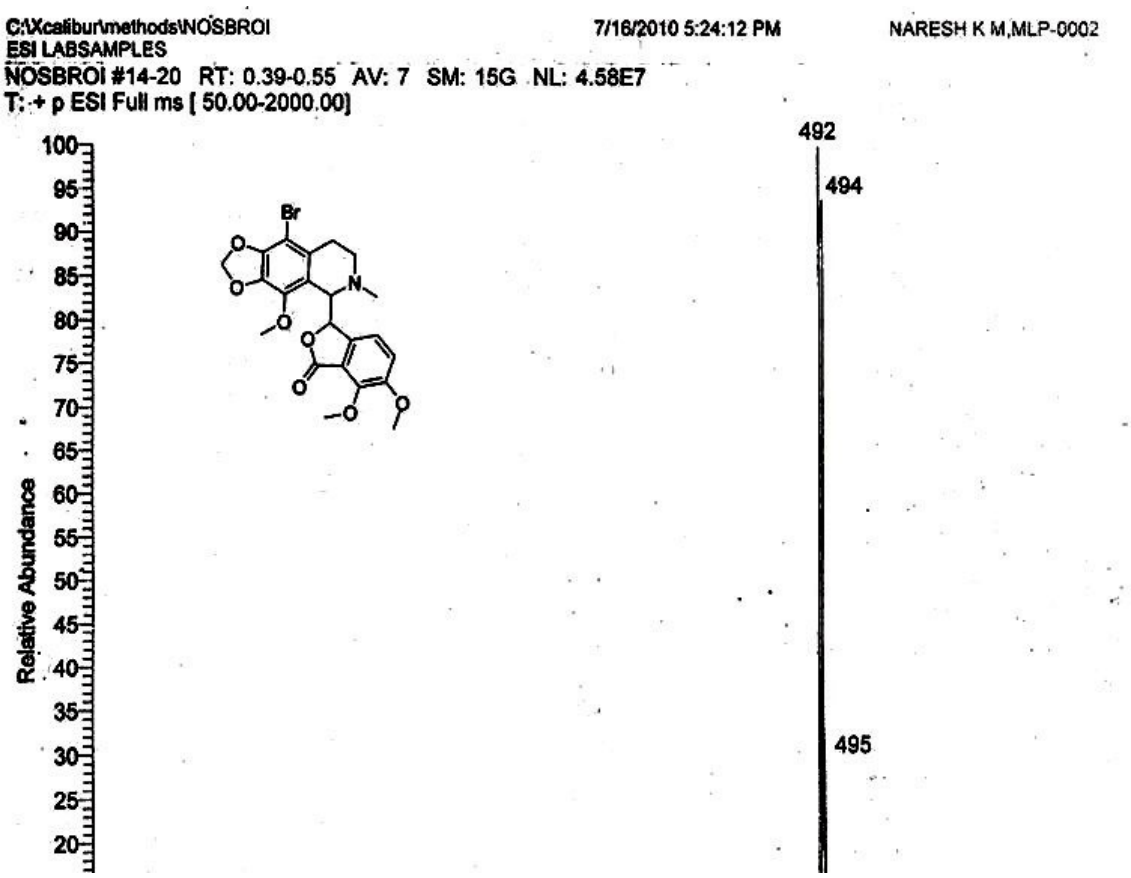
C:\Xcalibur\methods\NOSBROI
7/16/2010 5:24:12 PM
NARESH K M,MLP-0002
ESI LABSAMPLES
NOSBROI #14-20 RT: 0.39-0.55 AV: 7 SM: 15G NL: 4.58E7
T: + p ESI Full ms [50.00-2000.00]
Relative Abundance
100
95
90
85
80
75
70
65
60
55
50
45
40
35
30
25
20
492
494
495
Br

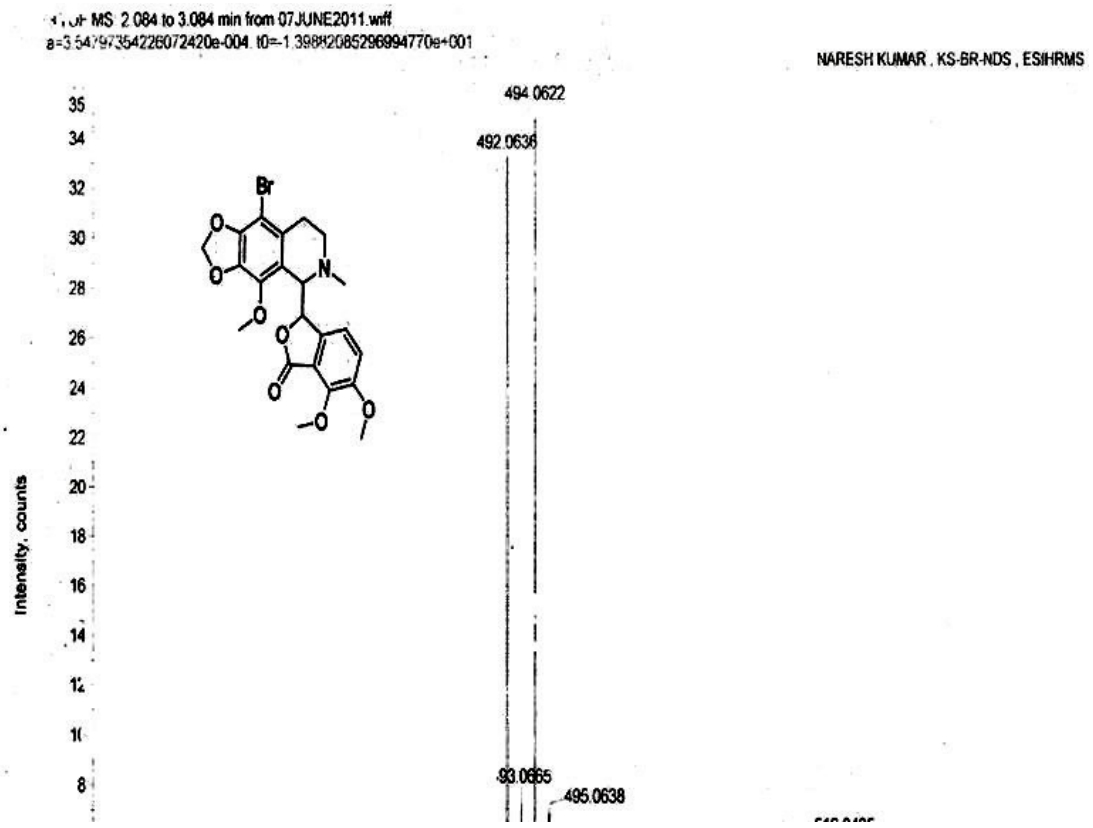

Elemental composition calculator

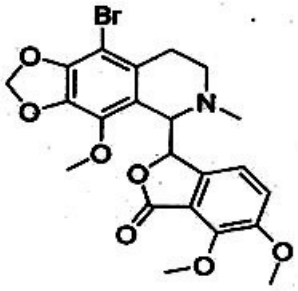

Target m/z: +492.0636 amu
Tolerance: +5.0000 ppm
Result type: Elemental
Max num of results: 100
Min DBE: -0.5000 Max DBE:
Electron state: OddAndEven
Num of charges: 0
Add water: N/A
Add proton: N/A
File Name: 07JUNE2011.wiff

	Elements	Min Number	
1	Br	0	1
2	C	0	22
3	H	0	23
4	N	0	1
5	Na	0	1
6	O	0	7

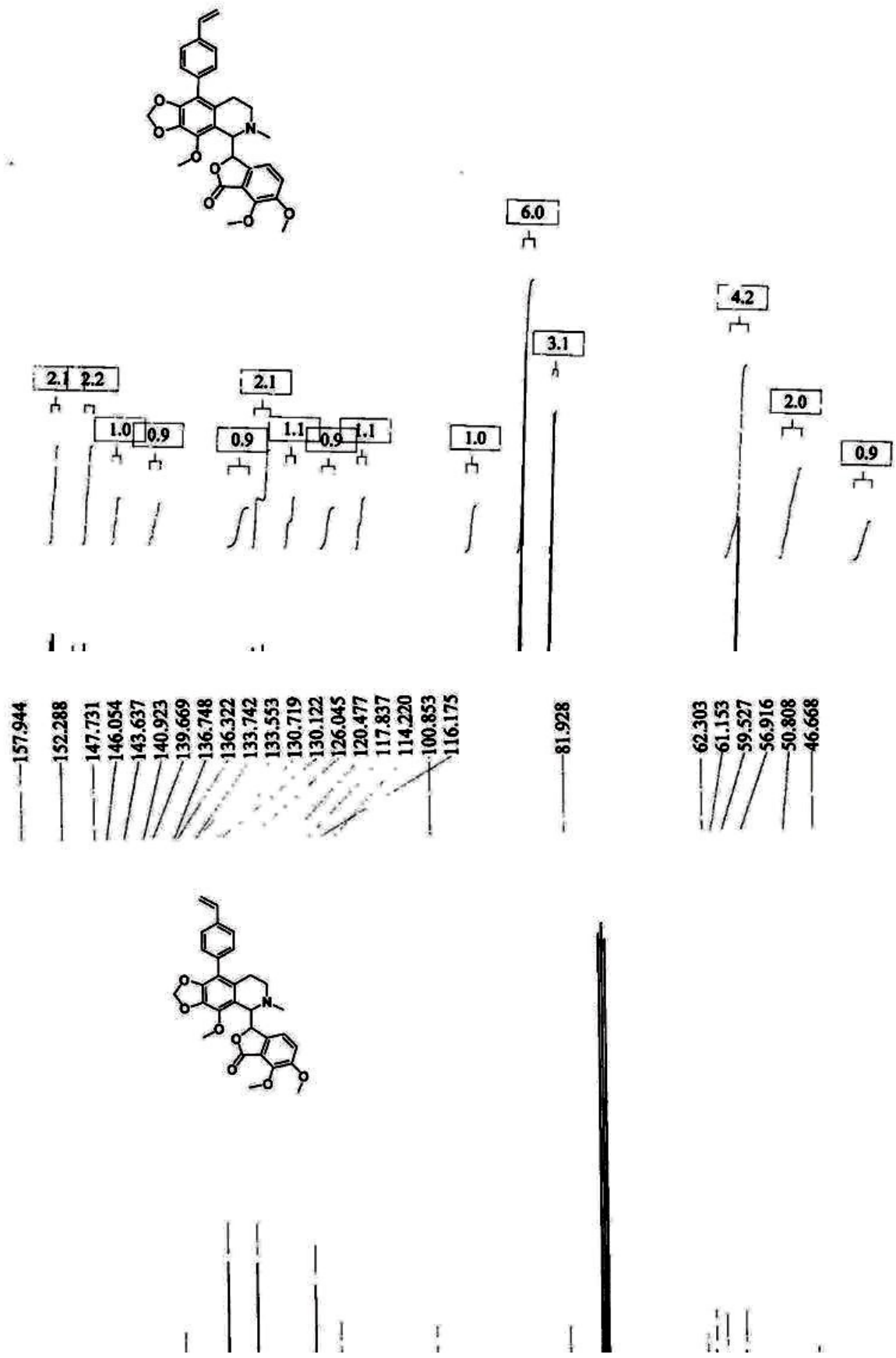
6.0
3.1
4.2
2.0
2.1
2.2
1.0
0.9
2.1
0.9
1.1
0.9
1.1
1.0
0.9
157.944
152.288
147.731
146.054
143.637
140.923
139.669
136.748
136.322
133.742
133.553
130.719
130.122
126.045
120.477
117.837
114.220
100.853
116.175
81.928
62.303
61.153
59.527
56.916
50.808
46.668

Acq. File: 26JULY2011.wiff Sample ID: TuneSampleID Acq. Date: Tuesday, Ju

Sample Comment: NARESH KUMAR.M., KS-SUZ-4 VINYLPHENYL, ESIHRMS, ESI-VE Acq. Time: 11:24

+TOF MS: 0.134 min from Sample 4 (KSSUZ4VINYLPHENYL) of 26JULY2011.wiff
a=3.5478369227217156e-004, t0=-1.4161538568994729e+001

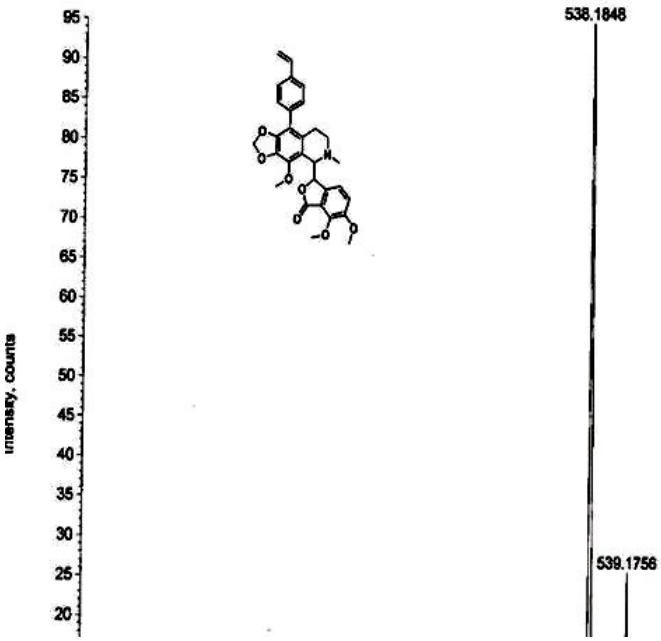

Acq. File: n/a Sample ID: n/a Acq. Date: n/a

Sample Comment: n/a Acq. Time: n/a

Elemental composition calculator

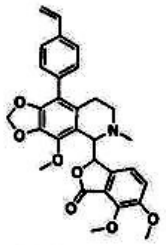

Target m/z: +538.1848 amu
Tolerance: +5.0000 ppm
Result type: Elemental
Max num of results: 100
Min DBE: -0.5000 Max DBE:
Electron state: OddAndEven
Num of charges: 0
Add water: N/A
Add proton: N/A
File Name: 26JULY2011.wiff

	Elements	Min Number	
1	C	0	31
2	H	0	32
3	N	0	2
4	Na	0	1
5	O	0	9

Supporting Information of 9-Amino noscapine

Copies of ^{1}H, ^{13}C NMR and mass spectra (ESI and HR-MS) of 9-amino-α-noscapine

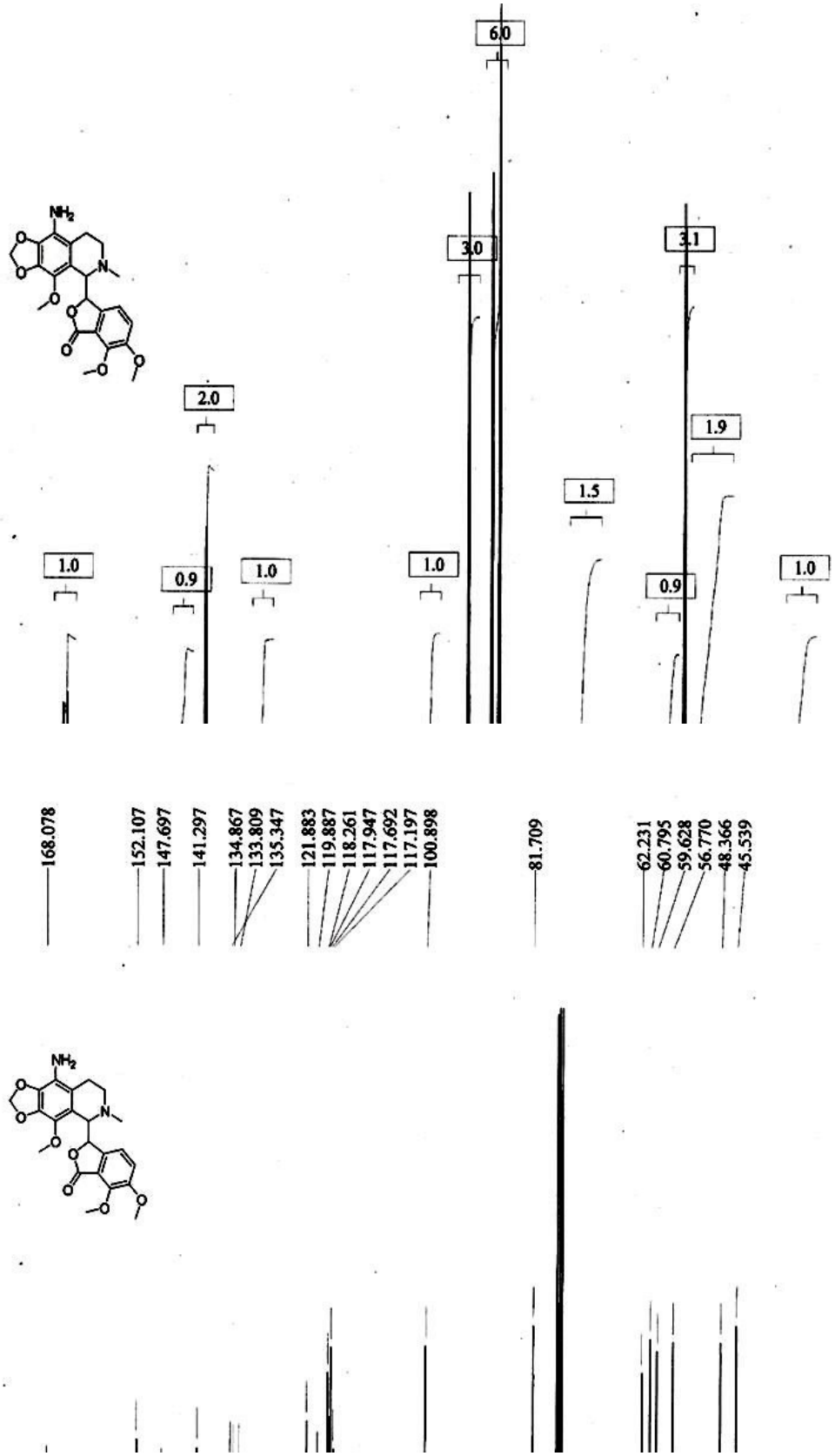

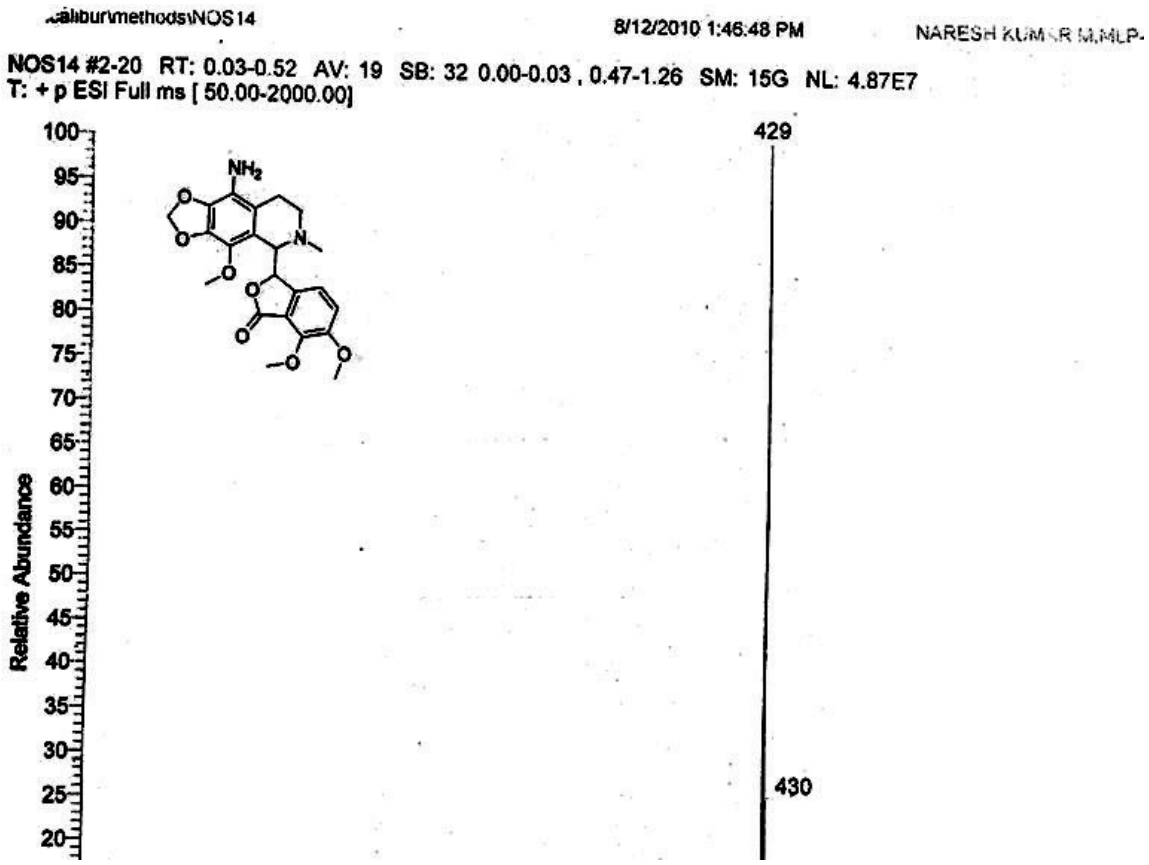
alibur\methods\NOS14
8/12/2010 1:46:48 PM
NARESH KUMAR M,MLP-
NOS14 #2-20 RT: 0.03-0.52 AV: 19 SB: 32 0.00-0.03 , 0.47-1.26 SM: 15G NL: 4.87E7
T: + p ESI Full ms [50.00-2000.00]
Relative Abundance
429
430
NH2

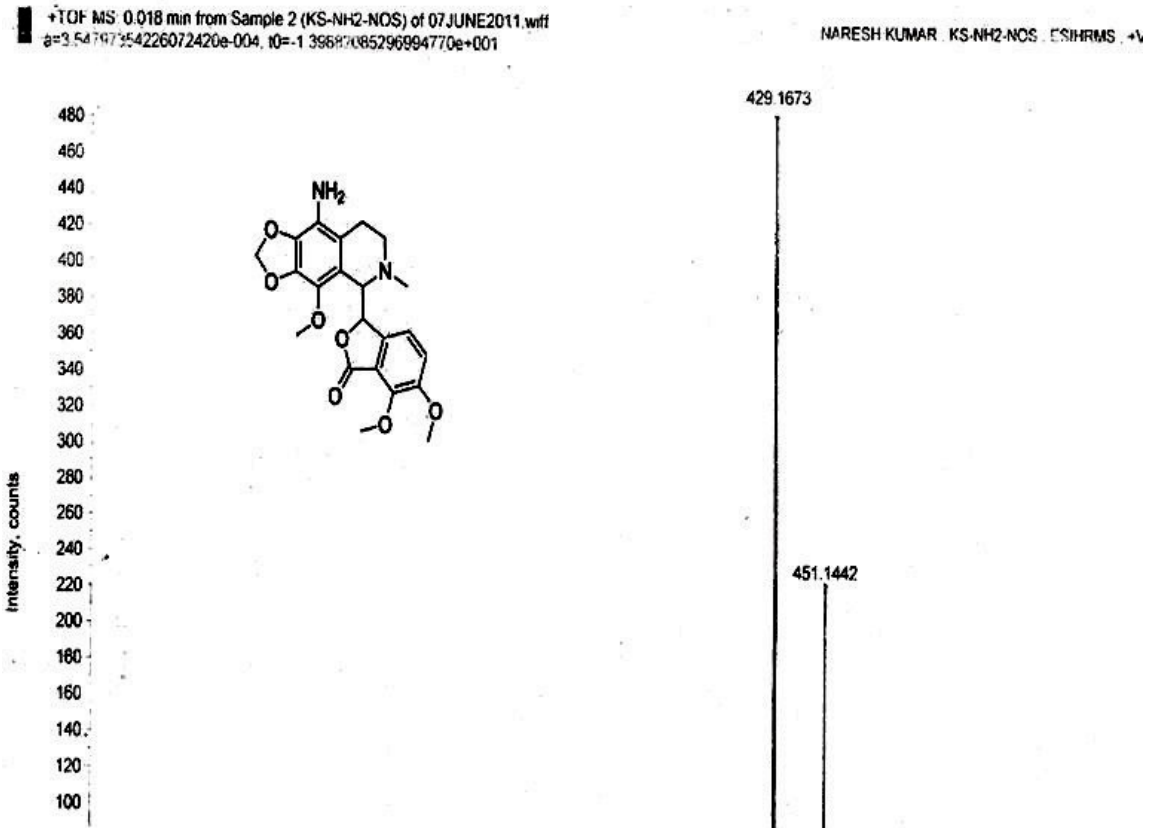
+TOF MS: 0.018 min from Sample 2 (KS-NH2-NOS) of 07JUNE2011.wiff
NARESH KUMAR, KS-NH2-NOS, ESIHRMS, +V
Intensity, counts
429.1673
451.1442
NH2

Sample ID: n/a Acq. Date: n/a

Acq. Time: n/a

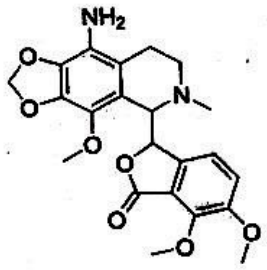

Elemental composition calculator

Target m/z: +429.1673 amu
Tolerance: +5.0000 ppm
Result type: Elemental
Max num of results: 100
Min DBE: -0.5000 Max DBE:
Electron state: OddAndEven
Num of charges: 0
Add water: N/A
Add proton: N/A
File Name: 07JUNE2011.wiff

	Elements	Min Number	
1	C	0	22
2	H	0	25
3	N	0	2
4	Na	0	1

Supporting Information of N-3-Br-Benzyl-noscapine

^{13}C NMR spectra of N-3-Br-Benzyl-noscapine

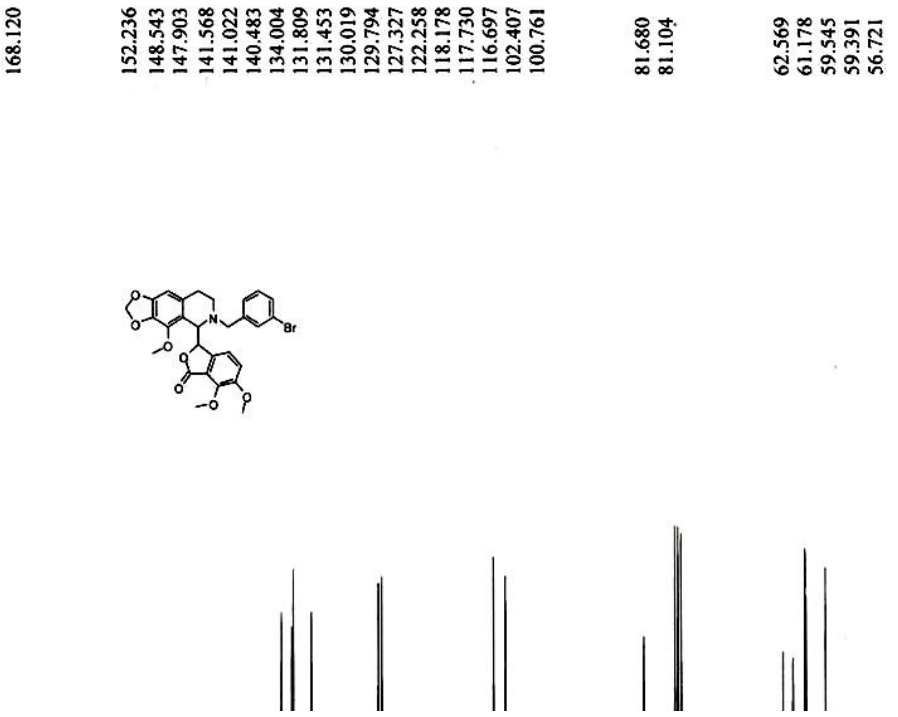

ESI spectra of N-3-Br-Benzyl-noscapine

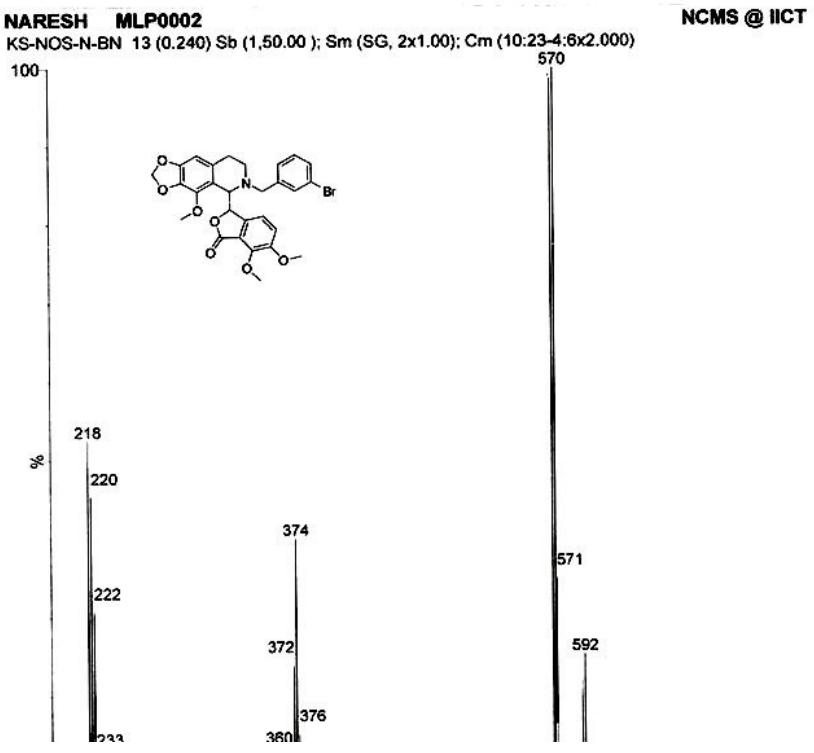

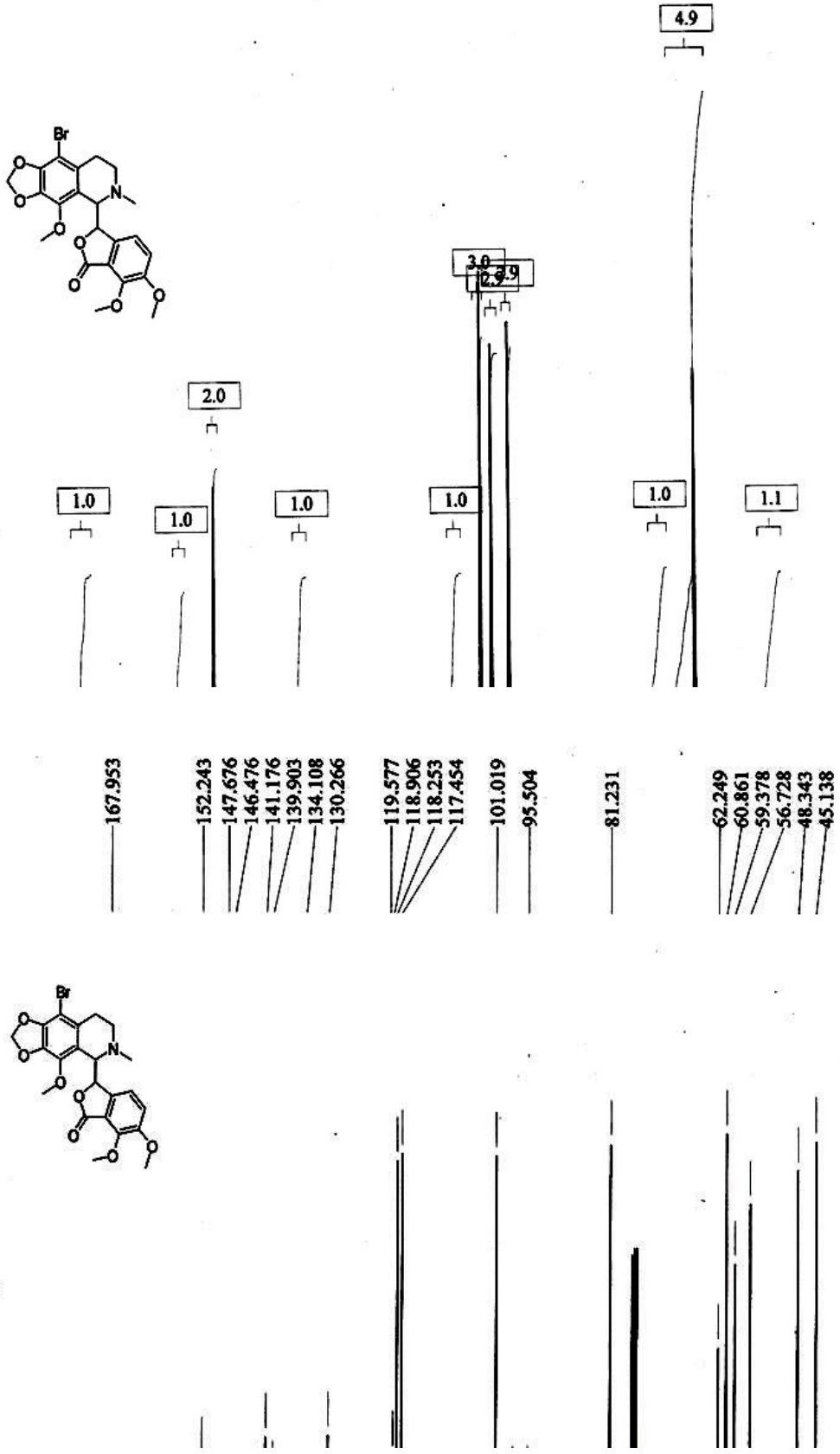
Br
O
O
N
O
O
O
O
4.9
3.0
2.9
2.0
1.0
1.0
1.0
1.0
1.0
1.1
167.953
152.243
147.676
146.476
141.176
139.903
134.108
130.266
119.577
118.906
118.253
117.454
101.019
95.504
81.231
62.249
60.861
59.378
56.728
48.343
45.138

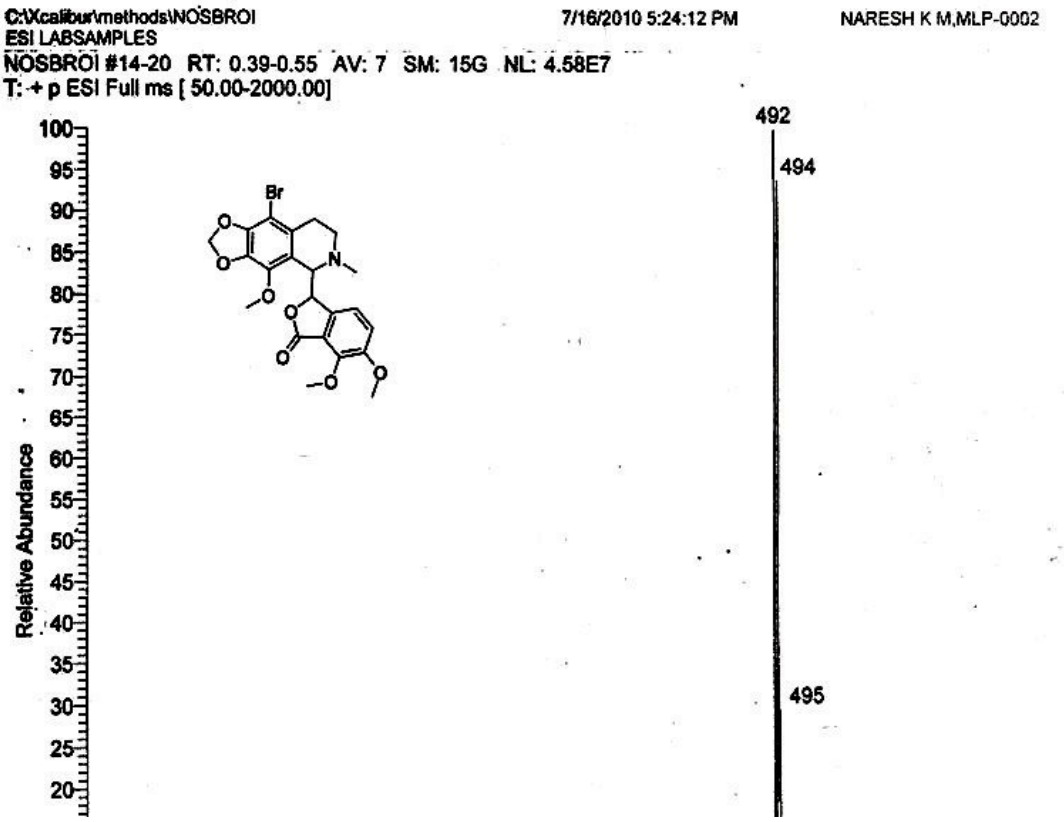

Supporting information of Br-TMB-noscapine

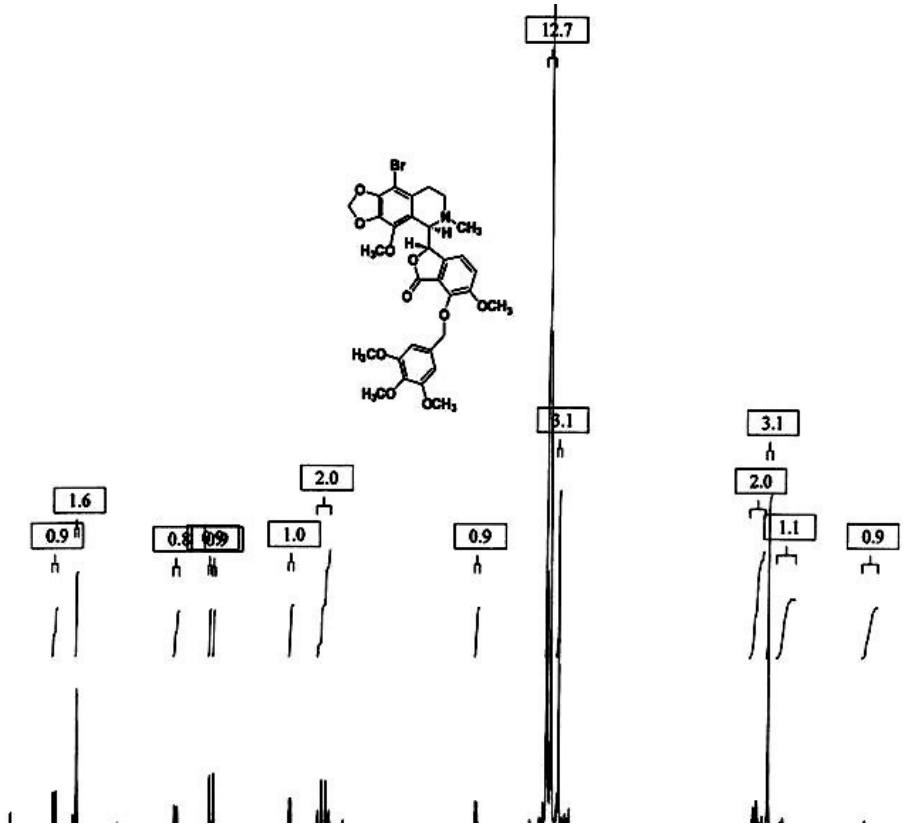

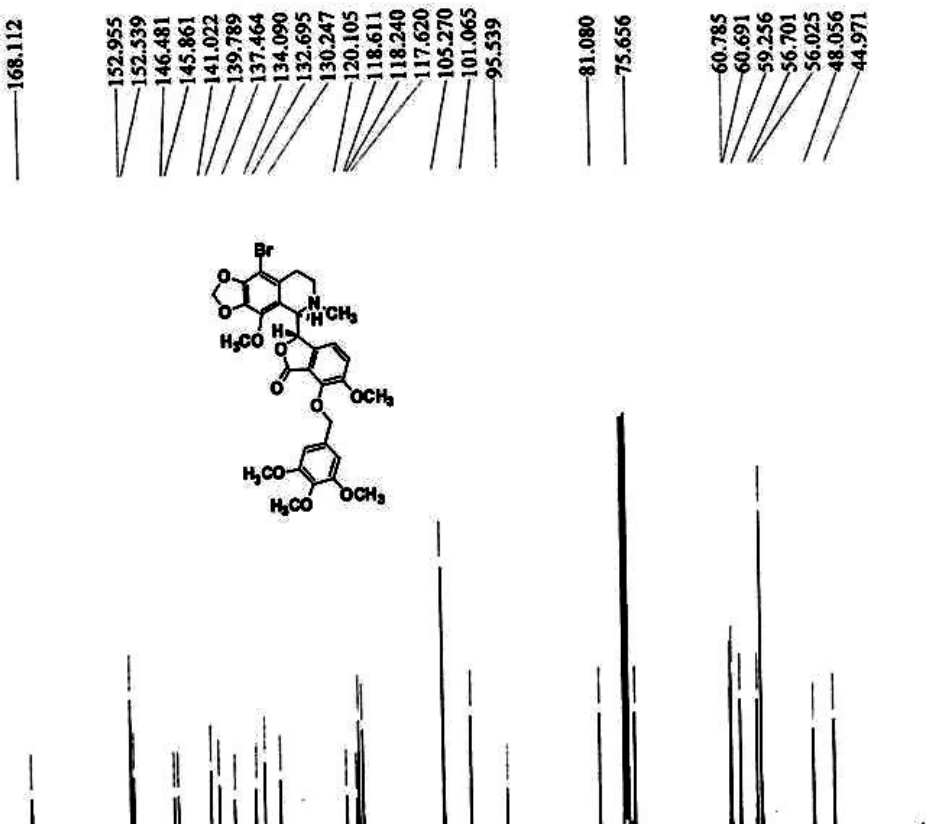

=== CPC DIVISION @ CSIR-IICT ===

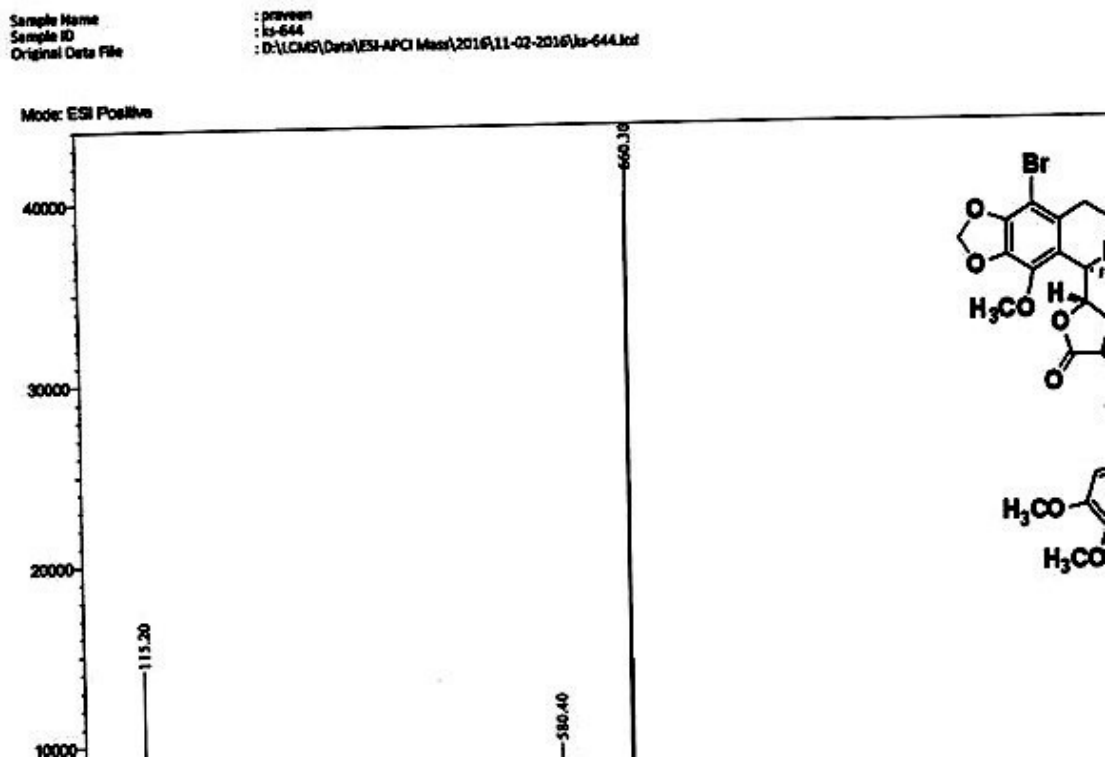

Supporting information of Pyridyl-3-Boronic Acid-noscapine

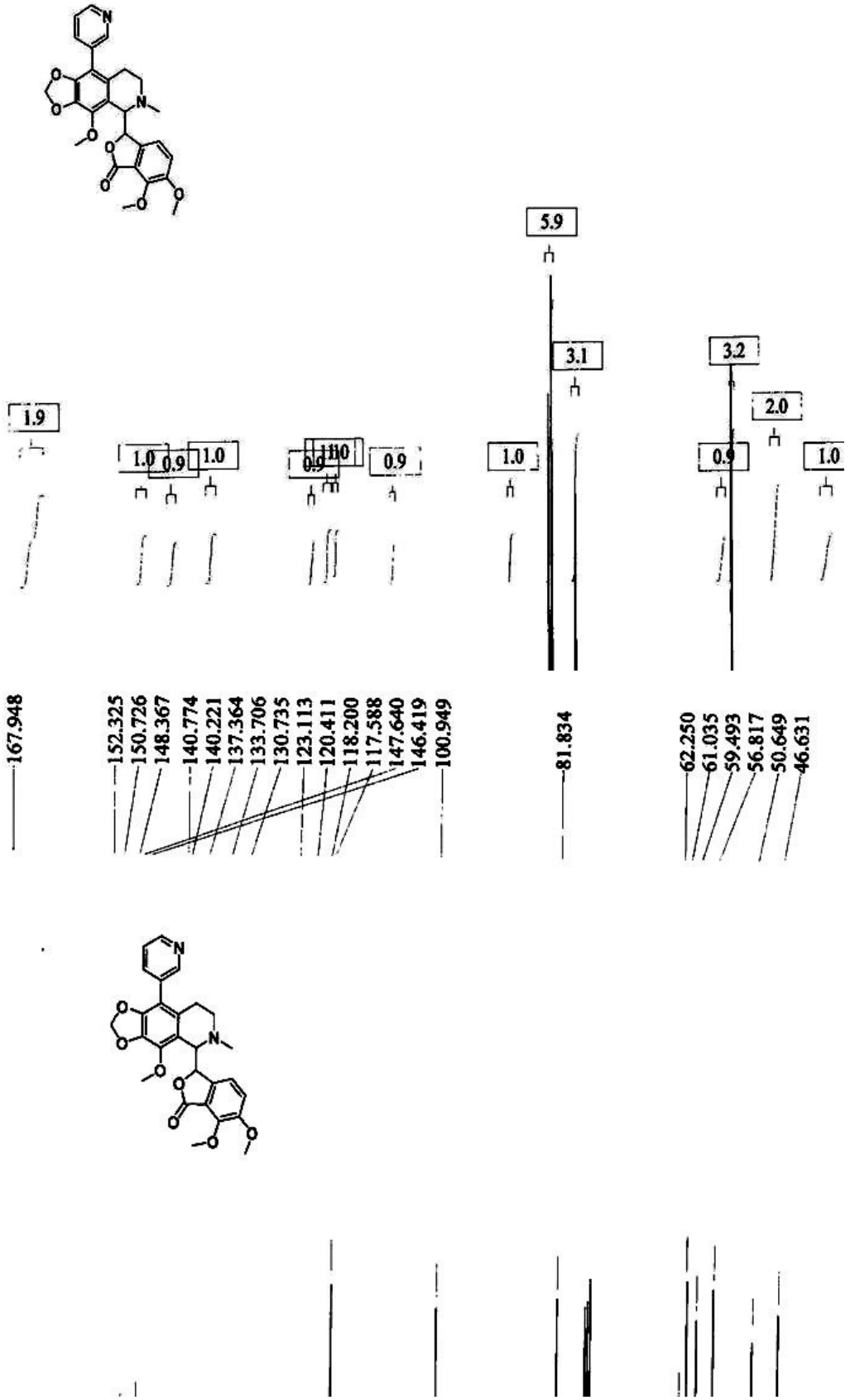

Acq. File: 26JULY2011.wiff Sample ID: TuneSampleID Acq. Date: Tuesday, July

Sample Comment: NARESH KUMAR M , KS-SUZ-PYRIDYL, ESIHRMS , +VE. Acq. Time: 11:13

+TOF MS: 1.868 to 1.734 min from 26JULY2011.wiff
a=3.5478369227217156e-004, t0=-1.4161538568947290e+001

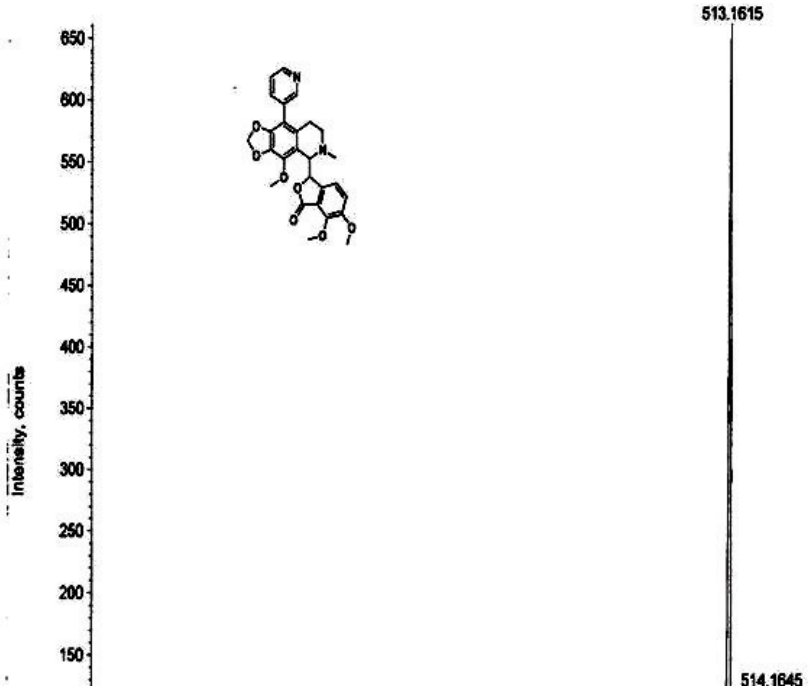

Table 4.2: VPN_DOX: Geometry of hydrogen bonds and hydrophobic interaction of VPN_DOX with the binding site residues of tubulin.

(a) VPN_Tubulin			(b) DOX_Tubulin		
Hydrogen bonding			**Hydrogen bonding**		
Hydrogen Donor (D)	**Hydrogen Acceptor (A)**	**Distance (D-A) in Å**	**Hydrogen Donor (D)**	**Hydrogen Acceptor (A)**	**Distance (D-A) in Å**
ASP D 357	OD1	3.67	UNK 900	O13	2.6
VAL D 355	O	4.22	UNK 900	O2	2.71
UNK 901	O16	3.16	GLY D 370	O	3.69
UNK 901	O21	4.39	ARG D 369	O	4.96
UNK 901	O18	3.13	ARG D 284	O	2.66
PRO D 245	O	4.48	GLN D 281	OE1	4.73
UNK 901	O19	4.11	GLN D 281	OE1	3.56
			UNK 900	O3	3.57
			GLN D 281	O	3.89
			UNK 900	O3	4.85
			UNK 900	O2	3.05
			UNK 900	O3	4.34
			UNK 900	O2	3.93
Hydrophobic interaction			**Hydrophobic interaction**		
VPN	**Tubulin**	**Distance**	**DOX**	**Tubulin**	**Distance**
ASP D 357	OD2	4.23	LYS D 372	NZ	4.11
ASP D 357	OD2	3.41	LYS D 372	NZ	4.53
ASP D 357	OD2	4.35	LYS D 372	NZ	4.83
ASP D 357	OD1	3.44	LYS D 372	CE	3.76
ASP D 357	OD1	3.23	LYS D 372	CE	4.58
ASP D 357	OD1	4.04	LYS D 372	CE	4.11
ASP D 357	CG	4.2	LYS D 372	CE	3.44
ASP D 357	CG	3.81	LYS D 372	CE	4.05
ASP D 357	CG	3.57	LYS D 372	CD	4.17
ASP D 357	CG	4.58	LYS D 372	CD	4.95
ASP D 357	CB	4.48	LYS D 372	CG	3.77
ASP D 357	CB	4.89	LYS D 372	CG	4.56
ASP D 357	CA	4.87	LYS D 372	CG	4.99
ASP D 357	N	3.99	LEU D 371	CD2	4.97
ASP D 357	N	4.97	LEU D 371	CD2	4.93
CYS D 356	C	4.57	LEU D 371	CD2	4.16
CYS D 356	CA	4.25	LEU D 371	CD2	4.11
CYS D 356	N	4.99	LEU D 371	CD2	3.16
CYS D 356	N	4.96	LEU D 371	CD2	3.58
VAL D 355	CG2	4.97	LEU D 371	CD2	4.16
VAL D 355	CB	4.84	LEU D 371	CD2	3.98
VAL D 355	CB	4.91	LEU D 371	CD2	4.23
VAL D 355	O	3.88	LEU D 371	CD2	3.79
VAL D 355	O	4.31	LEU D 371	CD2	4.8
VAL D 355	O	4.08	LEU D 371	CD1	4.09
VAL D 355	O	4.96	LEU D 371	CD1	4.82
VAL D 355	O	4.69	LEU D 371	CD1	4.95
VAL D 355	O	3.68	LEU D 371	CG	4.5
VAL D 355	O	3.32	LEU D 371	CG	4.78
VAL D 355	O	3.52	LEU D 371	CG	4.96
VAL D 355	O	2.82	LEU D 371	CG	4.24

VAL D 355	O	4.09	LEU D 371	CG	4.74
VAL D 355	C	4.82	LEU D 371	CG	4.25
VAL D 355	C	4.63	LEU D 371	CG	4.85
VAL D 355	C	4.42	GLY D 370	O	4.34
VAL D 355	C	4.47	GLY D 370	O	3.82
VAL D 355	C	4.17	GLY D 370	O	3.74
VAL D 355	C	4.04	GLY D 370	O	4.76
VAL D 355	CA	4.9	GLY D 370	O	4.24
VAL D 355	CA	4.86	GLY D 370	O	4.84
VAL D 355	CA	4.95	GLY D 370	C	4.79
VAL D 355	N	4.7	GLY D 370	C	4.58
VAL D 355	N	4.92	GLY D 370	C	4.47
VAL D 355	N	4.74	GLY D 370	CA	3.81
VAL D 355	N	4.32	GLY D 370	CA	4.95
VAL D 355	N	4.13	GLY D 370	CA	4.85
VAL D 355	N	4.47	GLY D 370	N	4.45
VAL D 355	N	4.32	ARG D 369	O	4.83
VAL D 355	N	4.84	ARG D 369	O	3.62
ALA D 354	CB	4.02	ARG D 369	O	4.02
ALA D 354	CB	3.88	ARG D 369	O	3.23
ALA D 354	CB	4.66	ARG D 369	C	4.36
ALA D 354	CB	4.8	ARG D 369	C	4.42
ALA D 354	CB	4.45	LEU D 286	CD2	3.92
ALA D 354	C	4.83	LEU D 286	CD2	4.34
ALA D 354	C	4.84	LEU D 286	CD2	4.3
ALA D 354	C	4.86	LEU D 286	CD2	4.85
ALA D 354	C	4.95	LEU D 286	CD2	4.39
ALA D 354	CA	4.37	LEU D 286	CD2	4.19
ALA D 354	CA	4.81	LEU D 286	CD1	4.87
ALA D 354	CA	3.87	LEU D 286	CG	4.34
ALA D 354	CA	4.54	LEU D 286	CG	4.68
ALA D 354	CA	4.92	LEU D 286	CG	4.91
ALA D 354	CA	4.29	LEU D 286	CG	4.96
ALA D 354	CA	4.67	LEU D 286	CB	3.48
ALA D 354	CA	4.78	LEU D 286	CB	4.96
ALA D 354	N	4.7	LEU D 286	CB	4.2
THR D 353	CG2	4.76	LEU D 286	CB	4.34
THR D 353	O	3.83	LEU D 286	CB	4.34
THR D 353	O	3.87	LEU D 286	CB	3.59
THR D 353	O	4.74	LEU D 286	CB	4.36
THR D 353	C	4.44	LEU D 286	CB	4.95
THR D 353	C	4.97	LEU D 286	CB	4.49
THR D 353	C	4.72	LEU D 286	O	4.75
ASP D 329	OD1	4.58	LEU D 286	CA	4.6
MET D 325	CE	4.7	LEU D 286	CA	3.84
MET D 325	CE	4.16	LEU D 286	CA	4.9
MET D 325	CE	3.41	LEU D 286	CA	4.86
MET D 325	CE	3.44	LEU D 286	N	4.39
MET D 325	CE	4.62	LEU D 286	N	4.96
MET D 325	CE	4.56	LEU D 286	N	4.13
MET D 325	SD	3.88	LEU D 286	N	4.25
MET D 325	SD	4.4	LEU D 286	N	4.15
MET D 325	SD	4.13	LEU D 286	N	4.87

MET D 325	SD	3.57	ALA D 285	CB	4.82
MET D 325	SD	4.33	ALA D 285	CB	4.37
MET D 325	CG	4.85	ALA D 285	CB	4.86
MET D 325	CG	4.66	ALA D 285	CB	4.92
LEU D 248	CB	4.24	ALA D 285	CB	3.82
LEU D 248	CB	4.34	ALA D 285	C	3.47
LEU D 248	CB	4.77	ALA D 285	C	4.67
LEU D 248	CA	4.8	ALA D 285	C	4.64
LEU D 248	CA	4.96	ALA D 285	C	4.7
LEU D 248	CA	4.91	ALA D 285	C	4.98
LEU D 248	N	4.07	ALA D 285	CA	3.47
GLN D 247	OE1	4.82	ALA D 285	CA	4.42
GLN D 247	NE2	3.26	ALA D 285	CA	3.66
GLN D 247	NE2	4.13	ALA D 285	CA	4.08
GLN D 247	NE2	4.14	ALA D 285	CA	4.74
GLN D 247	NE2	4.41	ALA D 285	CA	4.98
GLN D 247	CD	3.8	ALA D 285	CA	4.07
GLN D 247	CD	4.09	ALA D 285	N	4.96
GLN D 247	CD	3.82	ALA D 285	N	4.82
GLN D 247	CD	4.81	ARG D 284	O	4.92
GLN D 247	CD	4.78	ARG D 284	O	3.49
GLN D 247	CD	4.92	ARG D 284	O	3.91
GLN D 247	CG	4.4	ARG D 284	C	3.65
GLN D 247	CG	4.7	ARG D 284	C	4.56
GLN D 247	CG	3.71	ARG D 284	C	3.98
GLN D 247	CG	3.47	ARG D 284	C	4.71
GLN D 247	CG	4.78	GLN D 281	OE1	3.92
GLN D 247	CG	4.89	GLN D 281	OE1	4.62
GLN D 247	CG	3.54	GLN D 281	OE1	3.83
GLN D 247	CG	4.61	GLN D 281	OE1	3.59
GLN D 247	CG	4.31	GLN D 281	OE1	3.96
GLN D 247	CG	4.32	GLN D 281	OE1	4.76
GLN D 247	CB	3.71	GLN D 281	OE1	4.04
GLN D 247	CB	4.14	GLN D 281	OE1	3.63
GLN D 247	CB	4.77	GLN D 281	OE1	4.24
GLN D 247	CB	4.45	GLN D 281	NE2	3.8
GLN D 247	CB	4.55	GLN D 281	NE2	4.36
GLN D 247	CB	4.67	GLN D 281	NE2	4.87
GLN D 247	CB	4.96	GLN D 281	NE2	3.66
GLN D 247	CB	4.92	GLN D 281	NE2	4.17
GLN D 247	C	4.72	GLN D 281	NE2	4.98
GLN D 247	C	4.95	GLN D 281	NE2	3.9
GLN D 247	C	4.64	GLN D 281	NE2	3.52
GLN D 247	CA	4.6	GLN D 281	NE2	4.37
GLN D 247	CA	4.72	GLN D 281	NE2	4.85
GLN D 247	CA	4.79	GLN D 281	CD	4.66
GLN D 247	CA	4.73	GLN D 281	CD	3.45
GLN D 247	CA	4.25	GLN D 281	CD	3.71
GLN D 247	CA	4.88	GLN D 281	CD	4.23
GLN D 247	N	4.72	GLN D 281	CD	4.84
GLN D 247	N	4.01	GLN D 281	CD	4.43
GLN D 247	N	4.82	GLN D 281	CD	4.08
GLN D 247	N	4.49	GLN D 281	CD	3.85

GLN D 247	N	3.73	GLN D 281	CD	3.86
GLY D 246	O	4.21	GLN D 281	CD	3.99
GLY D 246	C	3.74	GLN D 281	CD	4.59
GLY D 246	C	3.98	GLN D 281	CD	4.7
GLY D 246	C	3.63	GLN D 281	CG	4.69
GLY D 246	C	4.16	GLN D 281	CG	3.44
GLY D 246	C	4.43	GLN D 281	CG	3.92
GLY D 246	CA	3.63	GLN D 281	CG	4.12
GLY D 246	CA	3.73	GLN D 281	CG	4.44
GLY D 246	CA	3.16	GLN D 281	CG	4.21
GLY D 246	CA	4.7	GLN D 281	CG	4.81
GLY D 246	CA	3.47	GLN D 281	CB	4.2
GLY D 246	CA	3.37	GLN D 281	CB	4.45
GLY D 246	CA	4.57	GLN D 281	CB	4.53
GLY D 246	CA	4.68	GLN D 281	CB	4.27
GLY D 246	CA	4.98	GLN D 281	CB	4.5
GLY D 246	N	3.84	GLN D 281	CB	4.01
GLY D 246	N	4.67	GLN D 281	O	4.34
PRO D 245	CB	4.82	GLN D 281	O	4.71
PRO D 245	O	4.78	GLN D 281	O	3.48
PRO D 245	O	3.81	GLN D 281	O	3.57
PRO D 245	O	4.48	GLN D 281	C	4.87
PRO D 245	O	4.39	GLN D 281	C	4.67
PRO D 245	O	4.17	GLN D 281	C	4.28
PRO D 245	C	4.42	GLN D 281	C	4.05
PRO D 245	C	4.85	GLN D 281	C	4.66
PRO D 245	C	4.79	GLN D 281	CA	4.51
PRO D 245	C	4.25	GLN D 281	CA	4.33
PRO D 245	C	4.78	GLN D 281	CA	4.84
TYR A 224	CE1	4.82	ARG D 278	NH2	3.95
TYR A 224	CE1	4.6	ARG D 278	CZ	3.83
TYR A 224	CD1	4.39	ARG D 278	CZ	4.92
TYR A 224	CD1	3.88	ARG D 278	CG	4.62
TYR A 224	CG	4.8	THR D 276	O	4.26
TYR A 224	CB	4.8	THR D 276	O	3.54
TYR A 224	N	4.47	THR D 276	O	4.26
THR A 223	OG1	4.83	THR D 276	C	4.64
THR A 223	OG1	4.74	THR D 276	N	4.47
THR A 223	CG2	4.82	THR D 276	N	4.62
THR A 223	CG2	4.62	LEU D 275	CD2	4.58
THR A 223	CG2	4.06	LEU D 275	CD2	4.27
THR A 223	CG2	4.06	LEU D 275	C	4.95
THR A 223	CG2	3.88	LEU D 275	CA	4.89
THR A 223	CG2	3.64	LEU D 275	CA	4.27
THR A 223	CG2	3.66	LEU D 275	N	4.98
THR A 223	CG2	3.9	LEU D 275	N	4.73
THR A 223	CG2	4.74	PRO D 274	CB	4.74
THR A 223	CG2	3.77	PRO D 274	CG	4.59
THR A 223	CG2	4.55	PRO D 274	CG	4.25
THR A 223	CG2	4.7	PRO D 274	CG	4.58
THR A 223	CB	4.72	PRO D 274	CG	4.55
THR A 223	CB	4.87	PRO D 274	O	4.16
THR A 223	CB	4.88	PRO D 274	O	3.15

THR A 223	CB	4.75	PRO D 274	O	3.45
THR A 223	CB	4.27	PRO D 274	O	4.62
THR A 223	CB	3.62	PRO D 274	C	4.23
THR A 223	CB	4.76	PRO D 274	C	4.34
THR A 223	CA	4.92	PHE D 272	CE2	4.43
THR A 223	CA	4.64	HIS D 229	NE2	3.46
ARG A 221	NH2	3.25	HIS D 229	NE2	4.1
ARG A 221	NH2	4.96	HIS D 229	NE2	3.69
ARG A 221	NH2	4.5	HIS D 229	CE1	4.6
ARG A 221	NH1	4.67	HIS D 229	CE1	4.29
ARG A 221	NH1	4.91	HIS D 229	CE1	4.53
ARG A 221	NH1	4.94	HIS D 229	CE1	3.91
ARG A 221	CZ	4.02	HIS D 229	CD2	4.51
ARG A 221	CZ	3.87	LEU D 217	CD2	4.1
ARG A 221	CZ	4.91	LEU D 217	CD2	3.95
ARG A 221	NE	4.62	LEU D 217	CD1	4.97

Table 4.3: Amino-Nos_DOX: Geometry of hydrogen bonds and hydrophobic interaction of Amino-Nos _DOX with the binding site residues of tubulin.

(a) Amino_Tubulin			**(b) DOX_Tubulin**		
Hydrogen bonding			**Hydrogen bonding**		
Hydrogen Donor (D)	**Hydrogen Acceptor (A)**	**Distance (D-A) in Å**	**Hydrogen Donor (D)**	**Hydrogen Acceptor (A)**	**Distance (D-A) in Å**
ASP D 357	OD1	4.23	O12 DOX	O13	2.6
Amino	O16	2.92	O3 DOX	O2	2.71
Amino	O19	2.8	GLY D 370	O	3.69
PRO D 245	O	4.03	ARG D 369	O	4.96
Amino	O21	3.46	ARG D 284	O	2.66
Amino	O21	3.43	GLN D 281	OE1	4.73
			GLN D 281	OE1	3.56
			NE2 DOX	O3	3.57
			GLN D 281	O	3.89
			NH2 DOX	O3	4.85
			NH2 DOX	O2	3.05
			NE DOX	O3	4.34
			NE DOX	O2	3.93
Hydrophobic interaction			**Hydrophobic interaction**		
Amino	**Tubulin**	**Distance**	**DOX**	**Tubulin**	**Distance**
C53 ASP D 357	OD2	3.89	C25 LYS D 372	NZ	4.11
C53 ASP D 357	OD2	3.89	C24 LYS D 372	NZ	4.53
C52 ASP D 357	OD2	3.69	C20 LYS D 372	NZ	4.83
C53 ASP D 357	OD1	3.42	C25 LYS D 372	CE	3.76
C52 ASP D 357	OD1	4.1	C24 LYS D 372	CE	4.58
C49 ASP D 357	OD1	4.68	C20 LYS D 372	CE	4.11
C45 ASP D 357	OD1	4.94	O8 LYS D 372	CE	3.44
C53 ASP D 357	CG	3.96	C19 LYS D 372	CE	4.05
C52 ASP D 357	CG	4.23	O8 LYS D 372	CD	4.17
C61 VAL D 355	O	3.01	C19 LYS D 372	CD	4.95
C60 VAL D 355	O	3.48	O8 LYS D 372	CG	3.77
C59 VAL D 355	O	4.58	C19 LYS D 372	CG	4.56

C57 VAL D 355	O	4.83	C16 LYS D 372	CG	4.99
C56 VAL D 355	O	3.85	C40 LEU D 371	CD2	4.97
C54 VAL D 355	O	4.4	C16 LEU D 371	CD2	4.93
C53 VAL D 355	O	4.87	C15 LEU D 371	CD2	4.16
C52 VAL D 355	O	4.52	O5 LEU D 371	CD2	4.11
C61 VAL D 355	C	4.15	O4 LEU D 371	CD2	3.16
C60 VAL D 355	C	4.46	C14 LEU D 371	CD2	3.58
C56 VAL D 355	C	4.88	C13 LEU D 371	CD2	4.16
C61 VAL D 355	CA	4.77	C12 LEU D 371	CD2	3.98
C64 VAL D 355	N	4.97	C7 LEU D 371	CD2	4.23
C61 VAL D 355	N	4.35	C6 LEU D 371	CD2	3.79
C60 VAL D 355	N	4.33	N1 LEU D 371	CD2	4.8
C59 VAL D 355	N	4.61	C12 LEU D 371	CD1	4.09
C58 VAL D 355	N	4.91	C11 LEU D 371	CD1	4.82
C57 VAL D 355	N	4.9	C6 LEU D 371	CD1	4.95
C56 VAL D 355	N	4.64	O4 LEU D 371	CG	4.5
C64 ALA D 354	CB	3.2	C14 LEU D 371	CG	4.78
C63 ALA D 354	CB	4.58	C13 LEU D 371	CG	4.96
O19 ALA D 354	CB	3.78	C12 LEU D 371	CG	4.24
C60 ALA D 354	CB	4.55	C7 LEU D 371	CG	4.74
C59 ALA D 354	CB	4.15	C6 LEU D 371	CG	4.25
C58 ALA D 354	CB	4.79	N1 LEU D 371	CG	4.85
C64 ALA D 354	CA	4.26	C14 GLY D 370	O	4.34
C63 ALA D 354	CA	4.15	C13 GLY D 370	O	3.82
O19 ALA D 354	CA	4.44	C6 GLY D 370	O	3.74
O18 ALA D 354	CA	4.94	C5 GLY D 370	O	4.76
C60 ALA D 354	CA	4.83	C3 GLY D 370	O	4.24
C59 ALA D 354	CA	4.41	C1 GLY D 370	O	4.84
C58 ALA D 354	CA	4.64	C6 GLY D 370	C	4.79
C63 ALA D 354	N	4.57	N1 GLY D 370	C	4.58
C63 THR D 353	O	3.03	C3 GLY D 370	C	4.47
C58 THR D 353	O	4.89	C3 GLY D 370	CA	3.81
C63 THR D 353	C	4.12	C2 GLY D 370	CA	4.95
N3 MET D 325	CE	3.45	C1 GLY D 370	CA	4.85
C62 MET D 325	CE	4.38	C3 GLY D 370	N	4.45
C56 MET D 325	CE	4.49	C4 ARG D 369	O	4.83
C55 MET D 325	CE	4.53	C3 ARG D 369	O	3.62
O17 MET D 325	CE	3.46	C2 ARG D 369	O	4.02
C54 MET D 325	CE	3.33	C1 ARG D 369	O	3.23
C52 MET D 325	CE	3.88	C3 ARG D 369	C	4.36
C51 MET D 325	CE	3.98	C1 ARG D 369	C	4.42
O21 MET D 325	SD	4.91	C43 LEU D 286	CD2	3.92
C55 MET D 325	SD	4.48	C40 LEU D 286	CD2	4.34
O17 MET D 325	SD	3.83	C39 LEU D 286	CD2	4.3
C54 MET D 325	SD	4.17	C38 LEU D 286	CD2	4.85
O17 MET D 325	CG	4.65	C16 LEU D 286	CD2	4.39
C64 LEU D 248	CG	4.85	C15 LEU D 286	CD2	4.19
O19 LEU D 248	CG	4.96	C40 LEU D 286	CD1	4.87
C64 LEU D 248	CB	3.67	C43 LEU D 286	CG	4.34
C63 LEU D 248	CB	4.37	C40 LEU D 286	CG	4.68
O19 LEU D 248	CB	3.55	C39 LEU D 286	CG	4.91
O18 LEU D 248	CB	4.62	O14 LEU D 286	CG	4.96
C59 LEU D 248	CB	4.78	C43 LEU D 286	CB	3.48

C64 LEU D 248	O	3.34	C41 LEU D 286	CB	4.96
C64 LEU D 248	C	4.05	C40 LEU D 286	CB	4.2
O19 LEU D 248	C	4.37	C39 LEU D 286	CB	4.34
C64 LEU D 248	CA	3.88	C38 LEU D 286	CB	4.34
O19 LEU D 248	CA	3.71	O14 LEU D 286	CB	3.59
C64 LEU D 248	N	3.32	C37 LEU D 286	CB	4.36
C63 LEU D 248	N	4.68	C36 LEU D 286	CB	4.95
C59 LEU D 248	N	4.03	C35 LEU D 286	CB	4.49
C58 LEU D 248	N	4.58	C35 LEU D 286	O	4.75
C65 GLN D 247	NE2	3.65	C43 LEU D 286	CA	4.6
C48 GLN D 247	NE2	3.71	O14 LEU D 286	CA	3.84
C46 GLN D 247	NE2	4.03	C37 LEU D 286	CA	4.9
C44 GLN D 247	NE2	4.52	C35 LEU D 286	CA	4.86
C65 GLN D 247	CD	4.32	C43 LEU D 286	N	4.39
O20 GLN D 247	CD	4.39	C38 LEU D 286	N	4.96
O16 GLN D 247	CD	3.56	C37 LEU D 286	N	4.13
C48 GLN D 247	CD	4.41	C36 LEU D 286	N	4.25
C46 GLN D 247	CD	4.65	C35 LEU D 286	N	4.15
C65 GLN D 247	CG	3.99	C34 LEU D 286	N	4.87
O20 GLN D 247	CG	3.66	O14 ALA D 285	CB	4.82
O19 GLN D 247	CG	4.53	O13 ALA D 285	CB	4.37
O18 GLN D 247	CG	3.97	C36 ALA D 285	CB	4.86
C59 GLN D 247	CG	4.33	C35 ALA D 285	CB	4.92
C58 GLN D 247	CG	4.07	O12 ALA D 285	CB	3.82
C57 GLN D 247	CG	4.55	O14 ALA D 285	C	3.47
O16 GLN D 247	CG	3.55	C37 ALA D 285	C	4.67
C48 GLN D 247	CG	4.64	O13 ALA D 285	C	4.64
C46 GLN D 247	CG	4.32	C36 ALA D 285	C	4.7
C44 GLN D 247	CG	4.42	C35 ALA D 285	C	4.98
C64 GLN D 247	CB	4.9	O14 ALA D 285	CA	3.47
C63 GLN D 247	CB	4.66	C37 ALA D 285	CA	4.42
O20 GLN D 247	CB	4.87	O13 ALA D 285	CA	3.66
O19 GLN D 247	CB	3.71	C36 ALA D 285	CA	4.08
O18 GLN D 247	CB	3.46	C35 ALA D 285	CA	4.74
C60 GLN D 247	CB	4.94	C34 ALA D 285	CA	4.98
C59 GLN D 247	CB	3.96	O12 ALA D 285	CA	4.07
C58 GLN D 247	CB	3.86	C37 ALA D 285	N	4.96
C57 GLN D 247	CB	4.78	C36 ALA D 285	N	4.82
O16 GLN D 247	CB	4.72	C38 ARG D 284	O	4.92
C64 GLN D 247	C	4.24	C37 ARG D 284	O	3.49
O19 GLN D 247	C	3.62	C36 ARG D 284	O	3.91
O18 GLN D 247	C	4.71	O14 ARG D 284	C	3.65
C59 GLN D 247	C	4.63	C37 ARG D 284	C	4.56
C64 GLN D 247	CA	4.34	O13 ARG D 284	C	3.98
O19 GLN D 247	CA	3.51	C36 ARG D 284	C	4.71
O18 GLN D 247	CA	4.37	C42 GLN D 281	OE1	3.92
C60 GLN D 247	CA	4.93	C41 GLN D 281	OE1	4.62
C59 GLN D 247	CA	4.13	C40 GLN D 281	OE1	3.83
C58 GLN D 247	CA	4.53	C39 GLN D 281	OE1	3.59
O16 GLN D 247	CA	4.85	C38 GLN D 281	OE1	3.96
C64 GLN D 247	N	3.42	C37 GLN D 281	OE1	4.76
C61 GLN D 247	N	4.85	C15 GLN D 281	OE1	4.04
C60 GLN D 247	N	3.8	C14 GLN D 281	OE1	3.63

C59 GLN D 247	N	3.31	C13 GLN D 281	OE1	4.24
C58 GLN D 247	N	4.08	C40 GLN D 281	NE2	3.8
C48 GLN D 247	N	4.67	C39 GLN D 281	NE2	4.36
C46 GLN D 247	N	4.86	C15 GLN D 281	NE2	4.87
C48 GLY D 246	O	4.23	C14 GLN D 281	NE2	3.66
C64 GLY D 246	C	3.95	C13 GLN D 281	NE2	4.17
O19 GLY D 246	C	3.73	C10 GLN D 281	NE2	4.98
C60 GLY D 246	C	4.22	C9 GLN D 281	NE2	3.9
C59 GLY D 246	C	4.15	C8 GLN D 281	NE2	3.52
O16 GLY D 246	C	4	C7 GLN D 281	NE2	4.37
C48 GLY D 246	C	4.07	C6 GLN D 281	NE2	4.85
O15 GLY D 246	C	4.57	C42 GLN D 281	CD	4.66
C46 GLY D 246	C	4.74	C40 GLN D 281	CD	3.45
C64 GLY D 246	CA	3.71	C39 GLN D 281	CD	3.71
O19 GLY D 246	CA	3.81	C38 GLN D 281	CD	4.23
C61 GLY D 246	CA	4.43	C37 GLN D 281	CD	4.84
C60 GLY D 246	CA	3.54	C15 GLN D 281	CD	4.43
C59 GLY D 246	CA	3.97	O5 GLN D 281	CD	4.08
O16 GLY D 246	CA	4	O4 GLN D 281	CD	3.85
C48 GLY D 246	CA	3.9	C14 GLN D 281	CD	3.86
O15 GLY D 246	CA	3.91	O3 GLN D 281	CD	3.99
C47 GLY D 246	CA	4.31	C13 GLN D 281	CD	4.59
C46 GLY D 246	CA	4.36	C8 GLN D 281	CD	4.7
C60 GLY D 246	N	4.72	C42 GLN D 281	CG	4.69
C48 GLY D 246	N	3.64	C40 GLN D 281	CG	3.44
C47 GLY D 246	N	4.21	C39 GLN D 281	CG	3.92
C46 GLY D 246	N	4.63	C38 GLN D 281	CG	4.12
C45 GLY D 246	N	4.99	O14 GLN D 281	CG	4.44
N2 PRO D 245	CB	3.86	C37 GLN D 281	CG	4.21
C48 PRO D 245	CB	3.97	O4 GLN D 281	CG	4.81
O15 PRO D 245	CB	3.04	C42 GLN D 281	CB	4.2
C47 PRO D 245	CB	4.08	C40 GLN D 281	CB	4.45
C45 PRO D 245	CB	4.45	C39 GLN D 281	CB	4.53
N2 PRO D 245	CG	4.66	C38 GLN D 281	CB	4.27
O15 PRO D 245	CG	4.39	O14 GLN D 281	CB	4.5
C61 PRO D 245	O	4.88	C37 GLN D 281	CB	4.01
C60 PRO D 245	O	4.51	C42 GLN D 281	O	4.34
C48 PRO D 245	O	4.69	C38 GLN D 281	O	4.71
C47 PRO D 245	O	4.16	C37 GLN D 281	O	3.48
C46 PRO D 245	O	5	C36 GLN D 281	O	3.57
C45 PRO D 245	O	4.27	C42 GLN D 281	C	4.87
N2 PRO D 245	C	4.45	O14 GLN D 281	C	4.67
O16 PRO D 245	C	4.85	C37 GLN D 281	C	4.28
C48 PRO D 245	C	4.1	O13 GLN D 281	C	4.05
O15 PRO D 245	C	3.44	C36 GLN D 281	C	4.66
C47 PRO D 245	C	4.16	O14 GLN D 281	CA	4.51
C46 PRO D 245	C	4.93	C37 GLN D 281	CA	4.33
C45 PRO D 245	C	4.62	O13 GLN D 281	CA	4.84
N2 PRO D 245	CA	4.79	C5 ARG D 278	NH2	3.95
C48 PRO D 245	CA	4.53	O2 ARG D 278	CZ	3.83
O15 PRO D 245	CA	3.81	C5 ARG D 278	CZ	4.92
C47 PRO D 245	CA	4.8	O3 ARG D 278	CG	4.62
C64 CYS D 241	SG	3.96	C10 THR D 276	O	4.26

C64 CYS D 241	CB	4.98	C9 THR D 276	O	3.54
N2 LEU D 42	CD2	4.45	C8 THR D 276	O	4.26
C65 TYR A 224	CD1	4.56	C9 THR D 276	C	4.64
C62 THR A 223	CG2	4.79	C10 THR D 276	N	4.47
C63 ARG A 221	NH2	4.84	C9 THR D 276	N	4.62
C55 ARG A 221	NH2	4.46	C11 LEU D 275	CD2	4.58
C55 ARG A 221	NH1	4.36	C10 LEU D 275	CD2	4.27
O21 ARG A 221	CZ	3.71	C10 LEU D 275	C	4.95
C55 ARG A 221	CZ	4.61	C11 LEU D 275	CA	4.89
			C10 LEU D 275	CA	4.27
			C11 LEU D 275	N	4.98
			C10 LEU D 275	N	4.73
			C40 PRO D 274	CB	4.74
			C40 PRO D 274	CG	4.59
			O4 PRO D 274	CG	4.25
			C12 PRO D 274	CG	4.58
			C11 PRO D 274	CG	4.55
			C12 PRO D 274	O	4.16
			C11 PRO D 274	O	3.15
			C10 PRO D 274	O	3.45
			C9 PRO D 274	O	4.62
			C11 PRO D 274	C	4.23
			C10 PRO D 274	C	4.34
			C11 PHE D 272	CE2	4.43
			C4 HIS D 229	NE2	3.46
			C2 HIS D 229	NE2	4.1
			C1 HIS D 229	NE2	3.69
			O1 HIS D 229	CE1	4.6
			C4 HIS D 229	CE1	4.29
			C2 HIS D 229	CE1	4.53
			C1 HIS D 229	CE1	3.91
			C4 HIS D 229	CD2	4.51
			C10 LEU D 217	CD2	4.1
			C9 LEU D 217	CD2	3.95
			C10 LEU D 217	CD1	4.97

Table 4.4: Br-Nos_DOX: Geometry of hydrogen bonds and hydrophobic interaction of Br-Nos _DOX with the binding site residues of tubulin.

(a) Br- Nos_Tubulin			**(b) DOX_Tubulin**		
Hydrogen bonding			**Hydrogen bonding**		
Hydrogen Donor (D)	**Hydrogen Acceptor (A)**	**Distance (D-A) in Å**	**Hydrogen Donor (D)**	**Hydrogen Acceptor (A)**	**Distance (D-A) in Å**
ASP D 357	OD2	4.89	O12 DOX 900	O13	2.6
VAL D 355	O	2.83	O3 DOX 900	O2	2.71
Bromo	BR1	3.12	N1 GLY D 370	O	3.69
Bromo	O15	3.95	N1 ARG D 369	O	4.96
Bromo	O21	2.83	O14 ARG D 284	O	2.66
Bromo	O19	2.99	O6 GLN D 281	OE1	4.73
Bromo	O16	3.8	O3 GLN D 281	OE1	3.56
			NE2 UNK 900	O3	3.57

			O14 GLN D 281	O	3.89
			NH2 DOX 900	O3	4.85
			NH2 DOX 900	O2	3.05
			NE DOX 900	O3	4.34
			NE DOX 900	O2	3.93
Hydrophobic interaction			**Hydrophobic interaction**		
BrBn_Nos_Tubulin	**Tubulin**	**Distance**	**DOX**	**Tubulin**	**Distance**
ASP D 357	OD2	3.79	C25 LYS D 372	NZ	4.11
ASP D 357	OD1	4.26	C24 LYS D 372	NZ	4.53
ASP D 357	CG	4.3	C20 LYS D 372	NZ	4.83
VAL D 355	CG2	3.83	C25 LYS D 372	CE	3.76
VAL D 355	CG2	4.73	C24 LYS D 372	CE	4.58
VAL D 355	CG2	4.59	C20 LYS D 372	CE	4.11
VAL D 355	CG2	4.71	O8 LYS D 372	CE	3.44
VAL D 355	CB	4.58	C19 LYS D 372	CE	4.05
VAL D 355	CB	4.95	O8 LYS D 372	CD	4.17
VAL D 355	CB	3.99	C19 LYS D 372	CD	4.95
VAL D 355	CB	4.29	O8 LYS D 372	CG	3.77
VAL D 355	CB	3.91	C19 LYS D 372	CG	4.56
VAL D 355	CB	4.48	C16 LYS D 372	CG	4.99
VAL D 355	O	3.74	C40 LEU D 371	CD2	4.97
VAL D 355	O	4.82	C16 LEU D 371	CD2	4.93
VAL D 355	O	4.97	C15 LEU D 371	CD2	4.16
VAL D 355	O	4.13	O5 LEU D 371	CD2	4.11
VAL D 355	O	4.51	O4 LEU D 371	CD2	3.16
VAL D 355	O	2.9	C14 LEU D 371	CD2	3.58
VAL D 355	O	4.8	C13 LEU D 371	CD2	4.16
VAL D 355	O	3.33	C12 LEU D 371	CD2	3.98
VAL D 355	O	3.41	C7 LEU D 371	CD2	4.23
VAL D 355	O	4.81	C6 LEU D 371	CD2	3.79
VAL D 355	C	3.96	N1 LEU D 371	CD2	4.8
VAL D 355	C	4.68	C12 LEU D 371	CD1	4.09
VAL D 355	C	4.7	C11 LEU D 371	CD1	4.82
VAL D 355	C	4.19	C6 LEU D 371	CD1	4.95
VAL D 355	C	3.74	O4 LEU D 371	CG	4.5
VAL D 355	C	4.56	C14 LEU D 371	CG	4.78
VAL D 355	C	4.42	C13 LEU D 371	CG	4.96
VAL D 355	CA	4.71	C12 LEU D 371	CG	4.24
VAL D 355	CA	4.32	C7 LEU D 371	CG	4.74
VAL D 355	CA	4.31	C6 LEU D 371	CG	4.25
VAL D 355	CA	4.53	N1 LEU D 371	CG	4.85
VAL D 355	CA	3.82	C14 GLY D 370	O	4.34
VAL D 355	CA	4.74	C13 GLY D 370	O	3.82
VAL D 355	N	3.44	C6 GLY D 370	O	3.74
VAL D 355	N	4.43	C5 GLY D 370	O	4.76
VAL D 355	N	4.2	C3 GLY D 370	O	4.24
VAL D 355	N	3.38	C1 GLY D 370	O	4.84
VAL D 355	N	4.37	C6 GLY D 370	C	4.79
VAL D 355	N	3.24	N1 GLY D 370	C	4.58
VAL D 355	N	4.54	C3 GLY D 370	C	4.47
ALA D 354	CB	4.4	C3 GLY D 370	CA	3.81
ALA D 354	CB	4.95	C2 GLY D 370	CA	4.95
ALA D 354	CB	4.84	C1 GLY D 370	CA	4.85

ALA D 354	CB	4.41	C3 GLY D 370	N	4.45
ALA D 354	CB	4.58	C4 ARG D 369	O	4.83
ALA D 354	CB	4.23	C3 ARG D 369	O	3.62
ALA D 354	CB	4.4	C2 ARG D 369	O	4.02
ALA D 354	CB	4.85	C1 ARG D 369	O	3.23
ALA D 354	O	4.83	C3 ARG D 369	C	4.36
ALA D 354	C	3.87	C1 ARG D 369	C	4.42
ALA D 354	C	4.47	C43 LEU D 286	CD2	3.92
ALA D 354	C	4.6	C40 LEU D 286	CD2	4.34
ALA D 354	C	4.02	C39 LEU D 286	CD2	4.3
ALA D 354	C	4.89	C38 LEU D 286	CD2	4.85
ALA D 354	C	4.59	C16 LEU D 286	CD2	4.39
ALA D 354	C	4.26	C15 LEU D 286	CD2	4.19
ALA D 354	CA	4.97	C40 LEU D 286	CD1	4.87
ALA D 354	CA	4.75	C43 LEU D 286	CG	4.34
ALA D 354	CA	3.78	C40 LEU D 286	CG	4.68
ALA D 354	CA	4.01	C39 LEU D 286	CG	4.91
ALA D 354	CA	4.28	O14 LEU D 286	CG	4.96
ALA D 354	CA	4.25	C43 LEU D 286	CB	3.48
ALA D 354	CA	3.91	C41 LEU D 286	CB	4.96
ALA D 354	CA	3.79	C40 LEU D 286	CB	4.2
ALA D 354	CA	4.24	C39 LEU D 286	CB	4.34
ALA D 354	CA	4.36	C38 LEU D 286	CB	4.34
ALA D 354	CA	4.36	O14 LEU D 286	CB	3.59
ALA D 354	N	4.89	C37 LEU D 286	CB	4.36
ALA D 354	N	4.48	C36 LEU D 286	CB	4.95
ALA D 354	N	4.29	C35 LEU D 286	CB	4.49
ALA D 354	N	4.51	C35 LEU D 286	O	4.75
ALA D 354	N	4.8	C43 LEU D 286	CA	4.6
ALA D 354	N	4.85	O14 LEU D 286	CA	3.84
ALA D 354	N	4.81	C37 LEU D 286	CA	4.9
THR D 353	CB	3.68	C35 LEU D 286	CA	4.86
THR D 353	CB	4.77	C43 LEU D 286	N	4.39
THR D 353	CB	4.78	C38 LEU D 286	N	4.96
THR D 353	OG1	4.75	C37 LEU D 286	N	4.13
THR D 353	CG2	4.14	C36 LEU D 286	N	4.25
THR D 353	CG2	4.36	C35 LEU D 286	N	4.15
THR D 353	O	3.08	C34 LEU D 286	N	4.87
THR D 353	O	3.3	O14 ALA D 285	CB	4.82
THR D 353	O	4.29	O13 ALA D 285	CB	4.37
THR D 353	O	3.51	C36 ALA D 285	CB	4.86
THR D 353	O	3.08	C35 ALA D 285	CB	4.92
THR D 353	O	3.47	O12 ALA D 285	CB	3.82
THR D 353	O	4.14	O14 ALA D 285	C	3.47
THR D 353	O	4.59	C37 ALA D 285	C	4.67
THR D 353	O	4.95	O13 ALA D 285	C	4.64
THR D 353	C	3.85	C36 ALA D 285	C	4.7
THR D 353	C	4.49	C35 ALA D 285	C	4.98
THR D 353	C	4.23	O14 ALA D 285	CA	3.47
THR D 353	C	4.66	C37 ALA D 285	CA	4.42
THR D 353	C	4.05	O13 ALA D 285	CA	3.66
THR D 353	C	3.99	C36 ALA D 285	CA	4.08
THR D 353	C	4.47	C35 ALA D 285	CA	4.74

THR D 353	C	4.9	C34 ALA D 285	CA	4.98
THR D 353	CA	4.19	O12 ALA D 285	CA	4.07
THR D 353	CA	4.98	C37 ALA D 285	N	4.96
THR D 353	N	4.37	C36 ALA D 285	N	4.82
ASP D 329	OD1	4.3	C38 ARG D 284	O	4.92
ASP D 329	OD1	4.49	C37 ARG D 284	O	3.49
MET D 325	CE	4.17	C36 ARG D 284	O	3.91
MET D 325	CE	3.51	O14 ARG D 284	C	3.65
MET D 325	CE	3.44	C37 ARG D 284	C	4.56
MET D 325	CE	3.82	O13 ARG D 284	C	3.98
MET D 325	CE	4.13	C36 ARG D 284	C	4.71
MET D 325	CE	4.45	C42 GLN D 281	OE1	3.92
MET D 325	CE	4.27	C41 GLN D 281	OE1	4.62
MET D 325	CE	3.58	C40 GLN D 281	OE1	3.83
MET D 325	CE	4.33	C39 GLN D 281	OE1	3.59
MET D 325	CE	4.2	C38 GLN D 281	OE1	3.96
MET D 325	SD	3.48	C37 GLN D 281	OE1	4.76
MET D 325	SD	3.55	C15 GLN D 281	OE1	4.04
MET D 325	SD	3.25	C14 GLN D 281	OE1	3.63
MET D 325	SD	3.98	C13 GLN D 281	OE1	4.24
MET D 325	SD	4.11	C40 GLN D 281	NE2	3.8
MET D 325	SD	4.51	C39 GLN D 281	NE2	4.36
MET D 325	SD	4.39	C15 GLN D 281	NE2	4.87
MET D 325	SD	4.72	C14 GLN D 281	NE2	3.66
MET D 325	CG	3.5	C13 GLN D 281	NE2	4.17
MET D 325	CG	4.22	C10 GLN D 281	NE2	4.98
MET D 325	CG	4.68	C9 GLN D 281	NE2	3.9
MET D 325	CB	4.8	C8 GLN D 281	NE2	3.52
LEU D 248	CD2	4.62	C7 GLN D 281	NE2	4.37
LEU D 248	CD1	4.82	C6 GLN D 281	NE2	4.85
LEU D 248	CG	4.45	C42 GLN D 281	CD	4.66
LEU D 248	CB	3.41	C40 GLN D 281	CD	3.45
LEU D 248	CB	4.26	C39 GLN D 281	CD	3.71
LEU D 248	CB	4.5	C38 GLN D 281	CD	4.23
LEU D 248	CA	4.16	C37 GLN D 281	CD	4.84
LEU D 248	CA	4.41	C15 GLN D 281	CD	4.43
LEU D 248	N	3.85	O5 GLN D 281	CD	4.08
LEU D 248	N	4.5	O4 GLN D 281	CD	3.85
GLN D 247	NE2	4.3	C14 GLN D 281	CD	3.86
GLN D 247	NE2	4.06	O3 GLN D 281	CD	3.99
GLN D 247	CD	4.47	C13 GLN D 281	CD	4.59
GLN D 247	CD	4.71	C8 GLN D 281	CD	4.7
GLN D 247	CD	4.57	C42 GLN D 281	CG	4.69
GLN D 247	CG	3.82	C40 GLN D 281	CG	3.44
GLN D 247	CG	4.5	C39 GLN D 281	CG	3.92
GLN D 247	CG	4.46	C38 GLN D 281	CG	4.12
GLN D 247	CG	4.59	O14 GLN D 281	CG	4.44
GLN D 247	CG	4.79	C37 GLN D 281	CG	4.21
GLN D 247	CG	4.15	O4 GLN D 281	CG	4.81
GLN D 247	CG	4.05	C42 GLN D 281	CB	4.2
GLN D 247	CG	4.76	C40 GLN D 281	CB	4.45
GLN D 247	CG	3.96	C39 GLN D 281	CB	4.53
GLN D 247	CB	4.26	C38 GLN D 281	CB	4.27

GLN D 247	CB	3.25	O14 GLN D 281	CB	4.5
GLN D 247	CB	3.85	C37 GLN D 281	CB	4.01
GLN D 247	CB	4.86	C42 GLN D 281	O	4.34
GLN D 247	CB	4.89	C38 GLN D 281	O	4.71
GLN D 247	CB	4.19	C37 GLN D 281	O	3.48
GLN D 247	C	4.66	C36 GLN D 281	O	3.57
GLN D 247	C	3.89	C42 GLN D 281	C	4.87
GLN D 247	C	4.96	O14 GLN D 281	C	4.67
GLN D 247	CA	4.99	C37 GLN D 281	C	4.28
GLN D 247	CA	3.45	O13 GLN D 281	C	4.05
GLN D 247	CA	4.85	C36 GLN D 281	C	4.66
GLN D 247	CA	4.59	O14 GLN D 281	CA	4.51
GLN D 247	N	3.9	C37 GLN D 281	CA	4.33
GLY D 246	C	3.86	O13 GLN D 281	CA	4.84
GLY D 246	C	4.79	C5 ARG D 278	NH2	3.95
GLY D 246	CA	3.99	O2 ARG D 278	CZ	3.83
GLY D 246	CA	4.62	C5 ARG D 278	CZ	4.92
GLY D 246	CA	4.52	O3 ARG D 278	CG	4.62
GLY D 246	CA	4.63	C10 THR D 276	O	4.26
GLY D 246	CA	4.71	C9 THR D 276	O	3.54
PRO D 245	O	4.66	C8 THR D 276	O	4.26
PRO D 245	O	4.21	C9 THR D 276	C	4.64
PRO D 245	C	4.96	C10 THR D 276	N	4.47
TYR A 224	CZ	4.72	C9 THR D 276	N	4.62
TYR A 224	CE1	4.5	C11 LEU D 275	CD2	4.58
TYR A 224	CE1	3.55	C10 LEU D 275	CD2	4.27
TYR A 224	CE1	4.07	C10 LEU D 275	C	4.95
TYR A 224	CE1	4.95	C11 LEU D 275	CA	4.89
TYR A 224	CD1	4.28	C10 LEU D 275	CA	4.27
TYR A 224	CD1	3.06	C11 LEU D 275	N	4.98
TYR A 224	CD1	3.5	C10 LEU D 275	N	4.73
TYR A 224	CD1	4.65	C40 PRO D 274	CB	4.74
TYR A 224	CG	3.97	C40 PRO D 274	CG	4.59
TYR A 224	CG	4.54	O4 PRO D 274	CG	4.25
TYR A 224	CB	4.34	C12 PRO D 274	CG	4.58
TYR A 224	CB	4.75	C11 PRO D 274	CG	4.55
TYR A 224	CA	4.6	C12 PRO D 274	O	4.16
TYR A 224	N	3.61	C11 PRO D 274	O	3.15
THR A 223	OG1	4.9	C10 PRO D 274	O	3.45
THR A 223	CG2	4.23	C9 PRO D 274	O	4.62
THR A 223	CG2	3.8	C11 PRO D 274	C	4.23
THR A 223	CG2	4.34	C10 PRO D 274	C	4.34
THR A 223	CG2	4.94	C11 PHE D 272	CE2	4.43
THR A 223	CG2	4.45	C4 HIS D 229	NE2	3.46
THR A 223	CB	3.74	C2 HIS D 229	NE2	4.1
THR A 223	CB	3.78	C1 HIS D 229	NE2	3.69
THR A 223	CB	4.47	O1 HIS D 229	CE1	4.6
THR A 223	CB	4.98	C4 HIS D 229	CE1	4.29
THR A 223	CB	4.65	C2 HIS D 229	CE1	4.53
THR A 223	C	4.69	C1 HIS D 229	CE1	3.91
THR A 223	C	4.27	C4 HIS D 229	CD2	4.51
THR A 223	CA	3.86	C10 LEU D 217	CD2	4.1
THR A 223	CA	3.89	C9 LEU D 217	CD2	3.95

THR A 223	CA	4.94	C10 LEU D 217	CD1	4.97
PRO A 222	O	4.98			
ARG A 221	NH2	4.1			
ARG A 221	NH2	3.35			
ARG A 221	NH2	4.57			
ARG A 221	NH2	3.55			
ARG A 221	NH2	3.42			
ARG A 221	NH2	4.4			
ARG A 221	NH1	3.15			
ARG A 221	NH1	4.97			
ARG A 221	NH1	4.75			
ARG A 221	NH1	4.67			
ARG A 221	NH1	4.85			
ARG A 221	CZ	3.5			
ARG A 221	CZ	4.66			
ARG A 221	CZ	4.29			
ARG A 221	CZ	4.25			
ARG A 221	CZ	4.37			
ARG A 221	CZ	4.45			
ARG A 221	CZ	4.85			
ARG A 221	NE	3.94			
ARG A 221	NE	4.91			
ARG A 221	CD	4.16			
THR A 179	CG2	4.25			
THR A 179	CG2	4.78			
SER A 178	O	4.58			
GLN A 176	O	4.8			

Table 4.5: Br-Bn_Nos_DOX: Geometry of hydrogen bonds and hydrophobic interaction of Br-Bn_Nos_DOX with the binding site residues of tubulin.

(a) Br-Bn_Nos_Tubulin			**(b) DOX_Tubulin**		
Hydrogen bonding			**Hydrogen bonding**		
Hydrogen Donor (D)	**Hydrogen Acceptor (A)**	**Distance (D-A) in Å**	**Hydrogen Donor (D)**	**Hydrogen Acceptor (A)**	**Distance (D-A) in Å**
			O12 UNK 900	O13	2.6
			O3 UNK 900	O2	2.71
			N1 GLY D 370	O	3.69
			N1 ARG D 369	O	4.96
			O14 ARG D 284	O	2.66
			O6 GLN D 281	OE1	4.73
			O3 GLN D 281	OE1	3.56
			NE2 UNK 900	O3	3.57
			O14 GLN D 281	O	3.89
			NH2 UNK 900	O3	4.85
			NH2 UNK 900	O2	3.05
			NE UNK 900	O3	4.34
			NE UNK 900	O2	3.93
Hydrophobic interaction			**Hydrophobic interaction**		
BrBn_Nos_Tubulin	**Tubulin**	**Distance**	**DOX**	**Tubulin**	**Distance**
C65 ASP D 357	OD1	4.67	C25 LYS D 372	NZ	4.11

C59 ASP D 357	OD1	4.99	C24 LYS D 372	NZ	4.53
C65 ASP D 357	CG	4.84	C20 LYS D 372	NZ	4.83
C65 ASP D 357	CB	4.82	C25 LYS D 372	CE	3.76
C65 ASP D 357	CA	4.88	C24 LYS D 372	CE	4.58
C65 ASP D 357	N	3.73	C20 LYS D 372	CE	4.11
C58 ASP D 357	N	4.86	O8 LYS D 372	CE	3.44
C65 CYS D 356	SG	3.44	C19 LYS D 372	CE	4.05
C64 CYS D 356	SG	4.57	O8 LYS D 372	CD	4.17
O19 CYS D 356	SG	3.57	C19 LYS D 372	CD	4.95
C58 CYS D 356	SG	4.89	O8 LYS D 372	CG	3.77
C65 CYS D 356	CB	3.97	C19 LYS D 372	CG	4.56
C64 CYS D 356	CB	4.09	C16 LYS D 372	CG	4.99
O21 CYS D 356	CB	4.57	C40 LEU D 371	CD2	4.97
O19 CYS D 356	CB	3.5	C16 LEU D 371	CD2	4.93
C58 CYS D 356	CB	4.51	C15 LEU D 371	CD2	4.16
C57 CYS D 356	CB	4.93	O5 LEU D 371	CD2	4.11
C65 CYS D 356	C	4.19	O4 LEU D 371	CD2	3.16
O19 CYS D 356	C	4.15	C14 LEU D 371	CD2	3.58
C58 CYS D 356	C	4.84	C13 LEU D 371	CD2	4.16
C65 CYS D 356	CA	3.57	C12 LEU D 371	CD2	3.98
C64 CYS D 356	CA	4.35	C7 LEU D 371	CD2	4.23
O21 CYS D 356	CA	4.38	C6 LEU D 371	CD2	3.79
O19 CYS D 356	CA	3.08	N1 LEU D 371	CD2	4.8
C59 CYS D 356	CA	4.77	C12 LEU D 371	CD1	4.09
C58 CYS D 356	CA	3.79	C11 LEU D 371	CD1	4.82
C57 CYS D 356	CA	4.35	C6 LEU D 371	CD1	4.95
C65 CYS D 356	N	4.7	O4 LEU D 371	CG	4.5
C64 CYS D 356	N	4.55	C14 LEU D 371	CG	4.78
C58 CYS D 356	N	4.18	C13 LEU D 371	CG	4.96
C57 CYS D 356	N	4.33	C12 LEU D 371	CG	4.24
C71 VAL D 355	CG2	4.26	C7 LEU D 371	CG	4.74
C70 VAL D 355	CG2	4.73	C6 LEU D 371	CG	4.25
C71 VAL D 355	CB	4.78	N1 LEU D 371	CG	4.85
C65 VAL D 355	O	4.39	C14 GLY D 370	O	4.34
C64 VAL D 355	O	4.26	C13 GLY D 370	O	3.82
C62 VAL D 355	O	4.89	C6 GLY D 370	O	3.74
C60 VAL D 355	O	3.91	C5 GLY D 370	O	4.76
C59 VAL D 355	O	3.63	C3 GLY D 370	O	4.24
C58 VAL D 355	O	2.88	C1 GLY D 370	O	4.84
C57 VAL D 355	O	2.86	C6 GLY D 370	C	4.79
C56 VAL D 355	O	3.28	N1 GLY D 370	C	4.58
C55 VAL D 355	O	3.73	C3 GLY D 370	C	4.47
C54 VAL D 355	O	4.28	C3 GLY D 370	CA	3.81
C53 VAL D 355	O	4.82	C2 GLY D 370	CA	4.95
C65 VAL D 355	C	5	C1 GLY D 370	CA	4.85
C64 VAL D 355	C	4.58	C3 GLY D 370	N	4.45
O21 VAL D 355	C	3.86	C4 ARG D 369	O	4.83
O19 VAL D 355	C	4.01	C3 ARG D 369	O	3.62
C59 VAL D 355	C	4.75	C2 ARG D 369	O	4.02
C58 VAL D 355	C	3.85	C1 ARG D 369	O	3.23
C57 VAL D 355	C	3.76	C3 ARG D 369	C	4.36
C56 VAL D 355	C	4.33	C1 ARG D 369	C	4.42
C55 VAL D 355	C	4.91	C43 LEU D 286	CD2	3.92

O21 VAL D 355	CA	4.82	C40 LEU D 286	CD2	4.34
C57 VAL D 355	CA	4.85	C39 LEU D 286	CD2	4.3
C71 VAL D 355	N	4.29	C38 LEU D 286	CD2	4.85
C66 VAL D 355	N	4.55	C16 LEU D 286	CD2	4.39
C62 VAL D 355	N	4.29	C15 LEU D 286	CD2	4.19
C57 VAL D 355	N	4.57	C40 LEU D 286	CD1	4.87
C56 VAL D 355	N	4.58	C43 LEU D 286	CG	4.34
C54 VAL D 355	N	4.7	C40 LEU D 286	CG	4.68
O21 ALA D 354	CB	4.19	C39 LEU D 286	CG	4.91
O18 ALA D 354	CB	3.49	O14 LEU D 286	CG	4.96
C56 ALA D 354	CB	4.94	C43 LEU D 286	CB	3.48
C54 ALA D 354	CB	4.3	C41 LEU D 286	CB	4.96
C71 ALA D 354	C	4.43	C40 LEU D 286	CB	4.2
C70 ALA D 354	C	4.95	C39 LEU D 286	CB	4.34
C66 ALA D 354	C	4.76	C38 LEU D 286	CB	4.34
C62 ALA D 354	C	4.86	O14 LEU D 286	CB	3.59
O18 ALA D 354	C	4.98	C37 LEU D 286	CB	4.36
C71 ALA D 354	CA	4.18	C36 LEU D 286	CB	4.95
C70 ALA D 354	CA	4.63	C35 LEU D 286	CB	4.49
C68 ALA D 354	CA	5	C35 LEU D 286	O	4.75
C67 ALA D 354	CA	4.6	C43 LEU D 286	CA	4.6
C66 ALA D 354	CA	4.18	O14 LEU D 286	CA	3.84
C62 ALA D 354	CA	4.45	C37 LEU D 286	CA	4.9
O18 ALA D 354	CA	4.21	C35 LEU D 286	CA	4.86
C54 ALA D 354	CA	4.72	C43 LEU D 286	N	4.39
C71 ALA D 354	N	4.51	C38 LEU D 286	N	4.96
C70 ALA D 354	N	4.51	C37 LEU D 286	N	4.13
C69 ALA D 354	N	4.66	C36 LEU D 286	N	4.25
C68 ALA D 354	N	4.79	C35 LEU D 286	N	4.15
C67 ALA D 354	N	4.82	C34 LEU D 286	N	4.87
C66 ALA D 354	N	4.7	O14 ALA D 285	CB	4.82
C71 THR D 353	CB	5	O13 ALA D 285	CB	4.37
C70 THR D 353	CB	4.02	C36 ALA D 285	CB	4.86
C69 THR D 353	CB	3.6	C35 ALA D 285	CB	4.92
C68 THR D 353	CB	4.3	O12 ALA D 285	CB	3.82
C69 THR D 353	OG1	4.75	O14 ALA D 285	C	3.47
C71 THR D 353	CG2	4.39	C37 ALA D 285	C	4.67
C70 THR D 353	CG2	3.44	O13 ALA D 285	C	4.64
C69 THR D 353	CG2	3.57	C36 ALA D 285	C	4.7
C68 THR D 353	CG2	4.57	C35 ALA D 285	C	4.98
C71 THR D 353	O	3.99	O14 ALA D 285	CA	3.47
C70 THR D 353	O	3.83	C37 ALA D 285	CA	4.42
C69 THR D 353	O	3.35	O13 ALA D 285	CA	3.66
C68 THR D 353	O	3	C36 ALA D 285	CA	4.08
C67 THR D 353	O	3.24	C35 ALA D 285	CA	4.74
C66 THR D 353	O	3.76	C34 ALA D 285	CA	4.98
C62 THR D 353	O	4.75	O12 ALA D 285	CA	4.07
C71 THR D 353	C	4.4	C37 ALA D 285	N	4.96
C70 THR D 353	C	4.13	C36 ALA D 285	N	4.82
C69 THR D 353	C	3.89	C38 ARG D 284	O	4.92
C68 THR D 353	C	3.92	C37 ARG D 284	O	3.49
C67 THR D 353	C	4.24	C36 ARG D 284	O	3.91
C66 THR D 353	C	4.49	O14 ARG D 284	C	3.65

C70 THR D 353	CA	4.74	C37 ARG D 284	C	4.56
C69 THR D 353	CA	4.32	O13 ARG D 284	C	3.98
C68 THR D 353	CA	4.61	C36 ARG D 284	C	4.71
C69 THR D 353	N	4.88	C42 GLN D 281	OE1	3.92
C68 THR D 353	N	4.89	C41 GLN D 281	OE1	4.62
C70 ASP D 329	OD2	4.45	C40 GLN D 281	OE1	3.83
C69 ASP D 329	OD2	4.48	C39 GLN D 281	OE1	3.59
C71 ASP D 329	OD1	4.28	C38 GLN D 281	OE1	3.96
C70 ASP D 329	OD1	3.08	C37 GLN D 281	OE1	4.76
C69 ASP D 329	OD1	3.37	C15 GLN D 281	OE1	4.04
C68 ASP D 329	OD1	4.67	C14 GLN D 281	OE1	3.63
C70 ASP D 329	CG	4.13	C13 GLN D 281	OE1	4.24
C69 ASP D 329	CG	4.27	C40 GLN D 281	NE2	3.8
C70 VAL D 328	CG1	4.75	C39 GLN D 281	NE2	4.36
C71 MET D 325	CE	4.66	C15 GLN D 281	NE2	4.87
C62 MET D 325	CE	4.69	C14 GLN D 281	NE2	3.66
C61 MET D 325	CE	4.72	C13 GLN D 281	NE2	4.17
N2 MET D 325	SD	4.98	C10 GLN D 281	NE2	4.98
C71 MET D 325	SD	3.39	C9 GLN D 281	NE2	3.9
C70 MET D 325	SD	4.06	C8 GLN D 281	NE2	3.52
C66 MET D 325	SD	4.27	C7 GLN D 281	NE2	4.37
C62 MET D 325	SD	4.35	C6 GLN D 281	NE2	4.85
C61 MET D 325	SD	4.57	C42 GLN D 281	CD	4.66
C71 MET D 325	CG	4.48	C40 GLN D 281	CD	3.45
C70 MET D 325	CG	4.81	C39 GLN D 281	CD	3.71
O18 LEU D 248	CB	4.06	C38 GLN D 281	CD	4.23
O18 LEU D 248	C	4.74	C37 GLN D 281	CD	4.84
O18 LEU D 248	CA	4.29	C15 GLN D 281	CD	4.43
C54 LEU D 248	N	4.21	O5 GLN D 281	CD	4.08
C50 GLN D 247	NE2	4.6	O4 GLN D 281	CD	3.85
C49 GLN D 247	NE2	4.93	C14 GLN D 281	CD	3.86
C48 GLN D 247	NE2	4.73	O3 GLN D 281	CD	3.99
C47 GLN D 247	NE2	4.33	C13 GLN D 281	CD	4.59
C46 GLN D 247	NE2	3.98	C8 GLN D 281	CD	4.7
C45 GLN D 247	NE2	4.84	C42 GLN D 281	CG	4.69
C44 GLN D 247	NE2	4.16	C40 GLN D 281	CG	3.44
O17 GLN D 247	CD	4.87	C39 GLN D 281	CG	3.92
C53 GLN D 247	CD	4.93	C38 GLN D 281	CG	4.12
C50 GLN D 247	CD	4.83	O14 GLN D 281	CG	4.44
C46 GLN D 247	CD	4.84	C37 GLN D 281	CG	4.21
C44 GLN D 247	CD	4.77	O4 GLN D 281	CG	4.81
N2 GLN D 247	CG	4.58	C42 GLN D 281	CB	4.2
O20 GLN D 247	CG	4.78	C40 GLN D 281	CB	4.45
C55 GLN D 247	CG	4.9	C39 GLN D 281	CB	4.53
C54 GLN D 247	CG	4.5	C38 GLN D 281	CB	4.27
O17 GLN D 247	CG	3.47	O14 GLN D 281	CB	4.5
C53 GLN D 247	CG	3.71	C37 GLN D 281	CB	4.01
C52 GLN D 247	CG	4.87	C42 GLN D 281	O	4.34
C51 GLN D 247	CG	4.22	C38 GLN D 281	O	4.71
C50 GLN D 247	CG	3.94	C37 GLN D 281	O	3.48
C49 GLN D 247	CG	4.26	C36 GLN D 281	O	3.57
C47 GLN D 247	CG	4.95	C42 GLN D 281	C	4.87
C46 GLN D 247	CG	4.7	O14 GLN D 281	C	4.67

C45 GLN D 247	CG	4.78	C37 GLN D 281	C	4.28
C44 GLN D 247	CG	4.26	O13 GLN D 281	C	4.05
N2 GLN D 247	CB	4.93	C36 GLN D 281	C	4.66
O18 GLN D 247	CB	4.36	O14 GLN D 281	CA	4.51
C54 GLN D 247	CB	4.21	C37 GLN D 281	CA	4.33
O17 GLN D 247	CB	3.44	O13 GLN D 281	CA	4.84
C53 GLN D 247	CB	4.23	C5 ARG D 278	NH2	3.95
C51 GLN D 247	CB	4.92	O2 ARG D 278	CZ	3.83
O18 GLN D 247	C	4.26	C5 ARG D 278	CZ	4.92
C54 GLN D 247	C	4.74	O3 ARG D 278	CG	4.62
O17 GLN D 247	C	4.67	C10 THR D 276	O	4.26
O18 GLN D 247	CA	4.07	C9 THR D 276	O	3.54
C54 GLN D 247	CA	4.16	C8 THR D 276	O	4.26
O17 GLN D 247	CA	3.83	C9 THR D 276	C	4.64
C53 GLN D 247	CA	4.74	C10 THR D 276	N	4.47
C57 GLN D 247	N	4.75	C9 THR D 276	N	4.62
C56 GLN D 247	N	3.95	C11 LEU D 275	CD2	4.58
C55 GLN D 247	N	4.3	C10 LEU D 275	CD2	4.27
C54 GLN D 247	N	3.1	C10 LEU D 275	C	4.95
C53 GLN D 247	N	3.93	C11 LEU D 275	CA	4.89
C54 GLY D 246	O	4.95	C10 LEU D 275	CA	4.27
O21 GLY D 246	C	4.86	C11 LEU D 275	N	4.98
O18 GLY D 246	C	3.81	C10 LEU D 275	N	4.73
C57 GLY D 246	C	4.63	C40 PRO D 274	CB	4.74
C56 GLY D 246	C	4.14	C40 PRO D 274	CG	4.59
C55 GLY D 246	C	4.49	O4 PRO D 274	CG	4.25
C54 GLY D 246	C	3.72	C12 PRO D 274	CG	4.58
O17 GLY D 246	C	3.92	C11 PRO D 274	CG	4.55
C53 GLY D 246	C	4.5	C12 PRO D 274	O	4.16
C64 GLY D 246	CA	4.09	C11 PRO D 274	O	3.15
O21 GLY D 246	CA	3.7	C10 PRO D 274	O	3.45
O19 GLY D 246	CA	4.78	C9 PRO D 274	O	4.62
O18 GLY D 246	CA	3.58	C11 PRO D 274	C	4.23
C60 GLY D 246	CA	4.13	C10 PRO D 274	C	4.34
C59 GLY D 246	CA	4.16	C11 PHE D 272	CE2	4.43
C58 GLY D 246	CA	4.01	C4 HIS D 229	NE2	3.46
C57 GLY D 246	CA	3.38	C2 HIS D 229	NE2	4.1
C56 GLY D 246	CA	3.22	C1 HIS D 229	NE2	3.69
C55 GLY D 246	CA	3.68	O1 HIS D 229	CE1	4.6
C54 GLY D 246	CA	3.33	C4 HIS D 229	CE1	4.29
O17 GLY D 246	CA	3.85	C2 HIS D 229	CE1	4.53
C53 GLY D 246	CA	4.2	C1 HIS D 229	CE1	3.91
C64 GLY D 246	N	4.5	C4 HIS D 229	CD2	4.51
C60 GLY D 246	N	4.57	C10 LEU D 217	CD2	4.1
C59 GLY D 246	N	4.31	C9 LEU D 217	CD2	3.95
C58 GLY D 246	N	4.31	C10 LEU D 217	CD1	4.97
C57 GLY D 246	N	4.12			
C56 GLY D 246	N	4.27			
C55 GLY D 246	N	4.55			
C54 GLY D 246	N	4.68			
C65 PRO D 245	CB	4.87			
C59 PRO D 245	CB	4.7			
C65 PRO D 245	CD	4.78			

C65 PRO D 245	O	3.03			
C64 PRO D 245	O	3.32			
C60 PRO D 245	O	3.81			
C59 PRO D 245	O	2.89			
C58 PRO D 245	O	2.65			
C57 PRO D 245	O	3.07			
C56 PRO D 245	O	3.85			
C55 PRO D 245	O	4.2			
C54 PRO D 245	O	4.85			
C65 PRO D 245	C	4.17			
C64 PRO D 245	C	4.17			
O21 PRO D 245	C	4.4			
O19 PRO D 245	C	3.96			
C60 PRO D 245	C	4.41			
C59 PRO D 245	C	3.77			
C58 PRO D 245	C	3.76			
C57 PRO D 245	C	3.97			
C56 PRO D 245	C	4.47			
C55 PRO D 245	C	4.73			
C65 PRO D 245	CA	4.76			
O19 PRO D 245	CA	4.94			
C59 PRO D 245	CA	4.84			
C58 PRO D 245	CA	4.99			
C65 PRO D 245	N	4.48			
C65 PHE D 244	CB	4.08			
O19 PHE D 244	CB	4.64			
C64 PHE D 244	O	4.45			
C65 PHE D 244	C	4.74			
C64 PHE D 244	C	4.99			
O19 PHE D 244	C	4.97			
C64 CYS D 241	SG	3.89			
O21 CYS D 241	SG	4.32			
O18 CYS D 241	SG	4.95			
C64 CYS D 241	CB	4.54			
C64 CYS D 241	CA	3.93			
O21 CYS D 241	CA	4.97			
C64 CYS D 241	N	4.14			
C64 THR D 240	CB	4.94			
C64 THR D 240	OG1	4.63			
C64 THR D 240	O	3.83			
C64 THR D 240	C	4.14			
C48 THR A 225	OG1	4.4			
C52 TYR A 224	CE1	4.24			
C49 TYR A 224	CE1	4.21			
C47 TYR A 224	CE1	4.58			
C45 TYR A 224	CE1	3.86			
C52 TYR A 224	CD1	4.46			
C49 TYR A 224	CD1	4.08			
O15 TYR A 224	CD1	3.87			
C47 TYR A 224	CD1	3.73			
C46 TYR A 224	CD1	4.82			
C45 TYR A 224	CD1	3.28			
O15 TYR A 224	CG	4.32			

C47 TYR A 224	CG	4.54			
C45 TYR A 224	CG	4.18			
C48 TYR A 224	CB	4.87			
O15 TYR A 224	CB	3.78			
C47 TYR A 224	CB	4.43			
C45 TYR A 224	CB	4.43			
O15 TYR A 224	C	4.72			
O15 TYR A 224	CA	4.17			
C47 TYR A 224	CA	4.86			
C45 TYR A 224	CA	4.71			
C49 TYR A 224	N	4.97			
C48 TYR A 224	N	4.94			
C47 TYR A 224	N	4.08			
C45 TYR A 224	N	3.73			
C48 THR A 223	OG1	4.97			
C47 THR A 223	OG1	4.7			
C45 THR A 223	OG1	4.77			
C52 THR A 223	CG2	4.94			
C49 THR A 223	CG2	4.69			
O15 THR A 223	CG2	4.81			
C47 THR A 223	CG2	4.6			
C45 THR A 223	CG2	4.25			
C52 THR A 223	CB	4.95			
C49 THR A 223	CB	4.57			
C48 THR A 223	CB	4.86			
O15 THR A 223	CB	3.9			
C47 THR A 223	CB	3.99			
C46 THR A 223	CB	4.92			
C45 THR A 223	CB	3.72			
O15 THR A 223	C	4.52			
C47 THR A 223	C	4.88			
C45 THR A 223	C	4.4			
C52 THR A 223	CA	4.81			
C49 THR A 223	CA	4.83			
O15 THR A 223	CA	4.61			
C47 THR A 223	CA	4.65			
C45 THR A 223	CA	4.01			
C71 ARG A 221	NH2	3.66			
C70 ARG A 221	NH2	3.4			
C69 ARG A 221	NH2	3.05			
C68 ARG A 221	NH2	3.03			
C67 ARG A 221	NH2	3.34			
C66 ARG A 221	NH2	3.66			
C62 ARG A 221	NH2	4.75			
C61 ARG A 221	NH2	3.87			
C52 ARG A 221	NH2	4.33			
C67 ARG A 221	NH1	4.84			
C66 ARG A 221	NH1	4.86			
C61 ARG A 221	NH1	3.42			
C52 ARG A 221	NH1	3.31			
C49 ARG A 221	NH1	4.65			
C71 ARG A 221	CZ	4.33			
C70 ARG A 221	CZ	4.24			

C69 ARG A 221	CZ	4.21			
C68 ARG A 221	CZ	4.3			
C67 ARG A 221	CZ	4.39			
C66 ARG A 221	CZ	4.41			
C61 ARG A 221	CZ	3.83			
C52 ARG A 221	CZ	4.16			
C71 ARG A 221	NE	4.73			
C70 ARG A 221	NE	4.46			
C69 ARG A 221	NE	4.66			
C61 ARG A 221	NE	4.78			

Table 4.6: PYBA-Nos_DOX: Geometry of hydrogen bonds and hydrophobic interaction of PYBA-Nos _DOX with the binding site residues of tubulin.

(a) PY3BA_Tubulin			**(b) DOX_Tubulin**		
Hydrogen bonding			**Hydrogen bonding**		
Hydrogen Donor (D)	**Hydrogen Acceptor (A)**	**Distance (D-A) in Å**	**Hydrogen Donor (D)**	**Hydrogen Acceptor (A)**	**Distance (D-A) in Å**
ASP D 329	OD1	4.35	UNK 900	O13	2.6
UNK 901	O18	2.9	UNK 900	O2	2.71
			GLY D 370	O	3.69
			ARG D 369	O	4.96
			ARG D 284	O	2.66
			GLN D 281	OE1	4.73
			GLN D 281	OE1	3.56
			UNK 900	O3	3.57
			GLN D 281	O	3.89
			UNK 900	O3	4.85
			UNK 900	O2	3.05
			UNK 900	O3	4.34
			UNK 900	O2	3.93
Hydrophobic interaction			**Hydrophobic interaction**		
PYBA	**Tubulin**	**Distance**	**DOX**	**Tubulin**	**Distance**
CYS D 356	CA	4.73	LYS D 372	NZ	4.11
CYS D 356	N	4.72	LYS D 372	NZ	4.53
VAL D 355	O	2.72	LYS D 372	NZ	4.83
VAL D 355	O	4.6	LYS D 372	CE	3.76
VAL D 355	O	4.99	LYS D 372	CE	4.58
VAL D 355	O	4.9	LYS D 372	CE	4.11
VAL D 355	O	4.16	LYS D 372	CE	3.44
VAL D 355	O	3.98	LYS D 372	CE	4.05
VAL D 355	C	3.93	LYS D 372	CD	4.17
VAL D 355	CA	4.97	LYS D 372	CD	4.95
VAL D 355	N	4.88	LYS D 372	CG	3.77
VAL D 355	N	4.77	LYS D 372	CG	4.56
VAL D 355	N	4.34	LYS D 372	CG	4.99
VAL D 355	N	4.43	LEU D 371	CD2	4.97
VAL D 355	N	4.68	LEU D 371	CD2	4.93
VAL D 355	N	4.86	LEU D 371	CD2	4.16
ALA D 354	CB	4.94	LEU D 371	CD2	4.11
ALA D 354	CB	4.06	LEU D 371	CD2	3.16

ALA D 354	CB	3.2	LEU D 371	CD2	3.58
ALA D 354	CB	2.94	LEU D 371	CD2	4.16
ALA D 354	CB	3.82	LEU D 371	CD2	3.98
ALA D 354	CB	4.28	LEU D 371	CD2	4.23
ALA D 354	CB	4.71	LEU D 371	CD2	3.79
ALA D 354	C	4.93	LEU D 371	CD2	4.8
ALA D 354	C	4.93	LEU D 371	CD1	4.09
ALA D 354	C	4.59	LEU D 371	CD1	4.82
ALA D 354	C	4.65	LEU D 371	CD1	4.95
ALA D 354	CA	4.73	LEU D 371	CG	4.5
ALA D 354	CA	4.95	LEU D 371	CG	4.78
ALA D 354	CA	4.13	LEU D 371	CG	4.96
ALA D 354	CA	4.28	LEU D 371	CG	4.24
ALA D 354	CA	4.71	LEU D 371	CG	4.74
ALA D 354	CA	4.12	LEU D 371	CG	4.25
ALA D 354	CA	3.49	LEU D 371	CG	4.85
ALA D 354	CA	3.8	GLY D 370	O	4.34
ALA D 354	CA	4.5	GLY D 370	O	3.82
ALA D 354	CA	4.27	GLY D 370	O	3.74
ALA D 354	N	4.97	GLY D 370	O	4.76
ALA D 354	N	4.32	GLY D 370	O	4.24
ALA D 354	N	4.73	GLY D 370	O	4.84
ALA D 354	N	4.86	GLY D 370	C	4.79
THR D 353	CB	3.95	GLY D 370	C	4.58
THR D 353	CB	4.27	GLY D 370	C	4.47
THR D 353	CB	4.76	GLY D 370	CA	3.81
THR D 353	CG2	4.14	GLY D 370	CA	4.95
THR D 353	CG2	4.88	GLY D 370	CA	4.85
THR D 353	CG2	4.69	GLY D 370	N	4.45
THR D 353	O	3.29	ARG D 369	O	4.83
THR D 353	O	3.1	ARG D 369	O	3.62
THR D 353	O	2.89	ARG D 369	O	4.02
THR D 353	O	3	ARG D 369	O	3.23
THR D 353	O	3.29	ARG D 369	C	4.36
THR D 353	O	4.27	ARG D 369	C	4.42
THR D 353	O	4.21	LEU D 286	CD2	3.92
THR D 353	C	3.66	LEU D 286	CD2	4.34
THR D 353	C	4.49	LEU D 286	CD2	4.3
THR D 353	C	4.3	LEU D 286	CD2	4.85
THR D 353	C	3.91	LEU D 286	CD2	4.39
THR D 353	C	3.83	LEU D 286	CD2	4.19
THR D 353	C	4.31	LEU D 286	CD1	4.87
THR D 353	C	4.64	LEU D 286	CG	4.34
THR D 353	CA	4.33	LEU D 286	CG	4.68
THR D 353	CA	4.44	LEU D 286	CG	4.91
THR D 353	CA	4.89	LEU D 286	CG	4.96
THR D 353	N	4.86	LEU D 286	CB	3.48
THR D 353	N	4.41	LEU D 286	CB	4.96
MET D 325	CE	4.39	LEU D 286	CB	4.2
MET D 325	CE	4.35	LEU D 286	CB	4.34
MET D 325	CE	3.74	LEU D 286	CB	4.34
MET D 325	CE	4.64	LEU D 286	CB	3.59
MET D 325	CE	4.38	LEU D 286	CB	4.36

MET D 325	CE	4.91	LEU D 286	CB	4.95
MET D 325	CE	5	LEU D 286	CB	4.49
MET D 325	SD	4.98	LEU D 286	O	4.75
MET D 325	SD	3.94	LEU D 286	CA	4.6
MET D 325	SD	4.37	LEU D 286	CA	3.84
MET D 325	SD	4.91	LEU D 286	CA	4.9
MET D 325	CG	4.42	LEU D 286	CA	4.86
LEU D 248	CD2	4.54	LEU D 286	N	4.39
LEU D 248	CG	4.99	LEU D 286	N	4.96
LEU D 248	CG	4.42	LEU D 286	N	4.13
LEU D 248	CB	4.43	LEU D 286	N	4.25
LEU D 248	CB	4.84	LEU D 286	N	4.15
LEU D 248	CB	4.99	LEU D 286	N	4.87
LEU D 248	CB	3.75	ALA D 285	CB	4.82
LEU D 248	CB	3.15	ALA D 285	CB	4.37
LEU D 248	CB	4.48	ALA D 285	CB	4.86
LEU D 248	O	3.69	ALA D 285	CB	4.92
LEU D 248	C	4.32	ALA D 285	CB	3.82
LEU D 248	C	4.52	ALA D 285	C	3.47
LEU D 248	CA	4.01	ALA D 285	C	4.67
LEU D 248	CA	3.76	ALA D 285	C	4.64
LEU D 248	N	4.76	ALA D 285	C	4.7
LEU D 248	N	3.35	ALA D 285	C	4.98
LEU D 248	N	4.18	ALA D 285	CA	3.47
LEU D 248	N	4.49	ALA D 285	CA	4.42
GLN D 247	NE2	4.87	ALA D 285	CA	3.66
GLN D 247	NE2	3.56	ALA D 285	CA	4.08
GLN D 247	CD	3.84	ALA D 285	CA	4.74
GLN D 247	CD	4.36	ALA D 285	CA	4.98
GLN D 247	CD	4.21	ALA D 285	CA	4.07
GLN D 247	CG	4.85	ALA D 285	N	4.96
GLN D 247	CG	3.97	ALA D 285	N	4.82
GLN D 247	CG	4.14	ARG D 284	O	4.92
GLN D 247	CG	3.56	ARG D 284	O	3.49
GLN D 247	CG	4.72	ARG D 284	O	3.91
GLN D 247	CG	4.52	ARG D 284	C	3.65
GLN D 247	CG	4.72	ARG D 284	C	4.56
GLN D 247	CG	4.69	ARG D 284	C	3.98
GLN D 247	CG	4.5	ARG D 284	C	4.71
GLN D 247	CG	4.79	GLN D 281	OE1	3.92
GLN D 247	CG	4.42	GLN D 281	OE1	4.62
GLN D 247	CB	4.63	GLN D 281	OE1	3.83
GLN D 247	CB	4.81	GLN D 281	OE1	3.59
GLN D 247	CB	4.97	GLN D 281	OE1	3.96
GLN D 247	CB	4.92	GLN D 281	OE1	4.76
GLN D 247	CB	4.61	GLN D 281	OE1	4.04
GLN D 247	CB	4.69	GLN D 281	OE1	3.63
GLN D 247	CB	4.39	GLN D 281	OE1	4.24
GLN D 247	CB	4.2	GLN D 281	NE2	3.8
GLN D 247	CB	4.28	GLN D 281	NE2	4.36
GLN D 247	CB	4.53	GLN D 281	NE2	4.87
GLN D 247	CB	4.67	GLN D 281	NE2	3.66
GLN D 247	C	4.74	GLN D 281	NE2	4.17

GLN D 247	C	4.25	GLN D 281	NE2	4.98
GLN D 247	C	4.24	GLN D 281	NE2	3.9
GLN D 247	C	4.93	GLN D 281	NE2	3.52
GLN D 247	CA	4.29	GLN D 281	NE2	4.37
GLN D 247	CA	4.25	GLN D 281	NE2	4.85
GLN D 247	CA	4.36	GLN D 281	CD	4.66
GLN D 247	CA	4.61	GLN D 281	CD	3.45
GLN D 247	CA	4.44	GLN D 281	CD	3.71
GLN D 247	N	3.34	GLN D 281	CD	4.23
GLN D 247	N	4.08	GLN D 281	CD	4.84
GLN D 247	N	3.52	GLN D 281	CD	4.43
GLN D 247	N	4.09	GLN D 281	CD	4.08
GLY D 246	C	4.42	GLN D 281	CD	3.85
GLY D 246	C	3.55	GLN D 281	CD	3.86
GLY D 246	C	3.95	GLN D 281	CD	3.99
GLY D 246	C	4.79	GLN D 281	CD	4.59
GLY D 246	C	4.24	GLN D 281	CD	4.7
GLY D 246	C	4.64	GLN D 281	CG	4.69
GLY D 246	CA	4.14	GLN D 281	CG	3.44
GLY D 246	CA	3.61	GLN D 281	CG	3.92
GLY D 246	CA	2.99	GLN D 281	CG	4.12
GLY D 246	CA	3.72	GLN D 281	CG	4.44
GLY D 246	CA	4.83	GLN D 281	CG	4.21
GLY D 246	CA	3.9	GLN D 281	CG	4.81
GLY D 246	CA	4.16	GLN D 281	CB	4.2
GLY D 246	N	4.77	GLN D 281	CB	4.45
PRO D 245	O	3.76	GLN D 281	CB	4.53
PRO D 245	C	4.59	GLN D 281	CB	4.27
PRO D 245	C	4.62	GLN D 281	CB	4.5
PRO D 245	C	4.83	GLN D 281	CB	4.01
CYS D 241	SG	4.36	GLN D 281	O	4.34
THR A 225	OG1	3.77	GLN D 281	O	4.71
THR A 225	CB	4.54	GLN D 281	O	3.48
THR A 225	N	4.97	GLN D 281	O	3.57
TYR A 224	CE1	4.94	GLN D 281	C	4.87
TYR A 224	CD1	4.28	GLN D 281	C	4.67
THR A 223	OG1	4.03	GLN D 281	C	4.28
THR A 223	CG2	4.5	GLN D 281	C	4.05
THR A 223	CG2	4.79	GLN D 281	C	4.66
THR A 223	CG2	3.5	GLN D 281	CA	4.51
THR A 223	CG2	4.69	GLN D 281	CA	4.33
THR A 223	CB	4.29	GLN D 281	CA	4.84
THR A 223	CB	4.26	ARG D 278	NH2	3.95
ARG A 221	NH2	4.64	ARG D 278	CZ	3.83
ARG A 221	NH2	4.44	ARG D 278	CZ	4.92
ARG A 221	NH2	3.68	ARG D 278	CG	4.62
ARG A 221	NH2	3.42	THR D 276	O	4.26
ARG A 221	NH2	4.16	THR D 276	O	3.54
ARG A 221	NH2	4.55	THR D 276	O	4.26
ARG A 221	NH2	3.8	THR D 276	C	4.64
ARG A 221	NH2	4.97	THR D 276	N	4.47
ARG A 221	NH1	3.82	THR D 276	N	4.62
ARG A 221	NH1	3.73	LEU D 275	CD2	4.58

ARG A 221	CZ	4.39	LEU D 275	CD2	4.27
ARG A 221	CZ	5	LEU D 275	C	4.95
ARG A 221	CZ	4.44	LEU D 275	CA	4.89
ARG A 221	CZ	4.24	LEU D 275	CA	4.27
ARG A 221	CZ	3.95	LEU D 275	N	4.98
ARG A 221	NE	4.91	LEU D 275	N	4.73
ARG A 221	NE	4.87	PRO D 274	CB	4.74
THR A 179	CG2	4.77	PRO D 274	CG	4.59
THR A 179	CG2	4.73	PRO D 274	CG	4.25
SER A 178	O	4.8	PRO D 274	CG	4.58
SER A 178	O	3.71	PRO D 274	CG	4.55
SER A 178	O	4.32	PRO D 274	O	4.16
SER A 178	C	4.78	PRO D 274	O	3.15
			PRO D 274	O	3.45
			PRO D 274	O	4.62
			PRO D 274	C	4.23
			PRO D 274	C	4.34
			PHE D 272	CE2	4.43
			HIS D 229	NE2	3.46
			HIS D 229	NE2	4.1
			HIS D 229	NE2	3.69
			HIS D 229	CE1	4.6
			HIS D 229	CE1	4.29
			HIS D 229	CE1	4.53
			HIS D 229	CE1	3.91
			HIS D 229	CD2	4.51
			LEU D 217	CD2	4.1
			LEU D 217	CD2	3.95
			LEU D 217	CD1	4.97

Table 4.7: Br-TMB-Nos_DOX: Geometry of hydrogen bonds and hydrophobic interaction of Br-TMB-Nos_DOX with the binding site residues of tubulin.

(a) Br-TMB_Tubulin			**(b) DOX_Tubulin**		
Hydrogen bonding			**Hydrogen bonding**		
Hydrogen Donor (D)	**Hydrogen Acceptor (A)**	**Distance (D-A) in Å**	**Hydrogen Donor (D)**	**Hydrogen Acceptor (A)**	**Distance (D-A) in Å**
BrTMB N2	ASP D 357 OD1	2.66	DOX N1	GLY D 370 O	3.69
GLN D 247 NE2	BrTMB O19	4.85	UNK 900 N1	ARG D 369 O	4.96
GLN D 247 N	BrTMB O20	2.78	UNK 900 O14	ARG D 284 O	2.66
			UNK 900 O6	GLN D 281 OE1	4.73
			UNK 900 O3	GLN D 281 OE1	3.56
			GLN D 281 NE2	UNK 900 O3	3.57
			UNK 900 O14	GLN D 281 O	3.89
			ARG D 278 NH2	UNK 900 O3	4.85
			ARG D 278 NH2	UNK 900 O2	3.05
			ARG D 278 NE	UNK 900 O3	4.34
			ARG D 278 NE	UNK 900 O2	3.93
Hydrophobic interaction			**Hydrophobic interaction**		
BrTMB	**Tubulin**	**Distance**	**DOX**	**Tubulin**	**Distance**
C62	ASP D 357 OD2	4.73	C25	LYS D 372 NZ	4.11

C61	ASP D 357 OD2	3.77	C24	LYS D 372 NZ	4.53
C53	ASP D 357 OD2	4.25	C20	LYS D 372 NZ	4.83
C51	ASP D 357 OD2	4.69	C25	LYS D 372 CE	3.76
C62	ASP D 357 OD1	3	C24	LYS D 372 CE	4.58
C61	ASP D 357 OD1	3.27	C20	LYS D 372 CE	4.11
C53	ASP D 357 OD1	4.08	O8	LYS D 372 CE	3.44
C52	ASP D 357 OD1	4.73	C19	LYS D 372 CE	4.05
C51	ASP D 357 OD1	3.82	O8	LYS D 372 CD	4.17
N2	ASP D 357 CG	3.55	C19	LYS D 372 CD	4.95
C62	ASP D 357 CG	4.17	O8	LYS D 372 CG	3.77
C61	ASP D 357 CG	3.91	C19	LYS D 372 CG	4.56
C53	ASP D 357 CG	4.4	C16	LYS D 372 CG	4.99
C51	ASP D 357 CG	4.55	C40	LEU D 371 CD2	4.97
N2	ASP D 357 CB	4.89	C16	LEU D 371 CD2	4.93
C60	CYS D 356 CA	4.31	C15	LEU D 371 CD2	4.16
C59	CYS D 356 CA	4.83	O5	LEU D 371 CD2	4.11
C60	CYS D 356 N	4.51	O4	LEU D 371 CD2	3.16
C59	CYS D 356 N	4.8	C14	LEU D 371 CD2	3.58
C72	VAL D 355 CG2	3.66	C13	LEU D 371 CD2	4.16
O22	VAL D 355 CG2	4.93	C12	LEU D 371 CD2	3.98
C72	VAL D 355 CB	4.3	C7	LEU D 371 CD2	4.23
C71	VAL D 355 O	4.74	C6	LEU D 371 CD2	3.79
C63	VAL D 355 O	4.73	N1	LEU D 371 CD2	4.8
C60	VAL D 355 O	2.79	C12	LEU D 371 CD1	4.09
C59	VAL D 355 O	3.11	C11	LEU D 371 CD1	4.82
C58	VAL D 355 O	3.62	C6	LEU D 371 CD1	4.95
C57	VAL D 355 O	3.75	O4	LEU D 371 CG	4.5
C56	VAL D 355 O	3.45	C14	LEU D 371 CG	4.78
C55	VAL D 355 O	3.03	C13	LEU D 371 CG	4.96
C54	VAL D 355 O	4.24	C12	LEU D 371 CG	4.24
C53	VAL D 355 O	3.81	C7	LEU D 371 CG	4.74
C60	VAL D 355 C	3.93	C6	LEU D 371 CG	4.25
C59	VAL D 355 C	4.14	N1	LEU D 371 CG	4.85
C58	VAL D 355 C	4.63	C14	GLY D 370 O	4.34
C57	VAL D 355 C	4.84	C13	GLY D 370 O	3.82
C56	VAL D 355 C	4.63	C6	GLY D 370 O	3.74
C55	VAL D 355 C	4.26	C5	GLY D 370 O	4.76
C53	VAL D 355 C	4.92	C3	GLY D 370 O	4.24
C72	VAL D 355 CA	4.74	C1	GLY D 370 O	4.84
C72	VAL D 355 N	3.88	C6	GLY D 370 C	4.79
C71	VAL D 355 N	4.72	N1	GLY D 370 C	4.58
C64	VAL D 355 N	4.87	C3	GLY D 370 C	4.47
C63	VAL D 355 N	4.41	C3	GLY D 370 CA	3.81
C59	VAL D 355 N	4.84	C2	GLY D 370 CA	4.95
C58	VAL D 355 N	4.63	C1	GLY D 370 CA	4.85
C57	VAL D 355 N	4.71	C3	GLY D 370 N	4.45
C71	ALA D 354 CB	3.28	C4	ARG D 369 O	4.83
C65	ALA D 354 CB	4.97	C3	ARG D 369 O	3.62
O20	ALA D 354 CB	4.19	C2	ARG D 369 O	4.02
C58	ALA D 354 CB	4.79	C1	ARG D 369 O	3.23
C72	ALA D 354 O	4.72	C3	ARG D 369 C	4.36
C72	ALA D 354 C	3.99	C1	ARG D 369 C	4.42
C71	ALA D 354 C	4.94	C43	LEU D 286 CD2	3.92

C72	ALA D 354 CA	3.91	C40	LEU D 286 CD2	4.34
C71	ALA D 354 CA	4.26	C39	LEU D 286 CD2	4.3
O22	ALA D 354 CA	4.73	C38	LEU D 286 CD2	4.85
C69	ALA D 354 CA	4.43	C16	LEU D 286 CD2	4.39
C68	ALA D 354 CA	4.81	C15	LEU D 286 CD2	4.19
C65	ALA D 354 CA	4.7	C40	LEU D 286 CD1	4.87
C64	ALA D 354 CA	4.36	C43	LEU D 286 CG	4.34
C63	ALA D 354 CA	4.68	C40	LEU D 286 CG	4.68
O20	ALA D 354 CA	4.78	C39	LEU D 286 CG	4.91
C73	ALA D 354 N	4.76	O14	LEU D 286 CG	4.96
C72	ALA D 354 N	4.22	C43	LEU D 286 CB	3.48
C69	ALA D 354 N	4.76	C41	LEU D 286 CB	4.96
C68	ALA D 354 N	4.76	C40	LEU D 286 CB	4.2
C74	THR D 353 CB	4.92	C39	LEU D 286 CB	4.34
C73	THR D 353 CB	3.48	C38	LEU D 286 CB	4.34
C72	THR D 353 CB	4.78	O14	LEU D 286 CB	3.59
O23	THR D 353 CB	4.09	C37	LEU D 286 CB	4.36
C68	THR D 353 CB	4.71	C36	LEU D 286 CB	4.95
C73	THR D 353 OG1	4.57	C35	LEU D 286 CB	4.49
C73	THR D 353 CG2	3.34	C35	LEU D 286 O	4.75
C72	THR D 353 CG2	4	C43	LEU D 286 CA	4.6
O23	THR D 353 CG2	4.38	O14	LEU D 286 CA	3.84
O22	THR D 353 CG2	4.95	C37	LEU D 286 CA	4.9
C68	THR D 353 CG2	4.97	C35	LEU D 286 CA	4.86
C74	THR D 353 O	3.01	C43	LEU D 286 N	4.39
C73	THR D 353 O	3.6	C38	LEU D 286 N	4.96
C72	THR D 353 O	4.02	C37	LEU D 286 N	4.13
C69	THR D 353 O	3.49	C36	LEU D 286 N	4.25
C68	THR D 353 O	2.95	C35	LEU D 286 N	4.15
C67	THR D 353 O	3	C34	LEU D 286 N	4.87
C66	THR D 353 O	3.52	O14	ALA D 285 CB	4.82
C65	THR D 353 O	3.96	O13	ALA D 285 CB	4.37
C64	THR D 353 O	3.95	C36	ALA D 285 CB	4.86
C74	THR D 353 C	4.01	C35	ALA D 285 CB	4.92
C73	THR D 353 C	4.02	O12	ALA D 285 CB	3.82
C72	THR D 353 C	4.24	O14	ALA D 285 C	3.47
O24	THR D 353 C	4.56	C37	ALA D 285 C	4.67
O23	THR D 353 C	4.16	O13	ALA D 285 C	4.64
O22	THR D 353 C	4.84	C36	ALA D 285 C	4.7
C69	THR D 353 C	4.35	C35	ALA D 285 C	4.98
C68	THR D 353 C	3.98	O14	ALA D 285 CA	3.47
C67	THR D 353 C	4.21	C37	ALA D 285 CA	4.42
C66	THR D 353 C	4.72	O13	ALA D 285 CA	3.66
C64	THR D 353 C	4.85	C36	ALA D 285 CA	4.08
C74	THR D 353 CA	4.41	C35	ALA D 285 CA	4.74
C73	THR D 353 CA	4.34	C34	ALA D 285 CA	4.98
O23	THR D 353 CA	4.62	O12	ALA D 285 CA	4.07
C68	THR D 353 CA	4.84	C37	ALA D 285 N	4.96
C74	THR D 353 N	3.68	C36	ALA D 285 N	4.82
C73	THR D 353 N	4.96	C38	ARG D 284 O	4.92
C74	LYS D 352 CD	4.35	C37	ARG D 284 O	3.49
C74	LYS D 352 CG	4.77	C36	ARG D 284 O	3.91
C74	LYS D 352 CB	4.2	O14	ARG D 284 C	3.65

C74	LYS D 352 C	4.54	C37	ARG D 284 C	4.56
C74	LYS D 352 CA	4.43	O13	ARG D 284 C	3.98
C73	ASP D 329 OD2	4.18	C36	ARG D 284 C	4.71
C73	ASP D 329 OD1	2.94	C42	GLN D 281 OE1	3.92
C72	ASP D 329 OD1	4.18	C41	GLN D 281 OE1	4.62
C73	ASP D 329 CG	3.89	C40	GLN D 281 OE1	3.83
O23	ASP D 329 CG	4.88	C39	GLN D 281 OE1	3.59
C72	VAL D 328 CG1	4.79	C38	GLN D 281 OE1	3.96
C72	MET D 325 CE	4.58	C37	GLN D 281 OE1	4.76
O22	MET D 325 CE	4.73	C15	GLN D 281 OE1	4.04
C63	MET D 325 CE	4.75	C14	GLN D 281 OE1	3.63
O18	MET D 325 CE	3.58	C13	GLN D 281 OE1	4.24
C56	MET D 325 CE	4.86	C40	GLN D 281 NE2	3.8
C54	MET D 325 CE	3.86	C39	GLN D 281 NE2	4.36
O17	MET D 325 CE	3.9	C15	GLN D 281 NE2	4.87
C72	MET D 325 SD	3.24	C14	GLN D 281 NE2	3.66
O22	MET D 325 SD	3.54	C13	GLN D 281 NE2	4.17
C69	MET D 325 SD	4.82	C10	GLN D 281 NE2	4.98
C63	MET D 325 SD	4.6	C9	GLN D 281 NE2	3.9
O18	MET D 325 SD	4.45	C8	GLN D 281 NE2	3.52
C54	MET D 325 SD	4.95	C7	GLN D 281 NE2	4.37
C72	MET D 325 CG	4.47	C6	GLN D 281 NE2	4.85
O22	MET D 325 CG	4.43	C42	GLN D 281 CD	4.66
C74	LEU D 248 CD2	4.13	C40	GLN D 281 CD	3.45
C74	LEU D 248 CD1	4.18	C39	GLN D 281 CD	3.71
C74	LEU D 248 CG	4.37	C38	GLN D 281 CD	4.23
C74	LEU D 248 CB	4.24	C37	GLN D 281 CD	4.84
C71	LEU D 248 CB	4.15	C15	GLN D 281 CD	4.43
O24	LEU D 248 CB	4.99	O5	GLN D 281 CD	4.08
C67	LEU D 248 CB	4.84	O4	GLN D 281 CD	3.85
C66	LEU D 248 CB	4.06	C14	GLN D 281 CD	3.86
C65	LEU D 248 CB	4.53	O3	GLN D 281 CD	3.99
O20	LEU D 248 CB	4.72	C13	GLN D 281 CD	4.59
C71	LEU D 248 O	3.78	C8	GLN D 281 CD	4.7
C71	LEU D 248 C	4.52	C42	GLN D 281 CG	4.69
C71	LEU D 248 CA	4.35	C40	GLN D 281 CG	3.44
C66	LEU D 248 CA	4.73	C39	GLN D 281 CG	3.92
O20	LEU D 248 CA	4.79	C38	GLN D 281 CG	4.12
C71	LEU D 248 N	3.7	O14	GLN D 281 CG	4.44
C66	LEU D 248 N	4.25	C37	GLN D 281 CG	4.21
C65	LEU D 248 N	4.31	O4	GLN D 281 CG	4.81
C48	GLN D 247 NE2	3.07	C42	GLN D 281 CB	4.2
C46	GLN D 247 NE2	4.35	C40	GLN D 281 CB	4.45
O16	GLN D 247 CD	3.86	C39	GLN D 281 CB	4.53
C48	GLN D 247 CD	4.04	C38	GLN D 281 CB	4.27
C65	GLN D 247 CG	4.38	O14	GLN D 281 CB	4.5
O21	GLN D 247 CG	4.06	C37	GLN D 281 CB	4.01
O20	GLN D 247 CG	4.53	C42	GLN D 281 O	4.34
O19	GLN D 247 CG	4.9	C38	GLN D 281 O	4.71
C58	GLN D 247 CG	4.91	C37	GLN D 281 O	3.48
C57	GLN D 247 CG	4.65	C36	GLN D 281 O	3.57
O16	GLN D 247 CG	3.76	C42	GLN D 281 C	4.87
C48	GLN D 247 CG	4.17	O14	GLN D 281 C	4.67

C46	GLN D 247 CG	4.93	C37	GLN D 281 C	4.28
C71	GLN D 247 CB	5	O13	GLN D 281 C	4.05
C66	GLN D 247 CB	4.17	C36	GLN D 281 C	4.66
C65	GLN D 247 CB	3.82	O14	GLN D 281 CA	4.51
C64	GLN D 247 CB	4.98	C37	GLN D 281 CA	4.33
O21	GLN D 247 CB	4.26	O13	GLN D 281 CA	4.84
O20	GLN D 247 CB	4.09	C5	ARG D 278 NH2	3.95
C58	GLN D 247 CB	4.88	O2	ARG D 278 CZ	3.83
C57	GLN D 247 CB	4.92	C5	ARG D 278 CZ	4.92
C71	GLN D 247 C	4.54	O3	ARG D 278 CG	4.62
C66	GLN D 247 C	4.95	C10	THR D 276 O	4.26
C65	GLN D 247 C	4.94	C9	THR D 276 O	3.54
O20	GLN D 247 C	4.34	C8	THR D 276 O	4.26
C71	GLN D 247 CA	4.48	C9	THR D 276 C	4.64
C65	GLN D 247 CA	4.72	C10	THR D 276 N	4.47
O21	GLN D 247 CA	4.96	C9	THR D 276 N	4.62
O20	GLN D 247 CA	3.86	C11	LEU D 275 CD2	4.58
C58	GLN D 247 CA	4.81	C10	LEU D 275 CD2	4.27
C71	GLN D 247 N	3.45	C10	LEU D 275 C	4.95
C65	GLN D 247 N	4.73	C11	LEU D 275 CA	4.89
C59	GLN D 247 N	4.38	C10	LEU D 275 CA	4.27
C58	GLN D 247 N	3.61	C11	LEU D 275 N	4.98
C57	GLN D 247 N	4.3	C10	LEU D 275 N	4.73
C71	GLY D 246 C	3.9	C40	PRO D 274 CB	4.74
O20	GLY D 246 C	3.4	C40	PRO D 274 CG	4.59
O19	GLY D 246 C	4.89	O4	PRO D 274 CG	4.25
C59	GLY D 246 C	4.29	C12	PRO D 274 CG	4.58
C58	GLY D 246 C	3.95	C11	PRO D 274 CG	4.55
C57	GLY D 246 C	4.81	C12	PRO D 274 O	4.16
C71	GLY D 246 CA	3.49	C11	PRO D 274 O	3.15
C70	GLY D 246 CA	4.13	C10	PRO D 274 O	3.45
O20	GLY D 246 CA	3.08	C9	PRO D 274 O	4.62
O19	GLY D 246 CA	4.25	C11	PRO D 274 C	4.23
C60	GLY D 246 CA	4.04	C10	PRO D 274 C	4.34
C59	GLY D 246 CA	3.09	C11	PHE D 272 CE2	4.43
C58	GLY D 246 CA	3.21	C4	HIS D 229 NE2	3.46
C57	GLY D 246 CA	4.27	C2	HIS D 229 NE2	4.1
C56	GLY D 246 CA	4.96	C1	HIS D 229 NE2	3.69
C55	GLY D 246 CA	4.85	O1	HIS D 229 CE1	4.6
C71	GLY D 246 N	4.8	C4	HIS D 229 CE1	4.29
C70	GLY D 246 N	3.96	C2	HIS D 229 CE1	4.53
C60	GLY D 246 N	4.49	C1	HIS D 229 CE1	3.91
C59	GLY D 246 N	3.88	C4	HIS D 229 CD2	4.51
C58	GLY D 246 N	4.37	C10	LEU D 217 CD2	4.1
C70	PRO D 245 CB	3.7	C9	LEU D 217 CD2	3.95
O19	PRO D 245 CB	4.95	C10	LEU D 217 CD1	4.97
C70	PRO D 245 CG	4.96			
C71	PRO D 245 O	4.96			
C70	PRO D 245 O	3.58			
C60	PRO D 245 O	3.16			
C59	PRO D 245 O	3.04			
C58	PRO D 245 O	4.2			
C55	PRO D 245 O	4.34			

C70	PRO D 245 C	3.72			
O19	PRO D 245 C	4.6			
C60	PRO D 245 C	4.11			
C59	PRO D 245 C	3.83			
C58	PRO D 245 C	4.72			
C70	PRO D 245 CA	4.38			
C71	CYS D 241 SG	4.14			
C62	LEU D 42 CD2	4.51			
C62	LEU D 42 CD1	4.89			
C48	TYR A 224 CD1	4.38			
C47	THR A 223 CG2	4.99			
C45	THR A 223 CG2	4.79			
O15	THR A 223 CB	4.6			
C73	ARG A 221 NH2	3.16			
C72	ARG A 221 NH2	4.2			
C69	ARG A 221 NH2	3.29			
C68	ARG A 221 NH2	3.23			
C67	ARG A 221 NH2	4.24			
C64	ARG A 221 NH2	4.36			
C69	ARG A 221 NH1	4.69			
C73	ARG A 221 CZ	4.26			
C72	ARG A 221 CZ	4.83			
O23	ARG A 221 CZ	4.13			
O22	ARG A 221 CZ	3.7			
C69	ARG A 221 CZ	4.21			
C68	ARG A 221 CZ	4.43			
C73	ARG A 221 NE	4.58			
C74	THR A 179 CG2	4.85			
O24	THR A 179 CG2	4.53			
C67	THR A 179 CG2	4.95			
C66	THR A 179 CG2	4.41			
C74	THR A 179 CA	4.49			
O24	THR A 179 CA	4.78			
C74	THR A 179 N	4.8			
C74	SER A 178 O	3.05			
C67	SER A 178 O	4.2			
C66	SER A 178 O	4.78			
C74	SER A 178 C	4.21			
O24	SER A 178 C	4.06			
O24	VAL A 177 C	4.81			

LIST OF PUBLICATIONS

1. **Shruti Gamya Dash**, Charu Suri, Praveen Kumar Reddy Nagireddy, Srinivas Kantevari and Pradeep Kumar Naik (2020). Rational design of 9-vinyl-phenyl noscapine as potent tubulin binding anticancer agent and evaluation of the effects of its combination on Docetaxel. ***Journal of biomolecular structure & dynamics***, *39*(14), 5276–5289. https://doi.org/10.1080/07391102.2020.1785945.

2. **Shruti Gamya Dash**, Srinivas Kantevari and Pradeep Kumar Naik (2021) Combination Regimen of Amino-Noscapine and Docetaxel for Evaluation of Anticancer Activity, ***Analytical Chemistry Letters***, 11:2, 215-229, DOI: 10.1080/22297928.2021.1896380.

3. **Shruti Gamya Dash**, Srinivas Kantevari, Swaroop Kumar Pandey and Pradeep Kumar Naik (2021). Synergistic interaction of N-3-Br-benzyl-noscapine and docetaxel abrogates oncogenic potential of breast cancer cells. ***Chemical biology & drug design***, *98*(3), 466–479. https://doi.org/10.1111/cbdd.13902.

BOOK CHAPTER

1. **Shruti Gamya Dash**, Harish Chandra Joshi and Pradeep Kumar Naik. Noscapinoids: a family of microtubule targeted anticancer agent. (Under Review in Springer Nature Singapore.)

CONFERENCE PRESENTATION

1. **Shruti Gamya Dash** and Pradeep Kumar Naik. "Development of synthetic derivatives on natural compounds" Oral Presentation in National Conference on Cancer Biology and Therapeutics from 29th to 30th November, 2019 organized by Institute of Life Science, Bhubaneswar, Rajiv Gandhi Center for Biotechnology, Thiruvananthapuram, Institute of Bioresource and Sustainable development, Imphal.

2. **Shruti Gamya Dash** and Pradeep Kumar Naik. "Design of synthetic derivatives of natural compound, Noscapine as tubulin binding chemotherapeutic agents and evalution of its synergistic effect with taxotere for the management of human breast cancer". Poster presentation in National Conference on Current research Trends in biotechnology,bioinformatics and intellectual Property management from 3rd to 4th March,2020.
3. **Shruti Gamya Dash** and Pradeep Kumar Naik. **"**Evaluation of synergistic effect of Noscapinoids and Docetaxel for management of human breast cancer". Poster presentation in the International Symposium on Emerging Trends and Challenges in Cancer Chemoprevention, Diagnosis and Therapeutics, from 17th -18th February, 2020.

4. **Shruti Gamya Dash** and Pradeep Kumar Naik. "9-vinyl phenyl noscapine: as potential tubulin binding effective anticancer drug" Oral Presentation in International Virtual Conferences on "Recent Advances in Applied Sciences, Technology & Health" - RASTH, 2021, SRM Institute of Science and Technology, Kattankulathur, Tamilnadu, India.

5. **Shruti Gamya Dash** and Pradeep Kumar Naik. "Comparative evaluation of Noscapinoids in combination with Docetaxel abrogates the anticancer potential as potent tubulin binding agent." Selected speaker in the virtual 3rd international JSPSAAE symposium, 26-28 September 2021.

JOURNAL OF BIOMOLECULAR STRUCTURE AND DYNAMICS
https://doi.org/10.1080/07391102.2020.1785945

Rational design of 9-vinyl-phenyl noscapine as potent tubulin binding anticancer agent and evaluation of the effects of its combination on Docetaxel

Shruti Gamya Dash[a], Charu Suri[b], Praveen Kumar Reddy Nagireddy[c], Srinivas Kantevari[c] and Pradeep Kumar Naik[a]

[a]Centre of Excellence in Natural Products and Therapeutics, Department of Biotechnology and Bioinformatics, Sambalpur University, Sambalpur, Odisha, India; [b]Drug Discovery Research Centre, Translational Health Science and Technology Institute, Pali, Haryana, India; [c]Fluoro and Agrochemicals Division, CSIR-Indian Institute of Chemical Technology, Hyderabad, India

Communicated by Ramaswamy H. Sarma

ABSTRACT

Docetaxel (DOX) based combination therapy is a novel therapeutic strategy that attracts great interest in breast cancer treatment but its clinical utility got limited due to side effects. In contrast, noscapine, an antitussive drug showed antitumor activity against many cancers without any side effects that targets microtubules and attenuates its dynamic instability. In the quest for an increase in the anticancer activity of noscapine, we strategically designed a novel derivative, 9-vinyl phenyl noscapine (VPN), based on our *in silico* molecular docking and molecular dynamics simulation effort. Molecular docking of VPN and DOX onto microtubule revealed a docking score of −4.82 kcal/mol and −6.67 kcal/mol respectively, while the docking score of VPN was changed to −3.23 kcal/mol when it was docked onto the co-complex of tubulin-DOX. Further, the binding free energy ($\Delta G_{bind,PBSA}$) of VPN and DOX with tubulin showed −24.04 and −18.65 kcal/mol respectively, while the binding free energy of DOX was increased further in combination with VPN ($\Delta G_{bind,\ PBSA}$ was reduced to −21.41 kcal/mol), denoting combination effect of both ligands. The IC_{50} value amounted to 30.17 μM and 19.92 μM for VPN and 0.621 μM and 0.193 μM for DOX, respectively for 48 h and 72 h. The dose dependent cytotoxicity of DOX has been reduced considerably with the combination dose regimen of VPN. Further, the combine effect of both the agents improved the apoptotic cell death 28.5% compared to single agent treatment 5.71% and 10.5% for VPN and DOX, respectively. Both agents bind effectively to tubulin in single and in combination to interfere with cell cycle progression in G2/M transition. This study provides novel concept of combination treatment of DOX and VPN to amend efficiency in breast cancer treatment.

ARTICLE HISTORY
Received 2 April 2020
Accepted 16 June 2020

KEYWORDS
9-vinyl-phenyl noscapine; anti-tumor activity; combination drug therapy; molecular docking; molecular dynamics simulations; noscapine; noscapinoids; tubulin binding affinity

Introduction

Microtubule-targeting drugs such as taxol derivatives and vinca alkaloids have been powerful chemotherapeutic agents for the treatment of a variety of human cancers. However, primarily because of the poor solubility of these compounds, the clinical uses of these compounds have been somewhat cumbersome and expensive. In addition, these drugs are plagued with serious toxicity (particularly, peripheral neuropathies, gastrointestinal toxicity, myelosuppression, and immunosuppression) owing to their non-selective action (Rowinsky & Donehower, 1991; Kavanagh & Kudelka, 1993; Rowinsky, 1997; Theiss & Meller, 2000; Topp et al., 2000; Zhou et al., 2005). Despite all these challenges, taxol was approved by the FDA in 1996 for the treatment of breast and ovarian cancers. Nevertheless, the success of taxol in the management of aggressive breast and ovarian cancers gives an impetus to identify compounds that target microtubules, but are less toxic, bind differently to tubulin, more soluble in aqueous solutions, available orally and significantly effective either as single agents or can efficiently synergize with currently-available drugs such as docetaxel (at low doses). In quest of searching such molecule, noscapine (an opium alkaloid, non-narcotic, non-sedative, traditionally used for decades as an innocuous anti-cough medicine) was discovered (Ye et al., 1998). This class of compounds set themselves apart from currently-available anticancer drugs like *taxanes* and *vincas* because they leave the microtubules arrays intact but merely attenuate microtubule dynamics just enough to activate mitotic checkpoints (Ye et al., 1998). Besides, unlike currently available microtubule drugs that either overpolymerize and bundle microtubules (*taxanes*) or depolymerize them (*vincas*), noscapinoids do not alter the monomer/polymer ratio of tubulin (Ye et al., 1998; Zhou et al., 2003) and thus they do not cause any hemo and neuronal toxicity based upon their unique mechanism of action. In pursuit of increasing its anticancer activity we have strategically designed a series of derivatives by modification of the scaffold structure.

CONTACT Pradeep Kumar Naik pknaik1973@gmail.com Centre of Excellence in Natural Products and Therapeutics, Department of Biotechnology and Bioinformatics, Sambalpur University, Jyoti Vihar, Burla, Sambalpur, Odisha 768 019, India

Supplemental data for this article can be accessed online at https://doi.org/10.1080/07391102.2020.1785945.

We have shown that these derivatives bind to tubulin with a higher affinity and do not alter the monomer/polymer ratio of tubulin In addition; these derivatives inhibit cellular proliferation and cause G2/M arrest in various human cancer cells followed by apoptotic cell death (Naik et al., 2011; Santoshi et al., 2011; Naik et al., 2012; Manchukonda et al., 2013; Manchukonda et al., 2014; Santoshi et al., 2015; Mahaddalkar et al., 2017). Noscapine and its derivatives were predicted to binds to α- and β- tubulin heterodimer interface near the colchicine site but not interfere with colchicine binding through use of computational docking techniques and molecular dynamic methods (Naik et al., 2011). This finding was supported by competitive binding experiments that indicated that noscapine was not competitive with colchicine (Naik et al., 2011). While several synthesized derivatives of noscapine showed promising *in vitro* activities against tumor cell lines, they were unable to achieve a complete elimination of the disease despite increased dosages.

Over the course of this decade, it is becoming well appreciated that more of a toxic drug at its maximum tolerated dose (MTD) is not necessarily better; and there is an opportunity to reduce its dose levels by using combination regimens of drugs that display synergistic interactions (Jordan & Wilson, 2004). In this context, the potential of combinatorial anti-microtubule therapy is an untapped source of chemotherapeutic wealth as the presence of diverse drug binding sites on tubulin suggest that rational combination of two or more drugs of this class might be able to enhance the anticancer efficacy and reduce toxic side effects, thereby, improving the therapeutic index. Previously it was demonstrated that the combination of docetaxel and other agents enhanced the anticancer activities of lung cancer (Hida et al., 2000; Hida et al., 2002; Nawrocki et al., 2004; Sweeney et al., 2005; Shaik et al., 2006) as well as breast cancer (Chougule et al., 2011). In the current study, we embark upon a approach to rationally designed a novel derivative of noscapine and evaluate its additive effect with the clinically approved anticancer agent, docetaxel, to enhance the anticancer activity.

Material and methods

Molecular modelling

Protein preparation

The co-crystallized structure of the colchicine-tubulin complex (PDB ID: 1SA0, resolution 3.58 Å) was used as a receptor protein. The errors in the PDB file were removed as per the procedure reported earlier (Santoshi & Naik, 2014). Further, refinement of the structure was achieved by energy minimization using Macromodel (Schrodinger package) and followed by molecular dynamic simulation of 100 ns using GROMACS 5.1.5 with similar parameters set up as reported earlier (Santoshi & Naik, 2014). A sum of 5000 frames was produced in the MD trajectories with a time step of 20 ps, from which the last 2000 frames were used to generate the average tubulin structure.

Rational design of novel derivative of noscapine

The lead molecule, noscapine is cytotoxic in a variety of different cancer cell lines (NCI 60 cell lines panel), although the IC_{50} value remain in the high micro-molar range (Naik et al., 2011). To enhance its anticancer activity further, efforts have been focused on rational designing and synthesis of new generation of noscapine derivatives. Noscapine docks onto $\beta-$tubulin near the interface between its dimerization partner, $\alpha-$tubulin (Checchi et al., 2003). This is supported by the earlier finding of 1:1 stoichiometry of tubulin binding (Ye et al., 1998). A closer look at the binding site revealed side chains around the putative binding pocket and the presence of an empty space around position 9 of noscapine. Inspired by the *in silico* findings, we have rationally coupled a bulky 4-vinyl phenyl functional group at the C-9 position of the noscapine scaffold in quest of developing a more potent derivative of noscapine (Figure 1).

Ligand preparation

The molecular structure of VPN and DOX was constructed using molecular builder of maestro (Schrodinger package). The built structures were energy minimized using Macromodel (Schrodinger package) and OPLS 2005 force field. For energy minimization, PRCG algorithm was used with 1000 steps and energy gradient of 0.001. Each ligand was assigned appropriate bond order using Ligprep. Further, the geometric optimization of the ligands was performed based on hybrid density functional theory with Becke's three-parameter exchange potential and the Lee-Yang-Parr correlation functional (B3LYP) (Lee et al., 1988; Becke, 1993) with basis set 3-21 G* (Binkley et al., 1980; Gordon et al., 1982; Pietro et al., 1982) using Jaguar (Schrödinger, LLC).

Molecular docking

Both VPN and DOX were docked onto αβ-tubulin heterodimer using "Extra Precision" (XP) algorithm of Glide docking (Schrödinger package) (Friesner et al., 2004; Halgren et al., 2004) in two cycles. The binding site of VPN is at the interface between α- and β- tubulin (noscapinoids binding site) (Naik et al., 2011), whereas the binding site of DOX is biased towards β-tubulin (taxol binding site) (Snyder et al., 2001). In the first cycle both DOX and VPN were docked onto their respective binding sites using Glide XP docking to calculate their individual binding affinity. In the second cycle, the VPN was docked onto the co-complex of DOX-tubulin and the DOX was docked onto the co-complex of VPN-tubulin. The binding sites were defined using a concentric grid box at the centroid of the binding site using the Glide grid-receptor generation program. An outer grid box of 12 Å x 12 Å x 12 Å was defined to confine the mass centre of the docked ligand. Besides, an enclosing grid box of 12 Å x 12 Å x 12 Å was defined which occupied all the atoms of the docked poses. The scale factor of 0.4 for van der Waals radii was applied to atoms of protein with absolute partial charges less than or equal to 0.25. The algorithm generated 10000 poses, out of which only 1000 poses were used for the minimization (conjugate gradients) and the final 30 structures

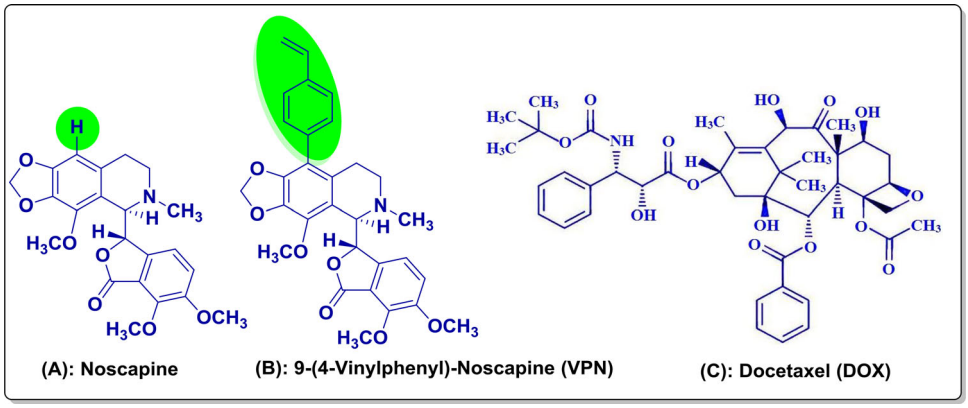

Figure 1. The molecular structures of (A) Noscapine (B) rationally designed derivative, 9-(4-vinylphenyl)-Noscapine (VPN) and (C) a clinical tubulin binding anti-cancer agent, Docetaxel (DOX) used in the study.

having the lowest energy conformations were evaluated for the favorable Glide docking score. A single best conformation for VPN and DOX was considered based on minimum docking score for MD simulation.

Molecular dynamics simulations

Co-complex of tubulin with both the ligands, VPN and DOX (Tub + VPN + DOX) was obtained from co-docking of DOX and VPN on Tubulin dimer (complex_1). GTP, GDP and magnesium ions were retained in the complex. Similarly, co-complex of tubulin-VPN (Complex_2) and Tubulin_DOX (Complex_3) were obtained by removing atoms of DOX and VPN from complex_1 respectively. Complex 4 with Tubulin only, without DOX and VPN, was also obtained. All simulations were performed using Amber 16 simulation suite (Case et al., 2016). The parameters for all 4 ligands such as DOX, VPN, GTP and GDP were estimated using Antechamber program of Amber 16 suite (Wang et al., 2006). All atomic point charges were calculated using AM1-BCC charge model (Jakalian et al., 2002). Topologies and internal coordinates for all complexes were generated using tleap program in Amber16. Missing Hydrogens were added and parameters were assigned to Protein and ligands using FF14SB and GAFF force-fields respectively (Maier et al., 2015). Each molecular system was neutralized by adding counter-ions and was subsequently solvated using TIP3P water model in a truncated octahedron with the distance of 12 Å between the atoms of protein and wall of the box (Jorgensen et al., 1983).

Once the topologies and internal co-ordinates for all complexes were obtained, three rounds of minimization were performed on each complex to relax the system and amend the bad contacts. Position restraints of 10 kcal/Å^2 and 2 kcal/Å^2 were imposed on the protein system for the first and the second rounds respectively, to relax the water molecules around protein. No restraints were imposed in the third round. After removal of bad contacts through minimization, all four molecular systems were equilibrated at 300 K and 1 atm for 500 ps. The equilibrated systems were then run for 100 ns each with time step of 2 fm. Throughout simulations the cut-off for non-bonded interaction was 10 Å, electrostatics was calculated using Particle Mesh Ewald (PME) and bonds were constrained using shake algorithm (Ryckaert et al., 1977; Darden et al., 1993; Essmann et al., 1995). Langevin thermostat was used to regulate the temperature of simulations. Co-ordinates were written every 20 ps to write 5000 frames for each molecular system. CPPTAJ implemented in Ambertools was used to analyze trajectories for Root Mean square deviation analyses (PTRAJ and CPPTRAJ, 2013).

Predictive binding affinity

Binding affinity of VPN and DOX was calculated when both ligands were bound to tubulin (complex 1). Binding affinity of VPN and DOX was also calculated when they were bound to tubulin separately in complex_2 and complex_3 respectively (Suri et al., 2015). Free energy of binding (ΔG_{bind}) was calculated as the ensemble average of the binding free energy of a total of 1000 snapshots, extracted every 20 ps from the last 20 ns of the MD simulation trajectory using MM-PBSA and MM-GBSA methods (Kollman et al., 2000; Massova & Kollman, 2000). as explained below:

$$\Delta G_{bind} = \Delta G_{complex} - \left[\Delta G_{Rec} + \Delta G_{lig}\right]$$
$$G = E_{gas} + G_{sol} - TS.$$
$$E_{gas} = E_{int} + E_{ele} + E_{vdw}$$
$$G_{sol} = G_{PB(GB)} + G_{sol-np}$$
$$G_{sol-np} = \gamma SAS$$

Where, G is Gibbs free energy, E_{gas} is the gas phase energy calculated as the sum of internal energy (E_{int}), energy generated as a result of the electrostatic interaction (E_{ele}) and the van der Waals interaction (E_{vdw}). G_{sol} is the solvation free energy calculated as the sum of polar ($G_{PB(GB)}$) and nonpolar contributions (G_{sol-np}). Polar interaction contribution ($G_{PB(GB)}$) was calculated as the summation of electrostatic contribution (E_{ele}) and polar solvation contribution ($G_{PB(GB)}$). The nonpolar solvation contribution (G_{sol-np}) is approximated as linearly dependent on the solvent accessible surface area (SAS) and γ is the surface tension constant that was set to 0.0072 kcal mol^{-1} Å^{-2} (Massova & Kollman, 2000).

Per residue energy decomposition

The contribution of each amino acid residue of tubulin was calculated to identify those residues which showed strong interaction with ligands (Suri et al., 2014). These calculations

were performed using MM-GBSA method implemented in Amber 16 over 1000 frames obtained every 20 ps from last 20 ns trajectory.

Chemistry

General

All the reactions were monitored by TLC (Precoated silica plates and visualizing under UVlight). Reagents and all solvents were analytically pure and were used without further purification. Air-sensitive reagents were transferred by syringe or double-ended needle. Evaporation of solvents was performed at reduced pressure by using heidolph rotary evaporator.^{1}H and ^{13}C NMR spectra of samples in $CDCl_3$were recorded on AVANCE-300 MHz, 400 MHz, 500 MHz spectrometer. Chemical shift reported are relative to an internal standard TMS ($\delta = 0.0$). Spin multiplicities are described as s (singlet), brs (broad singlet), d (doublet), t (triplet), q (quartet), or m (multiplet). Coupling constants are reported in hertz (Hz). Mass spectra were recorded in ESI conditions at 70 eV on LC-MSD (Agilent technologies) spectrometers. All high-resolution spectra were recorded on QSTAR XL hybrid MS/MS system (Applied Bio systems/MDS sciex, foster city, USA), equipped with an ESI source (IICT, Hyderabad). Column chromatography was performed on silica gel (60-120 mesh) supplied by Acme Chemical Co., India. TLC was performed on Merck 60 F-254 silica gel plates. Commercially available anhydrous solvents Dichloromethane, methanol, acetone and Ethylacetate were used as such without further purification. Natural α-noscapine was purchased from Sigma-Aldrich.

(S)-3-((R)-9-bromo-4-methoxy-6-methyl-5,6,7,8-tetrahydro-[1,3]dioxolo[4,5-g] isoquinolin-5-yl)-6,7-dimethoxyisobenzofuran-1(3H)-one (9-Br-nos)

To a suspension of natural α- noscapine (4.0 g, 9.7 mmol) was reacted with 48% aqueous HBr solution (15 mL) and saturated bromine water (~50 mL) following the procedure developed in our lab. The crude residue was purified over silica gel column chromatography eluted with 3:7 Ethyl acetate: Hexane (3:7) to give pure 9-bromonoscapine **2** (4.3 g, 90%) as white solid. mp 170 °C; $[\alpha]_D^{25}$=-106.8 ($c = 1$, Dichloromethane); ^{1}H NMR (300 MHz, $CDCl_3$) δ 6.96 (d, $J = 8.309$ Hz, 1H) , 6.26 (d, $J = 8.309$ Hz, 1H) , 6.023 (s,2H), 5.392 (d, $J = 4.721$ Hz, 1H), 4.270 (d, $J = 4.721$, 1H) , 4.077 (s, 3H), 3.999 (s, 3H) , 3.872 (s, 3H) , 2.831-2.746 (m, 1H), 2.670-2.579 (m, 1H) , 2.516(s, 3H), 2.496-2.422 (m, 1H), 2.024-1.913 (m, 1H). ^{13}C NMR (75 MHz, $CDCl_3$) δ 167.95, 152.24, 147.67, 146.47, 141.17, 139.90, 134.10, 130.26, 119.57, 118.90, 118.25, 117.45, 101.01, 95.50, 81.23, 62.24, 60.86, 59.37, 56.72, 48.34, 45.13, 25.85. MS (ESI) *m/z* 492 $[M+H]^+$; HR-MS (ESI) Calcd for $C_{22}H_{22}NO_7Br$ $[M+H]^+$:492.0657, found: 492.0636. The ^{1}H-NMR, ^{13}C-NMR and mass spectra (ESI and HR-MS) of the intermediate compound, 9-Br-noscapine are included as supporting material (S1 to S5).

(*S*) − 6,7-Dimethoxy-3- (*R*) − 4 - methoxy-6-methyl − 9 - (4-vinylphenyl) − 5,6,7,8 - tetrahydro-[1,3] dioxolo [4,5-*g*] isoquinolin-5-yl) isobenzofuran-1(3*H*) - zone (**9-VPN**): To a solution of 9-bromonoscapine (2.0 g, 4.1 mmol) in ethanol/toluene (1:1, v/v, 100 mL), $Pd(PPh_3)_4$ (0.59 g, 0.49 mmol), $NaHCO_3$ (8.2 mmol) and 4-vinylphenyl boronic acid (1.25 g, 8.2 mmol) were added sequentially, and the contents were stirred for 48 h at 120 °C. After the starting material was completely consumed in the reaction (judged by TLC), reaction mixture was cooled to room temperature, the solvents were evaporated under vacuum. The crude residue was extracted into dichloromethane (3 × 25 mL) and washed with brine solution. The organic layer was collected and passed through a Na_2SO_4 bed and later removed under reduced pressure. The crude residue was chromatographed over a triethylamine silica gel bed, using pet. ether/ethyl acetate (7:3) as eluents, to give pure compound as colourless solid. (1.32 g) Yield: 62%; m.p: 120-122 °C; $[\alpha]_D^{25}$ 120.22 ($c = 1$, dichloromethane); ^{1}H NMR (300 MHz, $CDCl_3$): δ 7.40 (d, $J = 8.24$ Hz, 2H), 7.17 (d, $J = 8.24$ Hz, 2H), 6.97 (d, $J = 8.16$ Hz, 1H), 6.74-6.66 (dd, $J = 10.81$ Hz, 17.51 Hz, 1H) 6.10 (s, 1H), 5.98 (s, 1H), 5.91 (s, 1H), 5.74 (d, $J = 17.51$ Hz, 1H), 5.48 (s, 1H), 5.25 (d, $J = 10.81$ Hz, 1H), 4.47 (s, 1H), 4.10 (s, 6H), 3.90 (s, 3H), 2.66-2.54 (m, 4H), 2.27-2.13 (m, 2H), 1.77-1.64 (m, 1H). ^{13}C NMR (75 MHz, $CDCl_3$): δ 157.9, 152.2, 147.7, 146.0, 143.6, 140.9, 139.6, 136.7, 133.7, 133.5, 130.7, 130.1, 126.0, 120.4, 117.8, 116.1, 114.2, 100.8, 81.9, 62.3, 61.1, 59.5, 56.9, 50.8, 46.6, 27.0, 23.2, 29.6. MS (ESI): m/z 538 $[M+Na]^+$; HRMS (ESI): Calcd for $C_{30}H_{29}NO_7$ $[M+Na]^+$; 538.1841; found: 538.1848. The ^{1}H-NMR, ^{13}C-NMR and mass spectra (ESI and HR-MS) of the final product, VPN are included as supporting material (S6 to S9).

Biology

Cell culture and reagents

The natural lead compound, noscapine and docetaxel were obtained from Sigma. All the chemical reagents and media used for cell culture were obtained from Mediatech, Cellgro. Human breast cancer cell line, MCF7 was obtained from the cell repository of the National Center for Cell Science Pune, Maharashtra, India. Stock solution (100 mM) of the newly synthesised noscapine derivative, VPN was prepared with dimethyl sulfoxide (DMSO) and stored at 4 °C until use. The cells were allowed to grow at a temperature of 37 °C in a 5% CO_2 and 95% humidity in Dulbecco's modified Eagle medium (DMEM, Pan Biotech), supplemented with 10% fetal bovine serum (FBS) and antibiotics.

In vitro cell proliferation assay

Inhibition of cell proliferation of MCF7 was assessed by 3-(4, 5-dimethylthiazol-2-yl)-2,5, ditetrazolium bromide (MTT) assay. Briefly, MCF 7 cells (3×10^3) were seeded into 96 well plates. After post attachment of 48 h, the cells were treated with different concentrations of VPN alone (10, 25, 50, 100 μM), DOX alone (0.001, 0.01, 0.1,1,10 μM) and in combination of VPN and DOX (10 μM VPN + 0.001 μM DOX, 15 μM VPN + 0.01 μM DOX, 20 μM VPN + 0.05 μM DOX, 25 μM VPN + 0.1 μM DOX, 30 μM VPN + 0.5 μM DOX). Cells were incubated for 48 h and 72 h. After the stipulated time the cells were incubated with 10 μl of MTT (5 mg/ml) for 4.0 h, at

37° C and the absorbance was measured in plate reader (Varioskan, Thermo Scientific) at 570 nm. The value of IC_{50} (the concentration of the drugs required to prevent cell proliferation by 50%) of VPN alone, DOX alone and in combination regimen of VPN and DOX was determined. The experiments were repeated in triplicates.

Cell cycle analysis

MCF7 (1×10^5) cells were seeded into a 6-well culture plate. After 24 h the cells were treated with VPN alone (20 μm), DOX alone (0.5 μm) or in combination regimen of VPN and DOX (25 μm VPN + 0.05 μm DOX). Cells were harvested after 24 h of treatment using trypsin-EDTA, washed properly with phosphate buffered saline (PBS) and fixed in 70% ethanol for 30 min. After fixation, the cells were stained with staining solution that included RNase (5 μg/ml), propidium iodide (5 μg/ml) and Triton X (0.1%). In Flow cytometer (FACS Calibur), the cells were analysed to monitor the inhibition in cell cycle progression. The experiment was performed in triplicates.

Apoptosis assay

MCF7 cells (5×10^4) were seeded in 35 mm plates. After 24 h, cells were treated with VPN alone (20 μm), DOX alone (0.5 μm) or in combination regimen of VPN and DOX (25 μm VPN + 0.05 μm DOX) at a temperature of 37 °C and 5% CO_2. Cells were sampled and analyzed using flow cytometry after 24 h of treatment. Briefly, the cells were stained with propidium iodide (PI) and Annexin-V-Alexa Fluor 488 (BD Pharmingen, San Diego, CA, USA) according to the manufacturer's protocol. Percentage of apoptotic cells were assessed using BD FACS Calibur (San Jose, CA, USA).

DAPI staining

The apoptotic cells in presence of VPN (20 μm), DOX (0.5 μm) and in combination regimen (25 μm VPN + 0.05 μm DOX) were visualized by staining with DAPI under fluorescence microscopy. In brief, MCF7 cells (3×10^3 cells) were grown on poly-l-lysine coated coverslips in 6-well plates and treated with single as well as in combination regimen for 48 h. The cells were then washed twice with ice-cold PBS. The coverslips were fixed with 70% ethanol and stained using DAPI, followed by imaging using BX60 fluorescence microscope (Olympus, Tokyo, Japan). Apoptotic cells were identified as changes in cellular morphology (e.g. nuclear condensation, membrane blebs formation, and apoptotic bodies).

Tubulin purification

Microtubules were isolated and purified from the goat brain through alternative cycles of GTP-dependent polymerization and depolymerisation in PEM buffer (50 mM pipes, 3 mM MgSO4, 1 mM EGTA, pH 6.8) (Hamel & Lin, 1981; Panda et al., 2000). The purified microtubules were preserved at −80 °C. The purified tubulin was estimated using the Bradford method as well as by SDS PAGE (Bradford, 1976).

Tryptophan quenching assay

Tubulin (2 μM) was incubated in a water bath with VPN at a concentration of 20 μM, DOX at a concentration of 0.5 μM and in combination regimen (DOX 0.05 μM + VPN 25 μM) in PEM buffer (50 mM pipes, 3 mM MgSO4, 1 mM EGTA, PH 6.8) for 45 min at 35 °C. The samples were excited at 295 nm and emission was measured at 310-400 nm. For the spectrofluorometric titrations a FlouroMax® 4 spectrofluorometer (Horiba Scientifc, Edison, NJ) assisted by Fluor Essence 3.5 software was used. The experiments were repeated twice.

ANS (8-Anilino-1-naphthalene sulfonic acid)-binding assay

ANS binding assay was performed to verify the structural integrity of the tubulin in presence of VPN and DOX in single as well as in combination regimen. Tubulin (2 μM) was incubated with VPN (20 μM and 50 μM), DOX (0.5 μM) and in combination regimen (DOX 0.05 μM + VPN 25 μM) at 35 °C for 30 min in PEM buffer. ANS (50 μM) was added and the samples were incubated in dark at 25 °C for 15 min. The samples were excited at 350 nm and the emission was measured at 410–470 nm using a Flourolog 3 spectrofluorometer (Horiba Scientific, Edition, NJ) assisted by fluorescence 3.5 software. The assays were repeated two times.

Results and discussion

Molecular modelling

Both noscapinoid and docetaxel were reported to bind to tubulin at a different site. Noscapinoids bind at the interface of α- and β- tubulin (Naik et al., 2011), whereas the binding of docetaxel was biased to β-tubulin (Snyder et al., 2001). Since both the ligands bind to tubulin, we are interested to determine the binding affinity of both VPN and DOX when both the ligands are docked at their respective binding site onto tubulin. We have performed two cycles of molecule docking with tubulin. In the first cycle DOX was docked onto its binding site and similarly VPN was docked onto noscapinoid binding site using Glide XP docking to calculate their binding affinity, individually. Both the ligands, VPN and DOX docked well into their binding site with a docking score of −4.82 kcal/mol and −6.67 kcal/mol respectively (Table 1). The DOX-tubulin complex was taken in the second cycle and the VPN was docked onto the noscapinoid binding site. Presence of DOX on its binding site interfered with the binding of VPN with a reduced docking score of −3.232 kcal/mol. It may be because of the alteration of the secondary conformation of tubulin due to binding of DOX.

MD simulation of the complex

We determine the binding mode of both VPN and DOX independently with tubulin (Tub-VPN and Tub-DOX complexes) as well as in the presence of both of them in their respective binding site onto tubulin (Tub-DOX + VPN) by molecule dynamic simulation of 100 ns to obtain a trajectory of 5,000 frames, each frame recorded every 20 ps. Root mean square deviations (RMSD) of Cα-atoms during the entire duration of

Table 1. Molecular docking results (Glide XP_{score}) and the relevent energy parameters of VPN and DOX in single as well as in combination with tubulin.

Ligands	Glide XP_{score} (kcal/mol)	Glide E_{vdw} (kcal/mol)	Glide E_{coul} (kcal/mol)	Glide energy (kcal/mol)
VPN	−4.82	−39.86	−8.16	−48.02
DOX	−6.67	−41.63	−8.46	−50.09
VPN-DOX	−3.23	−32.83	−9.27	−42.10

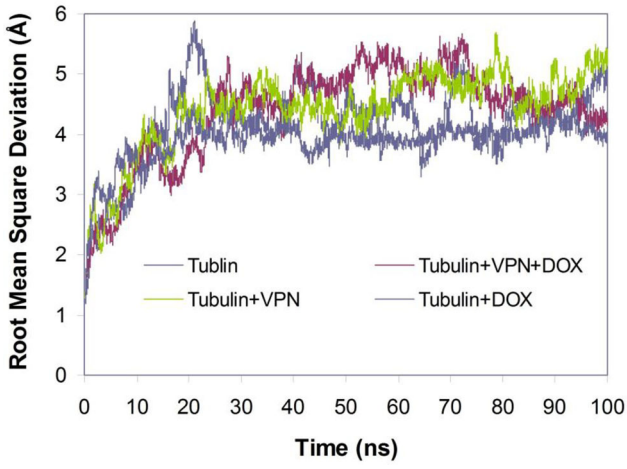

Figure 2. Root mean square deviations (RMSD) of Cα carbon atoms of tubulin only and in complex with VPN (Tubulin + VPN), with docetaxel (Tubulin + DOX) and with both docetaxel and VPN (Tubulin + DOX + VPN) during 100 ns of MD simulation. The relative fluctuation in the RMSD of the Cα atoms is very small after ~ 20 ns of the simulation. The time step of 20ps was used during the simulation that generated 5,000 frames which were used to generate the average structure.

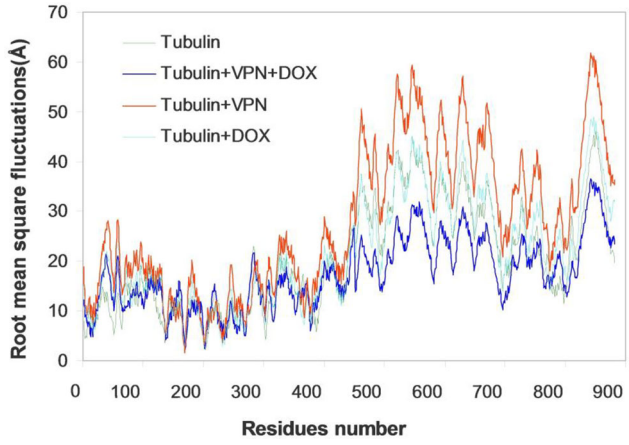

Figure 3. Root mean square fluctuation (RMSF) of the residues of tubulin of the docked ligands in the bound form and in the unbound form of tubulin heterodimer. Different levels of flexibility of these residues were noticed in the bound form of tubulin with VPN and DOX in single as well as in combination. Most of the residues showed flexibilities >5 Å in case of tubulin bound with VPN and DOX as compared to the free tubulin heterodimer, indicating that these residues seem to be more flexible as a result of binding.

simulation were calculated for all the frames to monitor the stability of the system (Figure 2).

All the systems got stabilized after 20 ns of simulation, since the relative fluctuation in the RMSD of Cα carbon atoms (Cα-rmsd) was very small after equilibration. The overall RMSD ranges from 0 to 2.582 Å. Furthermore, root mean square fluctuations (RMSF) of Cα-atoms were also calculated for all the systems to find any changes in the residue flexibilities. The RMSF values were plotted against residue numbers based on the 100 ns trajectory (Figure 3). The residues with higher RMSF tend to show more flexibility. Both VPN and DOX were well accommodated inside the binding cavity. The VPN docked well at the interface of α- and β- tubulin, whereas the binding of DOX is biased more towards β-tubulin (Figure 4a and b). Their binding mode with the tubulin was represented in two steps: (a) receptor residues that have strong interactions with the ligand, such as a favourable hydrogen-bonding interactions, and (b) receptor residues that are close to the ligand, but whose interactions with the ligand are weak or diffuse, such as hydrophobic interaction.

The differential mode of interactions of compounds VPN and DOX with the residues of tubulin are represented in the Ligplot. The differences in amino acids for binding of VPN with tubulin independently and in combination with DOX (Figure 4c and d) were mainly because of the change in conformation of tubulin due to binding of DOX. Similarly, the differences in amino acids for binding of DOX with tubulin, independently and in combination (Figure 4e and f) were due to change in the conformation of tubulin upon binding of VPN. As seen in the figure several hydrogen bonds and hydrophobic interactions are involved in their binding.

The amino acids of the binding site involved in the binding of VPN are Glu 336(D),Val 351(D), Leu 333(D),Pro 175(A), Glu 207(A), Arg 340(A), Asn 337(D), Lys 394(A) (Figure 4c), and the DOX are Val 23(D), Ala 233(D), His 229(D), Asp 226(D), Leu 219(D), Leu 371(D), Arg 278(D), Arg 369(D), Gly 370(D) (Figure 4d). The two hydrogen bonds contributed to the interactions of VPN with the binding pocket of tubulin. The oxygen atom (O_2) of the isoquinoline ring is hydrogen-bonded with the ND2 of the side chain of Leu D 286 with a distance of 3.04 Å. The carbonyl oxygen of isobenzofuran ring is hydrogen-bonded with the side chain of Arg D 278 with the distance of 3.05Å'. Similarly, binding of DOX involves two hydrogen bonds; the amino acids Lys 372, Leu 371, Gly 370, Leu 286 and Gln 281 contributed to hydrophobic interactions with the ligands. The isoquinoline ring is hydrogen-bonded with ND2 of the side chain of Asn D 337 with a distance of 3.21 Å and the isobenzofuran ring is hydrogen-bonded with the side chain of Lys A 394 with the distance of 2.90 Å. In contrast, there is significant difference in the amino acids involved in the interaction of VPN as well as DOX in the co-complex of tubulin with both the ligands together (Figure 4e and f) This clearly explains the changes in the binding mode of VPN and DOX when both the ligands are docked together with the tubulin so there is a chance of combination effect.

Calculated binding affinities of VPN and DOX

The binding free energy and its respective components of both VPN and DOX with tubulin were calculated independently as well as in combination and presented in Table 2. We have considered last 250 frames from the last 5 ns of trajectory

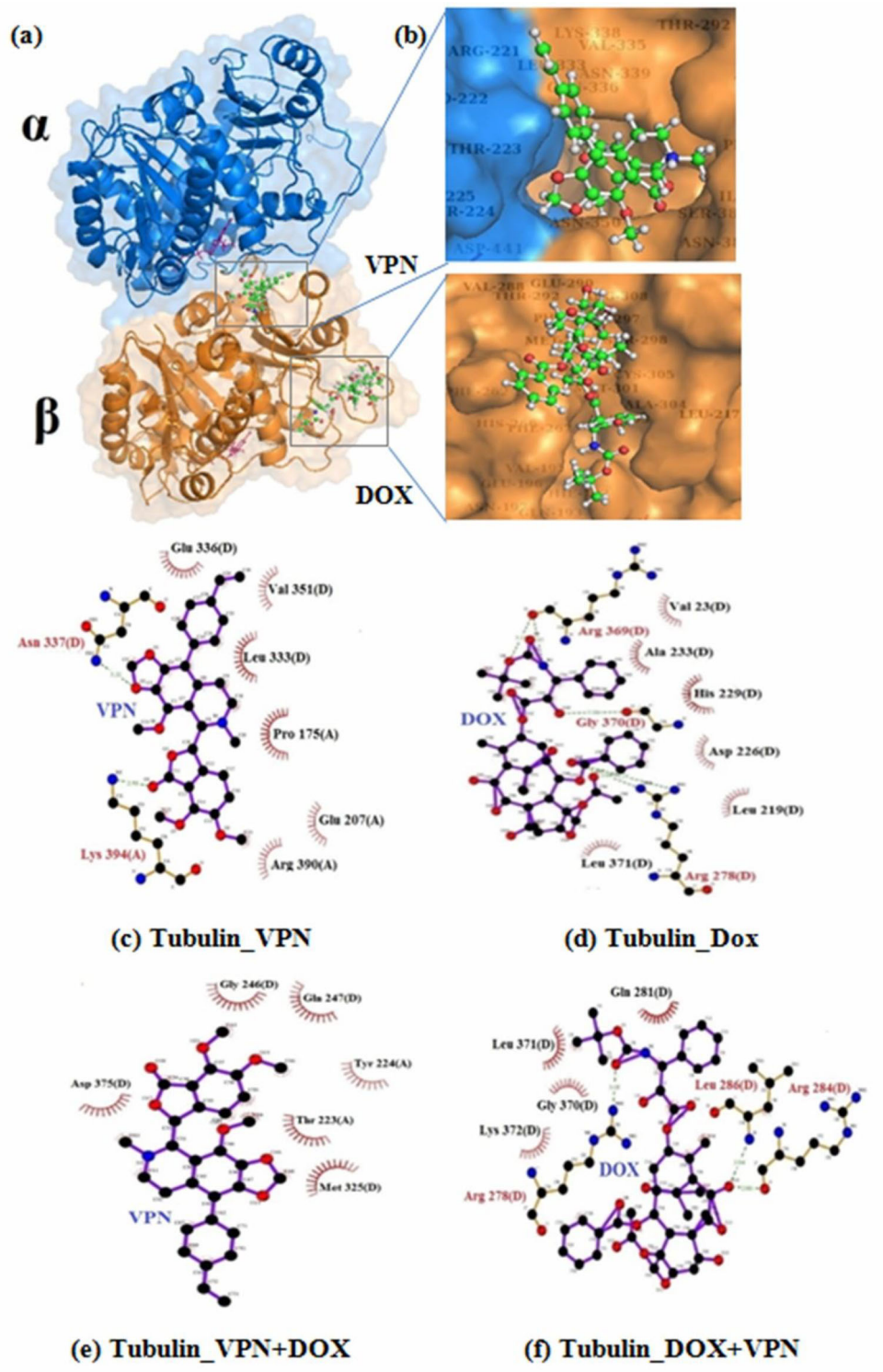

Figure 4. (a) Both VPN and DOX are well accomodated inside their respective binding site of tubulin. (b) Snapshot of both the ligands are obtained from the MD simulation. The binding site is represented as macromodel surface according to α- and β- tubulin (α-tubulin is represented in blue colour and β-tubulin is represented in brown colour). The ligplot analysis showing the interaction of binding site amino acids with the (c) VPN, (d) DOX, (e) VPN when it is docked into the co-complex of tubulin and DOX, and (f) DOX when it is docked into the co-complex of tubulin and VPN. The binding site residues involved in the interaction of VPN and DOX are slightly different in single as well as combine docking. The hydrogen bonds formed (if any) are represented as dotted lines.

to calculate the ensemble average of the free energy of binding using both MM-GBSA and MM-PBSA methods. For all complexes, the binding energy was decomposed into its various energy components (the electrostatic, van der Waals and solvation). Both van der Waals (ΔE_{VDW}) and the electrostatic component (ΔE_{ELE}) were observed to make very significant contributions to the free energy of binding. However, the net polar contribution ($\Delta G_{(ele,PB/GB)} = \Delta E_{ele} + \Delta G_{(PB/GB)}$) was rendered unfavourable due to very large penalty imposed by the desolvation component ($\Delta G_{PB/GB}$) while the net nonpolar component (ΔE_{vdw}) and ($\Delta G_{sol\text{-}np}$) were observed to have made highly favourable contribution to the binding free energy.

The results obtained from both the methods suggested very robust interactions of both VPN and DOX independently

as well as in combination. The predicted binding free energies (ΔG_{bind}) based on MM-GBSA method for VPN and DOX independently are −24.12 kcal/mol and −20.07 kcal/mol and in combination of both are −19.99 kcal/mol and −24.17 kcal/mol respectively. In contrary the ΔG_{bind} based on MM-PBSA for VPN and DOX independently are estimated to be −24.04 kcal/mol and −18.65 kcal/mol and in combination of both are −21.41 kcal/mol and −22.70 kcal/mol. The differences in the calculation of ΔG_{bind} between both the methods derived from the difference in calculation of the contribution to the polar solvation energy, which is slightly higher in the MM-PBSA calculation compared to MM-GBSA. Very robust van der Waals (ΔE_{VDW}) interactions of VPN, to the magnitude of −33.51 kcal/mol to −30.34 kcal/mol were observed for the single and combination with DOX. Similarly, the ΔE_{VDW} interactions of DOX, to the magnitude of −34.04 kcal/mol to −35.39 kcal/mol were observed for the DOX in single as well as in combination with VPN. The net polar component ($\Delta G_{GB\text{-}polar}$) was observed to be unfavourable in the interaction of VPN and DOX with tubulin (Table 2). The unfavourable polar contributions were observed to have overcome the highly favourable non-polar components ($\Delta G_{sol\text{-}np}$) among both the dimers. Interactions of VPN and DOX with tubulin seem to be steered by nonpolar component. This can be explained by the tendency of the nonpolar residues to readily bury themselves in the hydrophobic pockets and displaced water.

Table 2. Calculated binding energy and its various componentes (kcal/mol) of VPN and DOX in single as well as in combination binding with tubulin. The values in bold represent the ΔGbind energy of molecules with tubulin based on MM-GBSA and MM-PBSA methods.

Energy component	Tub_VPN	Tub_Dox	Tub_DOX + VPN	Tub_VPN + DOX
ΔE_{VDW}	−33.51	−34.04	−30.34	−35.39
ΔE_{ELE}	−289.96	−11.21	−313.55	−20.00
ΔE_{GAS}	−323.46	−45.26	−343.88	−55.40
$\Delta G_{GB\text{-}Polar}$	303.25	29.70	327.49	35.98
$\Delta G_{SOL\text{-}NP}$	−3.92	−4.51	−3.60	−4.75
$\Delta G_{SOL\text{-}GB}$	299.33	25.19	323.90	31.23
$\Delta G_{bind\text{-}GBSA}$	**-24.12**	**-20.07**	**-19.99**	**-24.17**
ΔG_{PB}	303.16	30.92	325.94	36.8913
$\Delta G_{SOL\text{-}NP}$	−3.74	−4.31	−3.46	−4.1931
$\Delta G_{SOL\text{-}PB}$	299.42	26.61	322.48	32.6982
$\Delta G_{bind\text{-}PBSA}$	**-24.04**	**-18.65**	**-21.41**	**-22.7061**

Per residue energy decomposition

Energy contribution of each residue in the binding of VPN and DOX was calculated using the MM-GBSA method to investigate the details of protein-ligand interactions at the atomic level. The predictive binding energy ($\Delta G_{bind,GB}$) of VPN and DOX independently was decomposed into per residue basis and included in (Figure 5a). Per residue contribution of binding free energy is an efficient way to investigate the details of protein–ligand interactions at the atomic level. We have identified the residues that have the greatest impact, in terms of total energy (ΔG_{bind}) contribution, known as hotspot amino acids. For the binding of VPN, residue Met323 showed the largest contribution (< -1.0 kcal/mol), while five other binding site residues (Glu183, Gln245, Asp327, Ala352 and Val353) contributed energy > -1.0 kcal/mol (Figure 5a). Moreover, the hot spot amino acids make considerable electrostatic energy contribution towards the binding of VPN. The hotspot amino acids in the binding of VPN were slightly different in presence of DOX. For the binding of DOX, residues Ala283, Leu361, Lys362 and Met363, showed the largest contribution of < -1.0 kcal/mol, whereas four other amino acids Tyr281, Arg282, Ala283 and Leu284) contributed > -1.0 kcal/mol energy (Figure 5b). All these hot spot amino acids make considerable van der Waals energy contribution towards the binding of DOX. The hospot amino acids were found to be diffferent in the presence of VPN.

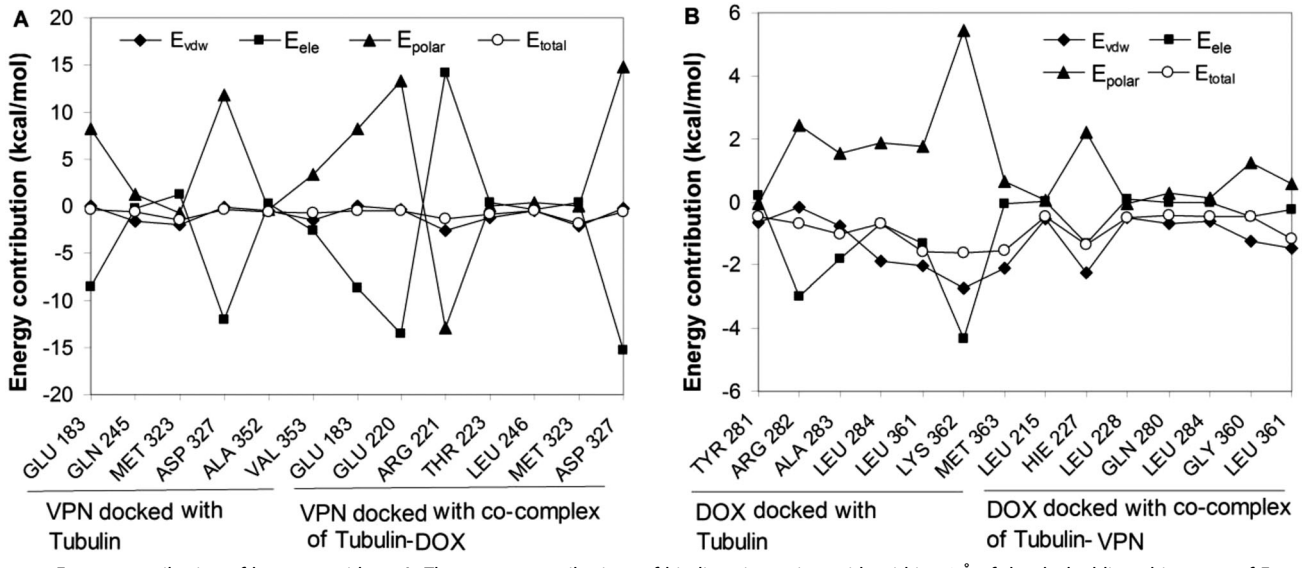

Figure 5. Energy contribution of hotspot residues. A. The energy contributions of binding site amino acids within 12 Å of the docked ligand in terms of E_{vdw}, E_{ele}, E_{polar} and E_{total} with VPN when it docked in single with the tubulin as well as in the co-complex of tubulin-DOX (A) and with DOX when it docked in single with the tubulin as well as in the co-complex of tubulin-VPN (B). For binding of VPN the hotspot amino acids make considerable electrostatic interaction energy, whereas for binding of DOX the hotspot amino acids make considerable van der Walls interaction energy. Further, for the binding of VPN and DOX with tubulin only and in co-complex with the ligands slightly different set of binding site amino acids are involved.

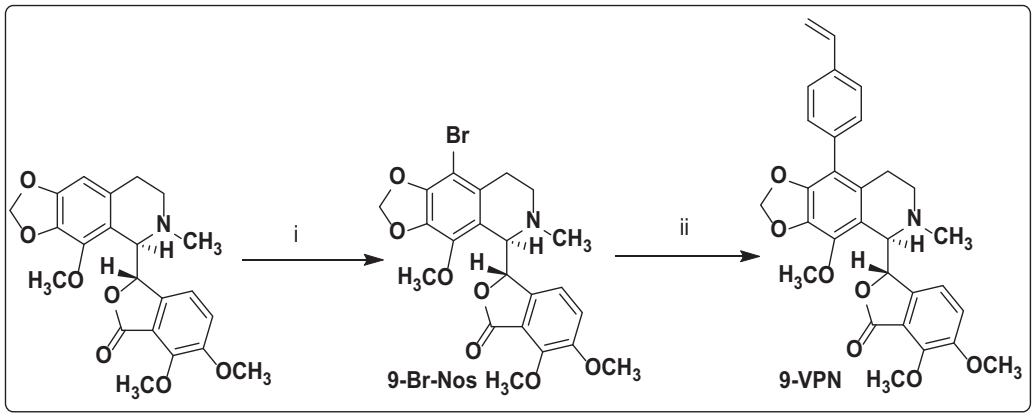

Scheme 1. Reaction Conditions. (i) 48% HBr, Br_2-water, RT, 2 h, 90% (ii) 4-Vinylphenyl boronic acid, Pd $(TPP)_4$, $NaHCO_3$, EtOH/Toluene, 120 °C, 48 h, 60%.

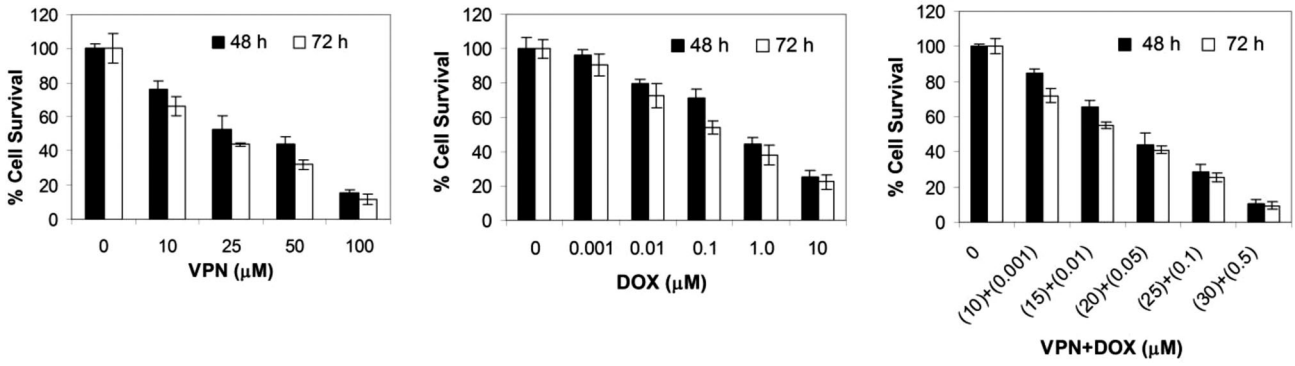

Figure 6. The inhibition of cellular proliferation of human breast cancer cell, MCF-7 with the treatment of VPN and DOX in single as well as in combination regimen at different concentration after 48 h and 72 h post-treatment. The IC_{50} value amounted to 30.17 μM and 19.92 μM, respectively for 48 h and 72 h with VPN. Similarly, the IC_{50} value amounted to 0.621 μM and 0.193 μM, respectively for 48 h and 72 h with DOX. In contrast, the approximately 50% inhibition of cellular inhibition was achieved in a combination regimen of VPN (20 μM) and DOX (0.05 μM) after 48 h and 72 h post-treatment.

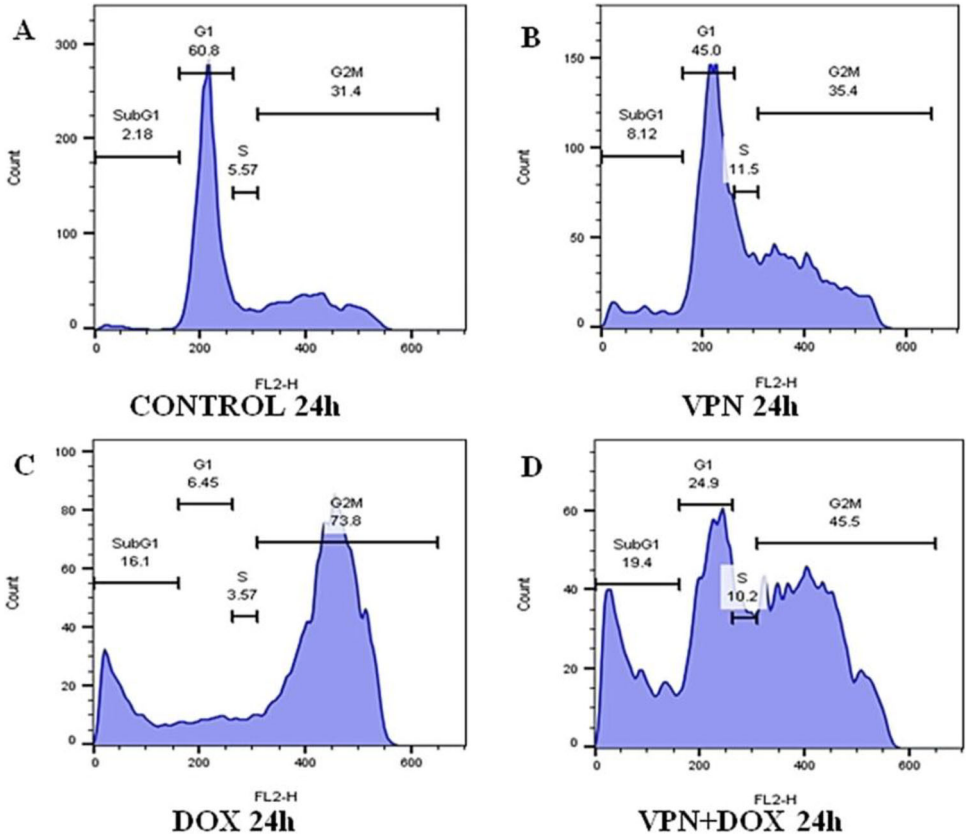

Figure 7. Panels (A) to (D) depicts cell cycle distribution of MCF-7 cells in a two-dimensional disposition as determined by flow cytometry at 24 h of treatment with 20 μM of VPN, 0.5 μM of DOX as single regimen and 25 μM of VPN + 0.05 μM of DOX in combination regimen. Results represent cell cycle progression at mitosis followed by the appearance of a characteristic hypodiploid (sub-G1) DNA peak is indicative of apoptosis.

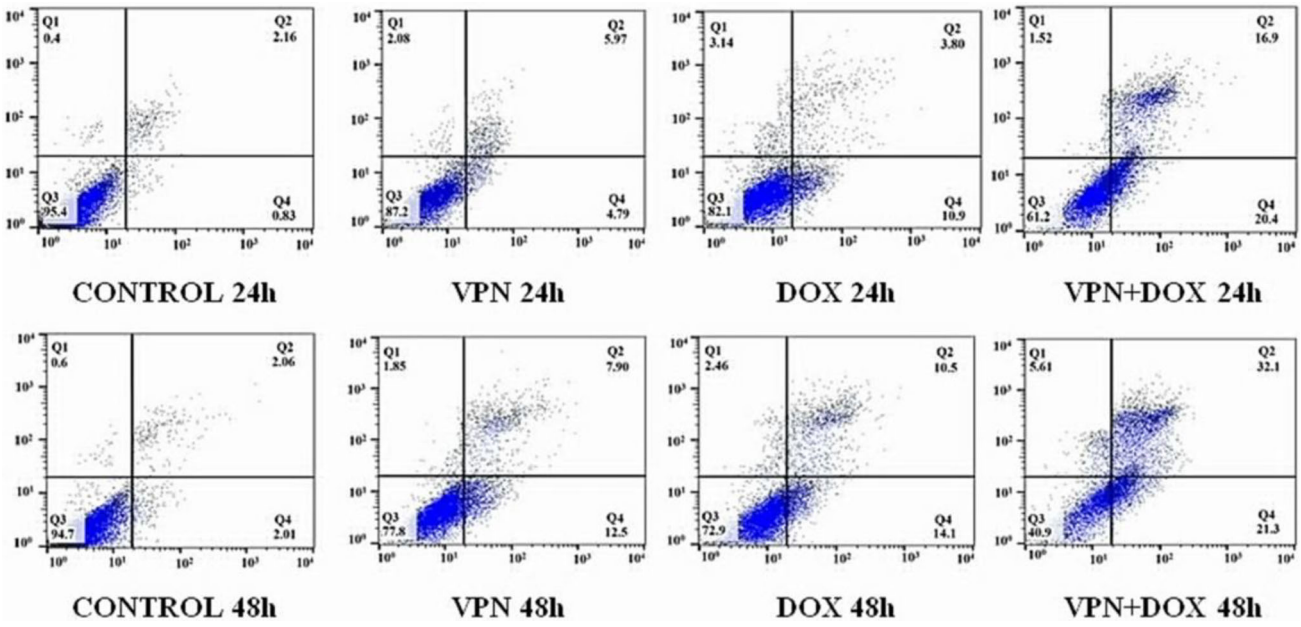

Figure 8. Induction of apoptosis caused by VPN (20 μM) and DOX (0.5 μM) alone and in their combination regimen (VPN, 25 μM + DOX, 0.05 μM) based on flow cytometric analysis. PE/Annexin V staining was used in combination with 7-Amino-Actinomycin (7-AAD) to distinguish among 4 subpopulations: cells negative for both 7-AAD and Annexin V staining were viable cells (in the lower left quadrant: Q3); 7-AAD-negative, Annexin V-positive cells were early apoptotic cells (in the lower right quadrant: Q4); 7-AAD-positive, Annexin V-positive cells were primarily late apoptotic/necrotic cells (in the upper right quadrant: Q2); and the 7-AAD-positive but annexin V-negative cells were necrotic cells (in the upper left quadrant: Q1).

Chemistry

It is always a challenge to synthesize the derivatives of noscapine because of their highly sensitive C-C bond between isoquinoline and isobenzofuranone ring components which are labile to strong acids and base. However, we have optimized the reaction conditions for the amalgamation of the VPN from 9-bromonoscapine as starting material without affecting the sensitive C-C bond (Scheme 1).

The starting material 9-bromo noscapine required was synthesized from natural α-noscapine in excellent yield (90%) using bromine water in 48% aqueous HBr by modifying the reaction conditions described in literature (Naik et al., 2011). 9-bromonoscapine reacted with 4-vinyl boronic acid, $Pd(TPP)_4$, $NaHCO_3$ in ethanol/toluene at 120 °C for 48 h to give VPN in 60% yield. Both 9-Br-Noscapine and VPN were fully characterised by ^1H, ^{13}C NMR and mass (ESI and HRMS), IR spectral data (supporting material S1-S9).

Biology

VPN inhibits proliferation of cancer cells

Inspired by the *in silico* prediction of binding affinity of VPN with tubulin dimer, we evaluated its efficacy in inhibiting proliferation of MCF7 cells in single and in combination regimen with DOX. The anti-proliferative activity for both VPN and DOX increases with the increasing concentration in single as well as in combination regimen (Figure 6). The IC_{50} value amounted to 30.17 μM and 19.92 μM, respectively for 48 h and 72 h with VPN. Similarly, the IC_{50} value amounted to 0.621 μM and 0.193 μM, respectively for 48 h and 72 h with DOX. Surprisingly, the inhibition of cellular proliferation was significantly achieved with the combination dose regimens of both VPN and DOX. The approximately 50% inhibition of cellular proliferation was found to be at VPN (20 μM) and DOX (0.05 μM). The dose dependent cytotoxicity of DOX has been reduced considerably with the combination dose regimen of VPN.

Cell cycle analysis

Inhibition in the progression of cell cycle of MCF7 with treatment of VPN (20 μM) and DOX (0.5 μM) in single regimen as well as in combination regimen (25 μM VPN + 0.05 μM DOX) was evaluated using flow cytometer. Both the compounds showed an increase in the sub-G1 cell populations compared to the control after 24 h of treatment in single and in combination regimen. The representative two-dimensional disposition of cell cycle profile is included in Figure 7. The sub-G1 population with treatment of VPN was increased to 8.12%, whereas with DOX it was increased to 16.1% and in combination it further increased to 19.4% in comparison to control. A cell must lose enough DNA to appear in the sub-G1 area. Therefore, both the compounds, VPN and DOX in single as well as in combination induce apoptosis to cancer cell. Maximum cells were arrested at the G2M transition phase.

Apoptosis assay

We approached to determine the induction of apoptotic cell death to breast cancer cell, MCF-7 by treatment of VPN and DOX in single as well as in combination regimen. Biochemically, the early apoptotic stage is characterized by the loss of lipid asymmetry between the two plasma membrane leaflets, resulting in an irregular externalization of phosphatidylserine (PS) from the inside leaflet to the outer leaflet, which can be measured fluorescently by annexin V

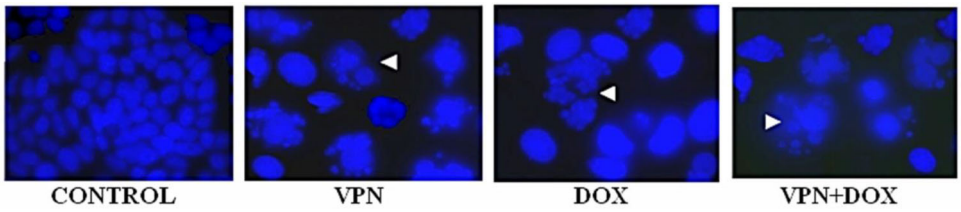

Figure 9. Morphologic indicators of apoptotic cell death include chromatin condensation along with nuclear envelope and plasma membrane blebbing followed by formation of small apoptotic bodies. Panels show morphological evaluation of nuclei stained with DAPI in the absence and presence of the VPN (20 μM) and DOX (0.5 μM) in single as well as in combination regimen (25 μM VPN + 0.05 μM DOX). Several typical features of apoptotic cells such as condensed chromosomes, numerous fragmented micronuclei, and apoptotic bodies are evident (indicated by white head arrows) upon 48 h of drug treatment. (Scale bar = 15 μm).

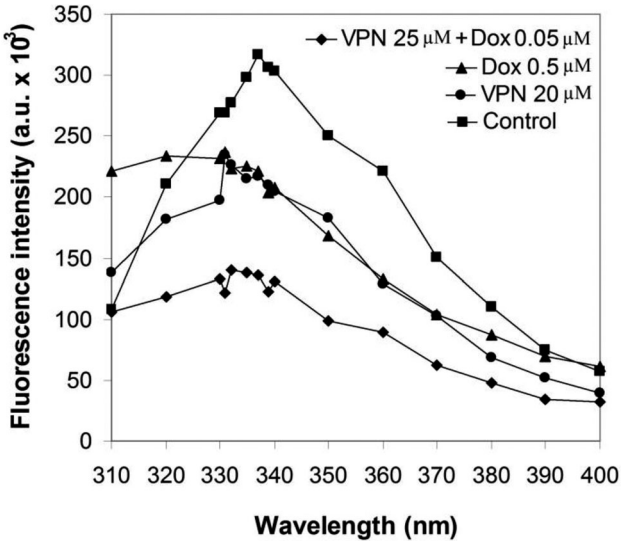

Figure 10. Decrease of fluorescence intensity of tubulin by VPN and DOX in single as well as in combination regimen. Tubulin (2.0 μM) was incubated with VPN (20 μM) and DOX (0.5 μM) alone as well as in combination regimen (25 μM of VPN + 0.05 μM of DOX) and the emission spectra were collected (310 nm – 400 nm). Both VPN and DOX in single as well as in combination regimen showed a concentration-dependent quenching of the intrinsic tubulin fluorescence emission intensity indicating the binding of both VPN and DOX to tubulin. The more reduction in tubulin fluorescence intensity in combination regimen of both VPN and DOX, compared to their single binding, revealed combination effect with the tubulin. The graph is a representative of three independent experiments.

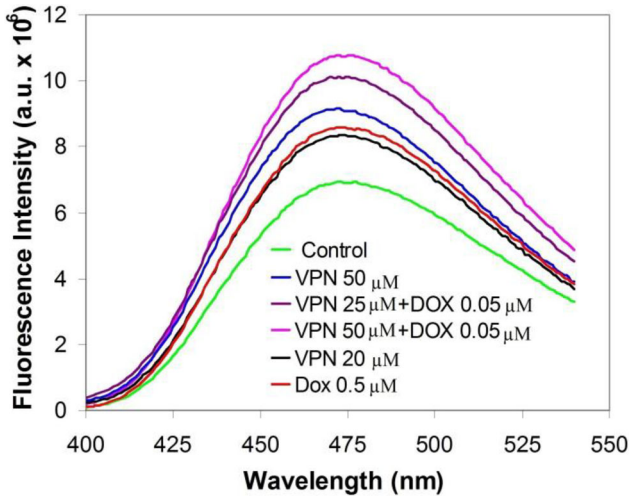

Figure 11. Enhancement of tubulin-ANS fluorescence by VPN and DOX in single as well as in combination regimen. Tubulin (2.0 μM) was incubated without (control) or with VPN (50 μM and 20 μM), DOX (0.5 μM) and in their combination regimen (VPN 25 μM + DOX 0.05 μM, VPN 50 μM + DOX 0.05 μM), followed by incubation with ANS (50 μM). The samples were excited at 380 nm and the emission spectra were collected (390 nm – 500 nm). Both VPN and DOX in single as well as in combination regimen showed a concentration-dependent increase in tubulin-ANS fluorescence indicating the binding of both VPN and DOX to tubulin. The increase is more in tubulin-ANS fluorescence in combination regimen of both VPN and DOX, compared to their single binding, revealed combination effect with the tubulin. The graph is a representative of three independent experiments.

binding. In contrast, a cell-impermeant DNA-binding fluorescent dye, propodium iodide can only enter the cells when it is at the stage of late apoptosis when membrane permeability is compromised. The apoptotic cells can be quantified to a large extent by FACS analysis. In FACS analysis, green Annexin V staining was used together with an impermeant red DNA binding dye, 7-Amino-Actinomycin (7-AAD), to quantitate the population of apoptotic, necroptotic and necrotic cells. Figure 8 depicts the density plots of 7-Amino-Actinomycin (7-AAD) versus PE conjugated Annexin V fluorescence obtained from untreated control and treated MCF7 cells. Cells negative for both 7-AAD and Annexin V staining were viable cells (in the lower left quadrant: Q3); 7-AAD-negative, Annexin V-positive cells were early apoptotic cells (in the lower right quadrant: Q4); 7-AAD-positive, Annexin V-positive cells were primarily late apoptotic/necrotic cells (in the upper right quadrant: Q2); and the 7-AAD-positive but annexin V-negative cells were necrotic cells (in the upper left quadrant: Q1). As anticipated, MCF-7 cells treated with both VPN (20 μM) and DOX (0.5 μM) in single as well as in combination regimen (VPN, 25 μM + DOX, 0.05 μM) for a duration of 24 h and 48 h resulted in significant increase of apoptotic cells compared to control untreated cells (Figure 8). The percentage of early apoptotic cells were measured to be 4.79%, 10.9%, 20.4% and late apoptotic cells were estimated to be 5.97%, 3.8%,16.9%, respectively with treatment of VPN and DOX in single as well as in combination regimen after 24 h of post-treatment. Parenthetically, a similar significantly high percentage of early apoptotic cells of 12,5%, 14.1% and 21.3% as well as late apoptotic cells of 7.90%, 10.5% and 32.1%, respectively with treatment of VPN and DOX in single as well as in combination regimen, after 48 h, was measured and compared to controlled untreated cells (Figure 8). The control untreated cell culture contained only very few early apoptotic (0.83% and 2.01% after 24 h and 48 h post-treatment) and late apoptotic cells (2.17% and 2.14% after 24 h and 48 h post-treatment), which were considered as the background cell death due to regular trauma during cell culture (Figure 8). This is mainly because we have taken unstained cell for gating

and put the stained control cells in the FACS analysis as per the standard protocol (Ji et al., 2017; Sivakumaran et al., 2018; Fan et al., 2018).

DAPI staining

The induction of apoptosis to cancer cells were observed under the inverted fluorescence microscope after treatment of VPN and DOX in single as well as in combination. The apoptotic cells have significant alteration in the membrane architecture, blebbing of plasma membrane, chromatin condensation and chromosomal breakdown (apoptotic bodies) which could be visualized using the 4′, 6-diamidino-2-phenylindole (DAPI) fluorescent dye. Both the compounds in both single and in combination, efficiently induced apoptosis to cancer cell as revealed in the (Figure 9).

Tryptophan quenching assay

Tubulin is autofluorescence due to presence of tryptophan amino acid. Thus any alteration in its conformation with ligand binding decreases emission fluorescence - a tool used to recognize a ligand binding. The reduced fluorescence intensity in presence of increasing concentration of VPN and DOX in single as well as in combination, indicates the binding of both the compounds with tubulin. The relative percentage of decrease in fluorescence intensity was 19.86% and 25.31% respectively in presence of 20 μM VPN and 0.5 μM of DOX and 55% in combination of DOX (0.05 μM) and VPN (25 μM) (Figure 10). The significant reduction in tubulin fluorescence intensity in the combine regimen of VPN and DOX indicate co-binding of both the ligands with tubulin.

ANS-binding assay (8-anilino-1-naphthalenesulfonic acid)

Next, we investigated the impact of VPN (20 and 50 μM) and DOX (0.5 μM) on tubulin conformation changes using ANS binding assay, a fluorescent probe that binds to the protein's hydrophobic patches. Treatment of tubulin with VPN (20 and 50 μM) showed increase in tubulin-ANS fluorescence intensity in a way dependent on the concentration (Figure 11). It showed 20% and 31.8% increase in fluorescence intensity at 20 and 50 μM of VPN, whereas 23.39% in presence of DOX (0.5 μM) in comparison to unbound tubulin. Similarly, the tubulin-ANS fluorescence intensity was increased to 45% in combination treatment of VPN (25 μM) and DOX (0.05 μM) as well as 54% in combination of VPN (50 μM) and DOX (0.05 μM). The relative increase in tubulin-ANS fluorescence intensity in combination treatment of VPN and DOX compared to single regimen indicates the synergistic effect in the binding of both the compounds onto their respective binding sites.

Conclusion

Our extensive molecular modelling, cellular and biochemical studies, revealed the combination effect of newly designed derivative of noscapine (VPN) and docetaxel. The calculated binding free energy with tubulin was found to be different when both the ligands bound together into their respective binding sites compared to their single binding. The molecular dynamic simulation for 100 ns also revealed stable interaction of both the ligands with the tubulin. The inhibition of proliferative activity was significantly enhanced when both the drugs were used for treatment together, compared to their single regimen treatment. Similarly, the combination regimen of VPN and DOX effectively interfered with the cell cycle progression and induced apoptosis to cancer cells compared to their single regimen treatment. Both the ligands also found to bind with tubulin efficiently at combination treatment. Taken together, it is concluded that the anticancer activity of both VPN and docetaxel could be combined for better therapeutic outcome with minimum toxicity. Thus the synergistic use of VPN and DOX could be a novel approach for the treatment of breast cancer.

Acknowledgements

We would like to acknowledge the financial support provided by the OHEPEE, Govt. of Odisha through World Bank. Shruti Gamya Dash wishes to acknowledge the award of student research fellowship (DST/INSPIRE/IF170022) by the Department of Science and Technology, Govt. of India. Further, we express our indebtedness to Dr. Manu Lopus, UM-DAE Centre for Excellence in Basic Sciences, Mumbai, for providing extended facilities. CSIR-IICT communication number: IICT/Pubs./2020/130.

Disclosure statement

No potential conflict of interest was reported by the authors.

References

Becke, A. D. (1993). A new mixing of Hartree-Fock and local density-functional theories. *The Journal of Chemical Physics*, *98*(2), 1372–1377. https://doi.org/10.1063/1.464304

Binkley, J. S., Pople, J. A., & Hehre, W. J. (1980). Self-consistent molecular orbital methods. 21. Small split-valence basis sets for first-row elements. *Journal of the American Chemical Society*, *102*(3), 939–947. https://doi.org/10.1021/ja00374a017

Bradford, M. M. (1976). A rapid and sensitive method for the quantitation of microgram quantities of protein utilizing the principle of protein-dye binding. *Analytical Biochemistry*, *72*, 248–254. https://doi.org/10.1006/abio.1976.9999

Case, D. A., Betz, R. M., Cerutti, D. S., Cheatham, T. E., III, Darden, T. A., Duke, R. E., Giese, T. J., Gohlke, H., Goetz, A. W., Homeyer, N., Izadi, S., Janowski, P., Kaus, J., Kovalenko, A., Lee, T. S., LeGrand, S., Li, P., Lin, C., Luchko, T., … Kollman, P. A. (2016). *AMBER 2016*. University of California.

Checchi, P. M., Nettles, J. H., Zhou, J., Snyder, J. P., & Joshi, H. C. (2003). Microtubule interacting drugs for cancer treatment. *Trends in Pharmacological Sciences*, *24*(7), 361–365. https://doi.org/10.1016/S0165-6147(03)00161-5

Chougule, M., Patel, A. R., Sachdeva, P., Jackson, T., & Singh, M. (2011). Anticancer activity of Noscapine, an opioid alkaloid in combination with Cisplatin in human non-small cell lung cancer. *Lung Cancer*, *71*(3), 271–282. https://doi.org/10.1016/j.lungcan.2010.06.002

Darden, T., York, D., & Pedersen, L. (1993). Particle mesh Ewald: An N. log (N) method for Ewald sums in large systems. *The Journal of Chemical Physics*, *98*(12), 10089–10092. https://doi.org/10.1063/1.464397

Essmann, U., Perera, L., Berkowitz, M. L., Darden, T., Lee, H., & Pedersen, L. G. (1995). A smooth particle mesh Ewald method. *The Journal of Chemical Physics*, *103*(19), 8577–8593. https://doi.org/10.1063/1.470117

Fan, B., Shi, S., Shen, X., Yang, X., Liu, N., Wu, G., Guo, X., & Huang, N. (2018). Effect of HMGN2 on proliferation and apoptosis of MCF-7 breast cancer cells. *Oncology Letters*, *17*(1), 1160–1166. https://doi.org/10.3892/ol.2018.9668

Friesner, R. A., Banks, J. L., Murphy, R. B., Halgren, T. A., Klicic, J. J., Mainz, D. T., Repasky, M. P., Knoll, E. H., Shelley, M., Perry, J. K., Shaw, D. E., Francis, P., & Shenkin, P. S. (2004). Glide: A new approach for rapid, accurate docking and scoring. 1. Method and assessment of docking accuracy. *Journal of Medicinal Chemistry*, *47*(7), 1739–1749. https://doi.org/10.1021/jm0306430

Gordon, M. S., Binkley, J. S., Pople, J. A., Pietro, W. J., & Hehre, W. J. (1982). Self-consistent molecular-orbital methods. 22. Small split valence basis sets for second-row elements. *Journal of the American Chemical Society*, *104*(10), 2797–2803. https://doi.org/10.1021/ja00374a017

Halgren, T. A., Murphy, R. B., Friesner, R. A., Beard, H. S., Frye, L. L., Pollard, W. T., & Banks, J. L. (2004). Glide: A new approach for rapid, accurate docking and scoring. 2. Enrichment factors in database screening. *Journal of Medicinal Chemistry*, *47*(7), 1750–1759. https://doi.org/10.1021/jm0306430

Hamel, E., & Lin, C. M. (1981). Glutamate-induced polymerization of tubulin: Characteristics of the reaction and application to the large scale purification of tubulin. *Archives of Biochemistry and Biophysics*, *209*(1), 29–40. https://doi.org/10.1016/0003-9861(81)90253-8

Hida, T., Kozaki, K., Ito, H., Miyaishi, O., Tatematsu, Y., Suzuki, T., Matsuo, K., Sugiura, T., Ogawa, M., Takahashi, T., & Takahashi, T. (2002). Significant growth inhibition of human lung cancer cells both *in vitro* and *in vivo* by the combined use of a selective cyclooxygenase 2 inhibitor, JTE-522, and conventional anticancer agents. *Clinical Cancer Research: An Official Journal of the American Association for Cancer Research*, *8*(7), 2443–2447.

Hida, T., Kozaki, K., Muramatsu, H., Masuda, A., Shimizu, S., Mitsudomi, T., Sugiura, T., Ogawa, M., & Takahashi, T. (2000). Cyclooxygenase 2 inhibitor induces apoptosis and enhances cytotoxicity of various anticancer agents in non small cell lung cancer cell lines. *Clinical Cancer Research: An Official Journal of the American Association for Cancer Research*, *6*(5), 2006–2011.

Jakalian, A., Jack, D. B., & Bayly, C. I. (2002). Fast, efficient generation of high-quality atomic charges. AM1-BCC model: II. Parameterization and validation. *Journal of Computational Chemistry*, *23*(16), 1623–1641. https://doi.org/10.1002/jcc.10128

Ji, Y., Yu, M., Qi, Z., Cui, D., Xin, G., Wang, B., Jia, W., & Chang, L. (2017). Study on apoptosis effect of human breast cancer cell MCF-7 induced by lycorine hydrochloride via death receptor pathway. *Saudi Pharmaceutical Journal: SPJ: The Official Publication of the Saudi Pharmaceutical Society*, *25*(4), 633–637. https://doi.org/10.1016/j.jsps.2017.04.036

Jordan, M. A., & Wilson, L. (2004). Microtubules as a target for anticancer drugs. *Nature Reviews Cancer*, *4*(4), 253–265. https://doi.org/10.1038/nrc1317

Jorgensen, W. L., Chandrasekhar, J., Madura, J. D., Impey, R. W., & Klein, M. L. (1983). Comparison of simple potential functions for simulating liquid water. *The Journal of Chemical Physics*, *79*(2), 926–935. https://doi.org/10.1063/1.445869

Kavanagh, J. J., & Kudelka, A. P. (1993). Systemic therapy for gynecologic cancer. *Current Opinion in Oncology*, *5*(5), 891–899. https://doi.org/10.1097/CAD.0000000000000057.

Kollman, P. A., Massova, I., Reyes, C., Kuhn, B., Huo, S., Chong, L., Lee, M., Lee, T., Duan, Y., Wang, W., Donini, O., Cieplak, P., Srinivasan, J., Case, D. A., & Cheatham, T. E. (2000). Calculating structures and free energies of complex molecules: Combining molecular mechanics and continuum models. *Accounts of Chemical Research*, *33*(12), 889–897. https://doi.org/10.1021/ar000033j

Lee, C., Yang, W., & Parr, R. G. (1988). Development of the Colle-Salvetti correlation-energy formula into a functional of the electron density. *Physical Review. B, Condensed Matter*, *37*(2), 785–789. https://doi.org/10.1103/physrevb.37.785

Mahaddalkar, T., Naik, P. K., Choudhary, S., Manchukonda, N., Kantevari, S., & Lopus, M. (2017). Structural investigations into the binding mode of a novel noscapine analogue, 9-(4-vinylphenyl) noscapine, with tubulin by biochemical analyses and molecular dynamic simulations. *Journal of Biomolecular Structure & Dynamics*, *35*(11), 2475–2484. https://doi.org/10.1080/07391102.2016.1222969

Maier, J. A., Martinez, C., Kasavajhala, K., Wickstrom, L., Hauser, K. E., & Simmerling, C. (2015). ff14SB: Improving the accuracy of protein side chain and backbone parameters from ff99SB. *Journal of Chemical Theory and Computation*, *11*(8), 3696–3713. https://doi.org/10.1021/acs.jctc.5b00255

Manchukonda, N. K., Naik, P. K., Sridhar, B., & Kantevari, S. (2014). Synthesis and biological evaluation of novel biaryl type α-noscapine congeners. *Bioorganic & Medicinal Chemistry Letters*, *24*(24), 5752–5575. https://doi.org/10.1016/j.bmcl.2014.10.046

Manchukonda, N. K., Naik, P. K., Santoshi, S., Lopus, M., Joseph, S., Sridhar, B., & Kantevari, S. (2013). Rational design, synthesis, and biological evaluation of third generation α-noscapine analogues as potent tubulin binding anti-cancer agents . *PLoS One*, *8*(10), e77970. https://doi.org/10.1371/journal.pone.0077970

Massova, I., & Kollman, P. A. (2000). Combined molecular mechanical and continuum solvent approach (MM-PBSA/GBSA) to predict ligand binding. *Perspectives in Drug Discovery and Design*, *18*(1), 113–135. https://doi.org/10.1023/A:1008763014207

Naik, P. K., Chatterji, B. P., Vangapandu, S. N., Aneja, R., Chandra, R., Kanteveri, S., & Joshi, H. C. (2011). Rational design, synthesis and biological evaluations of amino-noscapine: A high affinity tubulin-binding noscapinoid. *Journal of Computer-Aided Molecular Design*, *25*(5), 443–454. https://doi.org/10.1007/s10822-001-9430-4

Naik, P. K., Lopus, M., Aneja, R., Vangapandu, S. N., & Joshi, H. C. (2012). *In Silico* inspired design and synthesis of a novel tubulin-binding anticancer drug: Folate conjugated noscapine (Targetin). *Journal of Computer-Aided Molecular Design*, *26*(2), 233–247. Epub PMID: 22170255. https://doi.org/10.1007/s10822-011-9508-z

Naik, P. K., Santoshi, S., Rai, A., & Joshi, H. C. (2011). Molecular modelling and competition binding study of Br-noscapine and colchicine provide insight into noscapinoid-tubulin binding site. *Journal of Molecular Graphics & Modelling*, *29*(7), 947–955. https://doi.org/10.1016/j.jmgm.2011.03.004

Nawrocki, S. T., Sweeney-Gotsch, B., Takamori, R., & McConkey, D. J. (2004). The proteasome inhibitor bortezomib enhances the activity of docetaxel in orthotopic human pancreatic tumor xenografts. *Molecular Cancer Therapeutics*, *3*(1), 59–70.

Panda, D., Chakrabarti, G., Hudson, J., Pigg, K., Miller, H. P., Wilson, L., & Himes, R. H. (2000). Suppression of microtubule dynamic instability and treadmilling by deuterium oxide. *Journal of Biochemistry*, *39*(17), 5075–5081. https://doi.org/10.1021/bi992217f

Pietro, W. J., Francl, M. M., Hehre, W. J., Defrees, D. J., Pople, J. A., & Binkley, J. S. (1982). Self-consistent molecular orbital methods. 24. Supplemented small split-valence basis sets for second-row elements. *Journal of the American Chemical Society*, *104*(19), 5039–5048. https://doi.org/10.1021/ja00383a007

PTRAJ and CPPTRAJ. (2013). Software for Processing and Analysis of Molecular Dynamics Trajectory Data. *Journal of Chemical Theory and Computation*, *9*(7), 3084–3095. https://doi.org/10.1021/ct400341p.

Rowinsky, E. K. (1997). The development and clinical utility of the taxane class of antimicrotubule chemotherapy agents. *Annual Review of Medicine*, *48*, 353–374. https://doi.org/10.1146/annurev.med.48.1.353

Rowinsky, E. K., & Donehower, R. C. (1991). The clinical pharmacology and use of antimicrotubule agents in cancer chemotherapeutics. *Pharmacology & Therapeutics*, *52*(1), 35–84. https://doi.org/10.1016/0163-7258(91)90086-2

Ryckaert, J. P., Ciccotti, G., & Berendsen, H. J. (1977). Numerical integration of the cartesian equations of motion of a system with constraints: Molecular dynamics of *n*-alkanes. *Journal of Computational Physics*, *23*(3), 327–341. https://doi.org/10.1016/0021-9991(77)90098-5

Santoshi, S., Manchukonda, N. K., Suri, C., Sharma, M., Sridhar, B., Joseph, S., Lopus, M., Kantevari, S., Baitharu, I., & Naik, P. K. (2015). Rational design of biaryl pharmacophore inserted noscapine derivatives as potent tubulin binding anticancer agents. *Journal of Computer-Aided Molecular Design*, *29*(3), 249–270. https://doi.org/10.1007/s10822-014-9820-5

Santoshi, S., & Naik, P. K. (2014). Molecular insight of isotypes specific β-tubulin interaction of tubulin heterodimer with noscapinoids. *Journal of Computer-Aided Molecular Design*, *28*(7), 751–763. https://doi.org/10.1007/s10822-014-9756-9

Santoshi, S., Naik, P. K., & Joshi, H. C. (2011). Rational design of novel anti-microtubule agent (9-azido-noscapine) from quantitative structure activity relationship (QSAR) evaluation of noscapinoids. *Journal of Biomolecular Screening*, *16*(9), 1047–1058. https://doi.org/10.1177/1087057111418654

Shaik, M. S., Chatterjee, A., Jackson, T., & Singh, M. (2006). Enhancement of antitumor activity of docetaxel by celecoxib in lung tumors. *International Journal of Cancer*, *118*(2), 396–404. https://doi.org/10.1002/ijc.21325

Sivakumaran, N., Samarakoon, S. R., Adhikari, A., Ediriweera, M. K., Tennekoon, K. H., Malavige, N., Thabrew, I., & Shrestha, R. L. S. (2018). Cytotoxic and Apoptotic effects of Govaniadine isolated from *Corydalis govaniana* Wall. Roots on Human Breast Cancer (MCF-7) Cells. *BioMed Research International*, *2018*, 3171348. https://doi.org/10.1155/2018/3171348

Snyder, J. P., Nettles, J. H., Cornett, B., Downing, K. H., & Nogales, E. (2001). The binding conformation of Taxol in beta-tubulin: a model based on electron crystallographic density. *Proceedings of the National Academy of Sciences of the United States of America*, *98*(9), 5312–5316. https://doi.org/10.1073/pnas.051309398

Suri, C., Hendrickson, T. W., Joshi, H. C., & Naik, P. K. (2014). Molecular insight into γ-γ tubulin lateral interactions within the γ-tubulin ring complex (γ-TuRC). *Journal of Computer-Aided Molecular Design*, *28*(9), 961–972. https://doi.org/10.1007/s10822-014-9779-2

Suri, C., Joshi, H. C., & Naik, P. K. (2015). Molecular modeling reveals binding interface of γ-tubulin with GCP4 and interactions with noscapinoids. *Proteins: Structure, Function and Bioinformatics*, *83*(5), 827–843. https://doi.org/10.1002/prot.24773

Sweeney, C. J., Mehrotra, S., Sadaria, M. R., Kumar, S., Shortle, N. H., Roman, Y., Sheridan, C., Campbell, R. A., Murry, D. J., Badve, S., & Nakshatri, H. (2005). The sesquiterpene lactone parthenolide in combination with docetaxel reduces metastasis and improves survival in a xenograft model of breast cancer. *Molecular Cancer Therapeutics*, *4*(6), 1004–1012. https://doi.org/10.1158/1535-7163.MCT-05-0030

Theiss, C., & Meller, K. (2000). Taxol impairs anterograde axonal transport of microinjected horseradish peroxidase in dorsal root ganglia neurons *in vitro*. *Cell and Tissue Research*, *299*(2), 213–224. https://doi.org/10.1007/s004410050019

Topp, K. S., Tanner, K. D., & Levine, J. D. (2000). Damage to the cytoskeleton of large diameter sensory neurons and myelinated axons in vincristine-induced painful peripheral neuropathy in the rat. *The Journal of Comparative Neurology*, *424*(4), 563–576. https://doi.org/10.1002/1096-9861(20000904)424:4<563::AID-CNE1>3.0.CO;2-U

Wang, J., Wang, W., Kollman, P. A., & Case, D. A. (2006). Automatic atom type and bond type perception in molecular mechanical calculations. *Journal of Molecular Graphics & Modelling*, *25*(2), 247–260. https://doi.org/10.1016/j.jmgm.2005.12.005

Ye, K., Ke, Y., Keshava, N., Shanks, J., Kapp, J. A., Tekmal, R. R., Petros, J., & Joshi, H. C. (1998). Opium alkaloid noscapine is an antitumor agent that arrests metaphase and induces apoptosis in dividing cells. *Proceedings of the National Academy of Sciences of the United States of America*, *95*(4), 1601–1606. https://doi.org/10.1073/pnas.95.4.1601

Zhou, J., Gupta, K., Aggarwal, S., Aneja, R., Chandra, R., Panda, D., & Joshi, H. C. (2003). Brominated derivatives of noscapine are potent microtubule-interfering agents that perturb mitosis and inhibit cell proliferation. *Molecular Pharmacology*, *63*(4), 799–807. https://doi.org/10.1124/mol.63.4.799

Zhou, J., Liu, M., Luthra, R., Jones, J., Aneja, R., Chandra, R., Tekmal, R. R., & Joshi, H. C. (2005). EM012, a microtubule-interfering agent, inhibits the progression of multi drug-resistant human ovarian cancer both in cultured cells and in athymic nude mice. *Cancer Chemotherapy and Pharmacology*, *55*(5), 461–465. https://doi.org/10.1016/j.ejca.2010.02.017

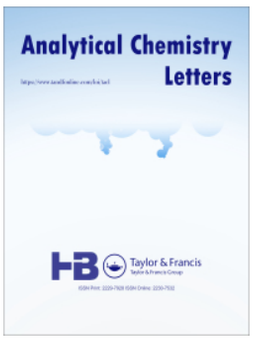

Analytical Chemistry Letters

ISSN: (Print) (Online) Journal homepage: https://www.tandfonline.com/loi/tacl20

Combination Regimen of Amino-Noscapine and Docetaxel for Evaluation of Anticancer Activity

Shruti Gamya Dash, Srinivas Kantevari & Pradeep Kumar Naik

To cite this article: Shruti Gamya Dash, Srinivas Kantevari & Pradeep Kumar Naik (2021) Combination Regimen of Amino-Noscapine and Docetaxel for Evaluation of Anticancer Activity, Analytical Chemistry Letters, 11:2, 215-229, DOI: 10.1080/22297928.2021.1896380

To link to this article: https://doi.org/10.1080/22297928.2021.1896380

Analytical Chemistry Letters

https://www.tandfonline.com/loi/tacl

Taylor & Francis
Taylor & Francis Group

ISSN: 2229-7928 (Print); ISSN: 2230-7532 (Online)

Article

Combination Regimen of Amino-Noscapine and Docetaxel for Evaluation of Anticancer Activity

Shruti Gamya Dash [1], Srinivas Kantevari [2] and Pradeep Kumar Naik [1]*

[1] Centre of Excellence in Natural Products and Therapeutics, Department of Biotechnology and Bioinformatics, Sambalpur University, Jyoti Vihar, Burla, Sambalpur-768 019, Odisha, India

[2] Fluoro and Agrochemicals Division, CSIR-Indian Institute of Chemical Technology, Hyderabad 500 007, India

Corresponding Author: pknaik1973@gmail.com (Pradeep Kumar Naik)

Received 19 January 2021; Received in revised form 23 February 2021; Accepted 25 February 2021

Abstract: Docetaxel (DOX) is one of the clinically used chemotherapeutic agents for the treatment of breast cancer, instead of its severe side effects. Noscapine, an antitussive opium alkaloid, on the other hand, has shown antitumor activity against a number of cancers without any significant side effects. Since both the compounds targeted tubulin, it is interesting to see the combined effect of both the compounds for the management of breast cancer. The binding energy of -3.49 and -4.18 kcal/mol respectively was noted by the molecular docking of amino-noscapine and DOX on the microtubule. In contrast, the binding energy was improved significantly (-6.27 kcal/mol) when the DOX was docked to the co-complex of amino-noscapine and tubulin, indicating the combined effect of both the ligands. The cell killing potential represented in terms of IC_{50} value was 38.07 μM and 28.4 μM for a treatment duration of 48 h and 72 h for amino-noscapine. Parenthetically the IC_{50} value was 0.61 μM and 0.08 μM for DOX respectively for the treatment duration of 48 h and 72 h. The cytotoxic effect of DOX was reduced significantly (to 0.05 μM) in combined treatment with amino-noscapine (20 μM). Apropos to the cytotoxic effect, both the compounds induced apoptosis to cancer cell by interfering with the cell cycle progression. Again, the induction of apoptosis was more effective in the combined treatment of both the compounds. This investigation offers a promising concept for the combination of DOX and amino-noscapine treatment to improve effectiveness in the treatment of breast cancer.

Keywords: Anti-tumor activity, Amino-Noscapine, MCF-7, Molecular Docking, Tubulin binding affinity, Alkaloids, Cancer therapy.

Introduction

Microtubule-interfering drugs like taxol derivatives and vinca alkaloids are effective chemotherapy agents for a variety of human cancers. However, these drugs are plagued by severe toxicity to patients [1-6]. More importantly, the patients have shown resistance to taxol derivatives. The success of taxol in the management of aggressive breast and ovarian cancers is a chance to identify other compounds that target microtubules but are less toxic, soluble in aqueous solutions and substantially effective both in single as well as in combination with currently available drugs such as docetaxel (low doses). Noscapine, a safe anti-tussive agent,

DOI: 10.1080/22297928.2021.1896380

is an excellent choice of treatment to use, which is not detrimental to healthy cells [7-8]. Joshi *et al.* have recently conducted multiple experiments to determine the mode of action of noscapine. [7-10].

It is a novel selective tubulin-binding anticancer drug that does not alter tubulin's organization (monomer/polymer ratio) across a wide range of concentrations [7,12]. This is a unique advantage over currently available antimicrotubule drugs that either inhibit the disassembly of the microtubule (taxanes, epothilone) or inhibit the assembly of tubulin (vincas, eribulin, estramustine) and therefore do not trigger any hemo and neuronal toxicity. In addition, the derivatives of noscapine inhibit cell proliferation and cause G2/M arrest in different human cancer cells followed by apoptotic cell death [13-19]. We have demonstrated that these compounds bind with a better binding affinity to tubulin. While several synthesized derivatives of noscapine showed promising *in vitro* activity against tumor cell lines, it would be unable to achieve complete elimination of the disease despite increased dosages. Over the course of this decade, it has become well understood that more toxic drugs are not necessarily better at their maximum tolerated dose (MTD) and that there is an opportunity to reduce their dose levels through the use of combination drug regimens that demonstrate synergistic interactions [20].

Different groups of compounds that include a ring structure and a nitrogen atom are alkaloids. The chemical structure of these alkaloids and their biosynthetic precursors is of significant concern. Due to their various significant biological activity and medicinal applications, alkaloids have been thoroughly researched. As an example, ephedrine was tested for antiasthmatic activity, morphine was tested for analgesic action and vinblastine was tested for its anticancer activity [21-23]. The widely used insole alkaloids include serotonin and other associated compounds. It is anticipated that about 2000 compounds are being classified as indole alkaloids. However, alkaloids are the most bioactive compounds in natural herbs. Some alkaloids were already used as chemotherapeutic agents viz. camptothecin (CPT), a common inhibitor of topoisomerase I (Topo I) [24] and vinblastine, a tubulin-binding agent. Vinblastine, strychnine, ajmaline, vincamine, vincristine and ajmalicine are among the most researched participants because of their pharmacological activities [25].

The existence of several drug binding sites on tubulin suggests that the rational combination of two or more drugs may increase the effectiveness of anticancer activity and reduce toxic side effects. The combination of docetaxel and other agents has earlier shown to increase the anticancer efficacy with lung cancer [26-30] and breast cancer [31]. In the current study, we approach to evaluate the anticancer activity with combination regimens of amino-noscapine and Docetaxel for the management of breast cancer.

Material and methods

Chemistry

The amino-noscapine was synthesized from the lead molecule, noscapine as per the method described earlier [32,33]. First of all, bromo-noscapine was synthesized from the noscapine by adding hydrobromic acid (~40 ml) and bromine water (~250 ml). The bromo-noscapine was converted to azido-noscapine in presence of sodium azide (40.63 mmol) and sodium iodide (4.063 mmol). Finally, amino-noscapine was synthesized from azido-noscapine by adding a solution of $SnCl_2$ in THF (10 ml), thiophenol and triphenylamine. The detailed of the synthetic scheme was mentioned below. The amino-noscapine was structurally elucidated based on ^{1}H NMR (300 MHz), ^{13}C NMR (75 MHz), HRMS, etc. as reported previously [34] and the final product as supporting information.

Molecular modelling

Protein preparation

The crystal structure of tubulin-amino noscapine (PDB ID: 6Y6D, resolution 2.20 Å) [35] was used for molecular docking of amino-noscapine and DOX. To prepare the protein structure, the protein preparation wizard (Schrödinger) was used and Macromodel (Schrödinger) was used for energy minimization [36]. For energy minimization, the OPLS 2005 force field with the Polak-Ribiere Conjugate Gradient (PRCG) algorithm with 1000 steps and an energy gradient of 0.001 kcal/mol was used.

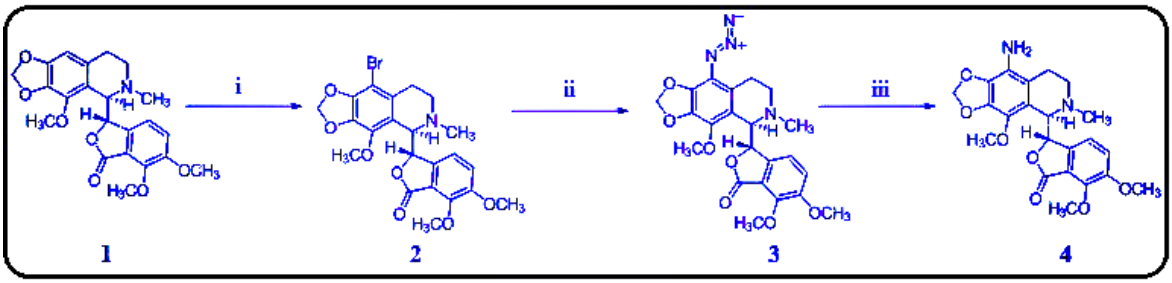

Scheme 1. Synthesis of 9-amino-noscapine. (i) HBr/Br_2-H_2O at 25°C/h, (ii) NaN_3/NaI in DMF at 80°C/15h, (iii) $SnCl_2$/PhSH/Et_3N in THF at 25°C/2h

Ligand preparation

The amino-noscapine and DOX molecular framework were developed using the maestro molecular builder (version 17.4, Schrodinger). Using Macromodel (version 17.4, Schrodinger) and OPLS 2005 force field, the constructed structures were energy minimized. A PRCG algorithm with 1000 steps and an energy gradient of 0.001 was used for energy minimization. Using Ligprep, a suitable bond order was allocated to each ligand. In addition, the ligands were DFT optimized using Jaguar (version 17.4, Schrödinger, LLC) applying Becke's three-parameter exchange potential and the Lee-Yang-Parr correlation functional (B3LYP) [37-38] with base set 3-21G* [39-41].

Molecular docking

Using Glide-XP (Extra Precision) (Schrödinger) [42], both amino-noscapine and DOX were docked to αβ-tubulin heterodimer at their respective binding cavities. The recorded noscapinoid [35] and DOX binding pockets [13] were established using a concentrated grid box at the center of the binding site using the Glide grid-receptor generation software. In order to contain the center mass of the docked ligand, a bounding box of size 14Å x 14Å x 14Å was specified. Also, specified larger enclosing box of size 20Å x 20Å x 20Å that occupied all the docked pose atoms. Using Glide-XP on the respective binding sites, both Amino-noscapine and DOX were docked. The DOX was docked onto the amino-noscapine and tubulin complex and the Amino-noscapine was docked onto the DOX and tubulin complex. The binding of ligands was evaluated using a parameter of the Glide XP score. For the ligand docking method, the scale factor of 0.4 for van der Waals radii was implemented to protein atoms with exact partial charges less than or equal to 0.25. Out of the 10000 poses sampled, 1000 were extracted by minimization (conjugate gradients) and favorable Glide docking performance was further evaluated by 30 structures with the lowest energy conformation.

Biology

Cell culture and reagents

Noscapine and docetaxel were obtained from Sigma. All the chemical reagents and media used for cell culture were obtained from Mediatech, Cellgro. The human breast cancer cell line, MCF7 was obtained from the cell repository of the National Center for Cell Science Pune, Maharashtra, India. The cells were grown in a 5% CO_2 and 95% humidity in Dulbecco's modified Eagle medium (DMEM, Pan Biotech) at a favorable temperature of 37°C, supplemented with 10 % fetal bovine serum (FBS) and antibiotics. For bioassays using trypsin-EDTA (0.25%), having a confluence with 70-80 % cells were subcultured.

In vitro cell proliferation MTT assay

The human breast cancer cell lines MCF-7 (3×10^3 cells per well) were seeded into 96-well plates. After incubation for 24 h (when cells reached 70-80% confluency), the medium was aspirated and the cells were treated with several concentrations of amino-noscapine alone (10, 25, 50, 100 µM), DOX alone (0.001, 0.01, 0.1,1,10 µM) and in combination of amino-noscapine and DOX (10 µM amino-noscapine+0.001 µM DOX, 15 µM amino-noscapine +0.01 µM DOX, 20 µM amino-noscapine +0.05 µM DOX, 25 µM amino-noscapine +0.1 µM DOX, 30 µM amino-noscapine +0.5 µM DOX). After 24h incubation,

10 µL of MTT (1 mg/mL) solution was added and the plates were incubated for an additional 4 h at 37°C and the absorbance was measured in a plate reader (Varioskan, Thermo Scientific) at 570 nm. The value of IC_{50} (the concentration of the drugs required to prevent cell proliferation by 50 %) of amino-noscapine alone, DOX alone and in the combination regimen of amino-noscapine + DOX was determined. The experiments were repeated in triplicates.

Cell cycle analysis

In Dulbecco's Modification of Eagle's Medium (DMEM), MCF7 cells were cultivated with 4.5 g/l glucose and L-glutamine, supplemented by 10 % bovine fetal serum and 1 % penicillin/ streptomycin. The MCF7 cells (1 X 10^5) were seeded with 35 mm plates. Cells were treated with amino-noscapine alone (25 µm), DOX alone (0.5 µm) or in combination with amino-noscapine and DOX (25 µm amino-noscapine+0.05 µm DOX) at 37°C temperatures and 5 % CO_2 after 24 hours. Cells were sampled after 24 h of treatment, followed by analysis using flow cytometry. The cells were briefly centrifuged, two times washed with ice-cold phosphate-buffered saline (PBS) and fixed with 70 % ethanol. The tubes containing the cell pellets have been deposited for 24 h at -20°C. Thereafter, the cells were centrifuged at 1000 x g for 10 minutes, and the supernatant was removed. The pellet was resuspended in 30 µl of phosphate/ citrate buffer (0.2 M Na_2HPO_4/0.1 M citric acid, pH 7.5) at room temperature for 30 min. Cells were then washed with 5 ml of PBS and incubated with 0.5 ml of propidium iodide (5 µg/ml in 0.1 % Triton-X in PBS) and 5 µg/ml of RNase A for 45 minutes in dark.

Apoptosis assay

Choline phospholipids such as phosphatidylcholine and sphingomyelin (PS) are exposed to the external leaflet during apoptosis, whereas amino-phospholipids (phosphatidylserine, phosphatidylethanolamine) are positioned exclusively on the lipid bilayer's cytoplasmic surface. The identification of PS by the fluorochrome-tagged 36 KDa anticoagulant protein Annexin V permits apoptotic incidence to be reliably calculated. Only in the presence of mM concentrations of divalent calcium ions, this probe reversibly binds to phosphatidylserine residues. Apoptosis in cancer cells has been identified by Annexin-V-FITC detection kit (Sigma-Aldrich, USA) based on the instruction provided by the manufacture.

In short, $5x10^4$ cells per well were seeded on a 35 mm plate and incubated for 24 h with a complete medium. After 24 hours, cells were treated with amino-noscapine alone (25 µm), DOX alone (0.5 µm) or in the combination regimen of amino-noscapine and DOX (25 µm amino-noscapine+0.5 µm DOX) at a temperature of 37°C and 5% CO_2. Cells were trypsinized and stained with surface marker antibodies (biotin-conjugated Annexin V, FITC conjugated streptavidin) and propiumdium iodide (PI). Cells were allowed to suspend in 1X binding buffer and incubated with Annexin-V-FITC conjugate for 20 minutes in dark conditions at room temperature. Flow cytometer data with 488 nm excitation for PI and emission at 530 nm were collected. Viable cells (Annexin V- / PI-), early apoptotic cells (Annexin V+ / PI-), late apoptotic/necrotic cells (Annexin V+ / PI+) and late necrotic cells (Annexin V- / PI+) were identified and determined their percentage, assessed using BD FACS Calibur (San Jose, CA, USA).

Tubulin purification

Microtubules were isolated and purified from the goat brain through alternative cycles of GTP-dependent polymerization and depolymerization in PEM buffer (50 mM pipes, 3 mM $MgSO_4$, 1 mM EGTA, pH 6.8) [43,44]. The purified microtubules were preserved at -80°C. The purified tubulin was estimated using the Bradford method as well as by SDS PAGE [45].

Tryptophan quenching assay

Tubulin (2 µM) was incubated in a water bath with amino-noscapine at a concentration of (20 µM), DOX (0.5 µM) and in combination regimen (DOX 0.05 µM+ amino-noscapine 25 µM) in PEM buffer (50 mM pipes, 3 mM $MgSO_4$, 1 mM EGTA, PH 6.8) for 45 minutes at 35°C. The samples were excited at 295 nm and emission was measured at 310-400 nm. For the spectrofluoro-

metric titrations, a FlouroMax® 4 spectrofluorometer (Horiba Scientifc, Edison, NJ) assisted by Fluor Essence 3.5 software was used. The experiments were repeated twice.

ANS (8-Anilino-1-naphthalene sulfonic acid)-binding assay

ANS binding assay was performed to verify the structural integrity of the tubulin in presence of amino-noscapine and DOX in a single as well as in combination regimen. Tubulin (2 μM) was incubated with two concentrations of amino-noscapine (25 μM and 50 μM), DOX (0.5 μM) and in combination regimen (DOX 0.05 μM+ amino-noscapine 25 μM, DOX 0.05 μM+ amino-noscapine 50 μM) at 35ºC for 30 min in PEM buffer. ANS (50 μM) was added and the samples were incubated in dark at 25ºC for 15 minutes. The samples were excited at 350 nm and the emission was measured at 410-470 nm using a Flourolog 3 spectrofluorometer (Horiba Scientific, Edition, NJ) assisted by fluorescence 3.5 software. The assays were repeated two times.

Results and discussion

Molecular modelling

It was reported that both noscapinoid and docetaxel bind to tubulin at a different binding site. Noscapinoids bind at the α- and β-tubulin interfaces [46, 47], while docetaxel binding was biased towards β-tubulin [48] (Figure 1). The difference in the mode of interactions of amino-noscapine and DOX with the residues of tubulin was also investigated in protein-ligand interaction profiler (PLIP), which is an automated detection and visualization tool of non-covalent protein-ligand interaction patterns from 3D structures. Results for each binding site were provided as 3D interaction diagrams for manual inspection (with PyMOL). The differences in amino acids for binding of amino-noscapine with tubulin independently and in combination with DOX (Figure 2) were mainly because of the change in conformation of tubulin due to binding of DOX. This clearly explains the changes in the binding mode of amino-noscapine and DOX when both the ligands were docked together with the tubulin

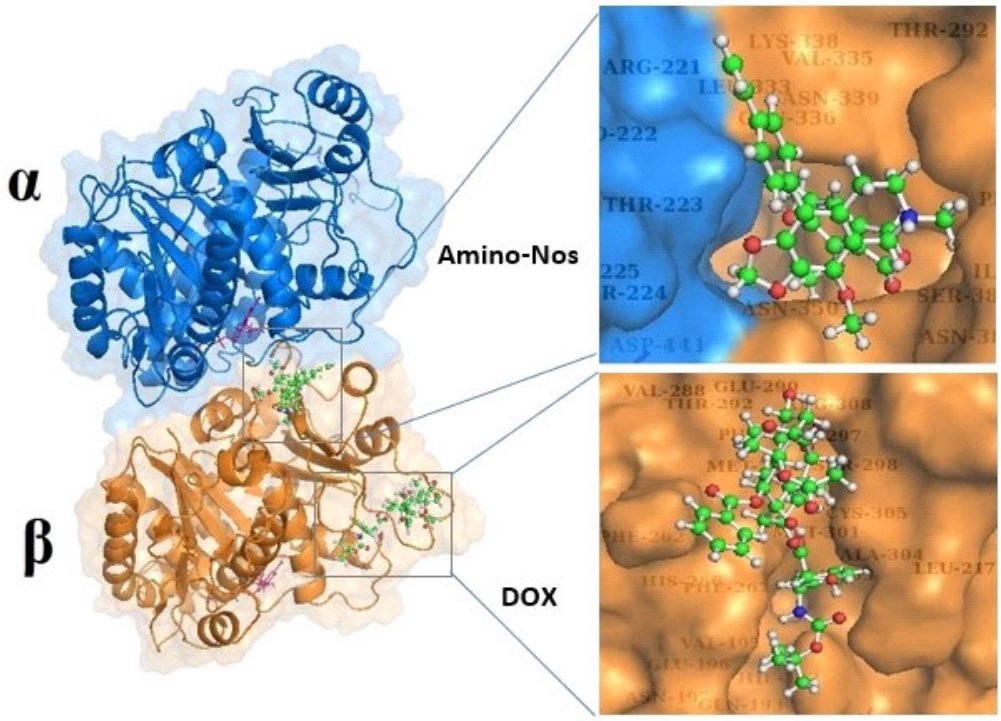

Figure 1. Both amino-noscapine and Docetaxel are well accomodated inside their respective tubulin binding site. (b) Snapshot of both the ligands obtained. The binding site is represented as macromodel surface according to α- and β-tubulin (α-tubulin is represented in green colour and β-tubulin is represented in brown colour)

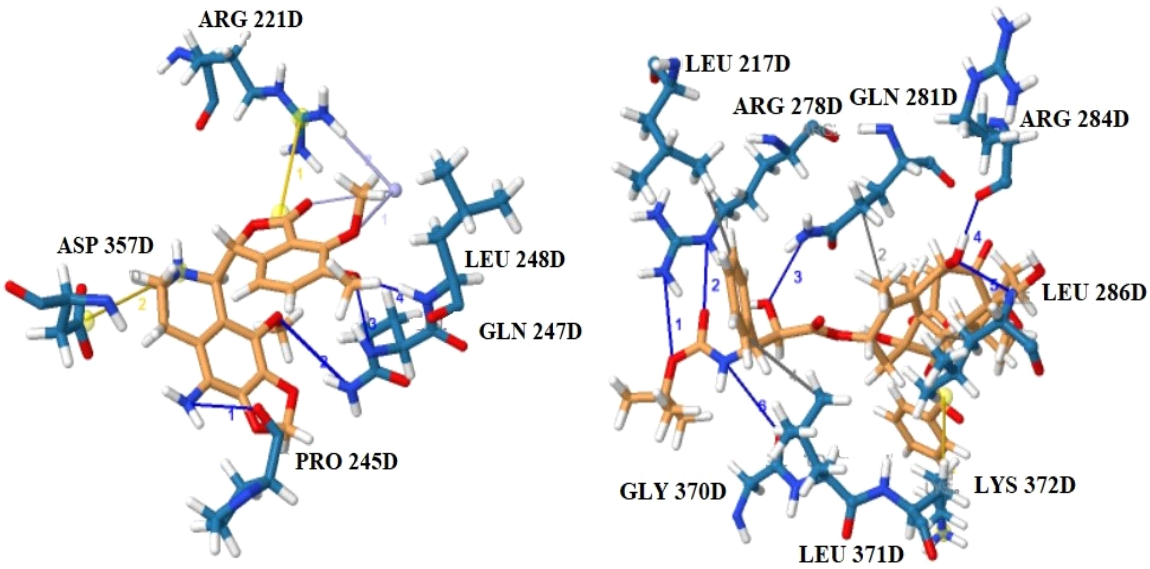

Figure 2. 3D ligplot representing the mechanism in which (a) Docetaxel and (b) Amino-noscapine interact with the binding sites of the amino acid. The protein-ligand interaction profiler (PLIP) was used to analyze the docked complex of DOX and Amino-noscapine with tubulin. In the figure, the hydrogen bonds involved in the binding of ligands are represented

Table 1. Molecular docking results (Glide XP_{score}) and the relevant energy parameters of amino-noscapine and docetaxel in single as well as in combination with tubulin

Ligands	Glide XPscore	Glide lipo	Glide Hbond	Glide Ecoul	Glide Evdw	Glide Emodel	Glide Energy
Amino-noscapine	-3.49	-1.56	-0.62	-31.16	-5.97	-42.37	-37.13
Docetaxel	-4.18	-0.99	-0.47	-28.17	-8.93	-44.44	-37.65
Amino-noscapine+Docetaxel	-6.27	-1.72	-0.01	-43.27	-6.46	-54.22	-49.97

so there is a chance of synergistic effect [48].

Towards determination of binding affinity of both the ligands in single as well as in combination, we have docked them at their respective binding pocket on tubulin in two cycles of molecular docking. It was found that both amino-noscapine and DOX docked well into their binding site with a binding score of -3.494 kcal/mol and -4.18 kcal/mol respectively (Table 1). The DOX-tubulin complex was taken in the second cycle and the amino-noscapine was docked onto the noscapinoid binding site. The presence of DOX on its binding site interferes with the binding of amino-noscapine with a reduced docking score of -6.27 kcal/mol. It is maybe because of the alteration of the secondary conformation of tubulin due to the binding of DOX [49].

Biology

In vitro cell proliferation MTT assay

The MTT assay was used to determine the effect of amino-noscapine and docetaxel individually and in their combination on cell viability. Amino-noscapine showed a dose-dependant cytotoxicity effect after 24 h in MCF-7 cell line. The antiproliferative activity increases with the increasing concentration of amino-noscapine and DOX in single as well as in combination. The percentage of cell survivability was reduced to ~50 % at 38.7 µM and 28.4 µM respectively at 48 h and 72 h of treatment with amino-noscapine (Figure 3a). In contrast, the DOX significantly revealed the dose-dependant cytotoxicity value of 0.61 µM and 0.08 µM respectively at 48 h and 72 h (Figure 3b). Further, the combination dose of amino-noscapine

(20 µM) and DOX (0.05 µM) revealed a reduction in ~50 % cell survival at 48 h and 72 h of treatment. The decrease in the concentration of DOX in combination with amino-noscapine in comparison to single regimen treatment revealed a chance of combined effect of both the drugs (Figure 3c).

Cell cycle analysis

The effect of amino-noscapine and DOX on the cell at the required concentration on the cell cycle profile of MCF-7 was evaluated by the induction of cell death using fluorescently labeled DNA deposition as a promising predictor of cell cycle

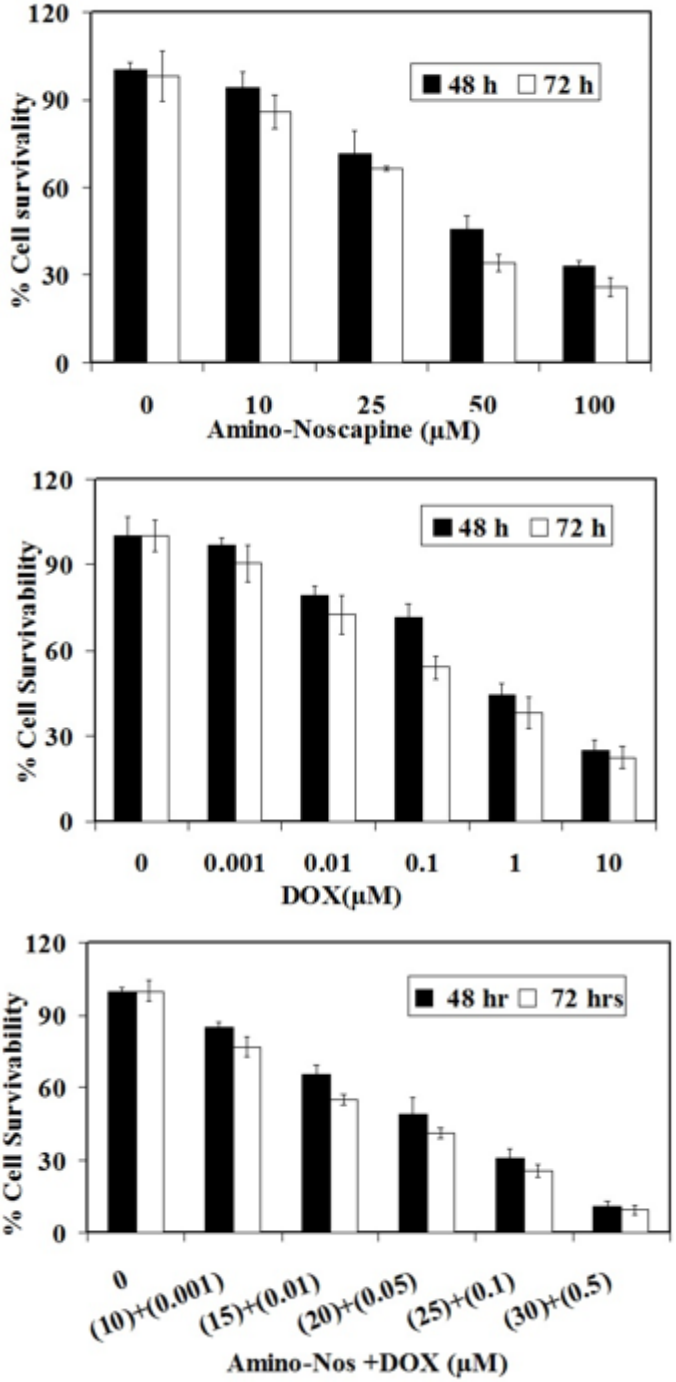

Figure 3. Reduction in percentage of cell survivability with the treatment of Amino-noscapine and Docetaxel in single as well as in combination regimen for MCF-7 cancer cell

progression and cell death. The un-replicated pattern of 2N DNA following characteristics of the G1 phase, while the duplicated 4N DNA cells describe the G2 and M phases. (Figure 4). During DNA duplication among peaks of 2N and 4N, the cells exhibit the S stage when DNA is synthesized. Less than 2N DNA appears in population groups of dying cells which deteriorate their DNA to varying degrees.

Treatment of MCF-7 cells with 25 µM treated test compounds for 24 h resulted in massive disruptions of the cell cycle profile. High cell aggregation during the G2/M transition phase at 24 h of treatment compared to untreated cells was observed in the FACS analysis (Table 2). The sub-G1 population with the treatment of amino-noscapine was increased to 9.62 %, whereas with DOX it was increased to 15.4 % and in combination, it further increased to 32.6 % in comparison to control.

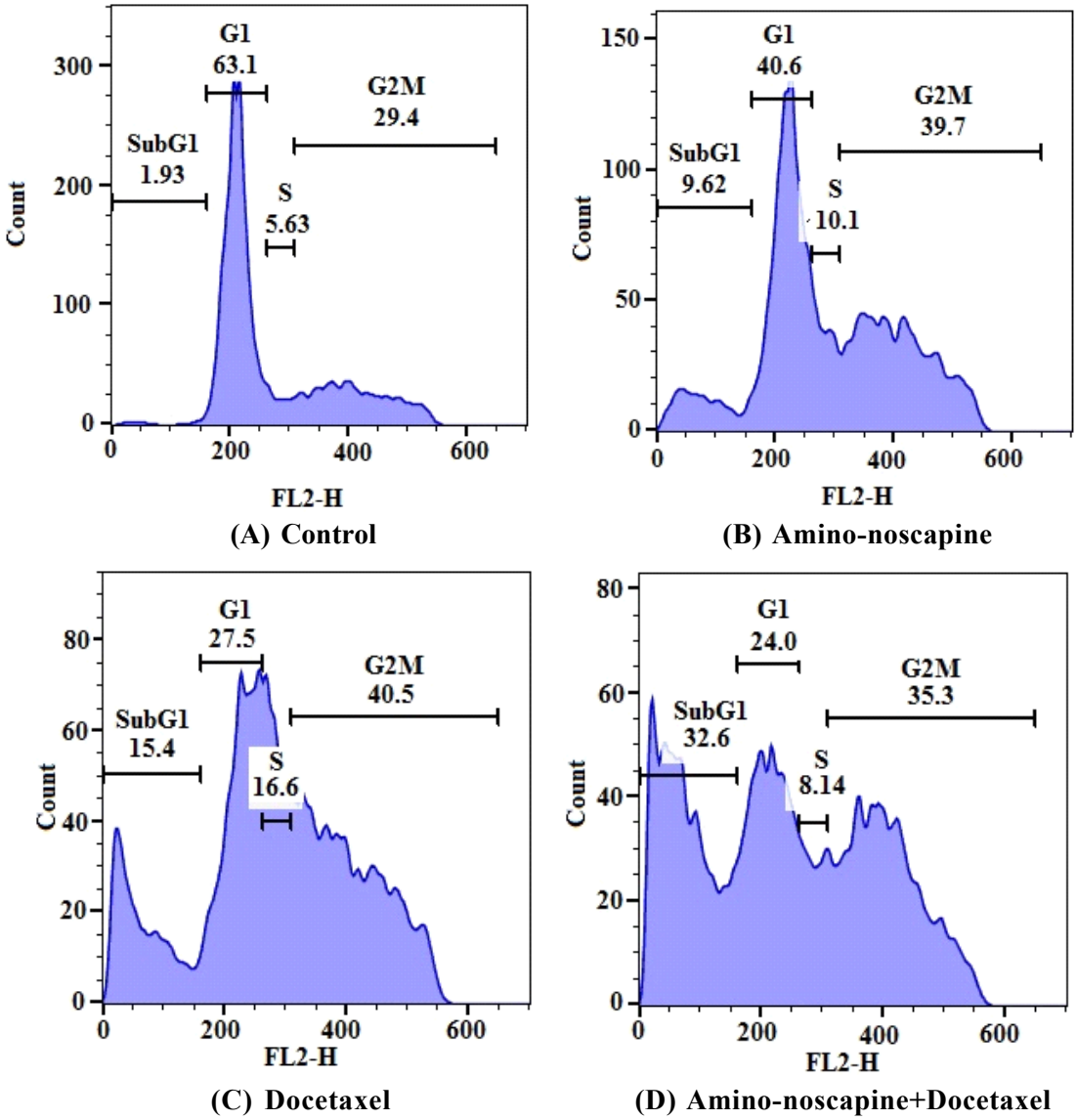

Figure 4. Amino-noscapine and docetaxel suppress the progression of the cell cycle at mitosis, indicated by characteristic hypodiploid (sub-G1) DNA peak, indicative of apoptosis. Figure A-D demonstrates the two-dimensional cell cycle distribution analysis as assessed by flow cytometry in MCF-7 cells treated with 25 µM of amino-noscapine, 0.5 µM of docetaxel single regimen, and 25 µM of amino-noscapine + 0.05 µM of docetaxel single regimen combination regimen.

Table 2. Effect of amino-noscapine (25 μM), docetaxel (0.5 μm) and their combination regimen (25 μm amino-noscapine + 0.05 μm docetaxel) on cell cycle progression of MCF-7 cells for 24 hours

	24 hr			
	Sub-G1	G_0/G_1	S	G_2/M
Control	1.93	63.1	5.63	29.4
Amino-noscapine (25 μm)	9.62	40.6	10.1	39.7
Docetaxel (0.5μm)	15.4	27.5	16.6	40.5
Amino-noscapine (25 μm) + Docetaxel (0.05 μm)	32.6	24.0	8.14	35.3

Apoptosis assay

The apoptotic phase is characterized by alterations in the lipid composition of the cell membrane, *i.e.*, phosphatidylserine, usually translocated to the outer leaflet on the inner leaflet of the cell membrane, which can be determined by using fluorescent binding Annexin V. In contrast, the cell impairment DNA-binding fluorescent dye *i.e.,* propidium iodide can only enter the cells at the stage of late apoptosis when membrane permeability is compromised. Apoptotic cells can be quantified by FACS analysis. There were very few apoptotic cells (~2 %) in the untreated cell cultures, which were assigned as the background cell death. MCF7 cells treated with amino-noscapine for 24 hours showed both early and late apoptosis (4.12 % and 2.42 %) respectively. In comparison, DOX demonstrates early and late apoptosis activation, 10.9 % and 3.80 % after 24 hours respectively. The combination treatment of DOX (0.05) and amino-noscapine (20) showed an increased rate of early and late apoptosis (15.1 % and 11.9 %) post 24 hours treatment (Figure 5).

Tryptophan quenching assay

The innate ability of proteins is to display the intrinsic fluorescence, which has provided a way to understand the environmental changes after interaction with the quencher. Tubulin is auto-fluorescence due to the presence of tryptophan amino acid. Tryptophan (Trp), tyrosine (Tyr) and phenylalanine (Phe) are the three natural amino acids that are fluorescent, but Trp does have the highest fluorescence quantum yield [50]. Thus, any alteration in its conformation with ligand binding decreases emission fluorescence - a tool used to recognize a ligand binding. The dynamic reduced fluorescence intensity in presence of increasing concentration of amino-noscapine and DOX in single as well as in combination, indicate the binding of both the compounds with tubulin. The relative percentage of decrease in fluorescence intensity was 28.87 % in presence of 20 μM amino-noscapine, 25.31 % in presence of 0.5 μM of DOX and 64 % in combination of DOX (0.05 μM) and amino-noscapine (25 μM) (Figure 6).

ANS-binding assay (8-anilino-1-naphthalene-sulfonic acid)

The impact of amino-noscapine (25 and 50 μM) and DOX on tubulin conformation changes using ANS binding assay, a fluorescent probe that binds to the protein's hydrophobic patches. Treatment of tubulin with amino-noscapine (25 and 50 μM) showed an increase in tubulin-ANS fluorescence intensity in a way dependent on the concentration (Figure 7). It showed 45 % and 62.4 % increase in fluorescence intensity at 25 and 50 μM of amino-noscapine, whereas 55.39 % in presence of DOX (0.5 μM) in comparison to unbound tubulin. Similarly, the tubulin-ANS fluorescence intensity was increased to 79 % in combination treatment of DOX (0.5 μM) and amino-noscapine (25 μM) as well as 88 % in combination of amino-noscapine (50 μM) and DOX (0.5 μM). The relative increase in tubulin-ANS fluorescence intensity in combination treatment of amino-noscapine and DOX compared to a single regimen indicate the synergistic effect in the binding of both the compounds onto their respective binding sites.

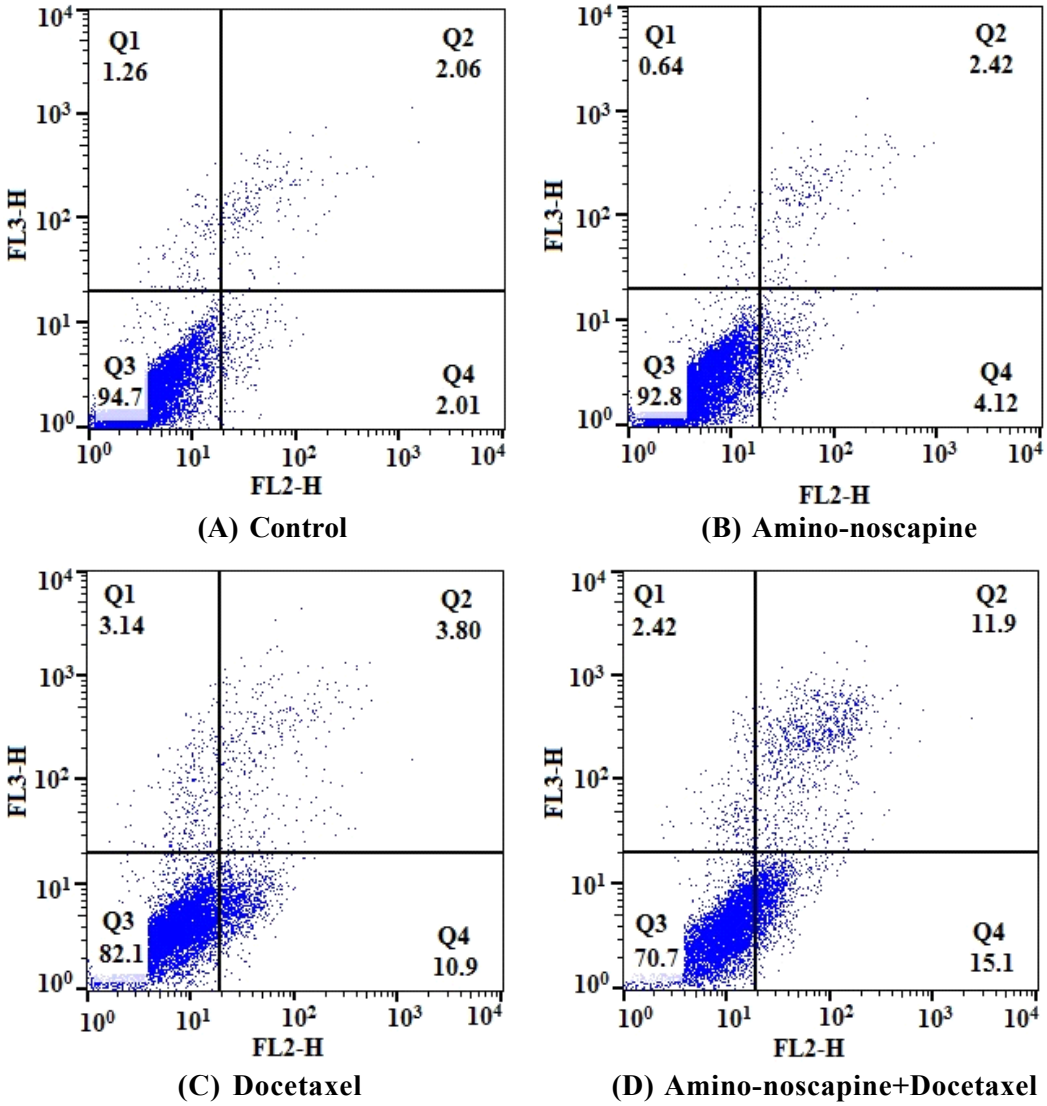

Figure 5. Analysis of apoptosis cell death induced by Amino-noscapine alone and in combination with Docetaxel based on flow cytometric analysis. In combination with 7-Amino-Actinomycin (7-AAD), Annexin V PE conjugate was used to distinguish the difference between 3 subpopulations: PE-and 7-AAD-the population indicates viable cells (lower left quadrant); PE-and 7-AAD+the population indicates early apoptotic cells (lower right quadrant); PE+ and 7-AAD+the population indicates late apoptotic cells (lower right quadrant) (top right quadrant).

Conclusion

We conclude that both amino-noscapine and docetaxel bind tubulin, alter the conformation of tubulin and inhibit the cell cycle at G2/M stage leading to induction of apoptosis. Regardless of its impressive anticancer bustle, docetaxel has a comparatively squat therapeutic index and its clinical significance is limited due to acute and chronic toxicities such as dose cumulative cardio-toxicity, myelosuppression, and immuno-suppression. Consequently, the dose-dosage regimen can be decreased in combination with other chemotherapeutic agents. However, the binding affinity of amino-noscapine increased to many folds in presence of docetaxel on its binding site, indicating the combined effect of both the molecules. Further, the antiproliferative and apoptosis activity increased significantly when both amino-noscapine and docetaxel were treated in combination compared to their single regimen

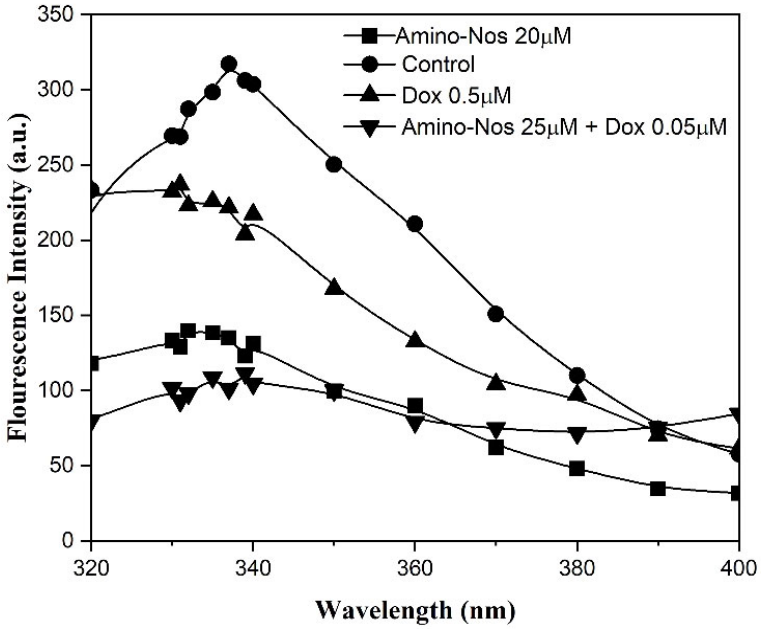

Figure 6. Interactions of amino-noscapine with tubulin alone and in combination with DOX showing concentration-dependent quenching of the intrinsic tubulin fluorescence emission intensity

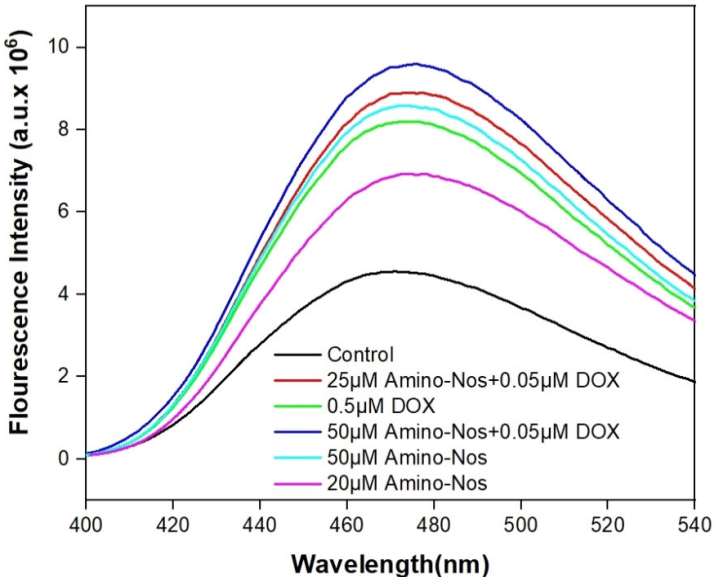

Figure 7. Interactions of the amino-noscapine with tubulin alone and in combination with DOX shown by concentration-dependent elevation of tubulin-ANS fluorescence

treatment. All these results taken together established a proof-of-concept that a rational combination of amino-noscapine and docetaxel could generate synergistic effects on cancer treatment, which is a highly promising and novel approach for the treatment of breast cancer.

Acknowledgments

The financial support by OHEPEE, Govt. of Odisha through World Bank is highly acknowledged. We would like to acknowledge the financial assistance provided by the Department of Science and Technology, Govt. of India (Award no: DST/INSPIRE/Code No.: IF170022) for providing a student research fellowship to Shruti Gamya Dash. We are grateful to Dr. Manu Lopus and UM-DAE Centre for Excellence in Basic Sciences for providing extended facilities.

References

1. **Rowinsky, E.K. (1997).** The development and clinical utility of the taxane class of antimicrotubule chemotherapy agents. Annual Review of Medicine. 48: 353-374.
2. **Rowinsky, E.K. and Donehower, R.C. (1991).** The clinical pharmacology and use of anti-microtubule agents in cancer chemotherapeutics. Pharmacology and Therapeutics. 52: 35-84.
3. **Kavanagh, J.J. and Kudelka, A.P. (1993).** Systemic therapy for gynecologic cancer. Current Opinion in Oncology**.** 5: 891-899.
4. **Zhou, J., Liu, M., Luthra, R., Jones, J., Aneja, R., Chandra, R., Tekmal, R.R. and Joshi, H.C. (2005).** EM012, a microtubule-interfering agent, inhibits the progression of multi drug-resistant human ovarian cancer both in cultured cells and in athymic nude mice. Cancer Chemo-therapy and Pharmacology. 55: 461-465.
5. **Theiss, C. and Meller, K. (2000).** Taxol impairs anterograde axonal transport of microinjected horseradish peroxidase in dorsal root ganglia neurons *in vitro*. Cell and Tissue Research. 299: 213-224.
6. **Topp, K.S., Tanner, K.D. and Levine, J.D. (2000).** Damage to the cytoskeleton of large diameter sensory neurons and myelinated axons in vincristine-induced painful peripheral neuropathy in the rat. Journal of Comparative Neurology. 424: 563-576.
7. **Ye, K., Ke, Y., Keshava, N., Shanks, J., Kapp, J.A., Tekmal, R.R., Petros, J. and Joshi, H.C. (1998).** Opium alkaloid noscapine is an antitumor agent that arrests metaphase and induces apoptosis in dividing cells. Proceedings of the National Academy of Sciences of the United States of America. 95: 1601-1606.
8. **Zhou, J., Liu, M., Aneja, R., Chandra, R., Lage, H. and Joshi, H.C. (2006).** Reversal of P glycoprotein mediated multidrug resistance in cancer cells by the c-jun NH2-terrminal kinase. Cancer Research. 66: 445-452.
9. **Joshi, H.C. and Zohu, J. (2000).** Noscapine and Analogues as Potential Chemotherapeutic Agents. Drug News and Perspectives. 13: 543-546.
10. **Y, Ke., K, Ye., Grossniklaus, H.E., Archer, D.R., Joshi, H.C. and Kapp, J.A. (2000).** Noscapine inhibits tumor growth with little toxicity to normal tissues or inhibition of immune responses. Cancer Immunology, Immunotherapy. 49: 217-225.
11. **Landen, J.W., Lang, R., McMahon, S.J., Rusan, N.M., Yvon, A.M., Adams, A.W., Sorcinelli, M.D., Campbell, R., Bonaccorsi, P., Ansel, J.C., Archer, D.R., Wadsworth, P., Armstrong, C.A. and Joshi, H.C. (2002).** Noscapine alters microtubule dynamics in living cells and inhibits the progression of Melanoma. Cancer Research. 62: 4109-4114.
12. **Zhou, J., Gupta, K., Aggarwal, S., Aneja, R., Chandra, R., Panda, D. and Joshi, H.C. (2003).** Brominated derivatives of noscapine are potent microtubule-interfering agents that perturb mitosis and inhibit cell proliferation. Molecular Pharmaceutics. 63: 799-807.
13. **Naik, P.K., Santoshi, S., Rai, A. and Joshi, H.C. (2011).** Molecular modelling and competition binding study of Br-noscapine and colchicine provide insight into noscapinoid-tubulin binding site. Journal of Molecular Graphics and Modelling. 29: 947-955.
14. **Santoshi, S., Naik, P.K. and Joshi, H.C. (2011).** Rational design of novel anti-microtubule agent (9-azido-noscapine) from quantitative structure activity relationship (QSAR) evaluation of noscapinoids. Journal of Biomolecular Screening. 16(9): 1047-1058.
15. **Mahaddalkar, T., Naik, P.K., Choudhary, S., Manchukonda, N., Kantevari, S. and Lopus, M. (2017).** Structural investigations into the binding mode of a novel noscapine analogue, 9-(4-vinylphenyl) noscapine, with tubulin by biochemical analyses and molecular dynamic simulations. Journal of Biomolecular Structure and Dynamics. 35(11): 2475-2484.
16. **Santoshi, S., Manchukonda, N.K., Suri, C., Sridhar, B., Joseph, S., Lopus, M., Kantevari, S., Baitharu, I. and Naik, P.K. (2015).** Rational design of biaryl pharmacophore inserted

noscapine derivatives as potent tubulin binding anticancer agents. Journal of Computer Aided Molecular Design. 29: 249-270.

17. **Manchukonda, N.K., Naik, P.K., Sridhar, B. and Kantevari, S. (2014).** Synthesis and biological evaluation of novel biaryl type ±-noscapine congeners. Bioorganic and Medicinal Chemistry Letters. 24(24): 5752-575.
18. **Manchukonda, N.K., Naik, P.K., Santoshi, S., Lopus, M., Joseph, S., Sridhar, B. and Kantevari, S. (2013).** Rational design, synthesis and biological evaluation of third generation α-noscapine analogues as potent tubulin binding anti-cancer agents. PLoS One. 8(10): e77970.
19. **Naik, P.K., Lopus, M., Aneja, R., Vangapandu, S.N. and Joshi, H.C. (2012).** *In Silico* inspired design and synthesis of a novel tubulin-binding anti-cancer drug: folate conjugated noscapine (Targetin). Journal of Computer Aided Molecular Design. 26(2): 233-247.
20. **Jordan, M.A., and Wilson, L. (2004).** Microtubules as a target for anticancer drugs. Nature Reviews Cancer. 4(4): 253-265.
21. **Lee, M.R. (2011).** The history of Ephedra (ma-huang). Journal of the Royal College of Physicians of Edinburgh. 41(1): 78-84.
22. **Benyhe, S. (1994).** Morphine: new aspects in the study of an ancient compound. Life Sciences. 55(13): 969–979.
23. **Weihong, Li., Shao, Y., Lihong, Hu., Zhang, Xiongwen., Chen, Yi., Tong, Li., Li, Chuan., Shen, Xu. and Ding, Ji. (2007).** BM6, a new semi-synthetic Vinca alkaloid, exhibits its potent *in vivo* anti-tumor activities via its high binding affinity for tubulin and improved pharmacokinetic profiles. Cancer Biology and Therapy. 6(5): 787-794.
24. **Huang, M., Gao, H., Chen, Y., Zhu, H., Cai, Y., Zhang, X., Miao, Z., Jiang, H., Zhang, J., Shen, H., Lin, L., Lu, W. and Ding, J. (2007).** Chimmitecan, a novel 9-substituted camptothecin, with improved anticancer pharmacologic profiles *in vitro* and *in vivo*. Clinical Cancer Research. 13(4): 1298-1307.
25. **Thawabteh, A., Juma, S., Bader, M., Karaman, D., Scrano, L., Bufo, A.S. and Karaman, R. (2019).** The Biological Activity of Natural Alkaloids against Herbivores, Cancerous Cells and Pathogens. Toxins. 11(656).
26. **Hida, T., Kozaki, K., Ito, H., Miyaishi, O., Tatematsu, Y., Suzuki, T., Matsuo, K., Sugiura, T., Ogawa, M., Takahashi, T. and Takahashi, T. (2002).** Significant growth inhibition of human lung cancer cells both *in vitro* and *in vivo* by the combined use of a selective cyclooxygenase 2 inhibitor, JTE-522, and conventional anticancer agents. Clinical Cancer Research. 8(7): 2443-2447.
27. **Hida, T., Kozaki, K., Muramatsu, H., Masuda, A., Shimizu, S., Mitsudomi, T., Sugiura, T., Ogawa, M. and Takahashi, T. (2000).** Cyclooxygenase 2 inhibitor induces apoptosis and enhances cytotoxicity of various anticancer agents in non-small cell lung cancer cell lines. Clinical Cancer Research. 6(5): 2006-2011.
28. **Nawrocki, S.T., Sweeney-Gotsch, B., Takamori, R. and McConkey, D.J. (2004).** The proteasome inhibitor bortezomib enhances the activity of docetaxel in orthotopic human pancreatic tumor xenografts. Molecular Cancer Therapeutics. 3: 59-70.
29. **Shaik, M.S., Chatterjee, A., Jackson, T. and Singh, M. (2006).** Enhancement of antitumor activity of docetaxel by celecoxib in lung tumors. International Journal of Cancer. 118: 396-404.
30. **Sweeney, C.J., Mehrotra, S., Sadaria, M.R., Kumar, S., Shortle, N.H., Roman, Y., Sheridan, C., Campbell, R.A., Murry, D.J., Badve, S. and Nakshatri, H. (2005).** The sesquiterpene lactone parthenolide in combination with docetaxel reduces metastasis and improves survival in a xenograft model of breast cancer. Molecular Cancer Therapeutics. 4(6): 1004-1012.
31. **Chougule, M., Patel, A.R., Sachdeva, P., Jackson, T. and Singh, M. (2011).** Anticancer activity of Noscapine, an opioid alkaloid in combination with Cisplatin in human non-small cell lung

cancer. Lung Cancer. 71(3): 271-282.

32. **Naik, P.K., Chatterji, B.P., Vangapandu, S.N., Aneja, R., Chandra, R., Kanteveri, S. and Joshi, H.C. (2011).** Rational design, synthesis and biological evaluations of amino-noscapine: a high affinity tubulin-binding noscapinoid. Journal of Computer Aided Molecular Design. 25(5): 443-54.
33. **Joshi, H.C., Aneja, R. and Vangapandu, S.N. (2014).** Noscapine analogs and their use in treating cancers (Patent No. 8889705). Emory University Link: https://www.freepatentsonline.com/8889705.html.
34. **Manchukonda, N.K., Sridhar, B., Naik, P.K., Joshi, H.C. and Kantevari, S. (2012).** Copper(I) mediated facile synthesis of potent tubulin polymerization inhibitor, 9-amino-±-noscapine from natural ±-noscapine. Bioorganic & Medicinal Chemistry Letters. 22(8): 2983-2987.
35. **Oliva, M.A., Prota, A.E., Rodriguez-Salarichs, J., Bennani, Y.L., Jimenez-barbero, J., Bargsten, K., Canales, A., Steinmetz, M.O. and Diaz, J.F. (2020).** Structural basis of noscapine activation for tubulin binding. Journal of Medicinal Chemistry. 63: 8495-8501.
36. **Santoshi, S. and Naik, P.K. (2014).** Molecular insight of isotypes specific ²-tubulin interaction of tubulin heterodimer with noscapinoids. Journal of Computer-Aided Molecular Design. 28: 751-763.
37. **Lee, C., Yang, W. and Parr, R.G. (1988).** Development of the Colle-Salvetti correlation-energy formula into a functional of the electron density. Physical Review B: Condensed Matter and Materials. 3: 785-789.
38. **Becke, A.D. (1993).** A new mixing of Hartree-Fock and local density-functional theories. Journal of Chemical Physics. 98: 1372-1377.
39. **Binkley, J.S., Pople, J.A. and Hehre, W.J. (1980).** Self-consistent molecular orbital methods. 21. Small split-valence basis sets for first-row elements. Journal of the American Chemical Society. 102: 939-947.
40. **Gordon, M.S., Binkley, J.S., Pople, J.A., Pietro, W.J. and Hehre, W.J. (1982).** Self-consistent molecular-orbital methods. 22. Small split valence basis sets for second-row elements. Journal of the American Chemical Society. 104: 2797-2803.
41. **Pietro, W.J., Francl, M.M., Hehre, W.J., Defrees, D.J., Pople, J.A. and Binkley, J.S. (1982).** Self-consistent molecular orbital methods. 24. Supplemented small split-valence basis sets for second-row elements. Journal of the American Chemical Society. 104: 5039-5048.
42. **Snyder, J.P., Nettles, J.H., Cornett, B., Downing, K.H. and Nogales, E. (2001).** The binding conformation of Taxol in tubulin: A model based on electron crystallographic density. Proceedings of the National Academy of Sciences of the United States of America. 98(9): 5312-5316.
43. **Hamel, E. and Lin, C.M. (1981).** Glutamate-induced polymerization of tubulin: characteristics of the reaction and application to the large-scale purification of tubulin. Archives of Biochemistry and Biophysics. 209: 29-40.
44. **Panda, D., Chakrabarti, G., Hudson, J., Pigg, K., Miller, H.P., Wilson, L. and Himes, R.H. (2000).** Suppression of microtubule dynamic instability and treadmilling by deuterium oxide. Journal of Biochemistry. 39: 5075-5081.
45. **Bradford, M.M (1976).** A rapid and sensitive method for the quantitation of microgram quantities of protein utilizing the principle of protein-dye binding. Analytical Biochemistry. 72: 248-254.
46. **Mishra, K.B., Mishra, R. C. and Tiwari, V. K. (2015).** First noscapine glycoconjugates inspired by click Chemistry. Royal Society of Chemistry Advances. 5: 51779-51789.
47. **Snyder, J.P., Nettles, J.H., Cornett, B., Downing, K.H. and Nogales, E. (2001).** The binding conformation of Taxol in tubulin: A model based on electron crystallographic density. Proceedings of the National Academy of Sciences of the United States of America. 98(9): 5312-

5316.

48. **Tomar, V., Kumar, N., Tomar, R., Sood, D., Dhiman, N., Dass, S.K., Prakash, S., Madan, J. and Chandra, R. (2019).** Biological Evaluation of Noscapine analogues as Potent and Microtubule-Targeted Anticancer Agents. Scientific Reports. 9(19542).
49. **Dash, S.G., Suri, C., Nagireddy, P.K.R., Kantevari, S. and Naik, P.K. (2020).** Rational design of 9-vinyl-phenyl noscapine as potent tubulin binding anticancer agent and evaluation of the effects of its combination on Docetaxel. Journal of Biomolecular Structure and Dynamics. 1: 1-14. .
50. **Sood, D., Kumar, N., Rathee, G., Singh, A., Tomar, V. and Chandra, R. (2018).** Mechanistic Interaction Study of Bromo-Noscapine with Bovine Serum Albumin employing Spectroscopic and Chemoinformatics Approaches. Scientific Reports. 8(16964).

Article type : Research Article

Synergistic interaction of N-3-Br-Benzyl-noscapine and docetaxel abrogates oncogenic potential of breast cancer cells

Running title: Synergistic effect of N-3-Br-Benzyl-noscapine and docetaxel

Shruti Gamya Dash[1], Srinivas Kantevari[2], Swaroop Kumar Pandey[3,4] and Pradeep Kumar Naik[1*]

[1]Centre of Excellence in Natural Products and Therapeutics, Department of Biotechnology and Bioinformatics, Sambalpur University, Jyoti Vihar, Burla, Sambalpur-768 019, Odisha, India

[2]Fluoro and agrochemicals Division, CSIR-Indian Institute of Chemical Technology, Hyderabad 500 007, India

[3]Bencos Research Solutions, New Link Road, Andheri West, Mumbai-400053, Maharashtra, India.

[4]Present address: Department of Life Sciences and the National Institute for Biotechnology in the Negev, Ben-Gurion University of the Negev, Beer-Sheva, 84105, Israel.

***For correspondence:** Phone No.: +91-9479268802; E-mail: pknaik1973@gmail.com

ABSTRACT

Noscapine, an opium alkaloid was discovered to bind tubulin, arrest dividing cells at mitosis, and selectively induced apoptosis to cancer cells. One of its derivatives, N-3-Br-Benzyl-Noscapine (Br-Bn-Nos) was demonstrated to have improved anticancer potential compared to noscapine. We approached to evaluate the single and combined effect of Br-Bn-Nos and docetaxel (DOX) based on molecular modelling and cellular study. The individual predicted free energy of binding ($\Delta G_{bind,pred}$) for Br-Bn-Nos and DOX with tubulin was found to be -28.89 kcal/mol and -36.07 kcal/mol based on MM-GBSA as well as -26.21 kcal/mol and -34.65 kcal/mol based on MM-PBSA, respectively. However, the $\Delta G_{bind,pred}$ of Br-Bn-Nos was significantly reduced (-33.02 kcal/mol and -30.24 kcal/mol using MM-GBSA and MM-PBSA) in presence of DOX on its binding pocket. Parenthetically, the $\Delta G_{bind,pred}$ of DOX was significantly reduced (-37.17 kcal/mol

and -32.80 kcal/mol using MM-GBSA and MM-PBSA) in the presence of Br-Bn-Nos on its binding pocket. The reduced $\Delta G_{bind,pred}$ in presence of Br-Bn-Nos and DOX together indicated a combination effect of both the ligands. The combined interaction of both the agents onto tubulin dimmer was also determined experimentally using purified tubulin, in which a combination regimen of Br-Bn-Nos and DOX reduced the fluorescence intensity of tubulin to a higher value (68%) compared to the single regimen. Further, isobologram analysis revealed the synergistic effect of Br-Bn-Nos and DOX in anti-proliferative activity using MCF-7 cell line at 48 h (sum FIC = 0.49) and at 72 h (sum FIC = 0.62). The combination dose regimen of Br-Bn-Nos and DOX blocks the cell cycle progression at the G2/M phase and induced apoptosis to cancer cells more effectively compared to the single regimen. Taken together, our study provides compelling evidence that the anticancer potential of noscapine derivatives may be substantially improved when it is used in a combined application with DOX for breast cancer.

Keywords: N-3-Br benzyl Noscapine, Molecular Docking, Combination therapy, Docetaxel, Breast cancer, Isobologram

Introduction

Chemotherapeutics regimens currently available for breast cancer have been hindered by poor selectivity towards cancerous cells and hence, associated with severe toxicity (Pace et al. 1996; Rowinsky, 1997; Crown and O'Leary, 2000; Theiss and Meller, 2000; Topp et al. 2000). Over the past few decades, these inadequate scenarios have pushed extensive research on finding more specific and less toxic drugs for cancer. Noscapine, a safe anti-tussive agent, is an excellent choice for cancer treatment because of its mechanism of action, which is not detrimental to healthy cells (Ye et al. 1996; Zhou et al. 2006). It doesn't significantly alter tubulin's stable monomer/polymer ratio over a broad range of concentrations (Ye et al. 1996; Zhou et al. 2003). This is a distinct benefit over currently available antimicrotubule medications, which either prevent microtubule disassembly (taxanes, epothilone) or tubulin assembly (vincas, eribulin, estramustine) and thus do not cause hemo and neuronal toxicity due to its inherent mechanism of action. To optimize its anticancer activity, we strategically developed more effective derivatives by changing the scaffold structure for therapeutics applications. A battery of noscapinoids has already developed, some of which have shown impressive anticancer activity in comparison to noscapine (Naik et al. 2011; Naik et al. 2012; Manchukonda et al. 2013; Manchukonda et al. 2014; Santoshi et al. 2015; Mahaddalkar et al. 2017). However, complete remission of cancer cells was not achieved even at a higher concentration based on *in vivo* animal study (Zhou et al. 2003;

2006). Therefore, new treatment modalities such as combination therapy could be beneficial for breast cancer.

The combination therapy of anti-microtubule agents is an undiscovered source of chemotherapeutic resources. Presence of multiple drug binding sites on the tubulin, suggests that a reasonable combination of two or more drugs of this class may increase the efficacy of anticancer drugs and diminish toxic side effects, thereby improving the therapeutic index. In this study, we approach to evaluate the combined effect of N-3-Br-Benzyl-noscapine and docetaxel towards better anticancer activity. The drug combination significantly reduces the cancer cell growth (sum FIC <1), which shows the synergism between N-3-Br-Benzyl-noscapine and docetaxel in their anticancer activity.

Materials and methods

A. Molecular modeling evaluation of N-3-Br-Benzyl Noscapine as tubulin binding agent and having combination effect with docetaxel

(a) Ligand preparation

The molecular structure of Br-Bn-Nos and docetaxel (DOX) were built using maestro molecular builder (Schrodinger). The constructed structures were energy minimized using Macromodel (version 17.4, Schrodinger) and OPLS 2005 force field. A PRCG algorithm with 1000 steps and an energy gradient of 0.001 was used for energy minimization. Using Ligprep, a suitable bond order was allocated to each ligand. In addition, the ligands were DFT optimized using Jaguar (version 17.4, Schrödinger, LLC) applying Becke's three-parameter exchange potential and the Lee-Yang-Parr correlation functional (B3LYP) (Lee et al. 1988; Becke, 1993) with a basis set 3-21G*(Binkley et al. 1980; Gordon et al. 1982). The various conformations of the molecules were generated using Ligprep (Schrodinger).

(b) Protein preparation

The co-crystal structure of amino-noscapine and tubulin (PDB ID: 6Y6D, resolution 2.20 Å) (Oliva et al. 2020) was used for the molecular docking and predicting the binding affinity of Br-Bn-Nos and DOX. The hydrogen atoms were added and the protein structure was prepared based on the multistep procedure of the protein preparation wizard (Schrodinger). Briefly, it involves minimization of added hydrogen atoms and optimization of hydrogen bonding networks. Further, refinement of the structure was achieved by molecular dynamic simulation of 100 ns

using GROMACS 5.1.5 with similar parameters setting as reported earlier (Santoshi and Naik, 2014).

(c) Molecular docking

The various conformations of Br-Bn-Nos generated above were docked onto the noscapinoids binding site (Oliva et al. 2020) at the interface of αβ-tubulin heterodimer (PDB ID: 6Y6D) prepared above. The binding site was specified by creating two grid boxes around it. An inner grid box of size 14Å x 14Å x 14Å was defined at the centroid of the noscapinoids binding site by selecting the co-complex ligand, amino-noscapine using the Glide grid-receptor generation program. This box defines the search space in which the diameter midpoint of each docked ligand is required to be present. Further, an outer grid box was also defined with a size of ≤ 24 Å of the co-complexed ligand, amino noscapine. It defines the volume within which all ligand atoms of a valid pose must be located. Similarly, the various conformations of the DOX generated above were docked onto the paclitaxel binding site of tubulin reported earlier (Nogales et al. 1998; Synder et al.2000; Canales et al. 2011; Winefield et al.2008). We have used the published co-crystal structure of paclitaxel-tubulin (PDB ID: 1TUB) (Nogales et al. 1998) to extract the binding site amino acids and their coordinates and mapped onto the above prepared protein structure using SiteMap (Schrodinger software package) to define the taxotere binding site. Further, this binding site was specified in the docking of DOX by creating two grid boxes using the grid receptor generation program (Schrodinger software package). An inner grid box of size 14Å x 14Å x 14Å was created at the centroid of the taxotere binding site to define the search space in which the diameter midpoint of each docked ligand is required to be present. Further, an outer grid box with a size of 20Å x 20Å x 20Å was defined within which all ligand atoms of a valid pose must be located. For the molecule docking of Br-Bn-Nos and DOX onto their respective sites we have used Glide-XP algorithm (Halgren et al. 2004) using Schrodinger package and evaluated their binding poses using Glide XP_{Score} function (Friesner et al. 2004; Halgren et al. 2004). Three cycles of molecular docking were performed to elucidate their binding affinity in single as well as in their combination. In the first cycle, both the ligands were docked individually into their respective binding site. In the second cycle, to the co-complex of Br-Bn-Nos and tubulin, DOX was docked to determine the combined effect of DOX with Br-Bn-Nos. Similarly, in the third cycle, to the co-complex of DOX and tubulin, Br-Bn-Nos was docked to determine its combination effect with

docetaxel. For the ligand docking method, the scale factor of 0.4 for van der Waals radii was implemented to protein atoms with exact partial charges less than or equal to 0.25. Out of the 10000 poses sampled, 1000 were extracted by minimization (conjugate gradients) and favorable Glide docking performance was further evaluated by 30 structures with the lowest energy conformation. The single best conformation for each ligand was used for further analysis.

(d) Molecular dynamics simulation

The docked complex of (a) Br-Bn-Nos with tubulin, (b) DOX with tubulin, (c) both Br-Bn-Nos and DOX in combination with tubulin, and (d) the tubulin only was considered for the MD simulation using Amber 16 (Case et al. 2016). The parameters for both the ligands including DOX and Br-Bn-Nos along with GTP and GDP were calculated using Amber 16 software Antechamber system (Wang et al. 2006). All charges for atomic points were determined using the charging model AM1-BCC (Jakalian et al. 2002). In Amber16, topologies and internal coordinates were created for all complexes using tleap programme. Missing hydrogen was added, and Protein and Ligand parameters were assigned using FF14SB and GAFF force fields, respectively (Maier et al. 2015). TIP3P water model in a truncated octahedron at 12 Å distance between the protein atoms and the wall of the box (Jorgensen et al. 1983) was added with dissolved counter ions to neutralize the system. Once the topologies and internal coordinates for all complexes have been obtained, three rounds of minimization have been carried out for each complex in order to relax the system. Position constraints of 10 kcal/Å^2 and 2 kcal/Å^2 have been imposed on the protein system for the first and second rounds, respectively, to relax the water molecules around the protein. In the third round, no restrictions were imposed. After removal of bad contacts through minimization, all four molecular systems were balanced at 300 K and 1 atm at 500 ps. The balanced systems were then run at 100 ns each with a time step of 2 fs. The cut-off for non-bonded interaction was 10 Å during simulations, electrostatics was measured using Particle Mesh Ewald (PME) and bonds were restricted using shake algorithm (Ryckaert et al. 1977; Darden et al. 1993; Essmann et al. 1995). The simulation temperature was regulated with the Langevin thermostat. Coordinates for each molecular system were written every 20 ps.

(e) Predicted free energy of binding using MM-GBSA and MM-PBSA

The predicted free energy of binding ($\Delta G_{bind,pred}$) of Br-Bn-Nos and DOX in their single binding and in co-binding with tubulin was determined as the ensemble average of the binding free energy of a total of 250 snapshots from the last 5 ns of the MD simulation trajectory of their respective molecular systems. We have used molecular mechanics generalized Born solvation area

(MM-GBSA) and molecular mechanics Poisson Boltzmann solvation area (MM-PBSA) methods (Kollman et al. 2000; Massova and Kollman, 2000) to obtain $\Delta G_{bind,pred}$ as explained below:

$\Delta G_{bind,pred} = \Delta G_{complex} - [\Delta G_{Rec} + \Delta G_{lig}]$

$G = E_{gas} + G_{sol} - TS.$

$E_{gas} = E_{int} + E_{ele} + E_{vdw}$

$G_{sol} = G_{PB(GB)} + G_{sol-np}$

$G_{sol-np} = \gamma SAS$

Where, G is Gibbs free energy, E_{gas} is the gas phase energy calculated as the sum of internal energy (E_{int}), energy generated as a result of the electrostatic interaction (E_{ele}) and the van der Waals interaction (E_{vdw}). G_{sol} is the solvation free energy calculated as the sum of polar ($G_{PB(GB)}$) and nonpolar contributions (G_{sol-np}). Polar interaction contribution ($G_{PB(GB)}$) was calculated as the summation of electrostatic contribution (E_{ele}) and polar solvation contribution ($G_{PB(GB)}$). The nonpolar solvation contribution (G_{sol-np}) is approximated as linearly dependent on the solvent accessible surface area (SAS) and γ is the surface tension constant that was set to 0.0072 kcal mol^{-1} $Å^{-2}$ (Massova and Kollman, 2000).

B. Biology

(a) Cell lines and Chemicals

Noscapine and docetaxel were purchased from Sigma. The novel derivative of noscapine, Br-Bn-Nos was chemically synthesized by reaction scheme mentioned below (Manchukonda et al., 2013) and HPLC purified (purity > 96%). The human breast cancer cell line MCF-7 was acquired from the cell registry of the National Centre for Cell Science in Pune, Maharashtra, India. All the chemical reagents and media used for cell culture were obtained from Mediatech, Cellgro. The cells were grown in a 5% CO_2 and 95% humidity in Dulbecco's modified Eagle medium (DMEM, Pan Biotech) at a favorable temperature of 37 °C, supplemented with 10 % fetal bovine serum (FBS) and antibiotics. For bioassays using trypsin-EDTA (0.25%), having a confluence with 70-80 % cells were sub cultured. Cell at 70-80% confluence was sub-cultured using trypsin-EDTA (0.25%) for assays.

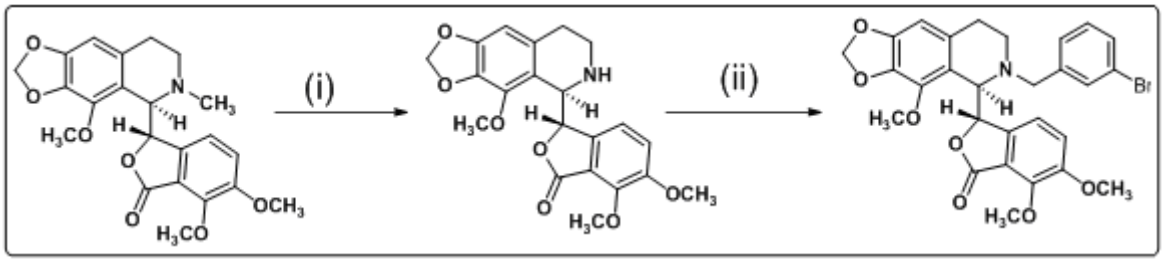

Reaction Scheme: Synthesis of N-3-Br benzyl noscapine: (i) a: *m*-CPBA, DCM; b: 2N HCl; C: $FeSO_4.7H_2O$; (ii) 3-Bromo benzyl bromide, KI, K_2CO_3, Acetone, RT, 97%.

(b) Cell viability assay

The cell proliferation analysis was conducted in 96-well plates using a human breast cancer cell line, MCF-7 at a density of 3 X 10^3 cells/well. The assay was performed with Br-Bn-Nos at variable concentrations of 5, 10, 25, and 50 µM. Similarly, the cells were incubated with DOX at a variable concentration of 0.001, 0.01, 0.1 and 1 µM. After 24 h and 48 h of treatment, the viability of the cell was checked by 3-(4, 5-dimethylthiazol-2-yl)-2, 5, ditetrazolium bromide (MTT) assay. The plate was read at a wavelength of 570 nm in a (Varioskan, Thermo Scientific) flash multimode reader. Fifty percent inhibitory concentration (IC_{50}) of tested drugs was obtained by transferring the data into a graphic program (e.g., Excel) and expressed as a percentage of the untreated controls and then evaluated by Logit regression analysis using a pre-programmed excel spreadsheet obtained from MMV group at Swiss Tropical Institute, Basel, Switzerland (Pandey et al. 2016).

(c) *In vitro* interaction of N-3-Br-Benzyl-noscapine and docetaxel

The cells were treated with a combination regimen of both Br-Bn-Nos and DOX by taking variable concentrations (50 µM Br-Bn-Nos+0.001µM DOX, 25 µM Br-Bn-Nos+0.01 µM DOX, 10 µM Br-Bn-Nos+0.1 µM DOX and 5 µM Br-Bn-Nos+1 µM DOX) directly onto the medium after 12h of cell attachment. The first and the last of these preparations had either Br-Bn-Nos or DOX alone. The cancer cells, MCF-7 at a density of 3 X 10^3 cells/well were exposed for 48 h and 72 h to these dilutions followed by MTT assay. The IC_{50} was determined by logit regression analysis. The fractional inhibitory concentration (FIC) was interpreted by the following formula:

$$FIC = \frac{Conc.of\ drug\ in\ combination\ to\ produce\ IC_{50}}{Conc.\ of\ drug\ alone\ require\ to\ produce\ IC_{50}}$$

The sum FIC value for each of the preparations determined by the following formula was used to classify the drug–drug interaction.

$$Sum\ FIC = \frac{IC_{50}\ of\ drug\ A\ in\ combination}{IC_{50}\ of\ drug\ A\ alone} + \frac{IC_{50}\ drug\ B\ in\ combination}{IC_{50}\ of\ drug\ B\ alone}$$

Sum FIC < 0.5 represents substantial synergism, sum FIC < 1 represents synergism, sum FIC = 1 represents additive interaction, sum FIC ≥ 1 represents antagonism. An Isobologram was plotted to show the drug interaction as per the method proposed earlier (Pandey et al. 2016).

(d) Cell cycle analysis

In Dulbecco's Modification of Eagle's Medium (DMEM), MCF7 cells were cultivated with 4.5 g/l glucose and L-glutamine, supplemented by 10% bovine fetal serum and 1% penicillin/streptomycin. MCF-7 cells ($1X10^5$) were seeded in a 6-well culture plate overnight and then treated with the indicated concentration of Br-Bn-Nos (20 μm) and DOX alone (0.1 μm) and combination regimen (25 μm Br-Bn-Nos+0.01 μm DOX). Staining solution RNase (5μg/ml), propidium iodide (5 μg/ml) and Triton X (0.1%) were used to determine the cell cycle phase and analyzed by flow cytometer (FACS Calibur) to estimate the percentage of cells in the different stages of the cell cycle. The experiment was performed in triplicates.

(e) Annexin V apoptosis assay

Choline phospholipids, like the phosphatidylcholine and sphingomyelin (PS), are subjected on the outer leaflet throughout apoptosis, whereas amino phospholipids (phosphatidylserine, phosphatidylethanolamine) are only found on the cytoplasmic edge of the lipid bilayer. Detection of PS by fluorochrome-tagged 36 KDa anticoagulant protein Annexin V allows for accurate estimation of apoptotic incidence. MCF-7 cells ($5 X 10^4$) were treated with Br-Bn-Nos (20 μm), DOX (0.1 μm) or in their combination regimen (25 μm Br-Bn-Nos+0.01 μm DOX) for apoptosis study using the Annexin V (BD Pharmingen, San Diego, CA, USA) binding assay according to the manufacturer's instructions. The cells were then analyzed using the BD FACS Calibur (San Jose, CA, USA).

(f) Tubulin purification

Two cycles of temperature- and GTP-dependent polymerization and depolymerization in the presence of 1 M glutamate were used to isolate microtubules from the goat brain (Hamel and Lin, 1981). Purified tubulin was extracted from the microtubule proteins by phosphocellulose chromatography based on the methods and procedures discussed earlier (Panda et al. 2000; Joshi and Zohu, 2001) and the amount of purified tubulin was estimated using the Bradford method as well as by SDS PAGE (Bradford, 1976). Aliquots were frozen in liquid nitrogen and preserved at -80 degrees Celsius until required.

(g) Tryptophan fluorescence quenching assay with purified tubulin

Tubulin (2 μM) was treated with desired concentrations of Br-Bn-Nos (20 μM and 50 μM), DOX (0.1 μM) and in combination regimen (DOX 0.01 μM+Br-Bn-Nos 25 μM) in a water bath (35 °C; 45 min). They were then excited at 295 nm and the emission reading at 310–400 nm was

obtained. A FlouroMax® 4 spectrofuorometer (Horiba Scientifc, Edison, NJ) supported by FluorEssence 3.5 software was used for the spectrofluorimetric titrations.

(h) ANS binding assay with purified tubulin

Fluorescence probe 8-anilino-1-napththalene sulfonate (ANS) is mostly used for the detection and analysis of conformational changes in proteins. Tubulin (2 μM) was incubated with 25 μM concentrations of Br-Bn-Nos, 0.1 μM concentration of DOX and in their combination regimen (DOX 0.01 μM+Br-Bn-Nos 25 μM) for 30 min at 35 °C in PEM buffer. ANS (50 μM) was then added to the samples and the samples were incubated in the dark (15 min; 25 °C). After the incubation, they were excited at 350 nm and the emission spectra were taken at 410–470 nm using a Flourolog 3 spectrofluorometer (Horiba Scientific, Edition, NJ) assisted by fluorescence 3.5 software. The assays were repeated two times.

Results

In a quest of increasing the anticancer activity of the noscapine, the –NCH3 group of isoquinoline ring has been substituted with various functional groups based on *in silico* combinatorial approach and screened out potent derivatives for chemical synthesis and experimental evaluation (Manchukonda et al. 2013). Many of these derivatives have shown anticancer activity at a lower concentration compared to noscapine. One of such derivative, N-3-Br-Benzyl noscapine has revealed higher tubulin binding affinity compared to noscapine (Manchukonda et al. 2013) and showed anti-proliferative activity using MDA-MB-231 breast cancer cell line (Cheriyamundath et al. 2019). This derivative of noscapine is different from the first generation noscapine derivatives (including 9-Br-noscapine) in which modification have been done at C-9 position of the isoquinoline ring (Figure 1A,B). Here in this study, we have used N-3-Br-Benzyl derivative of noscapine (Figure 1C) to evaluate its combined effect with docetaxel towards better therapeutic outcome by minimizing the concentration of docetaxel to preclude its side effect.

B. (a) Molecular modelling

In order to determine the predictive binding affinity of Br-Bn-Nos and DOX individually and in their combination, we have docked them at their respective binding pockets on tubulin in three cycles of molecular docking. In the first cycle, DOX and Br-Bn-Nos were docked into their respective binding pockets independently. Both Br-Bn-Nos and DOX docked well into their

binding site with a docking score of -4.99 and -5.88 kcal/mol respectively (Table 1). In the second cycle, the co-complex of tubulin-DOX was taken and Br-Bn-Nos was docked onto its binding site to determine the change in docking score in presence of DOX. The docking score of Br-Bn-Nos was reduced to -6.03 kcal/mol, indicating improvement in its binding affinity in presence of DOX. Similarly in the third cycle, DOX was docked into its binding site in the co-complex of tubulin-Br-Bn-Nos to determine its change in docking score in presence of Br-Bn-Nos. The presence of Br-Bn-Nos further reduced the docking score of DOX to -6.54 kcal/mol. The reduced docking score in presence of Br-Bn-Nos and DOX together indicated the combined effect of both the ligands.

Table 1: Molecular docking results (Glide XP_{score}) and the relevent energy parameters of Br-Bn-Nos and DOX in single as well as in combination with tubulin.

Ligands	Glide XP_{score} (kcal/mol)	Glide E_{vdw} (kcal/mol)	Glide E_{coul} (kcal/mol)	Glide Energy (kcal/mol)
Br-Bn-Nos	-4.99	-31.67	-8.29	-35.97
DOX	-5.88	-42.26	-11.96	-50.22
Br-Bn-Nos docked with Tubulin_DOX complex	-6.03	-39.07	-5.46	-52.53
DOX docked with Tubulin_ Br-Bn-Nos complex	-6.54	-41.24	-9.23	-59.24

(b) MD simulation of the complex

The binding of both Br-Bn-Nos and DOX with tubulin were evaluated independently (Tub-Br-Bn-Nos and Tub-DOX complexes) as well as in combination with tubulin (Tub-DOX+Br-Bn-Nos) by a molecular dynamic simulation of 100 ns. To analyse the system's stability, the root means square deviations (RMSD) of Cα-atoms were computed for all frames over the entire duration of simulation (Figure 2). The fluctuation in the RMSD of Cα carbon atoms was very small after equilibration and all of the systems were found to be stable after 20 ns of simulation. The root mean square fluctuations (RMSF) of Cα-atoms were also measured to see if there were any changes in residue flexibilities during the entire duration of MD simulation (Figure 3). The residues with higher RMSF tend to show more flexibility. Both Br-Bn-Nos and DOX were found to bind with tubulin during the entire duration of the simulation. However, the topmost five ligand-tubulin complexes based on the lowest total energy from the MD simulation trajectory were

obtained to generate the average structure in order to analyze the binding mode of ligands. Both Br-Bn-Nos and DOX were found to accommodate well inside the binding cavity. The Br-Bn-Nos docked well at the interface of α- and β- tubulin, whereas the binding of DOX is biased more towards β-tubulin (Figure 4a, b). Their binding mode with the tubulin was represented by ligplots in single as well as in combination (Figure 5a-d). The binding site amino acids involved in the binding of Br-Bn-Nos independently and in the presence of DOX were found albite different, which may be due to the change in conformation of tubulin in presence of DOX. None of the binding site amino acids were involved in hydrogen bonding with the Br-Bn-Nos when it was docked individually onto tubulin (Figure 5a). In contrast, the binding site amino acids Asp 357(D), Cys 356(D), Cys 241(D), and Gln 247(D) were involved in making 6 hydrogen bonding with Br-Bn-Nos in presence of DOX (Figure 5b). Parenthetically, the binding site amino acids Arg 278(D) and Arg 284(D) are involved in 2 hydrogen bonding with DOX when it was docked individually onto tubulin (Figure 5c). In contrast, the binding site amino acids Gly 370(D), Arg 278(D), Arg 284(D), and Gln 281(D) are involved in making 9 hydrogen bonds with DOX in presence of Br-Bn-Nos (Figure 5d).

(c) Calculated free energy of binding of Br-Bn-Nos and DOX with tubulin

The free energy of binding and its respective components of both Br-Bn-Nos and DOX with tubulin were calculated independently as well as in combination and presented in Table 2. The last 250 frames from the last 5 ns of trajectory were considered to calculate the ensemble average of the free energy of binding using both MM-GBSA and MM-PBSA methods. The free energy of binding for Br-Bn-Nos and DOX with tubulin was found to be -28.89 and -36.07 kcal/mol based on MM-GBSA as well as -26.21 and -34.65 kcal/mol based on MM-PBSA, respectively. Further, the free energy of binding of Br-Bn-Nos was reduced to -33.02 and -30.24 kcal/mol using MM-GBSA and MM-PBSA calculation when DOX was present on its binding pocket, indicating combination effect of both the ligands. Parenthetically, the free energy of binding of DOX was reduced to -37.17 and -32.80 kcal/mol using MM-GBSA and MM-PBSA, respectively when Br-Bn-Nos was present in binding tubulin. For all complexes, the binding energy was decomposed into its various energy components (the electrostatic, van der Waals, and solvation). Both van der Waals (ΔE_{VDW}) and the electrostatic component (ΔE_{ELE}) were observed to make very significant contributions to the free energy of binding. However, the net polar contribution ($\Delta G_{(ele,PB/GB)} = \Delta E_{ele} + \Delta G_{(PB/GB)}$) was rendered unfavorable due to very large penalty

imposed by the desolvation component ($\Delta G_{PB/GB}$) while the net nonpolar component (ΔE_{vdw}) and ($\Delta G_{sol\text{-}np}$) were observed to make a highly favourable contribution to the free energy of binding.

Table 2: Predicted free energy of binding ($\Delta G_{bind,pred}$) and its various componentes (kcal/mol) of Br-Bn-Nos and DOX in single as well as in combination binding with tubulin. The values in bold represent the ($\Delta G_{bind,pred}$ of molecules with tubulin based on MM-GBSA and MM-PBSA methods.

Energy Component	Br-Bn-Nos	Dox	Tub_DOX+ Br-Bn-Nos	Tub_Br-Bn-Nos+ DOX
ΔE_{VDW}	-31.61	-42.26	-41.24	-39.07
ΔE_{ELE}	-286.66	-21.21	-303.55	-30.00
ΔE_{GAS}	-333.46	-57.26	-348.88	-65.40
$\Delta G_{GB\text{-}Polar}$	308.85	39.70	307.49	32.98
$\Delta G_{SOL\text{-}NP}$	-3.62	-4.61	-3.69	-4.65
$\Delta G_{SOL\text{-}GB}$	279.35	29.19	323.90	31.03
$\Delta G_{bind\text{-}GBSA}$	**-28.89**	**-36.07**	**-33.02**	**-37.17**
ΔG_{PB}	323.16	30.62	335.94	36.69
$\Delta G_{SOL\text{-}NP}$	-3.54	-4.51	-3.36	-4.29
$\Delta G_{SOL\text{-}PB}$	279.22	29.61	320.48	33.69
$\Delta G_{bind\text{-}PBSA}$	**-26.21**	**-34.65**	**-30.24**	**-32.80**

B. Biology

(a) Inhibition of cellular proliferation

The Br-Bn-Nos inhibited proliferation of MCF-7 cells in a dose-dependent manner with IC_{50} values of 11.5 μM and 7.71 μM respectively at 48 h and 72 h (Figure 6a). Similarly, the DOX showed IC_{50} values of 0.39 μM and 0.016 μM against MCF-7 cells respectively at 48 h and 72 h (Figure 6b). In order to minimize the toxicity of DOX and to enhance the antiproliferative efficacy we have examined the antiproliferative activity with a combination of a lower concentration of DOX and a higher concentration of Br-Bn-Nos. Approximately, 50% inhibition of cellular proliferation was achieved in a combination regimen of Br-Bn-Nos (5 μM) and DOX (1μM) after 48 h and 72 h post-treatment (Figure 6c). Further, the interaction of both the agents has been analyzed on the basis of their sum FICs and isobologram plot (Figure 7). The sum FICs value was found to be 0.49 and 0.62 respectively at 48 h and 72 h. The isobologram of N-3-Br-Benzyl-

noscapine with docetaxel suggests that the combination has synergistic antiproliferative activity both at 48 h and 72 h exposure (sum FIC <1).

(b) Cell cycle effect

Both noscapinoids and docetaxel have been reported to bind tubulin and inhibit the cell cycle progression at G2/M phase, followed by induction of apoptosis to cancer cells (Ye et al. 1998; Dash et al. 2020). We examined the inhibition in cell cycle progression of MCF-7 cells with the treatment of Br-Bn-Nos and DOX in single as well as in combination regimens. The cells were treated with 20 μM of Br-Bn-Nos and 0.1 μM of DOX in the single regimen, whereas 25 μM Br-Bn-Nos+0.01 μM DOX for the combination regimen. The cell cycle distribution was evaluated via flow cytometric analysis. The presence of 2N DNA indicates that the cells are in the G1 phase, while the accumulation of duplicated 4N DNA indicates that the cells are in G2 and M phases. Accumulation of DNA in between 2N and 4N peaks represent, the cells are in the S phase. In contrast, less than 2N DNA indicates the apoptotic cells in which the DNA is degraded to different extents (sub-G1 phase). As shown in Figure 8, there is a high accumulation of cells in the G2/M phase. In contrast to the G2/M phase block, cells with sub-G1 phase were found to increase compared to the control after 48 h of treatment in single and in a combination regimen. The sub-G1 population with the treatment of Br-Bn-Nos was increased to 15.4%, whereas with DOX it was increased to 16.1% and in combination, it further increased to 23.2% in comparison to control. The combined effect of both Br-Bn-Nos and DOX on cell cycle progression could be useful for the induction of apoptosis.

(c) Induction of apoptosis

Induction of apoptosis to MCF-7 cells was investigated using PE Annexin V and 7-AAD apoptosis kit. The representative dot-plots illustrating apoptotic status was shown in Figure 9. The percentage of apoptotic cells (early apoptotic and late apoptotic cells) treated with Br-Bn-Nos (25 μm) + DOX (0.01 μm) was 24.1% and 20.3%, which was significantly high compared to single regimen treatment with 20 μm of Br-Bn-Nos (11.0 % and 3.73 %) or 0.1 μm of DOX (10.9 % and 3.80 %) respectively after 48h in comparison to controlled untreated cells. This study demonstrated that the proposed combination effect of Br-Bn-Nos and DOX would not only potentially induced apoptosis to the cancer cell, but also provide a promising prospect of order to reduce the toxicity of DOX.

(c) Both Br-Bn-Nos and DOX bind tubulin in single and in combination regimen

In order to experimentally validate our findings based on molecular modelling study with respect to the tubulin-binding affinity of Br-Bn-Nos and DOX in single as well as in their combination, we determined the quenching of fluorescence intensity of tubulin with the treatment of both the agents in single as well as in combination regimen. Due to the presence of the aromatic amino acid tryptophan, the tubulin is autofluorescence in nature. Any chemical compounds that bind with tubulin and alter its conformation leads to a decrease in its intrinsic fluorescence. The relative percentage of decrease in fluorescence intensity was 31.01% with the treatment of 25 μM of Br-Bn-Nos and 58% with the treatment of 0.1 μM of DOX, suggesting that both the agents bind to tubulin with different affinity. Further, the fluorescent intensity of tubulin was reduced to a higher value of 68% with the combination treatment of Br-Bn-Nos (25μM) and DOX (0.1μM) (Figure 10). Significant reduction in tubulin fluorescence intensity in the combination regimen of Br-Bn-Nos and DOX indicate co-binding of both the ligands with tubulin.

(d) Effect of Br-Bn-Nos and DOX on conformational changes of tubulin

In order to further investigate the structural changes on tubulin due to binding of Br-Bn-Nos and DOX in single as well as in combination regimen, we probed the tertiary structure of the protein using an ANS-binding assay. ANS is a fluorescent probe, whose fluorescence improves when attached to protein. ANS, when bound to hydrophobic patches on proteins, shows enhanced fluorescence. An increase in ANS fluorescence of tubulin suggests a loss of protein structural integrity. Purified tubulin with the treatment of Br-Bn-Nos (25μM) and DOX (0.1 μM) showed an increase in tubulin-ANS fluorescence intensity (Figure 11). It displayed a 29.8% increase in fluorescence intensity at 25 μM Br-Bn-Nos, and 40.39% in presence of DOX (0.1 μM) compared to unbound tubulin. Similarly, in combination treatment with Br-Bn-Nos (25 μM) and DOX (0.1 μM) the tubulin-ANS fluorescence intensity was further increased to 57.50% respectively, indicating a gradual incremental perturbation of the structural integrity of the tubulin by the binding of both the agents together.

Discussion

Poor clinical prospects of the current chemotherapy have triggered the development of new treatment modalities such as combination therapy for breast cancer. It is becoming well-appreciated that a toxic drug at its maximum tolerated dose given intermittently is not necessarily better and there exists an opportunity to reduce its dose levels by using combination regimens of drugs that display synergistic interactions (Jordan and Wilson, 2004). The presence of diverse

drug binding sites on tubulin suggests that rational combination of two or more drugs of anti-microbial therapy might be able to enhance the anti-cancer efficacy and reduce toxic side effects, thereby improving the therapeutic index. Tubulin binding drugs such as taxanes and vinca alkaloids are the most efficient anticancer agents for breast cancer treatment (Chougule et al.2011). However, due to the emergence of drug resistance and the subsequent serious side effects, their therapeutic utility is limited (Doddapaneni et al. 2016). In contrast, noscapine, a less toxic orally administered antimicrotubular agent, clearly indicates antitumor activity *in vitro* and *in vivo* against a number of cancers (Laden et al. 2002; Zohu et al.2002; Zhou et al. 2006). Therefore, to decrease the severe side effects of docetaxel and increase its anti-cancer effectiveness we adopt a combination treatment with one of the derivatives of noscapine i.e. Br-Bn-Nos. Similar studies have been conducted previously to demonstrate the combination effect of DOX and other anticancer agents for better therapeutic efficacy (Dash et al. 2020; Galsky and Vogelzang, 2010; Fisusi and Akala, 2019).

In this study, we have demonstrated the combined effect of Br-Bn-Nos and DOX based on molecular modeling and cellular study. Molecular docking of Br-Bn-Nos and DOX, individually, revealed a docking score of -4.99 kcal/mol and -5.88 kcal/mol respectively. However, the docking score of Br-Bn-Nos was significantly reduced (-6.03 kcal/mol) when it was docked onto a co-complex of tubulin-DOX and similarly docking score of DOX was reduced to a greater extent (-6.54 kcal/mol) when it was docked onto a co-complex of tubulin-Br-Bn-Nos, indicating co-binding of both the agents simultaneously to tubulin at two different binding pockets. Further, the significant reduction in free energy of binding based on MD simulation in combination with MM-GBSA and MM-PBSA calculation in presence of Br-Bn-Nos and DOX together compared to their individual binding with tubulin indicated a combination effect of both the ligands. The result obtained from theoretical prediction was validated through experiments by tubulin-binding assay and tubulin-ANS binding assay. Combination treatment of Br-Bn-Nos and DOX reduced the fluorescence intensity of tubulin to a higher value compared to their single regimen treatment, indicating the combined effect of both the agents. Similarly, a significant increase in fluorescent intensity of tubulin-ANS with the treatment of Br-Bn-Nos and DOX in combination regimen compared to single regimen treatment suggest co-binding of both the agents to tubulin. The combined effect of both Br-Bn-Nos and Dox was also revealed from the cellular study using the MCF-7 cancer cell line. Combination treatment of Br-Bn-Nos and DOX was found to be more effective in inhibiting cellular proliferation, blocking of cell cycle progression and induction of

apoptosis compared to single-drug treatment. Further, the isobologram analysis (sum FIC <1) of docetaxel with Br-Bn-Nos indicate significant synergism at 48 h and 72 h exposures.

In conclusion all these results taken together established a proof-of-concept that a rational combination of Br-Bn-Nos and DOX could generate synergistic effects on cancer treatment, which is a highly promising and novel approach for the treatment of breast cancer. Further studies need to be conducted to better understand the growth inhibition molecular mechanism in the combined treatment of breast cancer cells.

Acknowledgments

We would like to acknowledge the financial assistant provided by the Department of Science and Technology, Government of India (Award no- DST/INSPIRE/Code No.: IF170022) for providing student research fellowship to Shruti Gamya Dash and also the financial support by OHEPEE, Govt. of Odisha through World Bank. We are grateful to Dr. Manu Lopus and UM-DAE Centre for Excellence in Basic Sciences for providing extended facilities.

Conflict of Interest

The authors declare no conflict of interest.

REFERENCES

1. Becke, A.D. (1993). A new mixing of Hartree-Fock and local density-functional theories. *Journal of Chemical Physics*, 98, 1372-1377.https://doi:10.1063/1.464304.

2. Binkley, J.S., Pople, J.A., &Hehre, W.J. (1980). Self-consistent molecular orbital methods, Small split-valence basis sets for first-row elements.*Journal of the American Chemical Society*, 102, 939-947. https://doi.org/10.1021/ja00523a008.

3. Bradford, M.M. (1976). A rapid and sensitive method for the quantitation of microgram quantities of protein utilizing the principle of protein-dye binding. *Analytical Biochemistry*, 72, 248-254. https://doi.org/10.1016/0003-2697(76)90527-3.

4. Case, D.A., Betz, R.M., Cerutti, D.S., Cheatham, T.E. III., Darden, T.A., Duke, R.E., Giese, T.J., Gohlke, H., Goetz, A.W., Homeyer, N., Izadi, S., Janowski, P., Kaus, J., Kovalenko, A., Lee, T.S., LeGrand, S., Li, P., Lin, C., Luchko, T., Luo, R., Madej, B., Mermelstein, D., Merz, K.M., Monard, G., Nguyen, H., Nguyen, H.T., Omelyan, I., Onufriev, A., Roe, D.R., Roitberg, A., Sagui, C., Simmerling, C.L., Botello-Smith, W.M., Swails, J., Walker, R.C., Wang, J.,

Wolf, R.M., Wu, X., Xiao, L., &Kollman, P.A. (2016). *AMBER*. 2016. University of California, San Francisco.

5. Canales, A., Rodríguez-Salarichs, J., Trigili, C., Nieto, L., Coderch, C., Andreu, J. M., Paterson, I., Jiménez-Barbero, J., & Díaz, J. F. (2011). Insights into the interaction of discodermolide and docetaxel with tubulin. Mapping the binding sites of microtubule-stabilizing agents by using an integrated NMR and computational approach. *ACS chemical biology*, *6*(8), 789–799. https://doi.org/10.1021/cb200099u.

6. Cheriyamundath, S., Mahaddalkar, T., Reddy Nagireddy, P. K., Sridhar, B., Kantevari, S., & Lopus, M. (2019). Insights into the structure and tubulin-targeted anticancer potential of N-(3-bromobenzyl) noscapine. *Pharmacological reports : PR*, *71*(1), 48–53. https://doi.org/10.1016/j.pharep.2018.09.002.

7. Chougule, M. B., Patel, A. R., Jackson, T., & Singh, M. (2011). Antitumor activity of Noscapine in combination with Doxorubicin in triple negative breast cancer. *PloS one*, *6*(3), e17733. https://doi.org/10.1371/journal.pone.0017733.

8. Crown, J., & O'Leary, M. (2000). The taxanes: an update. *Lancet,* 355, 1176-1178.

9. Darden, T., York, D., & Pedersen, L. (1993). Particle mesh Ewald: An N. log (N) method for Ewald sums in large systems.*Journal of Chemical Physics*, 98, 10089-10092. https://doi.org/10.1063/1.464397

10. Dash, S. G., Suri, C., Nagireddy, P., Kantevari, S., & Naik, P. K. (2020). Rational design of 9-vinyl-phenyl noscapine as potent tubulin binding anticancer agent and evaluation of the effects of its combination on Docetaxel. *Journal of biomolecular structure & dynamics*, 1–14. Advance online publication. https://doi.org/10.1080/07391102.2020.1785945.

11. Doddapaneni, R., Patel, K., Chowdhury, N., & Singh, M. (2016). Noscapine chemosensitization enhances docetaxel anticancer activity and nanocarrier uptake in triple negative breast cancer. *Experimental cell research*, *346*(1), 65–73. https://doi.org/10.1016/j.yexcr.2016.05.006.

12. Essmann, U., Perera, L., Berkowitz, M.L., Darden, T., Lee, H., & Pedersen, L.G. (1995). A Smooth particle mesh: Ewald method. *Journal of Chemical Physics*, *103*, 8577-8593. https://doi.org/10.1063/1.470117.

13. Fisusi, F. A., & Akala, E. O. (2019). Drug Combinations in Breast Cancer Therapy. *Pharmaceutical nanotechnology*, *7*(1), 3–23. https://doi.org/10.2174/2211738507666190122111224.

14. Friesner, R. A., Banks, J. L., Murphy, R. B., Halgren, T. A., Klicic, J. J., Mainz, D. T., Repasky, M. P., Knoll, E. H., Shelley, M., Perry, J. K., Shaw, D. E., Francis, P., & Shenkin, P. S. (2004). Glide: a new approach for rapid, accurate docking and scoring. 1. Method and assessment of docking accuracy. *Journal of medicinal chemistry*, *47*(7), 1739–1749. https://doi.org/10.1021/jm0306430.

15. Galsky, M. D., &Vogelzang, N. J. (2010). Docetaxel-based combination therapy for castration-resistant prostate cancer. *Annals of oncology : official journal of the European Society for Medical Oncology*,21(11), 2135–2144. https://doi.org/10.1093/annonc/mdq050.

16. Gordon, M.S., Binkley, J.S., Pople, J.A., Pietro, W.J., &Hehre, W.J. (1982).Self-consistent molecular-orbital methods. Small split valence basis sets for second-row elements. *Journal of the American Chemical Society*, *104*, 2797-2803. https://doi.org/10.1021/ja00383a007.

17. Halgren, T.A., Murphy, R.B., Friesner, R.A., Beard, H.S., Frye, L.L., Pollard, W.T., & Banks, J.L. (2004). Glide: a new approach for rapid, accurate docking and scoring. 2. Enrichment factors in database screening. *Journal of Medicinal Chemistry*, 47, 1750-1759. https://doi.org/10.1021/jm030644s.

18. Hamel, E., & Lin, C.M. (1981). Glutamate-induced polymerization of tubulin: characteristics of the reaction and application to the large-scale purification of tubulin. *Archives of Biochemistry and Biophysics*, 209, 29-40.https://doi: 10.1016/0003-9861(81)90253-8.

19. Jakalian, A., Jack, D.B., &Bayly, C.I. (2002). Fast, efficient generation of high-quality atomic charges. AM1-BCC model: II. Parameterization and validation. *Journal of Computational Chemistry*, *23*, 1623-1641.https://doi.10.1002/jcc.10128.

20. Jordan, M. A., & Wilson, L. (2004). Microtubules as a target for anticancer drugs. *Nature reviews. Cancer*, *4*(4), 253–265. https://doi.org/10.1038/nrc1317.

21. Jorgensen, W.L., Chandrasekhar, J., Madura, J.D., Impey, R.W., & Klein, M.L. (1983). Comparison of simple potential functions for simulating liquid water. *Journal of Chemical Physics*, 79, 926-935. https://doi.org/10.1063/1.445869.

22. Joshi, H.C., &Zohu, J. (2000). Noscapine and Analogues as Potential Chemotherapeutic Agents. *Drug News & Perspectives,* 13, 543-546.https://doi: 10.1358/dnp.2000.13.9.858482.

23. Joshi, H.C., &Zohu, J. (2001). Gamma tubulin and microtubule nucleation in mammalian cells. *Methods Cell Biology*, 67, 179-193.doi: https://doi.org/10.1016/S0091-679X(01)67013-4.

24. Karlsson, M. O., Dahlstrom, B., Eckernas, S. A., Johansson, M. &Alm, A. T. (1990). Pharmacokinetics of oral noscapine. *European. Journal of Clinical. Pharmacology,* 39, 275–279. https://doi.org/10.1007/BF00315110

25. Kleeberg, U.R., Fink, M. Tessen, H.W., Nennecke, A., Hentschel, S. & Bartels, S. (2013). Adjuvant therapy reduces the benefit of palliative treatment in disseminated breast cancer-own findings and review of the literature. *Onkologie,* 36(6):348-56. doi: 10.1159/000351253.

26. Kollman, P.A., Massova, I., Reyes, C., Kuhn, B., Huo, S., Chong, L., Lee, M., Lee, T., Duan, Y., & Wang, W. (2000). Calculating structures and free energies of complex molecules: combining molecular mechanics and continuum models. *Accounts of Chemical Research*, 33(12), 889-897. doi: 10.1021/ar000033j

27. Lee, C., Yang, W., & Parr, R.G. (1988). Development of the Colle-Salvetti correlation-energy formula into a functional of the electron densityPhysical Review B: Condensed Matter and Materials Physics, 37, 785-789. https://doi: 10.1103/physrevb.37.785.

28. Mahaddalkar, T., Naik, P.K., Choudhary, S., Manchukonda, N., Kantevari, S., &Lopus, M. (2017). Structural investigations into the binding mode of a novel noscapine analogue, 9-(4-vinylphenyl) noscapine, with tubulin by biochemical analyses and molecular dynamic simulations. *Journal of Biomolecular Structure and Dynamics.35*, 2475-2482. https://doi: 10.1080/07391102.2016.1222969.

29. Maier, J.A., Martinez, C., Kasavajhala, K., Wickstrom, L., Hauser, K.E., & Simmerling, C. (2015). ff14SB: Improving the accuracy of protein side chain and backbone parameters from ff99SB. *Journal of Chemical Theory and Computation,11*, 3696-3713. https://doi.org/10.1021/acs.jctc.5b00255.

30. Manchukonda, N.K., Naik, P.K., Santoshi, S., Lopus, M., Joseph, S., Sridhar, B., &Kantevari, S. (2013). Rational design, synthesis and biological evaluation of third generation α-noscapine analogues as potent tubulin binding anticancer agents. *PLoS One.*, *8*, e77970.https://doi: 10.1371/journal.pone.0077970.

31. Manchukonda, N.K., Naik, P.K., Sridhar, B., &Kantevari, S. (2014). Synthesis and biological evaluation of novel biaryl type α-noscapine congeners. B*ioorganic & Medicinal Chemistry Letters*. 24, 5752-5757.

32. Massova, I., & Kollman, P.A. (2000). Combined molecular mechanical and continuum solvent approach (MM-PBSA/GBSA) to predict ligand binding. *Perspectives in Drug Discovery and Design*, 18(1), 113-135.

33. Naik, P.K., Chatterji, B.P., Vangapandu, S.N., Aneja, R., Chandra, R., Kanteveri, S., & Joshi, H.C. (2011). Rational design, synthesis and biological evaluations of amino-noscapine: a high affinity tubulin-binding noscapinoid. *Journal of Computer-Aided Molecular Design,* 25, 443-454. https://doi: 10.1007/s10822-011-9430-4.

34. Naik, P.K., Lopus, M., Aneja, R., Vangapandu, S.N., & Joshi, H.C. (2012). *Insilico* inspired design and synthesis of a novel tubulin-binding anti-cancer drug: folate conjugated noscapine (Targetin). *Journal of Computer-Aided Molecular Design*, 26, 233–247.

35. Naik, P.K., Santoshi, S., Rai, A., & Joshi, H.C. (2011). Molecular modelling and competition binding study of Br-noscapine and colchicine provide insight into noscapinoid-tubulin binding site. *Journal of Molecular Graphics and Modelling*, 29, 947-955.https://doi: 10.1016/j.jmgm.2011.03.004.

36. Nogales, E., Wolf, S. G., & Downing, K. H. (1998). Structure of the alpha beta tubulin dimer by electron crystallography. *Nature*, *391*(6663), 199–203. https://doi.org/10.1038/34465.

37. Oliva, M.A., Prota, A.E., Rodríguez-Salarichs, J., Bennani, Y.L., Jiménez-Barbero, J., Bargsten, K., Canales, A., Steinmetz, M.O., & Diaz, J.F. (2020). Structural basis of noscapine activation for tubulin binding. *Journal of Medicinal Chemistry*, 63, 8495-8501.https://doi.10.1021/acs.jmedchem.0c00855.

38. Pace, A., Bove, L., Nistico, C., Ranuzzi, M., Innocenti, P., Pietrangeli, A., Terzoli, E., &Jandolo, B. (1996). Vinorelbine neurotoxicity: clinical and neurophysiological findings in 23 patients. *Journal of Neuropsychology.*, 61, 409-411. https://doi:10.1136/jnnp.61.4.409.

39. Panda, D., Chakrabarti, G., Hudson, J., Pigg, K., Miller, H.P., Wilson, L., & Himes, R.H. (2000). Suppression of microtubule dynamic instability and treadmilling by deuterium oxide. *Journal of Biochemistry,* 39, 5075-5081. https://doi.org/10.1021/bi992217f.

40. Pandey, S.K, Biswas, S., Gunjan, S., Chauhan, B.S., Singh, S.K., Srivastava, K., Singh, S., Batra, S., Tripathi, R., (2016). Pyrrolidine-Acridine hybrid in Artemisinin-based combination: a pharmacodynamic study. *Parasitology*, 143(11), 1421-32. doi: 10.1017/S0031182016000937.

41. Rowinsky, E.K. (1997). The development and clinical utility of the taxane class of antimicrotubule chemotherapy agents. *Annual Review of Medicine*, 48, 353-374. https://doi:10.1146/annurev.med.48.1.353.

42. Ryckaert, J.P., Ciccotti, G., & Berendsen, H.J. (1977). Numerical integration of the cartesian equations of motion of a system with constraints: molecular dynamics ofn-alkanes. *Journal of Computational Physics,* 23, 327-341. https://doi.org/10.1016/0021-9991(77)90098-5.

43. Santoshi, S., & Naik, P.K. (2014). Molecular insight of isotypes specific β-tublin interaction of tubulin heterodimer with noscapinoids. *Journal of Computer-Aided Molecular Design*, *28*, 751-763. https://doi.10.1007/s10822-014-9756-9.

44. Santoshi, S., Manchukonda, N.K., Suri, C., Sharma, M., Sridhar, B., Joseph, S., Lopus, M., Kantevari, S., Baitharu, I., & Naik, P.K. (2015). Rational design of biaryl pharmacophore inserted noscapine derivatives as potent tubulin binding anticancer agents. *Journal of Computer aided Molecular Design*, 29, 249-270.https://doi: 10.1007/s10822-014-9820-5.

45. Snyder, J. P., Nettles, J. H., Cornett, B., Downing, K. H., & Nogales, E. (2001). The binding conformation of Taxol in beta-tubulin: a model based on electron crystallographic density. *Proceedings of the National Academy of Sciences of the United States of America*, *98*(9), 5312–5316. https://doi.org/10.1073/pnas.051309398.

46. Theiss, C., &Meller, K. (2000). Taxol impairs anterograde axonal transport of microinjected horseradish peroxidase in dorsal root ganglia neurons in vitro. *Cell Tissue Research*, 299 213-224. https://doi: 10.1007/s004419900120.

47. Topp, K.S., Tanner, K.D., & Levine, J.D. (2000). Damage to the cytoskeleton of large diameter sensory neurons and myelinated axons in vincristine-induced painful peripheral neuropathy in the rat. *ournal of Comparative Neurology*, 424, 563-576

48. Wang, J., Wang, W., Kollman, P.A., & Case, D.A. (2006). Automatic atom type and bond type perception in molecular mechanical calculations.*Journal of Molecular Graphics and Modelling,* 25, 247-260.

49. Winefield, R. D., Entwistle, R. A., Foland, T. B., Lushington, G. H., & Himes, R. H. (2008). Differences in paclitaxel and docetaxel interactions with tubulin detected by mutagenesis of yeast tubulin. *ChemMedChem*, *3*(12), 1844–1847. https://doi.org/10.1002/cmdc.200800288.

50. Y. Ke., K. Ye., Grossniklaus, H.E., Archer, D.R., Joshi, H.C., & Kapp, J.A. (2000). Noscapine inhibits tumor growth with little toxicity to normal tissues or inhibition of immune responses. *Cancer Immunology, Immunotherapy*, 49, 217-225. https://doi: 10.1007/s002620000109.

51. Ye, K., Ke, Y., Keshava, N., Shanks, J., Kapp, J.A., Tekmal, R.R., Petros, J., & Joshi, H.C. (1998). Opium alkaloid noscapine is an antitumor agent that arrests metaphase and induces apoptosis in dividing cells. *Proceedings of the NationalAcademy of Sciences of the United States of America,* 95, 1601-1606.doi: https://doi.org/10.1073/pnas.95.4.1601.

52. Zhou, J., Gupta, K., Aggarwal, S., Aneja, R., Chandra, R., Panda, D., & Joshi, H.C. (2003). Brominated derivatives of noscapine are potent microtubule-interfering agents that perturb mitosis and inhibit cell proliferation. *Molecular Pharmaceutics*, 63, 799-807. https://doi: 10.1124/mol.63.4.799.

53. Zhou, J., Gupta, K., Yao, J., Ye, K., Panda, D., Giannakakou, P., & Joshi, H. C. (2002). Paclitaxel-resistant human ovarian cancer cells undergo c-Jun NH2-terminal kinase-mediated apoptosis in response to noscapine. *The Journal of biological chemistry*, *277*(42), 39777–39785. https://doi.org/10.1074/jbc.M203927200

54. Zhou, J., Liu, M., Aneja, R., Chandra, R., Lage, H., & Joshi, H.C. (2006). Reversal of P glycoprotein mediated multidrug resistance in cancer cells by the c-jun NH2-terrminal kinase. *Cancer Research,* 66, 445-452. https://doi: 10.1158/0008-5472.CAN-05-1779.

Legends of Figures

Figure 1: Structures of the (A) first generation noscapinoids that identifies the 9th position modification in the noscapine scaffold, (B) molecular structure of the 9-Br-Noscapine and (C) N-3-Br Benzyl Noscapine.

Figure 2: Root mean square deviations (RMSD) of Cα carbon atoms of tubulin only and in complex with Br-Bn-Nos (Tubulin+ Br-Bn-Nos), with docetaxel (Tubulin+DOX) and with both docetaxel and Br-Bn-Nos (Tubulin+DOX+Br-Bn-Nos) during 100 ns of MD simulation. The relative fluctuation in the RMSD of the Cα atoms is very small after ~ 20 ns of the simulation. The time step of 20 ps was used during the simulation. The topmost 5 frames from the MD simulation trajectory with lowest total energy were considered to generate the average structure.

Figure 3: Root mean square fluctuation (RMSF) of the residues of tubulin of the docked ligands in the bound form and in the unbound form of tubulin heterodimer. Different levels of flexibility of these residues were noticed in the bound form of tubulin with Br-Bn-Nos and DOX in single as well as in combination. Most of the residues showed flexibilities >5 Å in case of tubulin bound with Br-Bn-Nos and DOX as compared to the free tubulin heterodimer, indicating that these residues seem to be more flexible as a result of binding.

Figure 4. (a) Both Br-Bn-Nos and DOX are well accomodated inside their respective binding site of tubulin. (b) Snapshot of both the ligands obtained. The binding site is represented as

macromodel surface according to α- and β- tubulin (α-tubulin is represented in blue colour and β-tubulin is represented in brown colour).

Figure 5. The ligplot analysis showing the binding mode of (a) Br-Bn-Nos with tubulin, (b) Br-Bn-Nos with the co-complex of Tubulin-DOX, (c) DOX with tubulin, and (d) DOX with the co-omplex of tubulin-Br-Bn-Nos. The binding mode of Br-Bn-Nos was different when docked to tubulin and to the co-complex of tubulin-DOX, in which different number of hydrogen bondings were involved with the binding site amino acids. Similarly, the binding mode of DOX was also different when docked to tubulin and to the co-complex of tubulin-Br-Bn-Nos, in which different number of hydrogen bonding involved with the binding site amino acids. The hydrogen bonds formed (if any) are represented as dotted lines and the value represents the bond distance.

Figure 6. Br-Bn-Nos and DOX in single as well as in combination regimen at different concentrations inhibit cellular proliferation of human breast cancer cell, MCF-7 after 48 h and 72 h treatment. The IC_{50} value amounted to 11.5 μM and 7.71 μM, respectively for 48h and 72h with Br-Bn-Nos. Similarly, the IC_{50} value amounted to 0.39 μM and 0.016 μM, respectively for 48h and 72h with DOX. In contrast, approximately 50% inhibition of cellular inhibition was achieved in a combination regimen of Br-Bn-Nos (5μM) and DOX (0.001μM) after 48 h and 72 h post-treatment.

Figure 7. Isobolograms showing *in vitro* interactions between Br-Bn-Nos and DOX. Sum FIC < 0.5 represents substantial synergism, sum FIC < 1 represents synergism, sum FIC = 1 represents additive interaction, and sum FIC >1 represents antagonism between two drugs.

Figure 8. Figure A-D depict represented figures of analyses of cell cycle distribution in a two-dimensional disposition as determined by flow cytometry in MCF-7 cells treated with 20 μM of Br-Bn-Nos, 0.1 μM of DOX as single regimen and 25 μM of Br-Bn-Nos + 0.01 μM of DOX in combination regimen. Both Br-Bn-Nos and DOX inhibit cell cycle progression at mitosis followed by the appearance of a characteristic hypodiploid (sub-G1) DNA peak, indicative of apoptosis.

Figure 9. Analysis of apoptosis cell death induced by Br-Bn-Nos alone and in combination with DOX based on flow cytometric analysis. PE conjugate of Annexin V was used in combination

with 7-Amino-Actinomycin (7-AAD) to distinguish among 3 subpopulations: PE^{--} and $7\text{-}AAD^{--}$ population indicates viable cells (bottom left quadrant); PE^{--} and $7\text{-}AAD^{+}$ population indicates early apoptotic cells (lower right quadrant); PE^{+} and $7\text{-}AAD^{+}$ population indicate late apoptotic cells (top right quadrant).

Figure 10. Decrease of fluorescence intensity of tubulin by Br-Bn-Nos and DOX in single as well as in combination regimen. Tubulin (2.0 μM) was incubated with Br-Bn-Nos (25 μM) and DOX (0.1 μM) alone as well as in combination regimen (25 μM of Br-Bn-Nos and 0.01 μM of DOX) and the emission spectra were collected (310 nm – 400 nm). Both Br-Bn-Nos and DOX in single as well as in combination regimen showed a concentration-dependent quenching of the intrinsic tubulin fluorescence emission intensity indicating the binding of both Br-Bn-Nos and DOX to tubulin. The more reduction in tubulin fluorescence intensity in combination regimen of both Br-Bn-Nos and DOX, compared to their single binding, revealed combination effect with the tubulin. The graph is a representative of three independent experiments.

Figure 11. Enhancement of tubulin-ANS fluorescence by Br-Bn-Nos and DOX in single as well as in combination regimen. Tubulin (2.0 μM) was incubated without (control) or with Br-Bn-Nos (25 μM), DOX (0.1 μM) and in their combination regimen (Br-Bn-Nos 25 μM+DOX 0.01 μM), followed by incubation with ANS (50 μM). The samples were excited at 380 nm and the emission spectra were collected (390 to 500 nm). The increase is more in tubulin-ANS fluorescence in combination regimen of both Br-Bn-Nos and DOX, compared to their single binding, and revealed combination effect with the tubulin. The graph is a representative of three independent experiments.

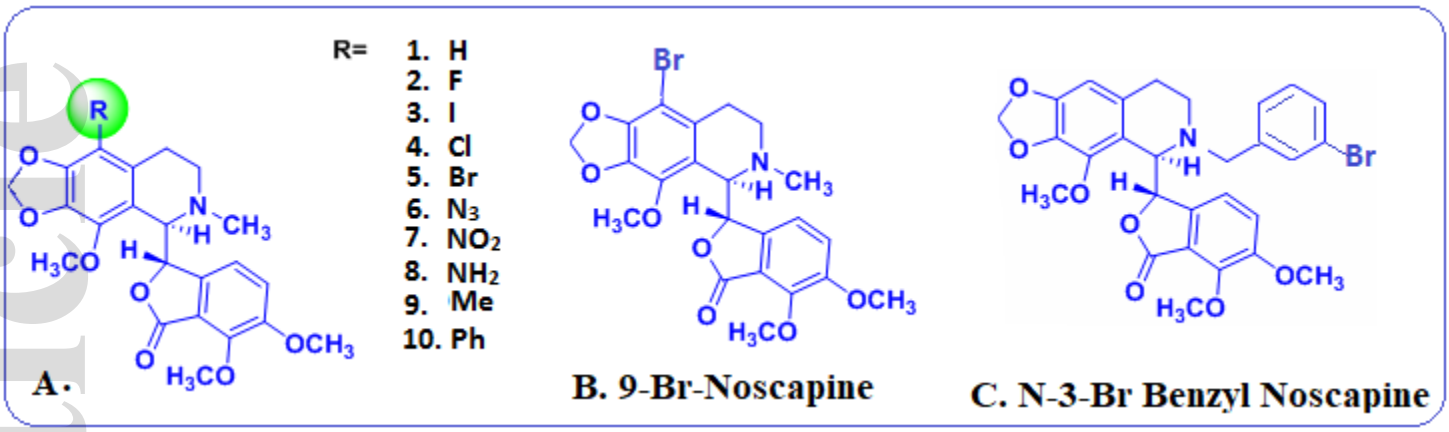

cbdd_13902_f1.tif

cbdd_13902_f2.tif

cbdd_13902_f3.tif

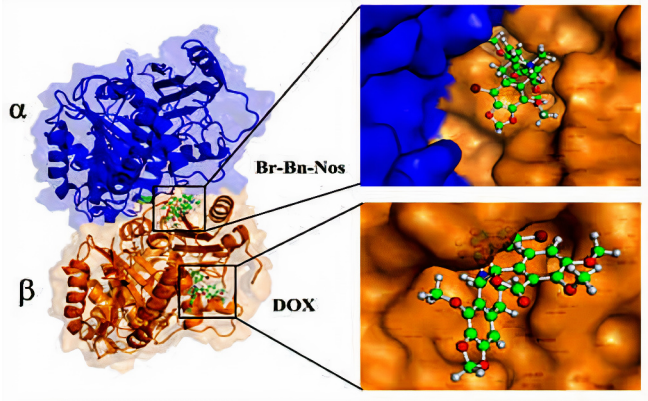

cbdd_13902_f4.jpg

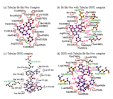

cbdd_13902_f5.tif

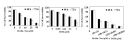

cbdd_13902_f6.tif

cbdd_13902_f7.tif

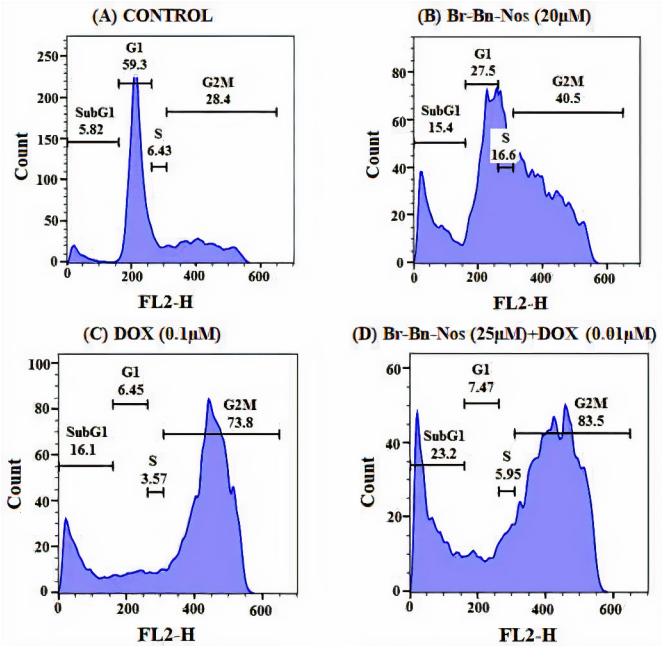

cbdd_13902_f8.jpg

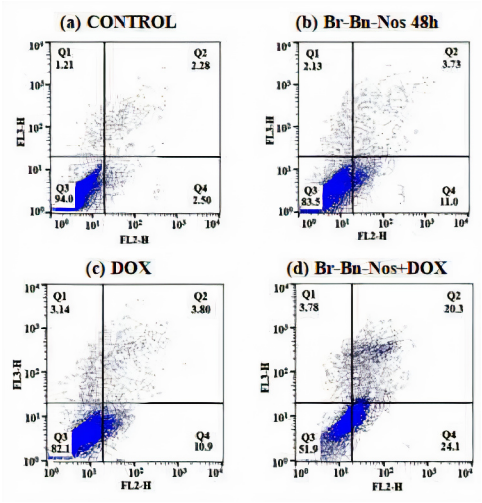

cbdd_13902_f9.jpg

cbdd_13902_f10.jpg

cbdd_13902_f11.jpg